UNIVERSITÀ DEGLI STUDI DI PARMA

DOTTORATO DI RICERCA IN
"*Scienza e Tecnologia dei Materiali*"

CICLO XXXII

Synthesis of NIR-harvesting Hybrid Nanomaterials

Coordinatore:
Chiar.mo Prof. Enrico Dalcanale

Tutore:
Chiar.mo Prof. Andrea Secchi

Dottoranda: Beatrice Cogliati

Anni 2016/2019

A Filippo.

Abstract

This PhD thesis describes the design, the study and the synthesis of NIR-harvesting hybrid nanomaterials, consisting of an inorganic (noble metal) and an organic component. Indeed, this strategy can be applied to enhance the emission of proper NIR dyes by exploitation the *plasmon-enhanced fluorescence* (PEF). This phenomenon rises from the coupling of the organic dyes with plasmonic nanostructures, such as nanoparticles (NPs), and nanorods (NRs). In the first part of the thesis, a *host-guest* approach was studied and exploited in order to have a control on the aggregation of nanostructures and, in principle, to modify their properties. In particular, the attention was focused on the synthesis of calix[n]arene derivatives used either as multivalent hosts for the decoration of noble metal NPs and NRs or as aggregators for properly functionalized NPs. In the second part of the thesis, the work was focused on the design and the synthesis of the organic part of the hybrid nanomaterial. Firstly, cyanine-type dyes characterized by a D-A-D structure (D = donor, A = acceptor) were prepared. The central acceptor core is represented by the croconic acid and for this reason these dyes are called *croconates* or *croconaines*. In order to have a better interaction and a major control on the effective coupling between the dye and the surface, the introduction of *linker* units, basically on the donor, was design. The linkers are characterized by the presence of a functional group in order to have a covalent grafting of the dyes on the metal (e.g. thiol, amine, carboxylic acid). Another type of NIR-compound is represented by acene class. On this topic, a research period of three months was spent in the laboratories of CEMES-CNRs of Toulouse (France) with the aim to obtain suitable precursors for the construction of long acenes and [16]starphene(5.5.5).

Keywords: NIR, NIR-harvesting, fluorescence, plasmon-enhanced fluorescence, noble metals, nanoparticles, anisotropic nanoparticles, nanorods, calix[n]arene, croconic acid, croconates, croconaines, DAD, quantum yield, acenes, starphenes.

Contents

CHAPTER 1
Introduction

1.1 Introduction to Nanotechnology

Over the past few decades, the global trend toward *miniaturization* is becoming increasingly popular.[1] The recent changes in societies' demand and research needs, due to the emerging and developing fields of technology, has forced the introduction of more and more microparts into various types of industrial products.[2] Therefore, the outgoing trend is to get ever more power into an even-smaller space[3]. However, it is essential to consider that the technologies that are known for the macro world cannot be applied and scaled to the micro or nanoworld.[1] In this context, the new concept of *nanotechnology* was introduced. Many different definitions of what exactly nanotechnology is and represent are present in the literature. This term usually covers very different research fields, and thus concepts such as inter- and multi-disciplinary are a fundamental part of it.[4]

Nanotechnology, in a general definition, can be expressed as the science of the nanoscale that creates nanostructures with designed features in the 1-100 nm size range.[5,6] In 1959 the physicist Richard Feynman in a talk entitled *"There's a Plenty of Room at the Bottom"* [7] introduced the concepts and the ideas behind nanoscience, as part of a process that could make scientists able to manipulate and rearrange atoms and molecules, in the perspective of the designing molecules one atom at a time. Only later, in 1974, Professor N. Taniguchi coined the term "nanotechnology".[8]
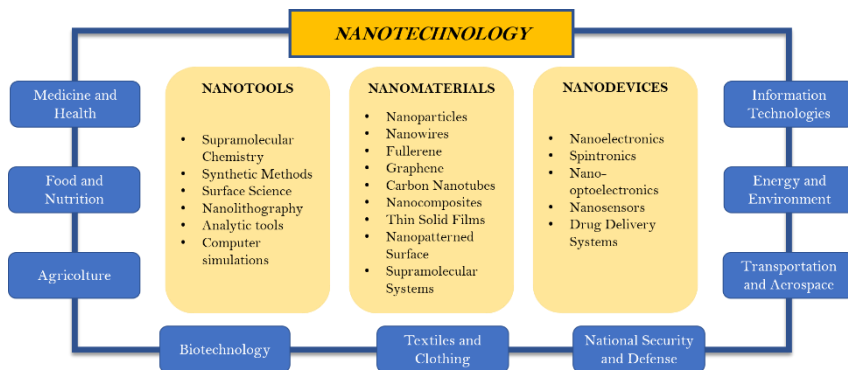
Figure 1.1 *Schematic illustration showing the development of nanotechnology and its several fields of application. Adapted from ref. [14] Copyright © 2012 John Wiley & Sons, Ltd.*

Nanotechnology is nowadays exploited in sever fields that span from pure scientific ones, such as drug delivery or biosensors, to more industrial oriented. Nanotechnologies are used in cosmetics, design of smart sports equipment, telecommunication, photovoltaic, or

environmental applications.[9] The first examples of nanotechnological applications come, however, from the far past. Indeed, in the middle age, colorful stained-glass windows (Figure 1.2) were manufactured by exploiting the different optical absorption properties of gold and silver particles of nanometric size, which are nowadays indicated as noble metal nanoparticles (see next chapters). In the same context, more than a thousand years ago, the Chinese were using gold nanoparticles as a dye to color ceramic artifacts. Of course, at that time, it was impossible to see with naked eye the atomic level of the matter, and indeed the age of nanotechnology was born after the development of tools and techniques, such as the scanning tunnel microscopy (STM), atomic force microscopy (AFM) or transmission electron microscopy (TEM) capable of investigating objects of those sizes.
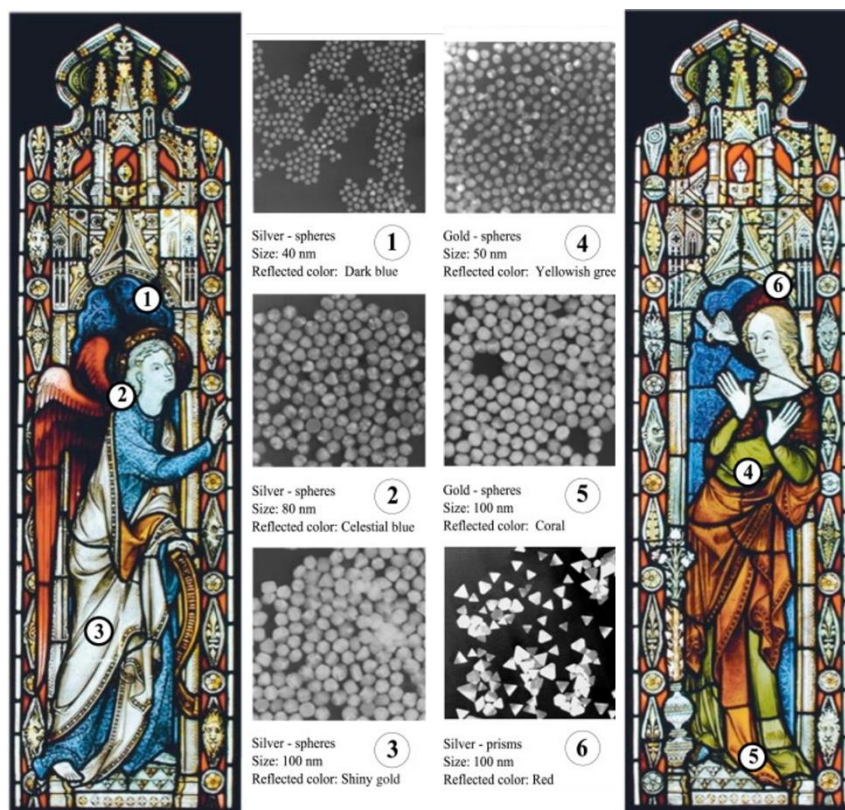
Figure 1.2 *Effect of silver and gold nanoparticles on the colors of the stained glass windows, varying parameters as size and shape.[10] Reproduced from ref. [10] Copyright © 2015 Elsevier Inc. All rights reserved.*

Recently, on the base of Feynman's concepts, the so-called "molecular" nanotechnology expresses precisely the concept of the manipulation of atom and molecules in order to design and create macroscale products.[11] In the fabrication of nanosized objects and nanomaterials,

two strategies can be used: the "bottom-up" and the "top-down" approach. The latter is used dominantly in the industry; it starts from bulk materials to get, through fragmentation, smaller nanostructures. The fragmentation is usually achieved by destructive techniques such as lithography.[12] The main disadvantages of this approach are that instrumental limits restrict the miniaturization level, and the resulting miniaturized structures may present imperfections and defects.

The bottom-up approach overcomes a large part of these limitations because the preparation of the nanostructures starts from the "bottom", that is atom by atom and then molecule by molecule. This can be achieved through direct manipulation of atoms and molecules for creating nano-objects. For example, in the literature, it is reported the possibility to "write" on a surface placing molecules on it. Hla and co-workers have reported a molecular artwork using an STM tip on a surface, where the number 2000 is written with 47 individually placed CO molecules on Cu(211) surface (Figure 1.3).[13] The principal limit of the direct manipulation of atoms/molecules is the fact that requires very sophisticated instrumentations (i.e., STM microscopes). Most important, the assembled objects usually do not exhibit any specific intrinsic function.
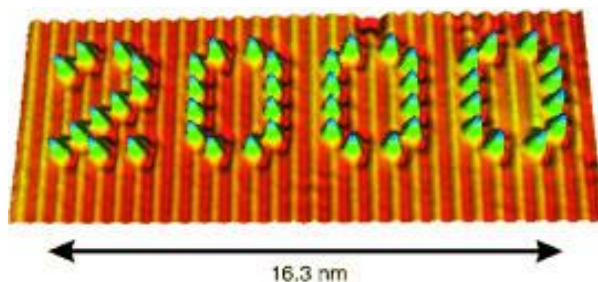
Figure 1.3 *Writing with an STM tip: CO single molecules are the green-blue protrusions placed on a Cu(211) surface. Reproduced with permission from ref. [13] Copyright © 2001 WILEY-VCH Verlag GmbH, Weinheim, Fed. Rep. of Germany.*

Nature taught us, instead, that the assembly of molecular structures such as oligopeptides, nucleic acids, etc. may originate nanosized structures capable of exhibiting specific functions (e.g., ATP-synthase). These assemblies do not originate from a random aggregation of species but are driven by specific intermolecular interactions. Taking inspiration from nature, it becomes thus possible exploiting the self-assembly between specific molecules as a bottom-up approach for the manufacturing of self-assembled structures (2D or 3D) as ideal building blocks for the creation of nanodevices endowed with specific novel functions.[14,15] These aspects are more conveniently studied through the application of the principles and methods of Supramolecular Chemistry.[16] This multidisciplinary branch of Chemistry mainly deals

15

with the reversibility of the multi-component systems, which are driven by non-covalent interactions (in this context also called supramolecular interactions), e.g., hydrogen bonding, electrostatic, π-π interactions. The resulting well-defined supermolecules (the nano-objects) are characterized by specific and tailored properties, that are not a simple superimposition of the properties of the single building block. The reversibility of these nanostructures allows the mimick of natural systems so that they could be responsive towards external stimuli (e.g., electrical, chemical, light, …). Striking examples are represented by artificial molecular nano-rotors or prototypes of molecular muscles (Figure 1.4).[17]
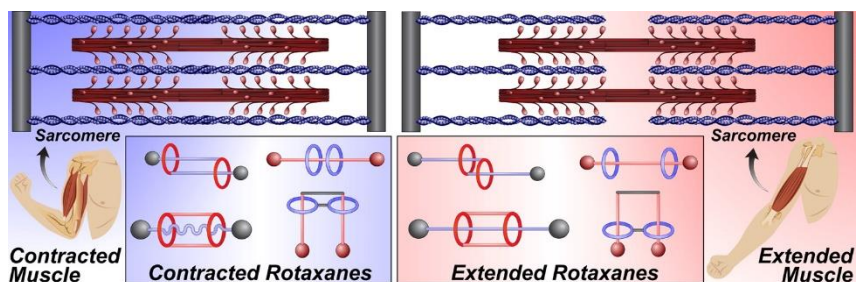
Figure 1.4 Examples of bistable mechanically interlocked molecules (MIMs), such as type of rotaxanes "molecular muscle" architectures that express contractile and extensile motion as in the actin-myosin system. Reproduced with permission from ref. [17] Copyright © 2014 American Chemical Society.

1.2 Hybrid Materials and Heterosupramolcular Chemistry

In recent years, increasing attention has grown towards materials consisting of an inorganic and an organic component, which are more commonly known as *hybrid materials*.[18] These materials may present new properties that are absent in the pure counterparts and are due to the interactions established between the inorganic and organic parts of the material. The explication of these new properties becomes increasingly important and interesting as the size of the hybrid material decreases.

The self-assembled monolayers (SAM) on surfaces represent a significant class of nano-sized hybrid materials that are characterized by a single layer of organic molecules spontaneously and ordinately assembled on an appropriate solid substrate.[19,20] The organic

molecules of the monolayer are equipped with a functional group capable of interacting covalently (or, more rarely, in a non-covalent way) with the surface atoms of the inorganic component. The chemisorption usually represents the driving force for the formation of SAMs. For this reason, a good chemical affinity between adsorbate and surface is required (e.g., thiol functional group on noble metals, especially gold, or carboxylic acid on silver or iron oxides). The adsorbate is often characterized by long alkyl chains that increase the SAM stability because of the highly ordered close-packing established by dispersive van der Waals interactions. When the organic layer contains domains capable of performing a specific function that combines with the intrinsic (optical, magnetic,...) properties of the inorganic substrate, then we usually talk of *smart materials*, also called *functional hybrid nanomaterials*.[21] In particular, the smartness of these materials is due to the presence of a "tail" group at the end of the alkyl chain (the "head" group is responsible for the chemisorption) that confers certain functionalities to the material (Figure 1.5).
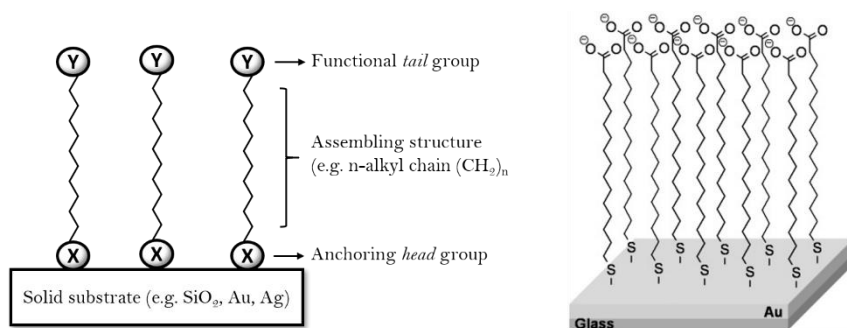
Figure 1.5 *(left) General schematic representation of a SAM and (right) schematic representation of a SAM based on ω-mercapto hexadecanoic acid.[22] Reproduced from ref. [22] Copyright © 2006 WILEY-VCH Verlag GmbH & Co. KGaA, Weinheim).*

SAMs are very often classified as 2D or 3D depending on the nature of the substrate. In the first case, a flat surface of an inorganic material (Au, Si, SiO$_2$, GaAs, etc.) is covered by the organic monolayer. In the second case, the inorganic structure has a well-defined three-dimensional shape (spherical, rod-like, prisms, etc.) still fully covered by the organic matter. 3D-SAM usually present more enticing properties than their 2D counterparts, because the properties of the organic monolayer are combined with those deriving from the quantum confinement typical of the nanosized 3D structures.

Among the various examples of 3D-SAM, those consisting of an inorganic component based on noble metals (Au, Ag, or Cu) are finding increasing employment in numerous applied fields such as nanosensoristic, nanoelectronic and catalysis. These nanostructures,

also commonly known as noble metal nanoparticles (NPs) or monolayer protected clusters (MPC),[23] have been indeed functionalized with a large variety of organic monolayers. Depending on the nature of the organic monolayer, it is possible, for example, to induce hydrophilicity or hydrophobicity to the entire nanostructure and therefore varying its solubility in solvents of different polarity. This topic will be discussed in detail in Chapter 2.

2D- and 3D-SAM are also extremely versatile from a supramolecular point of view. The possibility to exploit the host–guest approach to assemble nanostructures, to modify their properties, for signaling and sensing has indeed catalyzed the attention of the scientific community starting from the late nineties. As a matter of fact, in 1999, Fitzmaurice and co-workers introduced the new concept of *heterosupramolecular chemistry* as "a systematic covalent and non-covalent chemistry of condensed phase and molecular components".[24] Since then, the possibility to insert "host" molecules in the organic monolayer of 2D- and in particular of 3D-SAM has been explored by several groups[22,25] either to enhance the recognition properties of the host, through the multivalency, or to exploit the intrinsic properties of the metal substrate (plasmonic, magnetic, …) to signal the molecular recognition event (Figure 1.6).
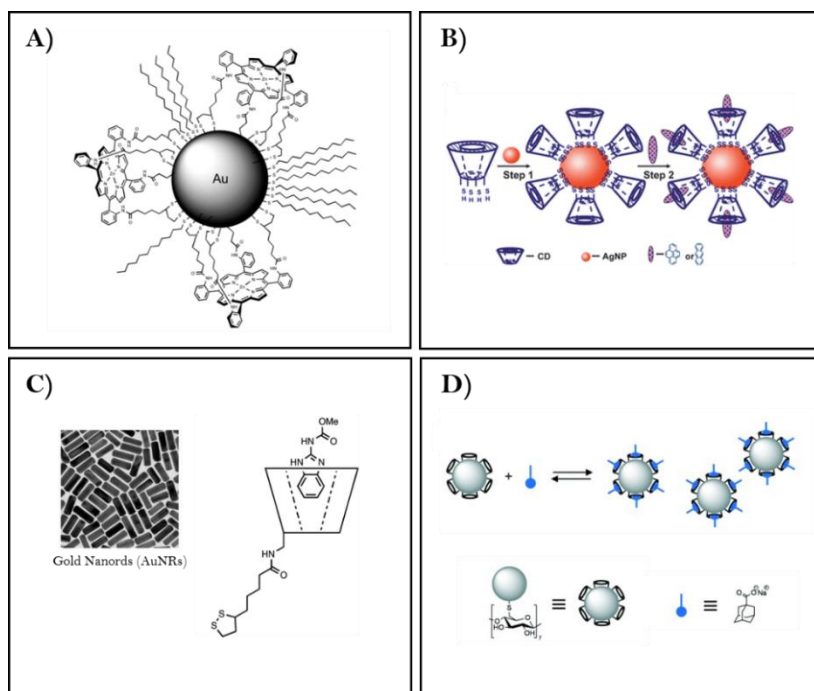
Figure 1.6 *Schematic representations of decorated 3D-SAM for molecular recognition. A) Reproduced from ref. [26] Copyright © 2004 The Royal Society of Chemistry. B) Reproduced from ref. [27] Copyright © The Royal Society of Chemistry 2010. D) Reproduced from ref. [22] Copyright © 2006 WILEY-VCH Verlag GmbH & Co. KGaA, Weinheim.*

As an example of multivalency, Beer and co-workers showed how the anions binding affinity of a free Zn-metalloporphyrin is lower than the binding affinity of preorganized Zn-metalloporphyrin grafted on a gold NP (AuNP), working as a good enhanced-surface anion sensor.[26] Zhao and Ozaki's group developed instead an enhanced-surface sensor for a kind of environmental pollutants, called polycyclic aromatic hydrocarbons (PAHs).[27] They designed decorated silver NPs (AgNPs) with an opportunely functionalized β-cyclodextrin (CD), to enhance the selectivity and the sensitivity of the hydrophobic cavity of the CD towards PAHs as anthracene and pyrene. CD host was also used for the detection of a benzimidazole-based fungicide (carbendazim), functionalizing the surface of anisotropic gold NPs, called nanorods (NRs).[28] The research group of Reinhoudt reported a nice experiment of host-guest complexation in which they decorated AuNPs with cyclodextrins (CD) capable of complexing adamantly carboxylate as a guest.[29]

Host-guest complexation could, in principle, be used for the formation of stable network aggregates (Figure 1.7). In the above-cited work, the authors investigated the formation of CD-adamantane host-guest supramolecular aggregates and, in this case, a bis(adamantly) guest molecule was used as a bi-functional bridge among CD-AuNPs. Another class of host exploited in this context is represented by cucurbit[n]uril (CB[n]), in particular, CB[8], which is usually used as linking molecule because of its capability to form 1:1:1 ternary complex with two guests.

As an example, Scherman et al. reported the formation of NP-polymer composites using viologen-functionalized AuNPs and naphthol-functionalized acrylamide copolymer.[30] When the CB[8] is added to the mixture of the two guest-components, polymerization is obtained, because of the high affinity of the CB[8] to complex viologen and naphthol (1:1:1 ternary complex). Moreover, it also possible the aggregation of NRs through an end-to-end alignment. The same research group, using the same system, functionalized the longitudinal ends of AuNRs with viologen guests, and they induced the aggregation adding CB[8] and bi-functional linker molecules with naphthol units at each end, acting as a bridging linker between AuNRs.[31]

Examples of *heterosupramolecular chemistry* that regard the use of calix[n]arene derivatives as a smart coating for Au and AgNPs will be discussed in detail in Chapter 2.

19
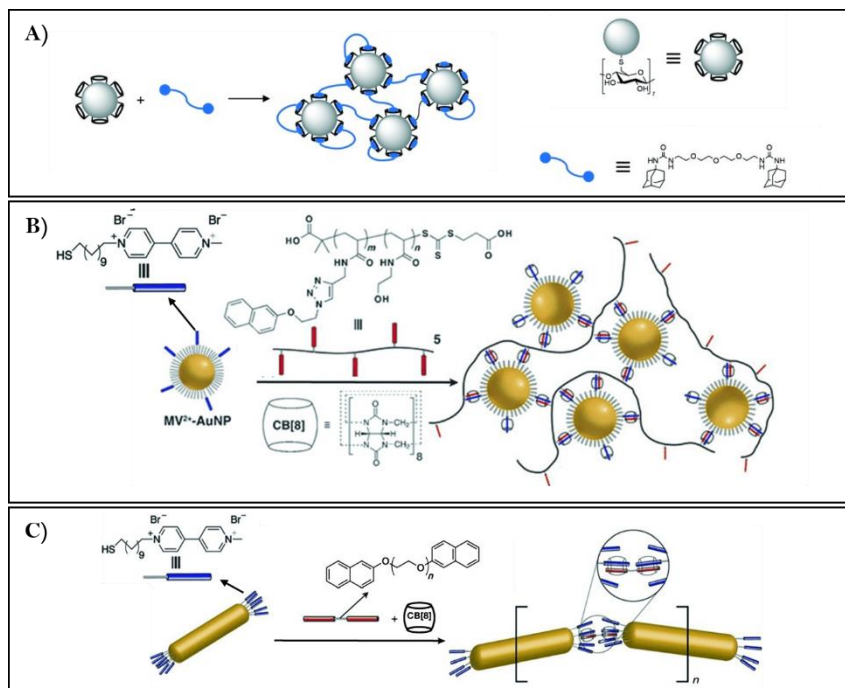
Figure 1.7 *Host-guest supramolecular aggregates. Adapted from A) ref. [22] Copyright © 2006 WILEY-VCH Verlag GmbH & Co. KGaA, Weinheim; B) ref. [30] Copyright © The Royal Society of Chemistry 2011; C) ref. [31] Copyright © The Royal Society of Chemistry 2013.*

1.3 Surface Plasmon Resonance: Fundamentals

The strong development of nanophotonic in recent years has brought considerable attention towards *plasmonic* that is the domain of optics in which the behavior and the properties of the light are considered at the nanometre scale and in which the excitation and the propagation of surface plasmon play a key role.[32]

Surface plasmon resonance (SPR) is one of the most outstanding features of metallic nanostructures, and it consists of a collective oscillation of metal conduction electrons induced by excitation from the electromagnetic field of the light. A good simplification for the theoretical description of the behavior of a metallic NP is to imagine it as an ionic lattice in which the conduction electrons are almost free to move. When a light beam interacts with the NP, the electromagnetic field induces a displacement of the conduction electrons inside the NP,

creating an electric dipole, since a negative charge will be accumulated in one side balanced by a positive charge on the other side (Figure 1.8).[33,34] In the case of a metallic NP with a size much smaller than the wavelength of the interacting photons (quasistatic approximation), the plasmons are non-propagating, and they are called *localized surface plasmons* (LSPs). In other words, the plasmon oscillation is distributed over the whole NP volume.[35–37] In turn, this generated dipole creates an opposite electric field (*near-field*) in order to restore the initial equilibrium positions of the conduction electrons. The restoring force is proportional to the electric dipole, i.e., to the electron displacement induced. The system is very similar to a linear oscillator: the displaced electrons, when the field is removed, will oscillate, and the oscillation frequency is called *resonant frequency*, or in the particular case of surface plasmon, the *plasmonic frequency*.[33] For a metallic NP, this plasmonic frequency is typically in the UV-Vis region. As a result, metallic NPs are characterized by absorption bands in this region of the electromagnetic spectrum.
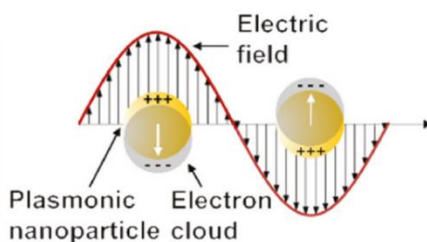
Figure 1.8 Schematic illustration of light interaction with a metallic NP, generating an LSP excitation. Adapted from ref. [34] *Copyright © 2017 Frank Vollmer et al.*

The most studied and exploited metal NPs are those of noble metals (Au, Ag, Cu), which are endowed with remarkable plasmonic properties.[38] NPs of metals with partially occupied d-states are, on the contrary, characterized by an increase of the SPR relaxation frequency, as a consequence of a high probability of the low-frequency interband (IB) transitions.[39–41] The SPR, and thus the relative optical properties, is strongly affected by size, shape, composition of the NPs, and by its dielectric environment, i.e., the nature of the solvent. These factors play a crucial role in the shape, width and position of the band generated by the SPR, called *surface plasmon resonance band* (SPRB or SPB). As regards spherical NPs, it is possible to obtain NPs of proper diameter choosing a suitable methodology. Although in the last years a high number of synthetic methods have been reported,[42–44] the NPs obtained have always a certain size dispersion, inducing a broadening of the absorption band.

Changing the shape of the NPs, the SPRB changes in turn and the most explicit example to explain this phenomenon is represented by nanorods (NRs). In this case, there are two different types of electron oscillation: one along the longitudinal rod axis (giving rise to the *longitudinal surface plasmon resonance band* – LSPRB) and one along the perpendicular transversal rod axis (giving rise to the *transversal surface plasmon resonance band* – TSPRB). Since the restoring force is proportional to the electron displacement, it will be smaller for longitudinal oscillation (LSPRB will fall at longer wavelength) with respect to the transversal one (at the same position of the SPRB of a spherical NP). As a result, two bands are observed (Figure 1.9). The "nanorods" topic will be discussed in more detail in Chapter 3.
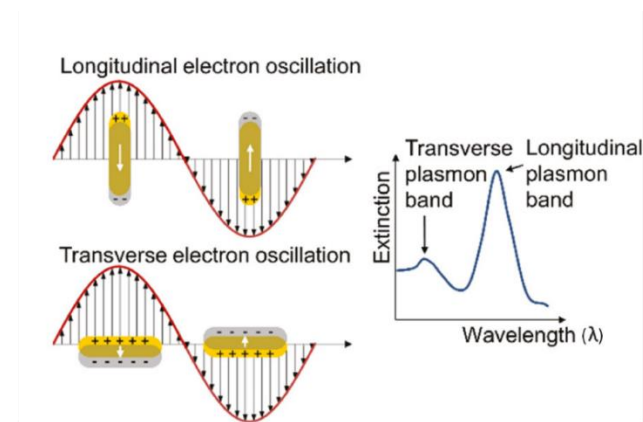
Figure 1.9 *Generation of LSPR and TSPR bands, depending on the different oscillation of the electrons along the longitudinal or the transversal rod-axis. Reproduced from ref. [34] Copyright © 2017 Frank Vollmer et al.*

The shape and geometry of other possible anisotropic NPs (e.g., nanoprisms, nanocubes, nanostars, etc.),[45,46] generally shift the SPRB towards longer wavelength (Figure 1.10).

The most critical effect due to the dielectric environment is the polarisation of this medium during the SPR excitation[47]. The dielectric medium can be the dispersing solvent or the coating of the metallic core in a hybrid material, e.g. SAMs.[37,48,49] The field created by the charge accumulation (due to the conduction electron displacement) induces the polarisation of the dielectric medium at the interface, which partially compensates the charge accumulation. This reduction depends on the dielectric function of the medium: the higher is this last one, the more significant is the polarisation, and so the smaller is the restoring force. Consequently, a shifting of the SPRB at longer wavelengths is observed (Figure 1.11).
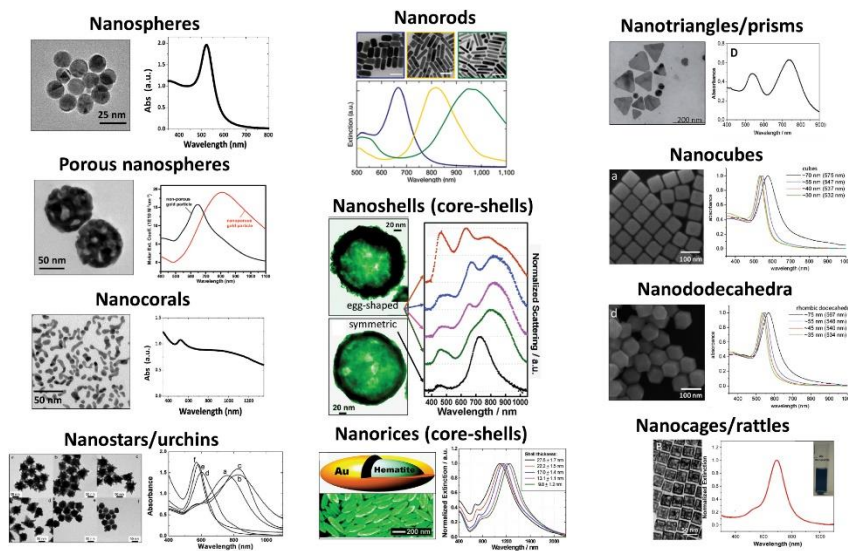
Figure 1.10 *Gold nanostructures with different shapes and corresponding optical extinction or scattering (dark-field) spectra. Reproduced from ref.* [37] *Copyright © 2017 IOP Publishing Ltd.*

Moreover, if plasmonic NPs are close enough, plasmons on different NPs can influence each other, depending on several factors, e.g., particle distance, geometry, coating, etc. These interparticle interactions, in general, induce a red-shift of the SRPB. Consequently, the tuning of the band position can be the result of NPs aggregation (see Chapter 2).
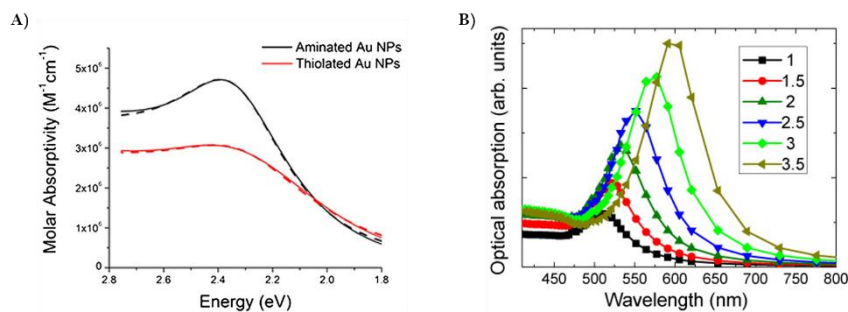
Figure 1.11 *Effects on SPRB of AuNPs of:* ***A)*** *different coatings* [48] *and* ***B)*** *different dielectric medium with different increasing dielectric function (expressed in the legend). A) Reproduced from ref.* [48] *Copyright © 2013 National Academy of Sciences B) Reproduced from ref.* [33] *Copyright © 2012 IOP Publishing Ltd.*

1.4 Applications

The potential applications of metallic NPs range over a wide variety of fields since their plasmonic properties are combined with their facile preparation (also in large scale for gold NPs) and functionalization.

1.4.1   Information and Communication Technology

In the field of *information and communication technology* (ICT), the optical properties of NPs can be especially exploited for light manipulation, that, in this field, is usually achieved by dielectric materials. The advantage of these materials is the good light penetration, but they show the disadvantage of focusing the light beam below the diffraction limit $(\lambda/2)$.[50,51]

In this context, where miniaturization is an important requirement, another problem is the optical information storage: the obtaining of reusable memories and rewritable optical devices is difficult and not easy to develop. The use of plasmonic materials allows new methods in the light manipulation, in the reading and the writing of optical information in sizes smaller than the light wavelength, in the design of subwavelength optical devices as nano-antennas or nano-waveguides.[50,52–56]

1.4.2   Environment and Energy

In the *catalysis* field, metallic NPs exhibit very good catalytic activity themselves[57] (improved upon light illumination to excite the SPR) by catalyzing many chemical reactions. They can also enhance photocatalytic efficiency when coupled to or incorporated in transition metal oxide NPs (e.g., TiO_2). For example, they can be used for the degradation of pollutants.[58]

In the energetic context, a significant challenge is the design and development of powerful *photovoltaic* devices, since these represent the most exploited way to harvest solar energy as renewable energy sources, but their main limitation is their efficiency. The incorporation of metallic NPs in solar cells can potentially increase their efficiency, since, for example, if NPs are placed at the junction interface, they can modify the charge separation, increasing the absorption efficiency.[59–63]

1.4.3   Biomedicine

One of the most explored fields of application of metallic NPs is *biomedicine*. Metal NPs, if properly functionalized, can interact with bio-species as cells, viruses or DNA chains, and they can increase two important parameters in the medical treatment: efficiency and specificity. NPs must be decorated adequately with molecules with an affinity (e.g., complementary functional groups) for the bio-species they have to interact with. This approach is used, for example, for *cell labeling*, for the identification of cancer cells, or *drug delivery*. In the last case, an important feature is a controlled release of the drug, and several examples in the literature report a strategy in which the drug is coated with a polymer with embedded metallic NPs. When the system reaches the unhealthy cell (e.g., tumoral cell), the region is irradiated, inducing the local enhancement of the field and, consequently, local heating, which causes the melting of the designed polymer, releasing the drug in that specific region and at the desired time.

Hyperthermia is another important application in which metallic NPs are involved. The local field enhancement at the surface of the NPs, induced by the conduction electron displacement, when the light reaches the NPs, ensures that local heating is produced. Using properly functionalized metallic NPs, it is possible to have *selective hyperthermia* (slightly increasing of the temperature of ~5-10 °C) only on unhealthy cells bind to the NPs.

1.4.3.1   Surface-Enhanced Raman Scattering (SERS)

An important role in this field is played by anisotropic NPs, in which the symmetry is broken because of the presence of asymmetrical axes. The most considerable example of anisotropic NPs is given by the nanorods (NRs),[64] briefly described in section 1.3.
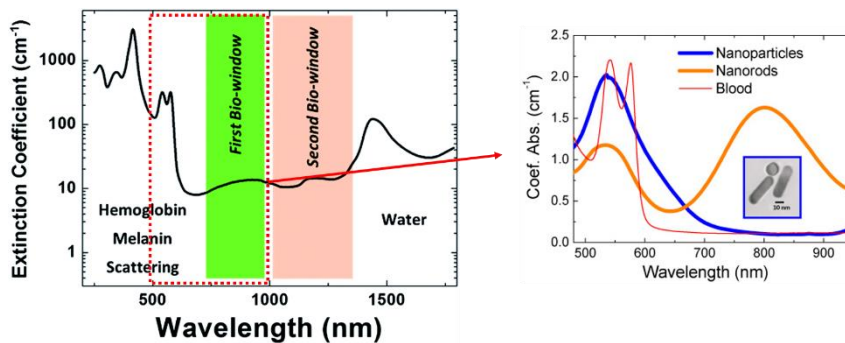

Figure 1.12 *Extinction coefficient of a tissue, in which it is possible to identify the "biological window" (divided into first and second).[65] On the right, comparison of absorption of AuNPs, gold NRs and blood. Adapted from ref. [65] Copyright © The Royal Society of Chemistry 2014 (left) and from ref. [33] Copyright © 2012 IOP Publishing Ltd (right).*

In particular, the LSPRB of NRs with a specific aspect ratio (AR, see Chapter 3) can fall in the NIR region of the electromagnetic spectrum. It is possible to tune the position of this band to reach the "biological window" between 700 and 1300 nm, in which tissue and blood are transparent, or better their absorption is very scarcely intense (Figure 1.12).

The possibility to tune the absorption of light is of high relevance in various sensing techniques. Among them, *surface-enhanced Raman scattering* (SERS)[66–68] is one of the most prominent examples since this spectroscopy is very useful for ultrasensitive detection and identification of a wide range of molecules. The scattering is referred to as those photons that are scattered by a molecule and, as a consequence, a difference of frequencies (because of the different scattered photon frequency) is observed ($\omega_{inc} - \omega_{vib}$). However, the Raman scattering signal is very low in intensity because only a few photons show inelastic scattering. In other words, since the changes in frequency are proportional to the difference in vibrational energy levels of the molecule (ω_{vib}), then this is very small compared to the frequency of the field and so the frequency of the outgoing field ω_R can be approximated to the excitation frequency ω_{inc} ($\omega_{inc} - \omega_{vib} \approx \omega_{inc}$). The coupling of a molecule of interest with a metallic nanostructure can enhance the scattering signal (Figure 1.13).
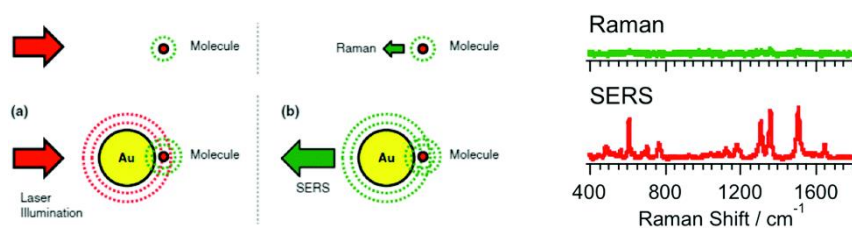
Figure 1.13 *Basic SERS electromagnetic mechanism. The AuNP enhances both (a) the incident laser field and (b) the scattered field, greatly boosting the Raman scattered signal from the nearby molecule. Spectra on the right are referred to an experiment, involving rhodamine 6G and assembled Au nanostars substrate.*[69] *Reproduced from ref.* [69] *Copyright ©The Royal Society of Chemistry 2017.*

There two theories to explain the reason why this Raman signal is enhanced: electromagnetic- or chemical-enhancement (Figure 1.14). First, SERS enhancement takes place when the excitation and outgoing field frequencies are in resonance with the SPR of the NPs, so the localized dipoles are generated, and this leads to an enhancement of the local field around the nanostructure. If the target molecule is spatially close to or in contact with the surface of the nanomaterial, then the enhanced local field caused, in turn, an induced dipole (increasing of the polarizability α) in the molecule. As a result, a Raman enhancement is

obtained. As the field strength decrease as $1/r^2$, the target molecule must be in the range between 0-10 nm from the surface of the plasmonic nanostructure. In the chemical-enhancement mechanism, the molecule has to be chemisorbed on the surface (chemical binding), generating a charge-transfer resonance, because of the electronic interaction between molecular orbital and conduction band of the nanomaterial. If this resonance couple to the vibrational states of the molecule, there will be a reallocation of electron density, changing α and consequently leading to a SERS enhancement.
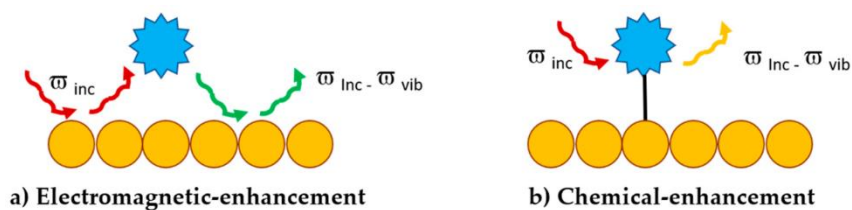
Figure 1.14 [70] *Two mechanisms at the base of the SERS. Used from ref.* [70] *under CC BY 2.0.*

Anisotropic NPs, compared to the spherical one, because of their elongated shape with edges and corners, can generate very highly intense near-fields and, consequently, stronger enhancements. The advantage of this morphology-type NPs is exactly the exploitation of their *intrinsic hotspots*.

As already mentioned, this spectroscopy is very sensitive for the detection of molecules, and recent examples report the possibility of quantitative detection. Khashab and co-workers introduce a new synthetic method to design a core-shell plasmonic NRs for selective and quantitative detection of tumoral cells by SERS.[71]

1.4.3.2   Plasmon-Enhanced Fluorescence (PEF)

Among the sensing techniques, another relevant type of surface-enhanced spectroscopy is represented by the *plasmon-enhanced fluorescence*,[72–75] observed soon after the discovery of SERS. The principles of this spectroscopy open the way to the design and creation of new photostable sensing fluorescent probes, increasing the sensitivity of single-molecule fluorescence, even for weakly emitters, and imaging resolution.[76]

The incident excitation frequency (expresses by excitation power P_0 in Figure 1.15) is absorbed from the metallic NP, inducing the SPR, and from the target molecule, that will reach the excited electronic state. The coupling of the generated local near-field with the emitter could increase the absorption and the emission efficiency, depending on

several factors such as size and shape of the NP or position and orientation of the fluorescent molecule.
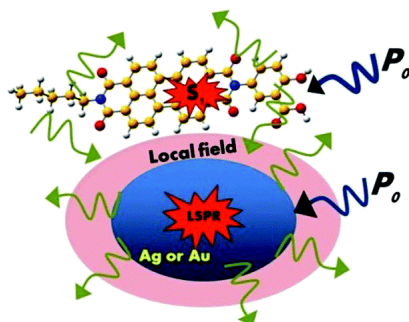
In both cases, PEF and SERS, the plasmonic nanostructure act as a *nanoantenna* to enhance an effect (fluorescence or scattering) of the target molecule. The nature of the organic molecules studied in this work, to be coupled to a surface, are described in the next section 1.5.

1.5 Near-Infrared Materials

Organic compounds that show an absorption or an emission in the near-infrared (NIR) region of the electromagnetic spectrum are usually characterized by an extended conjugated π-system, in which the π-electron are delocalized over the whole structure. The class of trans-polyacetylenes represents the most straightforward π-conjugated system. If they assume a cyclic structure, they are called cyclic π-conjugated polyene, and benzene can be considered as the simplest and smallest molecule of this class.

A way to extend the π-conjugation is to increase the number of annulated benzene rings. These compounds are called *acenes*, and they show a red-shifting of their low-energy absorption band with the extension of the π-system, i.e., the number of aromatic benzene rings. *Rylenes* represent another species derived by naphthalene that can be used as a simple building block. Unfortunately, acenes and rylenes are difficult to obtain, especially increasing the number of rings. The

synthesis of long acenes precursors is proposed and described in detail in Chapter 5.

A more stable and robust class of compounds are rylene diimides and studies have shown that the red-shifting of the absorption band is correlated to the length of π-system.[78] Moreover, this effect is observed even if in the molecular structure a donor-acceptor moiety is inserted or attaching electron-donating groups at the bay position.
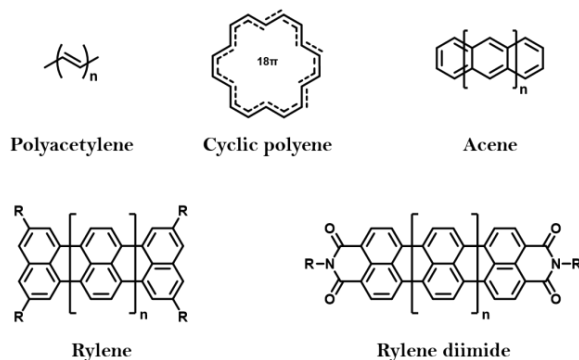
Figure 1.16 *Examples of conjugated π-systems.*

A crescent interest is addressed to the *polymethines* dyes, showing notable properties for various applications, such as bioimaging,[79–81] photovoltaics,[82,83] or non-linear optics.[84] These compounds are characterized by the presence of donor-acceptor substituents containing heteroatom at their endings, and they are categorized as shown in Figure 1.17.
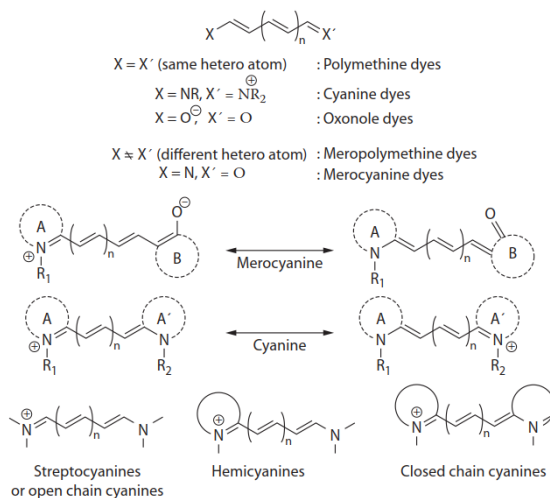
Figure 1.17 *Classes of polymethines.*[85] *Reproduced from ref.* [85] *Copyright © 2013 by Taylor & Francis Group, LLC.*

Highly relevant compounds belonging to this class are *cyanine*, used in industry as a pigment ("cyanin" from Greek means a shade of blue-green), but in the recent years employed as very interesting chromophores, especially in biomedicine, for their moderate absorption and emission in the "biological window". For this reason, to increase the shifting towards higher wavelengths in the NIR region, various modifications to their structure can be done. In particular, it is reported that increasing the length of the sp^2-bridge (i.e. chain length) and the addition of benzene rings could lead to a red-shift (HOMO-LUMO gap decreasing) of the absorption band and to an increase of the emission efficiency.

Another structural modification, in order also to improve the stability and the properties of cyanine dyes, is the enhancement of the rigidity of the chain, introducing alicyclic rings, such as the cyclochloroexanyl or those of oxocarbonic acids (e.g. squaric acid, croconic acid). Synthetic studies on this topic will be discussed in detail Chapter 4.
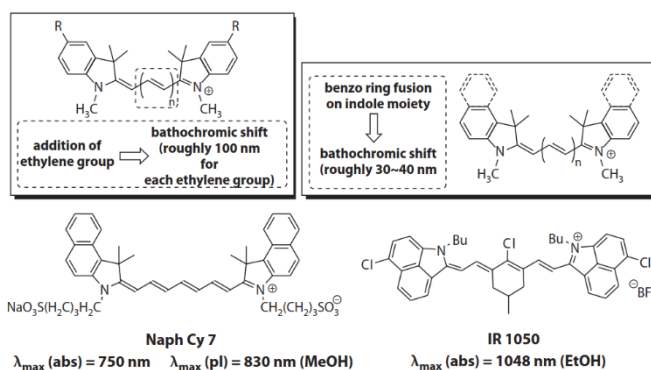
Figure 1.18 Structural modification on the polymethine framework and relative optical effect. Reproduced from ref. [85] Copyright © 2013 by Taylor & Francis Group, LLC.

Although optical properties such as the absorption in the NIR region and the possibility of wavelength tunability are good and suitable for the exploitation of cyanine derivatives as NIR harvesting substances, their emission properties, especially the quantum yield, are very low and negligible. A strategy reported in various examples, to overcome this problem, is to exploit PEF discussed in section 1.4.3.2, which is the coupling of organic dyes to metallic nanostructures, such as NPs, NRs, etc. Several fields of application could benefit from the emission improvement due to this approach, for example in the design of NIR probes for *in vitro* or *in vivo* imaging.[86,87]

References

[1] Z. Jiang, J. Zhao, H. Xie, *Microforming Technology: Theory, Simulation and Practice*, **2017**.

[2] B. Bhattacharyya, *Electrochemical Micromachining for Nanofabrication, MEMS and Nanotechnology*, Elsevier, **2015**.

[3] *Electronic Enclosures, Housings and Packages*, Elsevier, **2019**.

[4] G. Cao, *Nanostructures and Nanomaterials*, **2004**.

[5] S. Badal, R. Delgoda, *Pharmacognosy: Fundamentals, Applications and Strategy*, **2016**.

[6] P. Hyman, in *Adv. Appl. Microbiol.*, Academic Press, **2012**, pp. 55–73.

[7] R. P. Feynman, *A Plenty of Room at the Bottom*, Engineering And Science, **1959**.

[8] R. M. Bakker, H.-K. Yuan, Z. Liu, V. P. Drachev, A. V. Kildishev, V. M. Shalaev, R. H. Pedersen, S. Gresillon, A. Boltasseva, *Appl. Phys. Lett.* **2008**, *92*, 043101.

[9] T. Stedeford, in *Inf. Resour. Toxicol.*, Elsevier, **2009**, pp. 711–716.

[10] M. Loos, *Carbon Nanotube Reinforced Composites: CNT Polymer Science and Technology*, Elsevier Science, **2014**.

[11] G. Caruso, L. Merlo, M. Caffo, *Innovative Brain Tumor Therapy*, Elsevier, **2014**.

[12] M. Feldman, *Nanolithography: The Art of Fabricating Nanoelectronic and Nanophotonic Devices and Systems*, **2013**.

[13] S. W. Hla, G. Meyer, K. H. Rieder, *ChemPhysChem* **2001**, *2*, 361–366.

[14] P. Iqbal, J. A. Preece, P. M. Mendes, in *Supramolecular Chemistry: From Molecules to Nanomaterials*; Eds.: J. W. Steed, P. A. Gale; John Wiley & Sons Ltd: Chichester, UK, **2012**; *8*; 3589–3602.

[15] S. Zhang, in *Encycl. Mater. Sci. Technol.*, Elsevier, **2001**, 5822–5828.

[16] J. W. Steed, D. R. Turner, K. J. Wallace, *Core Concepts in Supramolecular Chemistry and Nanochemistry*, John Wiley, **2007**.

[17] C. J. Bruns, J. F. Stoddart, *Acc. Chem. Res.* **2014**, *47*, 2186–2199.

[18] G. Kickelbick, *Hybrid Materials: Synthesis, Characterization, and Applications*, Wiley, **2007**.

[19]   C. S. Park, R. Colorado, A. C. Jamison, T. R. Lee, in *Ref. Modul. Mater. Sci. Mater. Eng.*, Elsevier, **2016**.

[20]   S. Casalini, C. A. Bortolotti, F. Leonardi, F. Biscarini, *Chem. Soc. Rev.* **2017**, *46*, 40–71.

[21]   P. Gómez-Romero, C. Sanchez, *Functional Hybrid Materials*, Wiley, **2006**.

[22]   A. B. Descalzo, R. Martínez-Máñez, F. Sancenón, K. Hoffmann, K. Rurack, *Angew. Chemie Int. Ed.* **2006**, *45*, 5924–5948.

[23]   G. Schmid, *Nanoparticles From Theory to Application*, Wiley-VCH, **2011**.

[24]   S. Connolly, S. N. Rao, R. Rizza, N. Zaccheroni, D. Fitzmaurice, *Coord. Chem. Rev.* **1999**, *185–186*, 277–295.

[25]   V. Montes-García, J. Pérez-Juste, I. Pastoriza-Santos, L. M. Liz-Marzán, *Chem. - A Eur. J.* **2014**, *20*, 10874–10883.

[26]   P. D. Beer, D. P. Cormode, J. J. Davis, *Chem. Commun.* **2004**, *10*, 414.

[27]   Y. Xie, X. Wang, X. Han, X. Xue, W. Ji, Z. Qi, J. Liu, B. Zhao, Y. Ozaki, *Analyst* **2010**, *135*, 1389.

[28]   A. D. Strickland, C. A. Batt, *Anal. Chem.* **2009**, *81*, 2895–2903.

[29]   O. Crespo-Biel, A. Jukovic, M. Karlsson, D. N. Reinhoudt, J. Huskens, *Isr. J. Chem.* **2005**, *45*, 353–362.

[30]   R. J. Coulston, S. T. Jones, T.-C. Lee, E. A. Appel, O. A. Scherman, *Chem. Commun.* **2011**, *47*, 164–166.

[31]   S. T. Jones, J. M. Zayed, O. A. Scherman, *Nanoscale* **2013**, *5*, 5299.

[32]   S. Enoch, N. Bonod, *Plasmonics: From Basics to Advanced Topics*, Springer Berlin Heidelberg, **2012**.

[33]   M. A. Garcia, *Phys. D Appl. Phys.* **2011**, *44*, 283001.

[34]   J. Xavier, S. Vincent, F. Meder, F. Vollmer, *Nanophotonics* **2018**, *7*, 1–38.

[35]   U. Kreibig, M. Vollmer, *Optical Properties of Metal Clusters*, Springer Berlin Heidelberg, **2013**.

[36]   S. A. Maier, *Plasmonics: Fundamentals and Applications*, Springer US, **2007**.

[37]   V. Amendola, R. Pilot, M. Frasconi, O. M. Maragò, M. A. Iatì, *J. Phys. Condens. Matter* **2017**, *29*, 203002.

[38] K. L. Kelly, E. Coronado, L. L. Zhao, G. C. Schatz, *J. Phys. Chem. B* **2003**, *107*, 668–677.

[39] M. G. Blaber, M. D. Arnold, M. J. Ford, *J. Phys. Condens. Matter* **2010**, *22*, 143201.

[40] M. D. Arnold, M. G. Blaber, *Opt. Express* **2009**, *17*, 3835.

[41] M. B. Cortie, A. M. McDonagh, *Chem. Rev.* **2011**, *111*, 3713–3735.

[42] N. Toropov, T. Vartanyan, in *Compr. Nanosci. Nanotechnol.*, Elsevier, **2019**, pp. 61–88.

[43] F. Hubenthal, *Compr. Nanosci. Technol.* **2016**, *1*, 375–435.

[44] S. E. Lohse, C. J. Murphy, *Chem. Mater.* **2013**, *25*, 1250–1261.

[45] M. Grzelczak, J. Pérez-Juste, P. Mulvaney, L. M. Liz-Marzán, *Chem. Soc. Rev.* **2008**, *37*, 1783-1791.

[46] S. E. Lohse, N. D. Burrows, L. Scarabelli, L. M. Liz-Marzán, C. J. Murphy, *Chem. Mater.* **2014**, *26*, 34-43.

[47] M. M. Miller, A. A. Lazarides, *J. Phys. Chem. B* **2005**, *109*, 21556–21565.

[48] K. O. Aruda, M. Tagliazucchi, C. M. Sweeney, D. C. Hannah, G. C. Schatz, E. A. Weiss, *Proc. Natl. Acad. Sci.* **2013**, *110*, 4212–4217.

[49] M. A. Garcia, J. de la Venta, P. Crespo, J. LLopis, S. Penadés, A. Fernández, A. Hernando, *Phys. Rev. B* **2005**, *72*, 241403.

[50] W. . Steen, *Opt. Laser Technol.* **2000**, *32*, 385.

[51] I. Kaminow, T. Li, A. E. Willner, *Optical Fiber Telecommunications: Components and Subsystems: Sixth Edition*, **2013**.

[52] W. L. Barnes, A. Dereux, T. W. Ebbesen, *Nature* **2003**, *424*, 824–830.

[53] L. Shi, B. Iwan, R. Nicolas, Q. Ripault, J. R. C. Andrade, S. Han, H. Kim, W. Boutu, D. Franz, T. Heidenblut, et al., *Optica* **2017**, *4*, 1038-1043.

[54] J. M. Merlo, N. T. Nesbitt, Y. M. Calm, A. H. Rose, L. D'Imperio, C. Yang, J. R. Naughton, M. J. Burns, K. Kempa, M. J. Naughton, *Sci. Rep.* **2016**, *6*, 31710.

[55] M. Kaniber, K. Schraml, A. Regler, J. Bartl, G. Glashagen, F. Flassig, J. Wierzbowski, J. J. Finley, *Sci. Rep.* **2016**, *6*, 23203.

[56] A. G. Milekhin, S. A. Kuznetsov, I. A. Milekhin, L. L. Sveshnikova, T. A. Duda, E. E. Rodyakina, A. V. Latyshev, V. M. Dzhagan, D. R. T. Zahn, *Beilstein J. Nanotechnol.* **2018**, *9*, 2646–2656.

[57] M. Haruta, M. Daté, *Appl. Catal. A Gen.* **2001**, *222*, 427–437.

[58] M. Xiao, R. Jiang, F. Wang, C. Fang, J. Wang, J. C. Yu, *J. Mater. Chem. A* **2013**, *1*, 5790-5805.

[59] Q. Luo, C. Zhang, X. Deng, H. Zhu, Z. Li, Z. Wang, X. Chen, S. Huang, *ACS Appl. Mater. Interfaces* **2017**, *9*, 34821–34832.

[60] T. V. Pfeiffer, J. Ortiz-Gonzalez, R. Santbergen, H. Tan, A. S. Ott, M. Zeman, A. H. M. Smets, *Energy Procedia* **2014**, *60*, 3–12.

[61] H. R. Stuart, D. G. Hall, *Appl. Phys. Lett.* **1998**, *73*, 3815–3817.

[62] D. Derkacs, S. H. Lim, P. Matheu, W. Mar, E. T. Yu, *Appl. Phys. Lett.* **2006**, *89*, 093103.

[63] J. Xie, K. Shi, K. Cai, D. Zhang, J. Y. Wang, J. Pei, D. Zhao, *Chem. Sci.* **2016**, *7*, 499-504.

[64] N. D. Burrows, A. M. Vartanian, N. S. Abadeer, E. M. Grzincic, L. M. Jacob, W. Lin, J. Li, J. M. Dennison, J. G. Hinman, C. J. Murphy, *J. Phys. Chem. Lett.* **2016**, *7*, 632–641.

[65] D. Jaque, L. Martínez Maestro, B. del Rosal, P. Haro-Gonzalez, A. Benayas, J. L. Plaza, E. Martín Rodríguez, J. García Solé, *Nanoscale* **2014**, *6*, 9494–9530.

[66] M. Fleischmann, P. J. Hendra, A. J. McQuillan, *Chem. Phys. Lett.* **1974**, *26*, 163–166.

[67] M. G. Albrecht, J. A. Creighton, *J. Am. Chem. Soc.* **1977**, *99*, 5215-5217.

[68] D. L. Jeanmaire, R. P. Van Duyne, *J. Electroanal. Chem. Interfacial Electrochem.* **1977**, *84*, 1–20.

[69] J. Reguera, J. Langer, D. Jiménez de Aberasturi, L. M. Liz-Marzán, *Chem. Soc. Rev.* **2017**, *46*, 3866–3885.

[70] C. Kohout, C. Santi, L. Polito, *Int. J. Mol. Sci.* **2018**, *19*, 3385-3915.

[71] Y. Zhang, P. Yang, M. A. Habeeb Muhammed, S. K. Alsaiari, B. Moosa, A. Almalik, A. Kumar, E. Ringe, N. M. Khashab, *ACS Appl. Mater. Interfaces* **2017**, *9*, 37597–37605.

[72] A. M. Glass, P. F. Liao, J. G. Bergman, D. H. Olson, *Opt. Lett.* **1980**, *5*, 368-370.

[73] J. Gersten, A. Nitzan, *J. Chem. Phys.* **1981**, *75*, 1139–1152.

[74] A. Wokaun, H. -P. Lutz, A. P. King, U. P. Wild, R. R. Ernst, *J. Chem. Phys.* **1983**, *79*, 509–514.

[75] M. Moskovits, *Rev. Mod. Phys.* **1985**, *57*, 783–826.

[76] J. D. Flynn, B. L. Haas, J. S. Biteen, *J. Phys. Chem. C* **2016**, *120*, 20512–20517.

[77] J.-F. Li, C.-Y. Li, R. F. Aroca, *Chem. Soc. Rev.* **2017**, *46*, 3962–3979.

[78] N. G. Pschirer, C. Kohl, F. Nolde, J. Qu, K. Müllen, *Angew. Chemie - Int. Ed.* **2006**, *45*, 1401–1404.

[79] S. Zhu, B. C. Yung, S. Chandra, G. Niu, A. L. Antaris, X. Chen, *Theranostics* **2018**, *8*, 4141–4151.

[80] S. Luo, E. Zhang, Y. Su, T. Cheng, C. Shi, *Biomaterials* **2011**, *32*, 7127–7138.

[81] L. Prodi, S. Biffi, L. Petrizza, C. Garrovo, E. Rampazzo, L. Andolfi, P. Giustetto, I. Nikolov, G. Kurdi, M. Danailov, et al., *Int. J. Nanomedicine* **2016**, *11*, 4865–4874.

[82] D. Saccone, S. Galliano, N. Barbero, P. Quagliotto, G. Viscardi, C. Barolo, *European J. Org. Chem.* **2016**, 2244–2259.

[83] E. Seliverstova, N. Ibrayev, *IOP Conf. Ser. Mater. Sci. Eng.* **2018**, *289*, 012011.

[84] R. A. Ganeev, R. I. Tugushev, A. A. Ishchenko, N. A. Derevyanko, A. I. Ryasnyanskii, T. Usmanov, *Opt. Spectrosc.* **2003**, *95*, 435–441.

[85] Z. Y. Wang, *Near-Infrared Organic Materials and Emerging Applications*, CRC Press, **2013**.

[86] J. Yu, X. Zhang, X. Hao, X. Zhang, M. Zhou, C. S. Lee, X. Chen, *Biomaterials* **2014**, *35*, 3356–3364.

[87] C. Niu, Q. Song, G. He, N. Na, J. Ouyang, *Anal. Chem.* **2016**, *88*, 11062–11069.

CHAPTER 2
Synthesis and Aggregation of Calixarenes-decorated Noble Metal Nanoparticles

2.1 Introduction

Colloidal noble metal nanoparticles (NPs) for centuries have been of crucial interest in different scientific fields because of their unique plasmonic optical properties. Noble metal nanomaterials are indeed extensively used because they are characterized by an SPR band in the visible region of the electromagnetic spectrum. The exploitation of these plasmonic properties is strictly related to the synthesis and the manipulation of NPs in a controlled way. Varying the size, nature, and geometry of NPs, it is possible to red-shift the absorption in the NIR region, creating nanomaterials suitable for several applications. Good and promising results can be obtained taking advantage of the near-field effects (see Chapter 1) present in mono-dimensional arrays of aligned NPs. In this way, it becomes possible to design the so-called *plasmonic waveguides*,[1] in which the light can be transported below the diffraction limit, thus allowing the design and the creation of optoelectronic devices. Indeed, they are also called *low-loss* nanoscale plasmonic waveguides, in contrast to the macroscale waveguides (e.g. glass fibers), in which the propagation is based on classical optics.[2] Recently, Roller and co-workers have developed this type of nano-waveguides, creating hetero-trimers of gold and silver NPs (Au-Ag-Au NPs).[3] Exploiting this designed mono-dimensional aggregates, they demonstrated the possibility of having an energy-transfer between NPs through the near-field interactions. The smaller AgNP between the two larger AuNPs acts as a virtual transmitter (the AgNP is characterized by a plasmon resonance energy higher than that of the AuNP). To take advantage of this phenomenon a precise control over the spatial arrangement of the NPs is required. To this aim, the research group of Roller proposed the exploitation of a *DNA origami* nanotechnology (Figure 2.1), which is the decoration of the NPs with short DNA linkers that promote a specific binding of these nanomaterials on the DNA-base fiber.
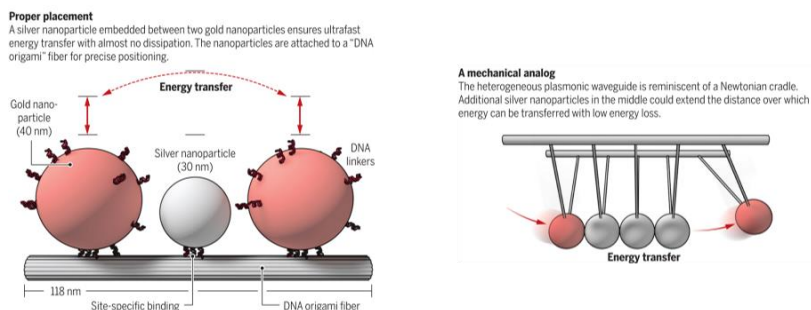
Figure 2.1 *Schematic representation of the low-loss nano-waveguide designed by Roller. Reproduced from ref. [2] and used under CC BY-NC 4.0 license.*

The supramolecular chemistry can offer the right tools for the creation of controlled aggregates of NPs. In general, an increasing interest is addressed to the introduction on the NPs' surface of synthetic molecular receptors in order to combine their complexing abilities with the optical properties of the nanomaterial (e.g., surface plasmons) and, therefore, to realize *functional hybrid nanomaterials* (see section 1.2 in Chapter 1).[4–6] This type of approach has been defined by Fitzmaurice and co-workers as *hetero-supramolecular chemistry*,[7] because it benefits from the principles and methods of supramolecular chemistry to improve the properties of these nanostructures.[8,9] The complexation processes, driven by *host-guest* interactions, where the *host* species is a synthetic molecular receptor and the *guest* is a complementary species to be recognized, can, in fact, also occur at the level of the organic monolayer stabilizing the nanostructures. This process can be therefore used to control their aggregation.

In this last decade, several examples have been reported in the literature, where different types of hosts, such as cyclodextrins, cucurbit[n]urils, and pillar[n]arenes (see section 1.2 in Chapter 1) have been used as smart organic coating of noble metal NPs. Different strategies can be employed in order to have control over the complexation process and, thus, on the nanostructures' aggregation. Among these strategies, one involves the functionalization of the metal surface with host-containing organic monolayers and using a bifunctional guest as the aggregator (*Strategy I* in Figure 2.2). On the contrary, a second possibility consists in the grafting of the guest on the nanostructure surface and employing a bifunctional host as the aggregator (*Strategy II* in Figure 2.2). Finally, it is possible to functionalize the nanomaterial differently with the host and with a complementary guest and to exploit their interaction to obtain aggregation (*Strategy III* in Figure 2.2).
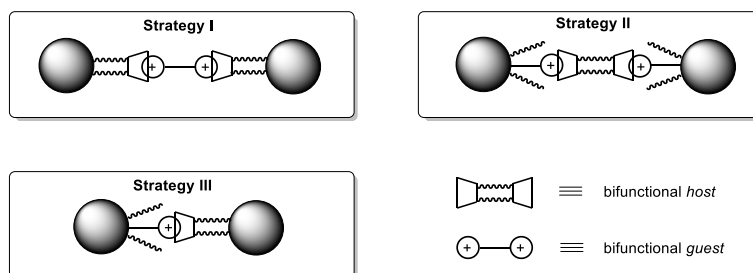
Figure 2.2 *Schematic representation of the different strategies of supramolecular aggregation exploiting host-guest interactions.*

In this Chapter, the use of calix[n]arene derivatives as multivalent hosts for the decoration or the aggregation of noble metal NPs will be

discussed. Before the discussion of the results obtained, in the following paragraph is presented a brief review on the use of calix[n]arene derivatives as smart coatings for noble metal NPs.

2.1.1 Calixarenes and Noble Metal NPs

In 2005 Pochini and co-workers published one of the first examples of calixarene-capped AuNPs employed for host-guest studies.[10] The designed calixarene derivatives were properly functionalized thiolated 1,3-dialkoxycalix[4]arenes, which were known to form endo-cavity inclusion complexes with N-alkyl pyridinium ion pairs in weakly polar solvents,[11,12] and they demonstrated the enhancement of the host binding affinity of the calix[4]arene derivatives supported on the NPs with respect to the corresponding unsupported host. The two ω-alkanethiol chains at the lower rim of the calix[4]arene (derivatives **2a** and **2b** in Scheme 2.1) allow the grafting host on the gold surface. In this case, the thiolated calixarene host has been inserted on the NPs surface through a ligand-exchange reaction carried out on 2nm dodecanethiol-capped AuNPs.
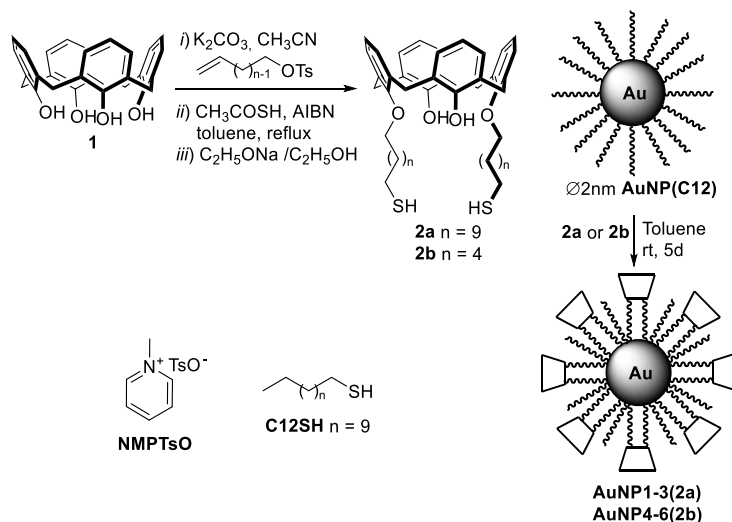
Scheme 2.1 *Synthesis of the bidentate calix[4]aren **2a** and **2b** and schematic representation of the synthesis of **AuNP1-6** with a mixed organic monolayer containing **2a** or **2b** and C12SH in different molar ratios.*

The authors synthesized a series of NPs (**AuNP1-6** in Scheme 2.1) characterized by a different ratio between host **2a** or **2b** and the dodecanthiol chain (C12SH). The binding ability of these decorated AuNPs was evaluated versus N-methyl pyridinium tosylate (NMPTsO). The results showed a remarkable enhancement up to twice

the value of the log$K$ with respect to the measured one for the unsupported host. In particular, this enhancement was more marked for the derivative **2a** (having longer C11 ω-thiolate alkyl chains), suggesting the importance of the distance of the cavity from the surface.

The organic monolayer in SAMs or NPs has crucial importance. It affects, depending on its nature, the nanostructure stability for steric reasons, but it could also induce hydrophilicity or hydrophobicity to the entire nanostructure tuning the solubility of the NPs in solvents of different polarity. For example, extremely stable, water-soluble calix[4]arene-decorated AuNPs were reported.[13] Even in this case, these nanostructures are capable of specific molecular recognition of pyridinium ions, but in aqueous solutions. To make the nanoparticles soluble in aqueous solution, some thioalkylated oligoethylene glycol chains (**3**) were used as the organic monolayer, in combination with the calix[4]arene derivative **2a** in different molar ratios (Figure 2.3). Following the *Strategy II*, depicted in Figure 2.2, the recognition abilities of this functional water-soluble AuNPs were demonstrated using two different inorganic substrates, opportunely functionalized with *N*-(11-mercaptoundecyl)pyridinium tosylate (**4**) as the guest. In the first case, a SAM of ligands **4** on Au flat surface was employed, while in the second one silica molecular sieves were loaded with the same ligand **4**. In both the experiments, the binding properties of the host cavity were measured, showing good efficiency even in this very polar media.
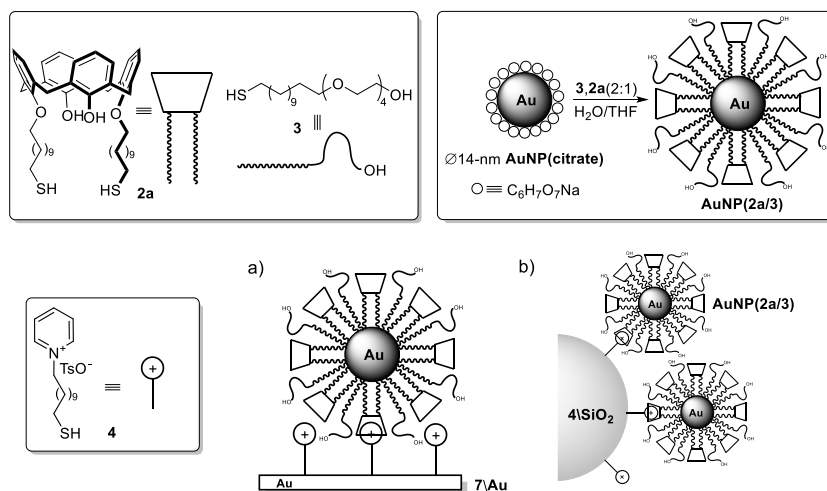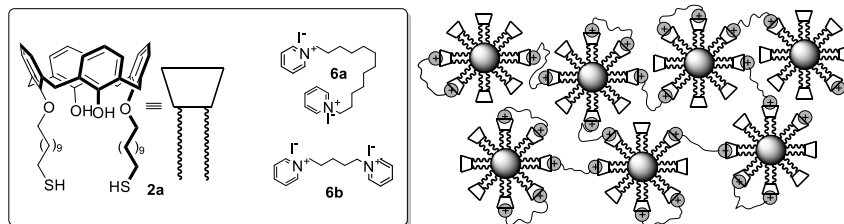
Figure 2.3 *Schematic representation of the synthesis of water-soluble calix[4]arene-decorated AuNPs (top, right) and two different experiments to evaluate binding affinities of **AuNP(2a/3)** and guest(**4**)-decorated a)Au surface or b) SiO₂ molecular sieve beads in aqueous solution.*

Even if the preparation and the study of AgNPs endowed with a functional organic monolayer is still under active investigation by the scientific community, some examples regarding their preparation are present in the literature. Guerrini and co-workers developed a sensor using a self-assembled monolayer of the dithiocarbamate calix[4]arene **5** on AgNPs (Figure 2.4).[14] They studied the complexation of pyrene molecules exploiting the SERS effect, investigating the use of different methods and different reducing agents. Moreover, they showed that a good efficiency of the sensor is correlated to an optimum coverage of the surface with the receptor. Only in these typical conditions, the host can assume an optimum conformation able to complex the guest molecule (Figure 2.4).
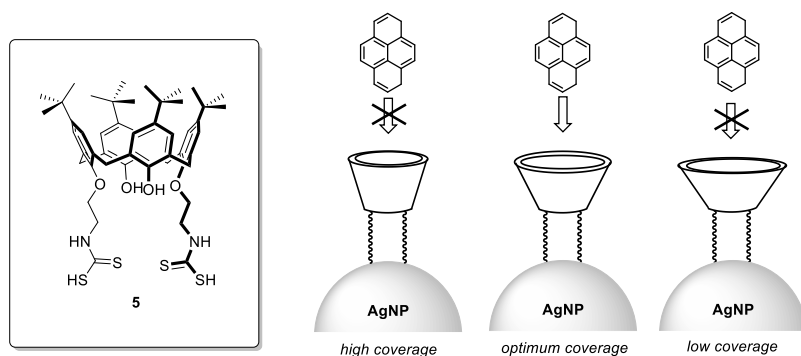

Figure 2.4 *Dithiocarbamate calix[4]arene derivative **5** and schematic representation of its structure at different surface coverages in the complexation of pyrene guests.*

Concerning the self-assembly of the decorated-NPs, in order to control and to study the aggregation, the *Strategy I* is the most extensively used (Figure 2.2). Ciesa et al. have functionalized lipophilic ~6nm AuNPs with calix[4]arene **2a** through a ligand-exchange reaction starting from AuNPs electrostatically stabilized with tetraoctylammonium bromide (TOABr).[15] The guest-induced self-assembly process between these **2a@AuNPs** has been studied using different bifunctional pyridinium guests (**6a** and **6b**) that can act as a "supramolecular bridging linker" (Figure 2.5). The size and the solubility of the aggregates strongly depend on the length and rigidity of the linker. In particular, they demonstrated that the long and flexible guest **6a** gives rise to super-aggregates of NPs, still soluble in common low polar organic solvents.

43

Figure 2.5 *Schematic representation of the guest-driven aggregation of the **2a@AuNPs**.*

In more recent studies, the same research group reported an interesting example in which the same **2a@AuNPs** were employed in the fabrication of hybrid systems based on the reversible assembly on a Si(100) surface.[16] Together with the derivative **2a**, they employed a tris(*N*-phenylureido)-calix[6]arene **7**, bearing three ω-undecenyl chains on its lower rim. Indeed, in a previous study, Zanoni and co-workers reported the surface grafting of a calix[4]arene derivative on Si(100) surface through extra-mild photochemical activation via visible light of C=C terminating anchoring chains.[17] The assembly was mediated by a series of hierarchical and reversible complexation steps involving a bifunctional guest **8** (Figure 2.6). This supramolecular linker **8** presents two binding sites separated by a flexible C12 chain: a pyridinium unit, as good guest for the calix[4]arene **2a**, and a redox-active bis-pyridinium unit, able to form a stable inclusion complex with calix[6]arene derivatives.[18] Upon the application of an electrochemical stimulus, it is possible to obtain a controlled release of the nanoparticles **2a@AuNP** from the silicon surface, since the reduced unit has a very weak affinity towards the host **7**.
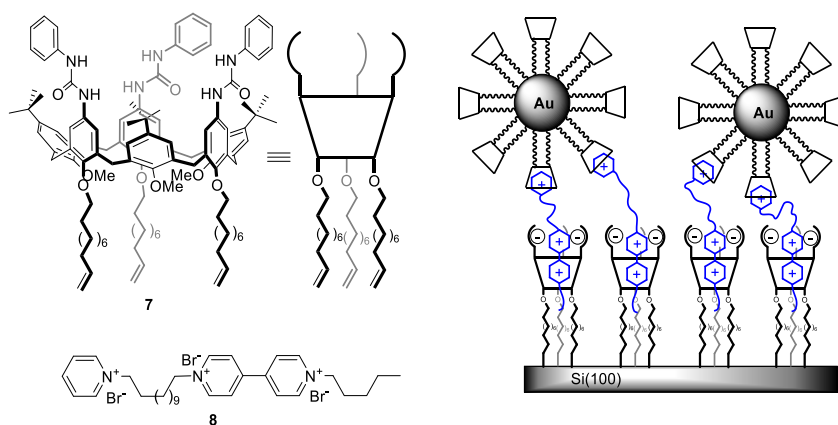
Figure 2.6 *Schematic representation of the designed calix[6]arene derivative **7**, used for the photochemical grafting on Si(100) surface and schematic representation of the aggregation with **2a@AuNPs** using the bifunctional linker **8**.*

2.2 Result and Discussion

In the first part of this section, the synthesis of a series of lipophilic noble metal NPs of gold, silver, and copper will be presented. Successively, a particular type of Host/Guest aggregation strategy, indicated in Figure 2.2 as *Strategy II*, will be used to promote a controlled aggregation of the synthesised NPs by exploiting the host/guest interactions between an *N*-alkyl pyridinium-based guest interdigitated in the lipophilic monolayer of the NPs and a bifunctional calix[4]arene host. In the last part of the section, some examples of aggregation studies using the Host/Guest *Strategy I* will be introduced using calix[n]arene-decorated AgNPs and bispyridinium-based bifunctional guests.

Several examples are reported in the literature concerning the functionalization of noble metal NPs with calix[4]arene derivatives. On the contrary, the use of calix[6]arene derivative is still less explored. This is mainly due to the difficulty in the synthesis of these derivatives and in the possibility to obtain stable and soluble NPs decorated with these macrocycles. In section 2.2.3.1, it will be discussed the synthesis of a calix[6]arene derivative, characterized by the presence of three ω-thiolated C11 chains at the lower rim of the macrocycle, allowing its grafting on the surface of noble metal NPs.

### 2.2.1 Synthesis of Noble Metal Nanoparticles

The lipophilic nanoparticles of gold, silver, and copper used in the studies reported in this chapter were prepared using *wet chemical* methods. These NPs can be thoroughly dried and re-dispersed in an organic solution without observing irreversible aggregation processes. This property makes them excellent precursors for further functionalization and applications.

In the last decades, many improvements have been accomplished regarding the synthetic methodologies used for the preparation of noble metal nanoparticles. These improvements were mainly aimed to have better control of crucial parameters affecting the dimensionality of the nanoparticles (size and monodispersity). Among the various methods of synthesis available, the most common one involves the chemical reduction, in solution, of a metal salt precursor with a reducing agent. A stabilizing agent is then used to passivate the surface of the growing nanostructures and to prevent their aggregation once they have been

formed. The nature of this stabilizing agent also determines the solubility properties of the resulting NPs.

The lipophilic gold nanoparticles (AuNPs) used in the subsequent aggregation studies were all prepared from batch toluene solutions of underivatized ~5nm AuNPs stabilized with tetraoctylammonium bromide (TOABr). These very stable colloidal solutions, which can survive without significant deterioration for periods of at least one year, were synthesized using the two-phase protocol reported by Schiffrin et al. in 1998.[19] This method involves the use of tetrachloroauric acid (HAuCl$_4$) as the metal precursor. In brief, the anion ([AuCl$_4$]-) is transferred from the aqueous phase to the organic phase (typically toluene) through the TOABr, which acts as a phase-transfer catalyst. Successively, the Au(III) precursor is reduced to Au(0) thanks to the addition of a water solution of sodium borohydride (NaBH$_4$). The TOABr salt still present in the organic solution also plays the fundamental role of electrostatically stabilizer of the newly formed AuNPs.

The TOABr monolayer of these AuNPs can be then easily replaced by alkyl thiol-based ligands, which are well-known to form stable covalent interactions with the gold surface. For example, a toluene solution of ~5nm **TOABr@AuNPs** was treated overnight at r.t. with a large stoichiometric excess of 1-dodecanethiol (C12SH), to obtain the dodecanthiol-capped AuNPs indicated in Scheme 2.2 as **C12S@AuNPs**. The purification of the resulting functionalized AuNPs from the unbound excess of alkyl thiol and replaced tetralkylammonium salt was achieved for precipitation by adding ethanol to the reaction mixture in toluene (in the ratio of 2:1). After an ultracentrifugation cycle, the sedimented AuNPs could be dispersed in most of the weakly polar solvents such as CH$_2$Cl$_2$, CHCl$_3$, and toluene. The purified **C12S@AuNPs** were characterized by UV-Vis (see Figure 2.12, black line) and TEM measurements (see Figure 2.17a).
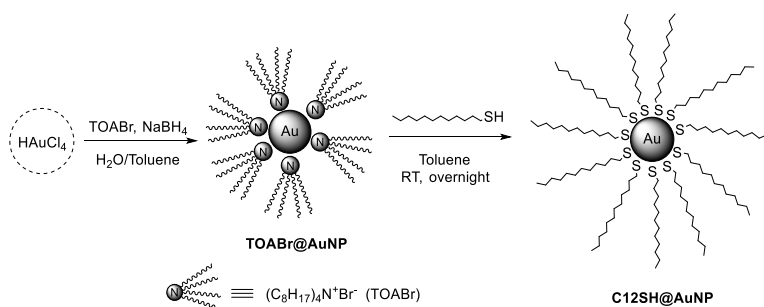
Scheme 2.2 *Synthesis of* **TOABr@AuNPs** *and* **C12SH@AuNPs** *after the ligand-exchange reaction.*

To prepare the batch solutions of lipophilic dodecanthiol-capped AgNPs (**C12S@AgNPs**) to be used in the subsequent aggregation studies, we initially employed a modification[20] of the two-phase Brust-Schiffrin procedure originally reported for the synthesis of AuNPs.[21] With this method, the reducing agent ($NaBH_4$) is added to a toluene organic phase in which the alkylthiol stabilizing group is already present along with the silver precursor ($AgNO_3$). However, the AgNPs synthesized following this procedure are characterized by a smaller mean diameter (~1-3 nm) than the AuNPs synthesized with Schiffrin's methodology. Moreover, the Brust-Schiffrin method does not allow the use of thiol ligands with specific functional groups (esters, acids, imines, aldehydes or ketones), because they can react, since the presence of the sodium borohydride $NaBH_4$ as reducing agent.

An alternative method for the synthesis of ~4nm alkyl thiol-capped AgNPs has recently been developed.[22] This method was adapted from a previous one, reported by Wang et al. in 2008 [23] in which the synthesis of monodisperse AuNPs and AgNPs covered with dodecylamine ($C12NH_2$) is accomplished in a biphasic system. The main difference with the Brust-Schiffrin method is the absence of a phase-transfer catalyst, although the synthesis takes place in a two-phase system (water/cyclohexane), and the use of formaldehyde as the reducing agent in place of $NaBH_4$. The formaldehyde is transferred from the aqueous phase into the organic one through the reaction with the dodecylamine. The formed reducing intermediate (RCH_2NHCH_2OH) allows the reduction of the Ag(I) ions (from the $AgNO_3$ precursor salt in the aqueous solution) to Ag(0), obtaining AgNPs stabilized by a dodecylamine organic monolayer in cyclohexane (**C12NH₂@AgNPs** in Figure 2.7).
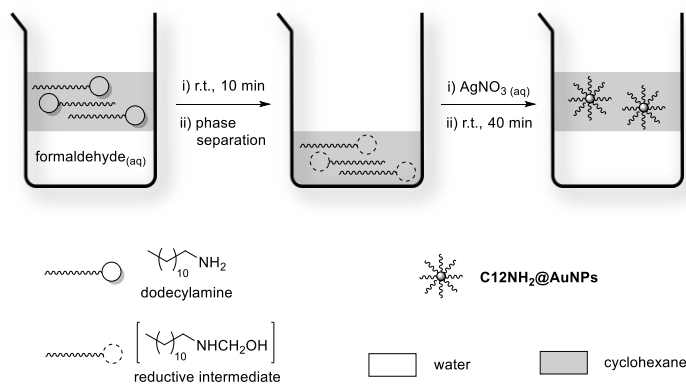
Figure 2.7 *Schematic synthesis of* **C12NH₂@AgNPs**.

According to the modification of this method, in a second step, the resulting AgNPs undergo an exchange reaction with the thiol chains (e.g., C12SH or C8SH), replacing the weak amine ligands. The purification of the exchanged AgNPs was accomplished in a similar way to the AuNPs previously described. The precipitation of the AgNPs was induced by the addition of an aliquot of ethanol to the cyclohexane phase, followed by an ultracentrifugation step to obtain **C12S@AgNPs,** readily dispersible in most of the weak polar solvents, such as CH_2Cl_2 or toluene. The purified **C12S@AgNPs** were characterized by UV-Vis measurements (see Figure 2.24).

The synthetic methods previously reported for the preparation of AuNPs and AgNPs cannot be adapted to the synthesis of copper nanoparticles (CuNPs). This metal is indeed easily oxidizable and thus not very stable in its metallic colloidal state as the precursor for the synthesis of lipophilic CuNPs. Wei et al. reported the first method used for the preparation of lipophilic CuNPs.[24] This procedure, based on the Brust-Schiffrin method, involves the use of TOABr in an inert atmosphere to transfer the anion $[CuBr_4]^{2-}$ from the aqueous to the organic phase. This precursor was obtained from an ionic exchange between $CuCl_2$ and KBr in water. As for the protocol used for AuNPs and AgNPs, in this case, the addition of 1-dodecanthiol takes place before the addition of the aqueous solution of $NaBH_4$, which leads to the reduction of Cu(II) to Cu(0). However, the application of this published method for the synthesis of lipophilic **C12S@CuNPs** to be used in our aggregation studies did not lead to successful results, mainly because of the formation of high polydisperse and unstable colloids. We thus moved to a very effective alternative method based on the thermal decomposition of a copper(II) salt in the presence of oleylamine (OAM).[25] The reaction was carried out at 155 °C in an inert atmosphere in diphenyl ether by using copper (II) acetylacetonate $[Cu(acac)_2]$ as the precursor salt, OAM as the solvent and surfactant, and 1,2-tetradecanediol (1,2-TDD) as the reducing agent (Scheme 2.3).
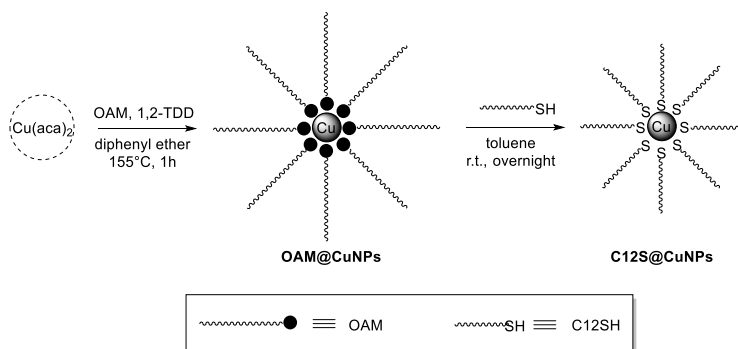
Scheme 2.3 *Synthesis of* **C12S@CuNPs** *by thermal decomposition method.*

The purification of the resulting ~9nm CuNPs (**OAM@CuNPs**) was carried out following the procedure previously reported for the Au and AgNPs, which is precipitation induced by the addition of ethanol followed by ultracentrifugation to recover the sediment of the CuNPs. Since these CuNPs are very sensitive to oxidation, they were immediately subjected to an exchange reaction with dodecanthiol. The ligand exchange was accomplished by mixing the alkylthiol with the solution of **OAM@CuNPs** in CH_2Cl_2. Once again, the purification of the exchanged dodecanthiol-capped CuNPs was carried out with the usual precipitation/ultracentrifugation steps. The sediment of pure and monodisperse **C12S@CuNPs** becomes readily dispersible in most of the weak polar solvents, such as CH_2Cl_2 or toluene. The purified **C12S@CuNPs** were characterized by UV-Vis measurements. In Figure 2.8 were reported the UV-Vis spectra in toluene with the SPB centered at 608 nm.
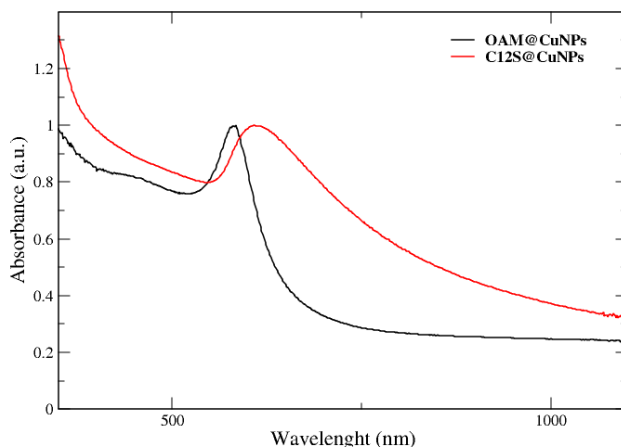

Figure 2.8 *UV-Vis spectra of exchanged CuNPs in toluene.*

The broadness of the plasmon band of the exchanged **C12S@CuNPs** could derive either to a high size dispersion or to aggregation in toluene. Nevertheless, TEM measurements (not shown) carried out on the sample of **2a|C12S@CuNPs** evidenced a rather size-monodispersed sample.

2.2.2   Aggregation studies: Strategy *(II)*

In this section, it will be discussed the aggregation studies carried out on the series of previously prepared NPs by exploiting the Host/Guest strategy *II* (Figure 2.2b). With the aim to gain better control on the extent of aggregation, we considered a slightly different aggregation

strategy based on the already reported bilayer surfactant assemblies that consist of the formation of a secondary interdigitated monolayer in C12SH-capped NPs.[26–29] The *N*-octyl pyridinium iodide (**NOPI**) was identified as the surfactant (Figure 2.9). Its long octyl chain can potentially interdigitate in the organic layer of C12SH-capped NPs. In our intentions, this interdigitation should be driven by non-specific interactions between the methylene groups of the alkyl chain of the **NOPI** with the same groups present in the alkylthiol ligand covering the NPs. The aggregation process between the NPs would be then promoted by the complexation of the charged "head" of these **NOPI** guests by the calix[4]arene-based bifunctional host **11** (Figure 2.9). This host is indeed characterized by the presence of two preorganized electron-rich aromatic cavities. These two units are linked together by two bridging C6 alkyl chains in the 1,3 alternated positions of the phenolic units of both macrocycles. The high affinity of the pyridinium moiety of **NOPI** for the π-rich aromatic cavity of the bis-calix[4]arene derivative **11** has been already reported.[30]
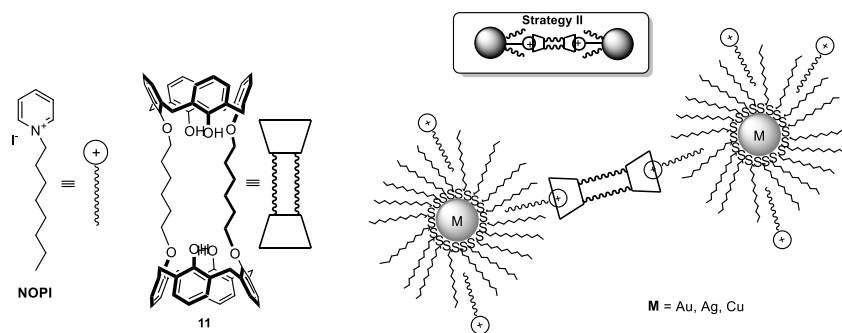
Figure 2.9 *Schematic representation of Strategy II, using **NOPI** and **11**. The interdigitation of the alkyl chain of the guest into the C12SH monolayer of the NPs allows the complexation of the charged "head" by the bis-calix[4]arene host **11**.*

2.2.2.1 Synthesis of guest and bifunctional host aggregator

The *N*-octyl pyridinium iodide salt (**NOPI**) was synthesized through a nucleophilic substitution reaction between pyridine and 1-iodooctane in CH_3CN at reflux to give the salt in 80% yield (Scheme 2.4). As regards the bis-calix[4]arene derivative **11**, Beer et al. synthesized similar difunctional hosts in low overall yields using a long multiple-step synthesis.[31,32] Our bifunctional host was instead synthesized adopting a one-pot strategy in which two building blocks, the calix[4]arene derivative **10** and the bis-electrophile alkylating agent **9** were reacted together in the presence of a base.[30] This strategy allows a higher control over the possible formation of oligomeric species. In brief, the reaction was carried out refluxing in CH_3CN compounds **10** and **9** in a 1:2 stoichiometric ratio in the presence of K_2CO_3 as the base. The

different acidity of the phenolic -OH groups allows the regioselective introduction of the alkyl chains and a correct stoichiometric ratio between **10** and the alkylating agent allows the introduction of the desired number of bridges.
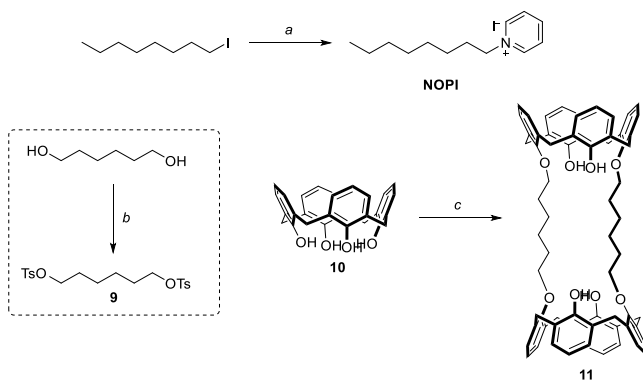
Scheme 2.4 *Synthesis of* **NOPI** *and bis-functional host* **11**. *Reagents and conditions: a) pyridine, CH₃CN, reflux, 48h, 80%; b) TsCl, Et₃N, CH₂Cl₂, rt, overnight, 86%; c)* **9**, *K₂CO₃, CH₃CN, reflux, 4 days, 11%.*
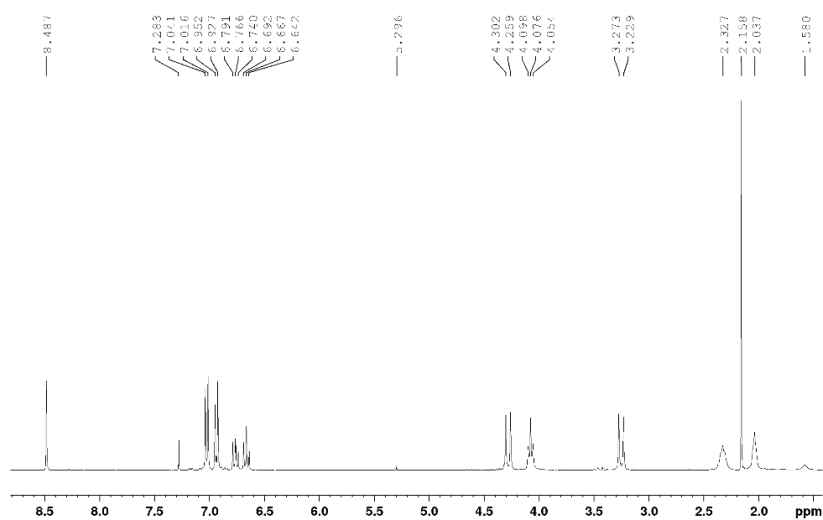
Figure 2.10 *¹H NMR (CDCl₃, 300MHz) of bis-calix[4]arene derivative* **11**.

In the ¹H NMR of **11** in CDCl₃ (Figure 2.10), the identity of the bis-calix[4]arene is confirmed by the high symmetry in the pattern of the signals. In particular, the occurred alkylation in the 1,3 positions of the two macrocycles is evidenced by the presence of some diagnostic signals, such as the singlet for 4 protons at 8.47 ppm relative to the two -OH group at the lower rim of each cavity, the typical pattern of two triplets and two doublets in the aromatic region, which is relative to the 24 protons of the macrocycles aromatic rings, and the triplet centered

at 4.06 ppm that corresponds to the four methylene groups in α-position with respect to the four alkylated aromatic rings. The alkylation ensures that each calix[4]arene macrocycle is in a *cone* conformation. Indeed, two doublets, with geminal coupling, are visible in the spectrum at 4.26 and 3.23 ppm. These two signals are diagnostic for the cone conformation because of two diasterotopic protons of each methylene bridge between the aromatic rings. The blocking of the calix[4]arene macrocycle in the cone conformation is a fundamental requisite for **11** because, in this conformation, the receptor presents a well-defined and π-rich aromatic cavities capable to complex, in low polarity solvents, *N*-alkyl pyridinium-based guest with relatively high binding constants.[30]

### 2.2.2.2   Synthesis of the NOPI-decorated NPs

The samples of the noble metal NPs (generally indicated as **NMNPs**) to be employed in the aggregation studies were prepared by mixing a dichloromethane solution of the dodecanthiol-capped nanoparticles (**C12S@NMNPs**) with a solution of the guest (**NOPI**) in the same solvent. In general, aliquots of guest solution were added to 1 mL of solution characterized by an absorbance value of ~1.8. To study the effect of the concentration in the monolayer of the charged "head" of the guest (interdigitation grade), several batches of the **NMNPs** solution were treated with increasing aliquots of a 10^{-3} M solution of the guest in CH_2Cl_2 (Figure 2.11).
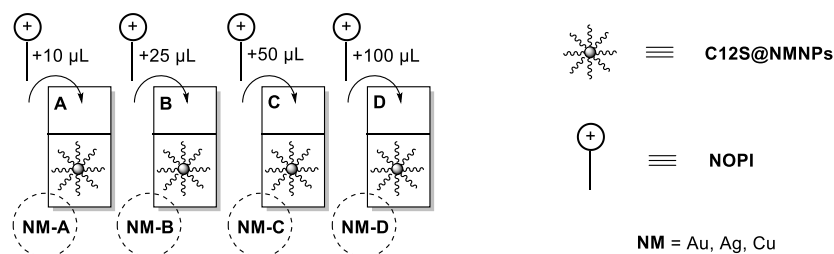
Figure 2.11 *Schematic representation of the increasing additions of the **NOPI** solution in CH_2Cl_2 to the **C12S@NMNPs** solution in CH_2Cl_2.*

To discard the hypothesis that the addition of the guest could itself induce aggregation, a blank titration experiment was accomplished by adding increasing aliquots of the **NOPI** solution (c = 10^{-3} M in CH_2Cl_2) to the solution of **C12S@NMNPs**. As an example, in Figure 2.12 has been reported the collection of spectra of the blank titration carried out on the sample of **C12S@AuNPs**. The titration shows an absorption reduction of the SPB band centered at 527 nm. This reduction is likely due to a small dilution effect and insertion of the guest in the dodecanthiol-based monolayer of the lipophilic NPs. As expected, the addition of the guest solution to the AuNPs does not induce any red-

shift of the SPB. This behavior is an indication that the interactions of the guest with the nanoparticles monolayer at this stage does not induce aggregation of these nanostructures. The blank titrations repeated on the samples of either **C12S@AgNPs** and **C12S@CuNPs** gave similar results.
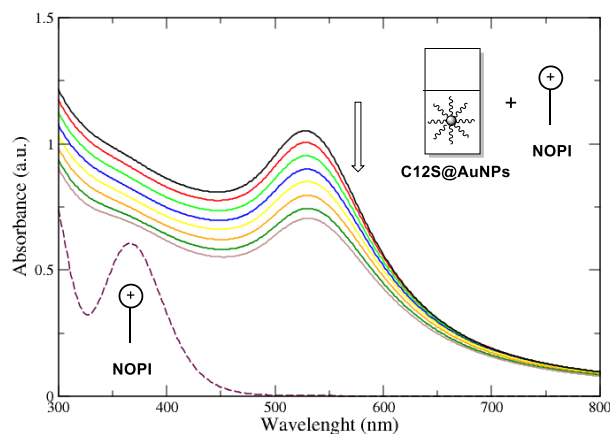

Figure 2.12 Titration of **C12S@AuNPs** with **NOPI** solution in CH₂Cl₂ (c = 10⁻³ M).

In the following sections, the resulting NOPI-decorated NPs will be indicated as **NMNPs(NOPI)** or, in detail, with the name of the solutions indicated in Figure 2.11 (e.g. Au-A).

2.2.2.3   Aggregation studies and characterization

The ability of the resulting NMNPs(NOPI) to give rise to a superlattice of nanoparticles through the complexation of the bifunctional host **11** was evaluated in dichloromethane solution using UV-vis spectroscopy as an investigation tool. With this technique, it is indeed possible to monitor the shifting of the maximum of the SPB of the NPs, which is sensitive to the size of the nanoparticles as well as to nanoparticle-nanoparticle electromagnetic coupling.[33,34] The UV-Vis measurements were carried out in a quartz cuvette with an optical path of 1 cm. In a typical UV-Vis titration experiment, aliquots of a 10^{-4} M solution of the bifunctional host **11** were added to the solutions of previously prepared NMNPs(NOPI). The position of the SPB of the NPs was monitored after each host addition.

Concerning AuNPs, the titrations carried out on the AuNPs solutions containing 10, 25 and 50 μl of **NOPI** (**Au-A**, **Au-B**, and **Au-C**, respectively, as indicated in Figure 2.11) were gathered in Figure 2.13. The addition of **11** determines a small red shifting of the SPB maximum for the solutions **Au-B** and **Au-C** (Figure 2.13b and Figure 2.13c, respectively).
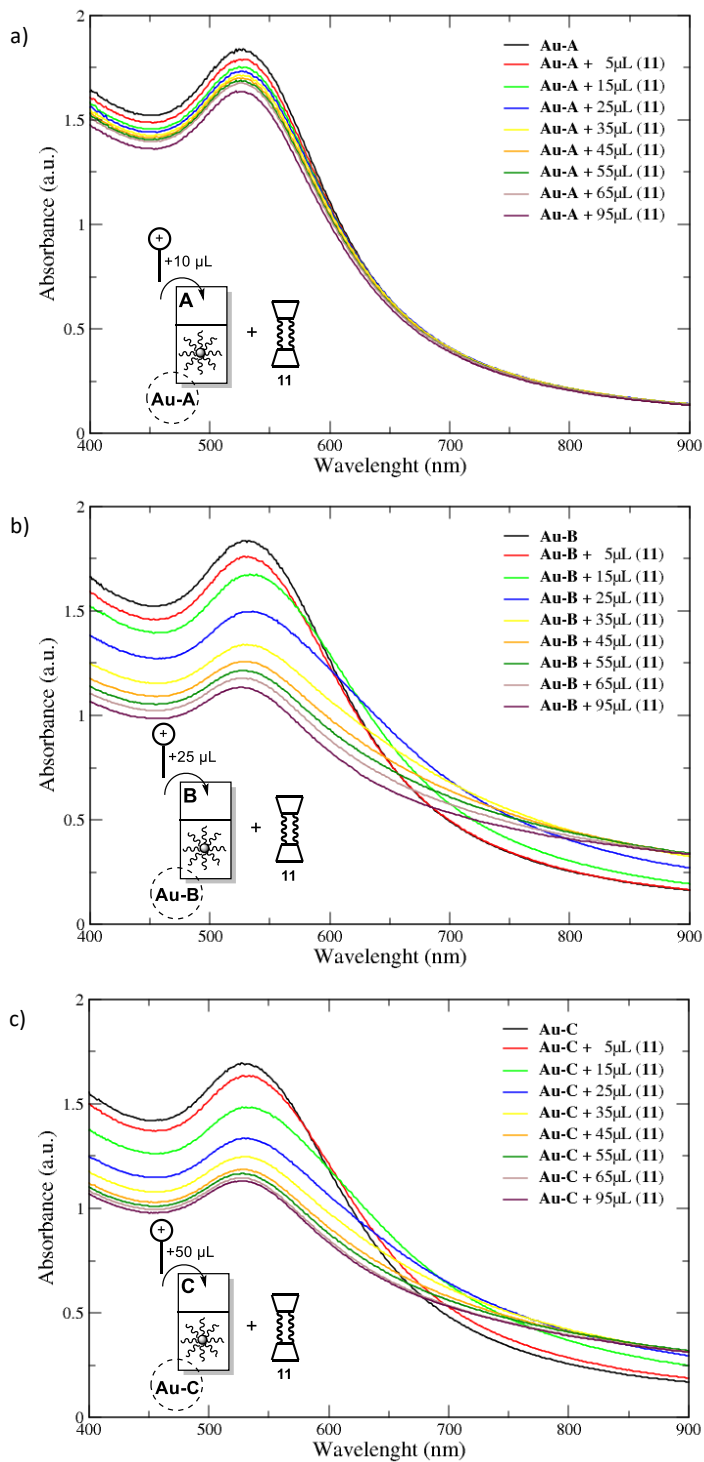
Figure 2.13 *Titration studies with increasing aliquots of **11** (c=10⁴ M) in CH₂Cl₂ on: a) **Au-A** (**C12S@AuNPs** + 10 µL **NOPI**), b) **Au-B** (**C12S@AuNPs** + 25 µL **NOPI**), c) **Au-C** (**C12S@AuNPs** + 50 µL **NOPI**).*
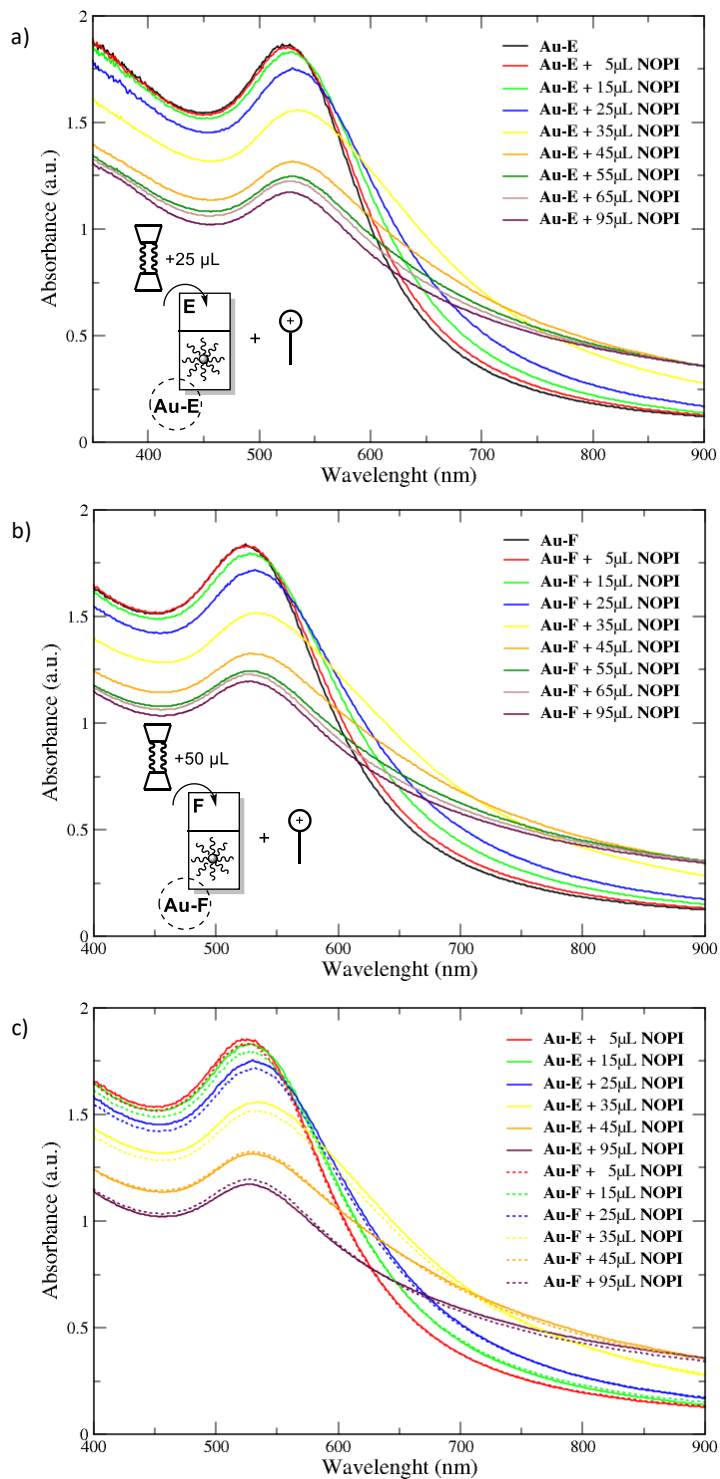
Figure 2.14 *Titration studies with increasing aliquots of **NOPI** (c=10⁻³ M) in CH₂Cl₂ on: a)* ***Au-E*** *(**C12S@AuNPs** + 25 µL **11**), b)* ***Au-F*** *(**C12S@AuNPs** + 50 µL **11**), c) superimposition of the two titration experiments. Solutions of **11** c=10⁻⁴ M in CH₂Cl₂.*

The redshift is more evident for the solution **Au-B** (by approximately 25-30 nm). This behavior suggests that in these conditions of concentration, in the **Au-C** solution, the **NOPI** is in excess and the increasing aliquots of **11** tend to complex the "free" guest present in the solution instead of the interdigitated one. However, for both **Au-B** and **Au-C**, the red-shift of the SPB is accompanied by peak broadening and extinction reduction. After the stepwise addition of 5 μL of the solution of **11**, the further additions progressively shift the maximum of the SPB with the formation of a recognizable isosbestic point. In the titration of the **Au-A** solution (Figure 2.13a), the redshift of the SPB band was never observed even for the largest addition of the solution of **11** (95 μl). This behavior was explained considering that the amount of the interdigitated **NOPI** in the organic monolayer of the **C12S@AuNPs** was not sufficient to promote their observable aggregation.

To demonstrate that the aggregation phenomena observed with **Au-B** and **Au-C** is due to a hierarchical interaction between nanoparticles monolayer, *N*-octyl pyridinium cation and aromatic cavities of **11**, two reversal titration experiments were also carried out by adding fixed aliquots of the bifunctional host **11** (25 μl and 50 μl for solutions **Au-E** and **Au-F**, respectively) to the nanoparticles solution, followed by the addition of incremental aliquots of the **NOPI** solution. The collections of spectra depicted in Figure 2.14 show that the incremental addition of the pyridinium guest induces an initial redshift of the SPB along with its progressive broadening. Once again, this behavior witnesses that the aggregation of the nanoparticles occurs thanks to the synergic contribution of the host and the guest present simultaneously in solution. It is worth to note that in the two solutions, the aggregation occurs almost independently from the amount of **11** initially added to the AuNPs (in both cases, extensive SPB broadening starts after the addition of 35 μl aliquot of **NOPI**). This behavior seems to suggest that the critical event triggering the aggregation is the diffusion of a sufficient amount of the pyridinium guest in the monolayer of the nanoparticles.

To verify the effect of bifunctional host concentration on the extent of the aggregation, a new titration experiment was devised on the **Au-C** solution. To this latter solution, incremental aliquots of a 10^{-3} M solution of **11** were added, and a UV spectrum was recorded after 5 min from each host addition. The resulting collection of spectra was gathered in Figure 2.15. The addition of **11** is witnessed by the increase of the band centered at 279 nm. After each addition, the color of the solution progressively turns from ruby red to blue, and indeed a broadening of the SPB, due to light scattering, is observed. This effect is here more pronounced than in the titrations carried out with a 10^{-4} M

solution of **11** (see Figure 2.13), sign that a higher amount of this bifunctional host in solution favors the NPs networking.
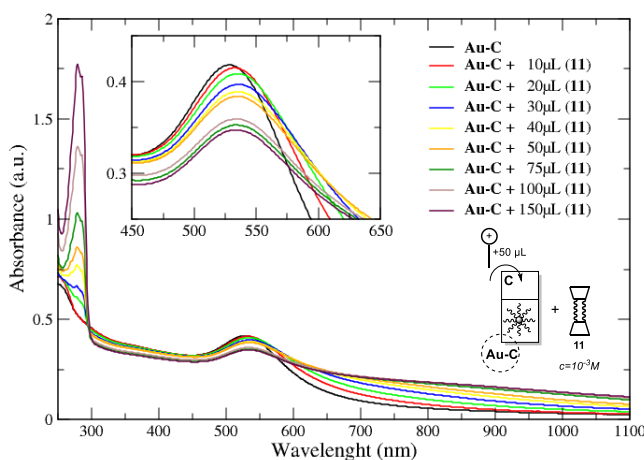
Figure 2.15 *Titration studies on **Au-C** (**C12S@AuNPs** + 50 µL **NOPI**) with increasing aliquots of **11** (c=10⁻³ M) in CH₂Cl₂.*

A second experiment was then repeated to study the kinetics of the process. The amount of **NOPI** in solution was doubled (100 µl, **Au-D**), and the variation of the SPB was monitored with time. The results of this experiment, depicted in Figure 2.16, show that the nanoparticles' aggregation increases with time with the formation of a large absorption band centered at ~600 nm, which extends up to the NIR region (blue-colored solution) after half-an-hour from the mixing of the components.
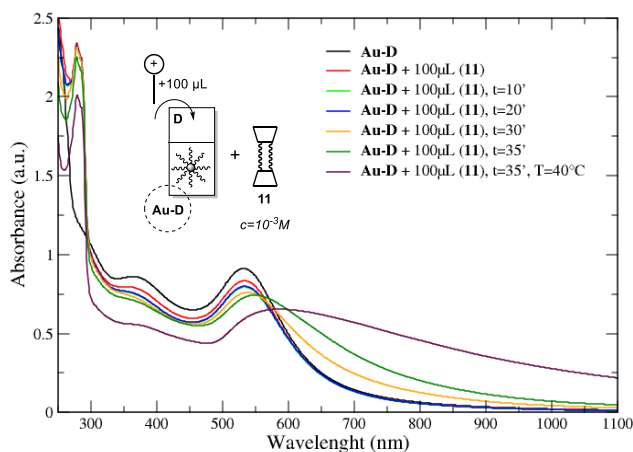
Figure 2.16 *Kinetics studies on **Au-D** (**C12S@AuNPs** + 100 µL **NOPI**) with the addition of **11** (c=10⁻³ M) in CH₂Cl₂*

The aggregation phenomena induced by the host/guest complexation was also studied through a series of TEM measurements. Four samples to be analyzed were prepared. In the first sample (Figure 2.17a), a drop of the **C12S@AuNPs** solution in CH_2Cl_2 was deposited on the TEM grid. On further two grids, drops of solutions prepared by mixing the previous nanoparticles' solution with solutions of **11** (Figure 2.17b) and **NOPI** (Figure 2.17c), respectively, were deposited. On the fourth grid, a solution of the three components was deposited (Figure 2.17d).
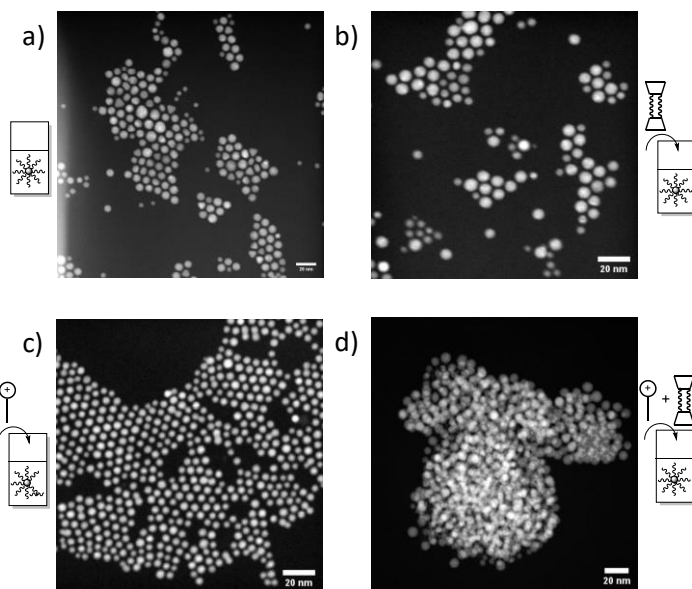
Figure 2.17 *TEM measurements of different solutions: a)* **C12S@AuNPs***; b)* **C12S@AuNPs** *+ host 11; c)* **C12S@AuNPs** *+* **NOPI** *guest; d)* **C12S@AuNPs** *+ 11 +* **NOPI**.

The same type of aggregation study was carried out also with the solutions of the AgNPs(NOPI), which were prepared in the same way as the AuNPs(NOPI). No significant results were obtained during the titrations performed on the **Ag-A**, **Ag-B**, and **Ag-C** solutions. The decrease in the absorption intensity upon the addition of the solution of **11** seems due to a dilution effect. Nevertheless, upon the addition of 95 µl of the bifunctional host solution, it is possible to observe a minimal red-shift with the appearance of an isosbestic point on the right shoulder of the considerable absorption band. As a straightforward example, in Figure 2.18a it has been depicted the titration carried out on the **Ag-B** solution, in which the isosbestic point is found at ~480 nm. Encouraged by this minimal result, the titration was repeated with the **Ag-D** solution that contains a higher amount of **NOPI** (100 µL, c = 10^{-3} M). In this case, even if less evident than the results obtained with the corresponding AuNPs solutions, it is clearly possible to see the presence

of an isosbestic point (~ 515 nm). However, there was no significant red-shift of the SPB maximum (~5 nm). It is worth to note that the small band at ~350 nm is referred to the absorption maximum of the **NOPI** guest (Figure 2.18b).
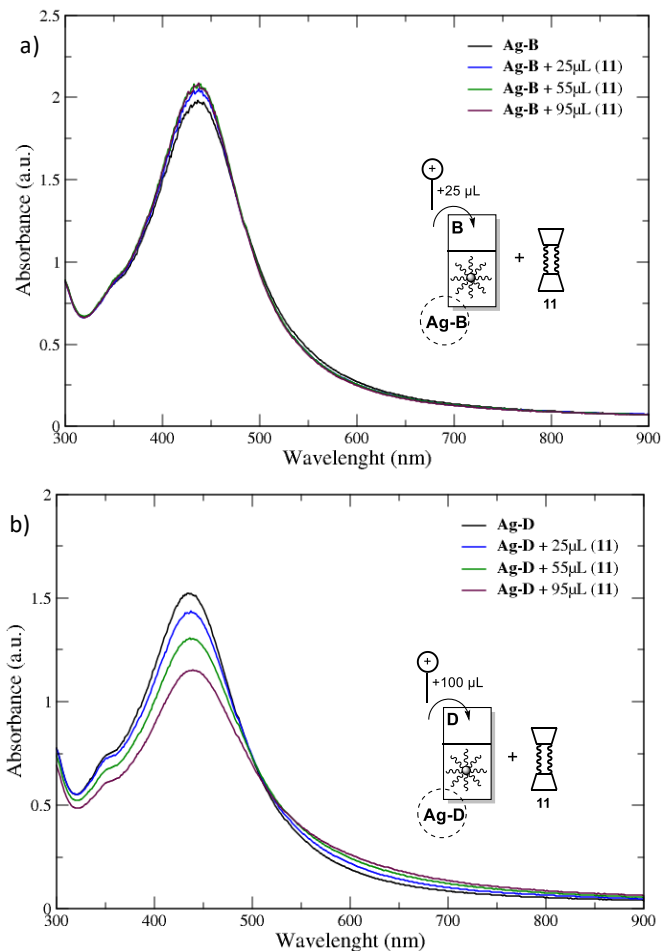
Figure 2.18 *Titration studies with increasing aliquots of* **11** *(c=10⁻⁴ M) in CH₂Cl₂ on: a)* ***Ag-B*** *(C12S@AgNPs + 25 μL* ***NOPI***), *b)* ***Ag-D*** *(C12S@AgNPs + 100 μL* ***NOPI***).

Finally, some preliminary experiments were done to study the aggregation process among CuNPs(NOPI). As usual, four solutions (**Cu A-D**) with increasing amounts of **NOPI** were prepared and titrated with the bifunctional host **11** (c = 10⁻⁴ M). Even in the titration experiment carried out on the **Cu-D** solution (100 μL of **NOPI**, c = 10⁻³ M), no appreciable red-shifting or broadening of the SPB was visible. However, even if not very apparent, it is possible to observe that, after each addition of the host solution, the SPB band slightly decreases in intensity increasing the time of equilibration. To highlight this trend,

the absorbance profiles measured after the mixing of the host solution with that of the CuNPs were indicated with continuous lines in Figure 2.19a, while those obtained 10 minutes after the addition with dashed lines. Surprisingly, however, the measure recorded after 100 minutes from the addition of 95 µl of the solution of **11** revealed (garnet dotted line in Figure 2.18a) a marked absorption increasing. Probably, this effect is due to the approaching of the metal nuclei one to each other, changing the interparticle spacing, followed by a possible coupling of plasmon modes of nearby metallic cores.[35] The same measurements were done using a more concentrated solution of the bifunctional host **11** (c = 10^{-3} M), and a similar trend was evidenced (Figure 2.19b).
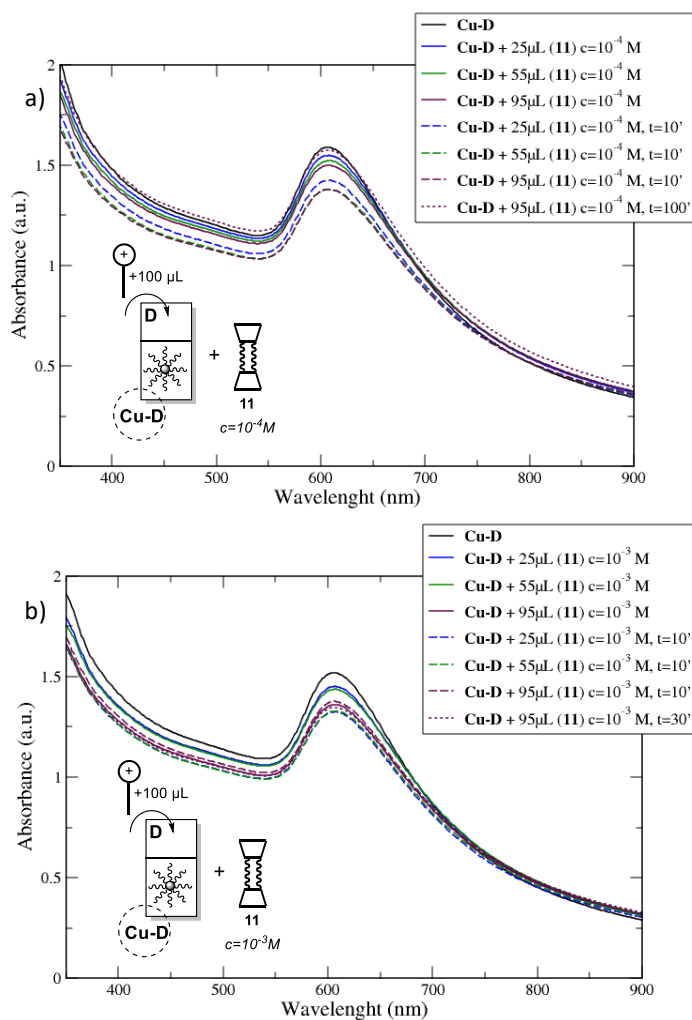
**Figure 2.19** *Titration studies on* **Cu-D** *with increasing aliquots of different concentration of* **11** *solution in CH₂Cl₂: c=10^{-4} M (a) and c=10^{-3} M (b).*

2.2.3 Aggregation studies: Strategy *(I)*

In this section, we present a study in which silver NPs having a mean core size of ~ 4 nm are coated with the thiolate calix[4]arene derivative **2a** (Figure 2.20). The resulting NPs are able to self-assemble through supramolecular interactions with bifunctional guests based on the dialkyl pyridinium salt (Figure 2.20) to yield aggregates whose sizes and solubility can be controlled by the different concentration of bifunctional guest used as a linker between nanoparticles. It will be also discussed the synthesis of a calix[6]arene derivative (**21** in Figure 2.20) for a future functionalization of the NPs and the following aggregation studies with a suitable bis-dipyridinium guest (Figure 2.20).

2.2.3.1 Synthesis of functional hosts

In a previous paper,[36], the use of a thiolate calix[6]arene derivative as a functional organic coating for AuNPs was reported. This host presents three methoxy groups alternate with three ω-thiolate C11 alkyl chain at the macrocycle lower rim and six *tert*-butyl groups at its upper rim. To increase the recognition abilities of the calix[6]arene macrocycle towards bipyridinium-based guests, we designed the insertion of three phenylureido moieties at the upper rim (**21**, Figure 2.20). The synthesis of this derivative is not trivial because of the presence of several functional groups that have to be orthogonal to each other and resistant to particular reaction conditions.
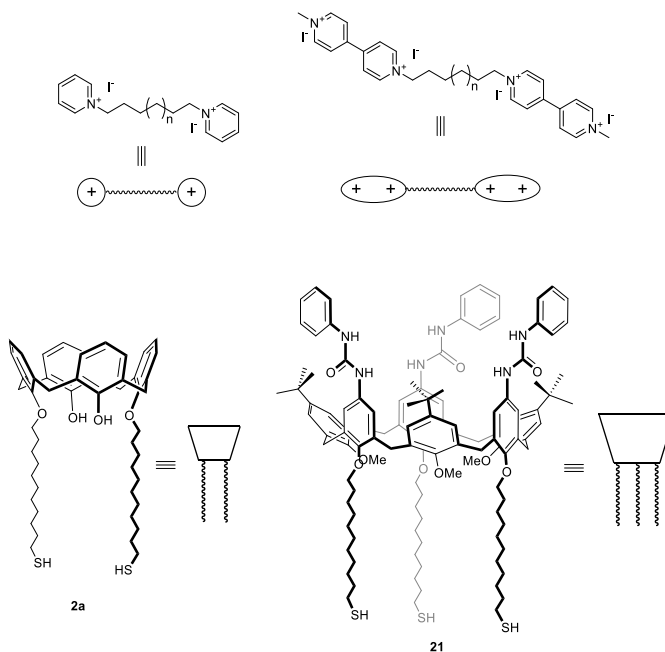
Figure 2.20 *Schematic representation of calix[n]arene derivative **2a** and **21** and their complementary guest.*

Calix[4]arene derivative **2a** was synthesized following a reported method (Scheme 2.5).[10,36]
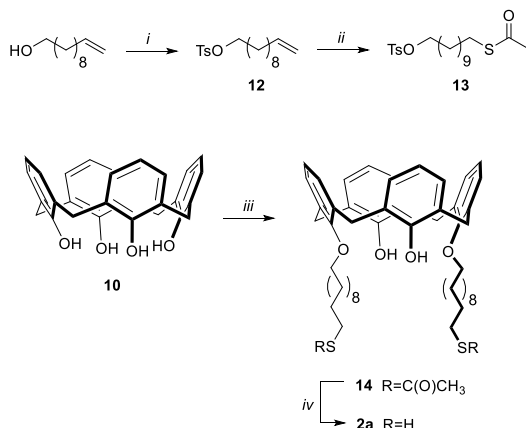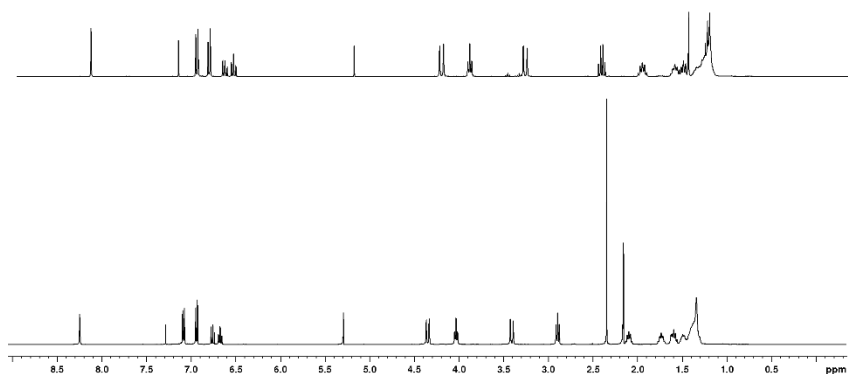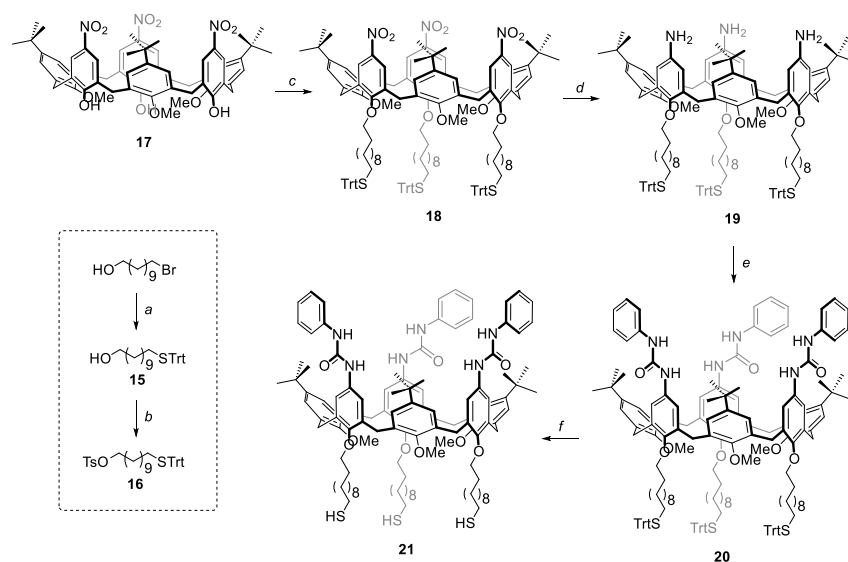

Scheme 2.5 *Synthesis of calix[4]derivative **2a**. Reagents and conditions: i) TsCl, Et₃N, DMAP, CH₂Cl₂, rt, overnight, 96%; ii) CH₃COSH, AIBN, toluene, reflux, 5h, 70%; iii) **13**, K₂CO₃,KI, CH₃CN, reflux, 48h, 64%; iv) HCl 10%v/v, THF/H₂O, reflux, 48h, quant. yield.*

Firstly, the ω-thioacetyl C11 alkyl chain **13** was synthesized. The functional thiol-anchoring group was protected as a thioester group (SCOCH₃) to avoid oxidation, with the formation of disulfide bridges, and to prevent unwanted side-reactions. The first step involved the reaction of 10-undecen-1-ol with 4-toluenesulfonyl chloride (TsCl) in the presence of triethylamine (Et₃N), using 4-dimethyl aminopyridine (DMAP) as the catalyst. The resulting tosylate **12** was used as a reactant in the radical reaction with thioacetic acid in the presence of AIBN as the initiator. The product **13** was obtained with 70% yield and was characterized by NMR and ESI-MS spectroscopy (see compound **L-4** in section 4.2.5 in Chapter 4). This compound was then used as the alkylating agent in the reaction with the calix[4]arene derivative **10** carried out in CH₃CN in the presence of K₂CO₃ as the base. The resulting mixture was purified by chromatography on silica gel to give compound **14** in 64%yield. The removal of the protecting group was carried out in a 1: 1 mixture of THF/HCl (10% v/v) and allowed to obtain the target thiolate derivative **2a**, with a quantitative yield. Its ¹H NMR spectrum, recorded in CDCl₃ (Figure 2.21, top), presents the diagnostic multiplet centered at 2.56 ppm, relative to the methylene protons adjacent to the free thiol function, demonstrating the effective deprotection of the ester group. It is possible to observe also the disappearance of the singlet (at 2.34 ppm in Figure 2.21, bottom) relative to the methyl protons of the thioester group in compound **14**. As in the case of compound **11** previously described, the alkylated calix[4]arene derivative is in a blocked *cone* conformation as indicated

by the characteristic pattern of aromatic signals and the two doublets relative to the diasterotopic protons of the methylene bridge.

Figure 2.21 *¹H NMR stack plot of **2a** (300 MHz, CDCl₃, top) and **14** (400 MHz, CDCl₃, bottom).*

Scheme 2.6 *Synthesis of calix[6]arene derivative **21**. Reagents and conditions: a) (Ph)₃CSH, NaOH, toluene/EtOH, rt, 6h, 88%; b) TsCl, Et₃N, DMAP, CH₂Cl₂, rt, overnight, 78%; c) **16**, K₂CO₃, KI, DMF, 110°C, 10 days, 21%; d) SnCl₂•2H₂O, EtOH, reflux, 12h, 62%; e) PhNCO, CH₂Cl₂, rt, 4h, 50%; f) NaBH₃CN, TFA, CH₂Cl₂, rt, 3h, 55%.*

Concerning the synthesis of the calix[6]arene derivative **21**, a convergent pathway was followed (Scheme 2.6). The synthesis of the

calix[6]arene building block **17** was already developed and reported by our research group.[37] Parallelly, the C11 ω-thiol-protected alkylating chain **16** was synthesized. The thiol function was protected employing the triphenylmethyl (trityl) group (Tr), while at the other end it was introduced a good leaving group, the tosyl (-OTs), which allows a faster functionalization of the OH groups at the lower rim of derivative **17**. The alkylating agent **16** was obtained in two synthetic steps. The first one consists of the protective-reaction of 11-bromoundecan-1-ol with triphenylmethanethiol in basic condition, to give **15** in 88% yield. The resulting compound **15** was reacted with TsCl in the presence of Et_3N as the base, to give the desired compound **16** in 78% yield. In the corresponding ^1H NMR spectrum (Figure 2.22), the diagnostic signals of the tosylate group are observed as two doublets (J = 7.9 Hz) and a singlet at 7.82, 7.37 and 2.47 ppm, respectively. Moreover, the signals related to methylene protons in α-positions to the two terminal functional groups are clearly visible as two triplets at 4.05 and 2.17 ppm assigned to -C$\underline{H}_2$-OTs and -C$\underline{H}_2$-SR, respectively.
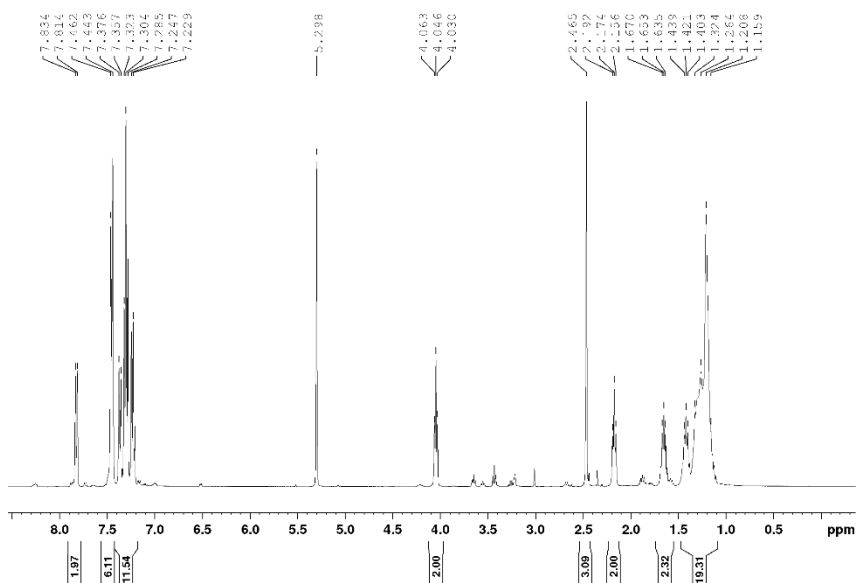
Figure 2.22 ^1H NMR spectrum (CDCl$_3$, 400 MHz) of **16**.

The first step for the preparation of the calix[6]arene derivative **21** was the alkylation of compound **17** with the ω-thiol-protected alkyl chain **16**. The reaction was carried out in a Schlenk tube, at high pressure and temperature, in anhydrous CH_3CN in the presence of K_2CO_3 and KI. The pure derivative **18** was obtained with 21% yield, after purification by column chromatography on silica gel. The NO_2 group was then reduced to NH_2 with $SnCl_2$•2H$_2$O, and the resulting amino derivative **19** was reacted without any further purification with phenyl isocyanate

to give the compound **20** in 50% yield, after purification by column chromatography on silica gel. The last reaction step consists of the deprotection of the thiol group through a reaction carried out in stoichiometric excess of $NaBH_3CN$ in a TFA/DCM mixture (1:2), in anhydrous conditions to avoid the hydrolysis of phenyl urea moieties at the upper rim of the derivative. After purification by column chromatography on silica gel, the target molecule **21** was obtained in 55% yield. The ^{1}H NMR spectrum (Figure 2.23, top) shows the presence of a quadruplet at 2.53 ppm, corresponding to -C<u>H</u>$_2$-SH, while the triplet at 2.10 ppm (Figure 2.23, bottom), corresponding to -C<u>H</u>$_2$-S-Tr was absent. Moreover, a notable reduction of the signals in the aromatic region further confirmed the successful trityl removal.
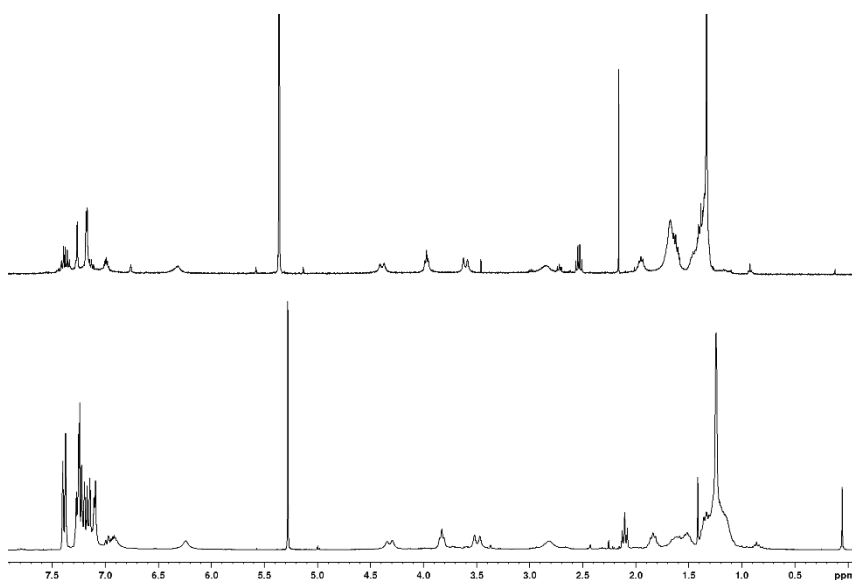
Figure 2.23 *^{1}H NMR stack plot of **21** (300 MHz, CD$_2$Cl$_2$, top) and **20** (300 MHz, CDCl$_3$, bottom).*

2.2.3.2 Synthesis and characterization of the calix[n]arene-coated NPs

The synthesis and the aggregation studies of AgNPs entirely decorated with thiolate calix[4]arene **2a** were already reported by our research group.[38] In particular, a dichloromethane solution of **C12S@AgNPs**, synthesized by using the methodic reported by Fitzmaurice et al.,[20] was mixed with a solution of **2a** in the same solvent. The ligand-place exchange reaction was left to proceed for at least seven days. After the purification, the XPS measurements suggested that the C12SH monolayer was totally displaced by calix[4]arene **2a**. This result is not surprising considering the large affinity of this bidentate thiolated ligand with respect to the monodentate one (C12SH). In order to gain

better control over the aggregation and solubility of the resulting AgNPs and relative aggregates, a different approach to obtain AgNPs coated with a mixed monolayer of C12SH and the calix[n]arene derivative was devised. Starting from the precursor solution of **C12NH₂@AgNPs**, prepared using the biphasic method[22] explained in section 2.2.1. Therefore, the ligand place exchange reaction was carried out by mixing a 1:1 cyclohexane/toluene solution containing C12SH and **2a** in a 1:5 stoichiometric ratio, with a cyclohexane solution of **C12NH₂@AgNPs** (Scheme 2.7). The ligand exchange reaction was left to proceed overnight. This shortened time of ligand exchange reaction would, in principle, increase the probability to obtain AgNPs with a mixed monolayer of **C12S** and **2a** rather than a full exchange of the ligand as occurred with the previously adopted methodology (7 days). The exchanged nanoparticles **2a|C12S@AgNPs** were then precipitated through the addition of methanol to the reaction mixture and separated by ultracentrifugation at 9000 rpm for 15 minutes. Finally, the resulting precipitated NPs were redispersed in CH₂Cl₂.

C12NH₂@AgNPs   **2a|C12S@AgNPs**
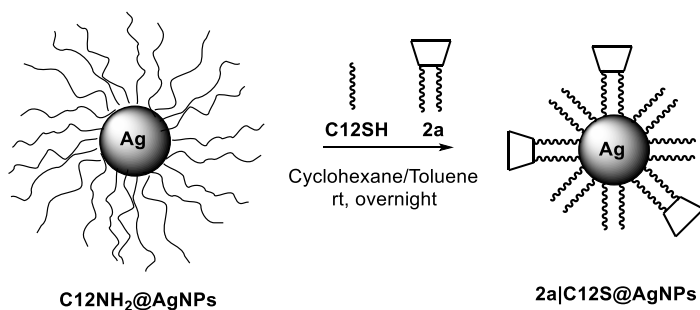
**Scheme 2.7** *Schematic synthesis of **2a|C12S@AgNPs**.*
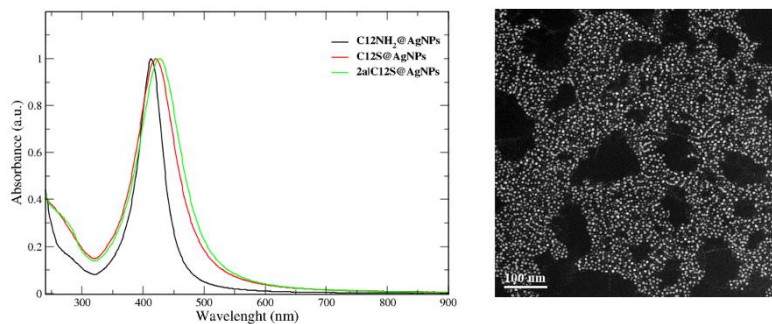
Figure 2.24 *UV-Vis characterization of AgNPs in CH₂Cl₂ (left) and STEM image of **2a|C12S@AgNPs** (right).*

These NPs were characterized by UV-Vis and STEM measurements. The UV/Vis spectrum clearly evidences a notable red-shift of the SPB (~ 15 nm), as a proof of the occurred exchange of the monolayer (Figure 2.24 left). The STEM measurements show a rather monodispersed sample of **2a|C12S@AgNPs**. On average, the observed interparticle distance of approximately 4 nm was consistent with grafting of the bulkier calix[4]arene **2a** on the surface of the AgNPs (from simple molecular modeling calculation).

2.2.3.3 Aggregation studies and characterization

The dipyridinium diiodide **PyC12Py** (Figure 2.25) was chosen as the bifunctional guest to promote the aggregation of the nanoparticles. This salt was synthesized in high yields (>90%) by the reaction of pyridine in refluxing acetonitrile with 1,12-diododododecane. It is characterized by two pyridinium units linked through a flexible C12 alkyl chain. Furthermore, it shows good solubility in low polarity solvents such as chloroform and toluene. The affinity of this type of guest for the aromatic cavity of preorganized calix[4]arene derivatives has been already documented[39,40] and, thus, can be employed for the aggregation of **2a|C12S@AgNPs** (*Strategy I*).
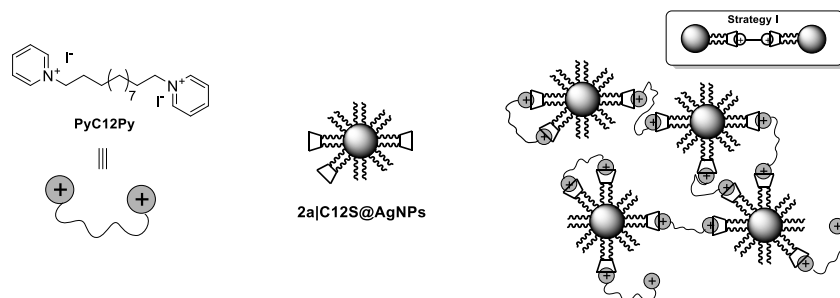
Figure 2.25 *Schematic representation of the aggregation among **2a|C12S@AgNPs** and bifunctional guest **PyC12Py**, following a Strategy I.*

The aggregation processes were followed by UV-Vis absorption spectrophotometry and were carried out in a cuvette with an optical path of 1 cm. In detail, the titrations were accomplished by adding increasing aliquots (10 to 100 μL) of a solution of the salt **PyC12Py** in CH_2Cl_2 to a 1.5 mL solution of **2a|C12S@AgNPs** in the same solvent. Following each guest solution addition, the change and displacement of the SPB maximum were monitored. The titration depicted in Figure 2.26a was done using a solution of **PyC12Py** with a concentration of 10^{-4} M, and it showed that the addition of the guest determines a small red-shift of the SPB maximum (~10 nm), accompanied by peak broadening and extinction reduction only for the highest aliquots of the added guest. Thus, another titration was done increasing the concentration of

PyC12Py to 10^{-3} M. As indicated by the collection spectra of Figure 2.26b, the red-shift of the SPB maximum is much more marked, by approximately 25 nm. Moreover, the peak broadening is higher and visible since the first aliquot of the guest solution added (10 µL).
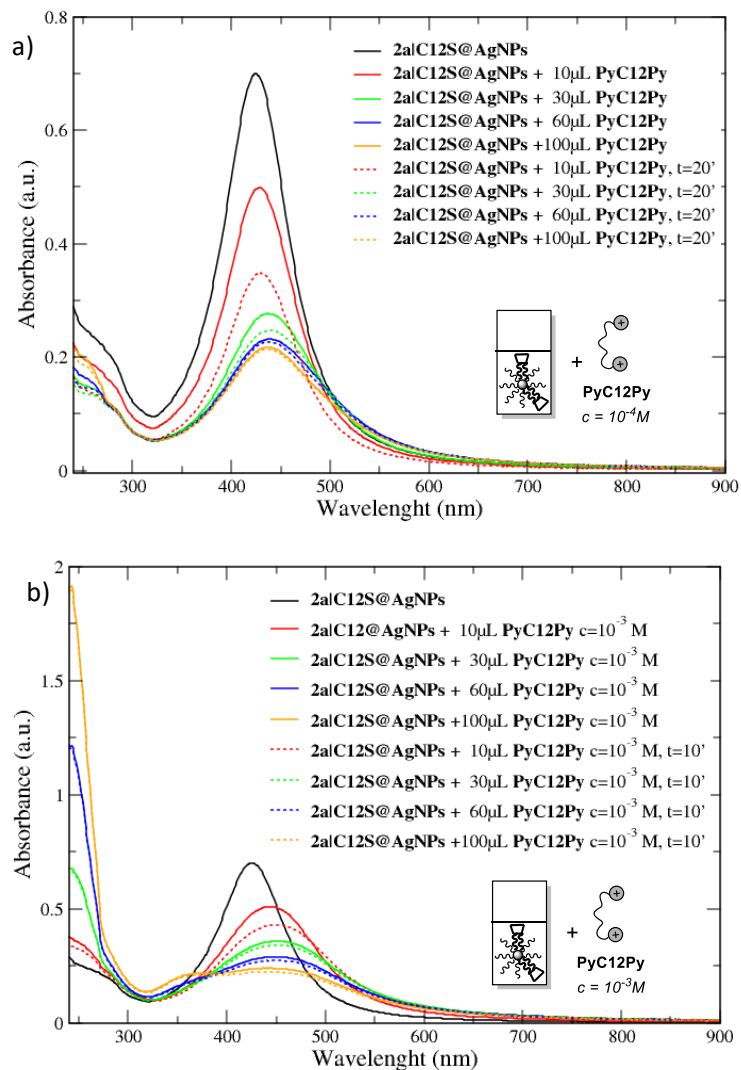
Figure 2.26 *Titration studies on **2a/C12S@AgNPs** with increasing aliquots of different concentration of **PyC12Py** solution in CH₂Cl₂: c=10⁴ M (a) and c=10³ M (b).*

To confirm that these aggregation processes were effectively driven by the complexation of **PyC12Py** by the several units of calix[4]arene **2a** resident on the surface of different NPs, a complementary titration was devised. The experiment was accomplished by adding a dichloromethane solution of **PyC12Py** to a solution of **C12S@AgNPs** in the same solvent. It is easily predicted that these NPs, presenting any

receptor on their surface, cannot aggregate upon the action of the supramolecular bifunctional linkers. Indeed, the collection of spectra recorded (Figure 2.27) shows that the addition of **PyC12Py** (c = 10^{-4} M and c = 10^{-3} M) does not induce any red-shift of the SPB. The intensity reduction is reasonably due to a dilution effect.

69
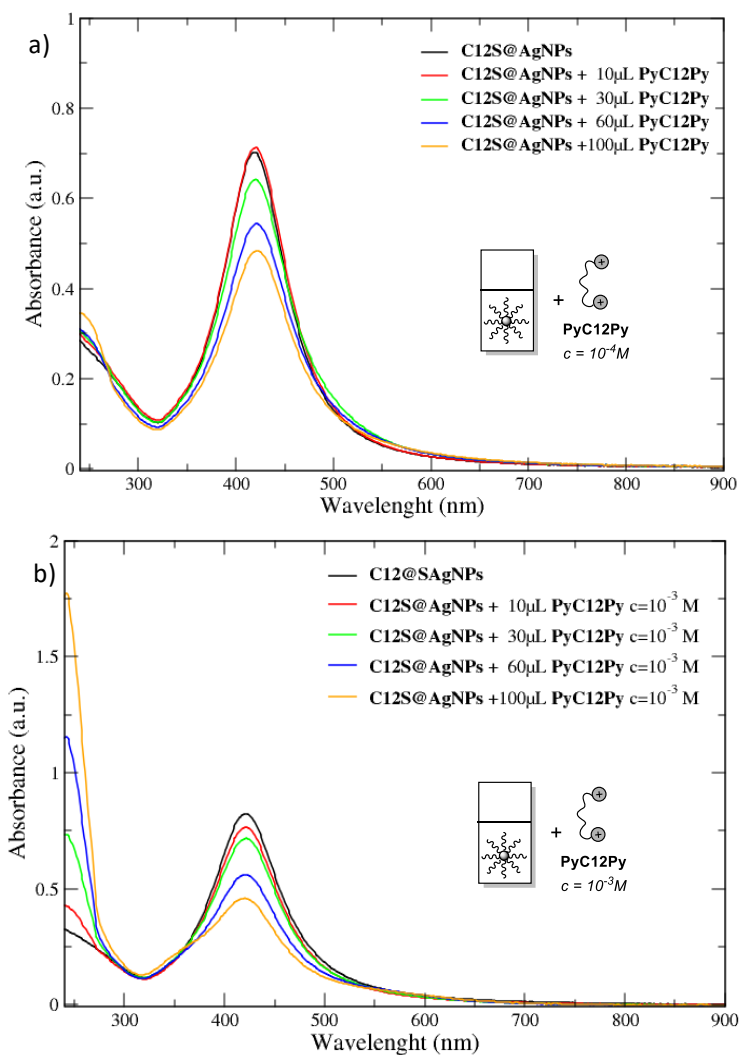
Figure 2.27 *Titration studies on* **C12S@AgNPs** *with increasing aliquots of different concentration of* **PyC12Py** *solution in CH₂Cl₂: c=10⁻⁴ M (a) and c=10⁻³ M (b).*

2.3 Experimental Section

All solvents were dried using standard procedures. All other reagents were of reagent-grade quality, obtained from commercial suppliers and were used without further purification. "Brine" refers to a saturated aqueous solution of NaCl. Unless otherwise specified, solutions of common inorganic salts used in workups are aqueous solutions. Reactions were monitored by TLC using 0.25 mm Merck silica gel plates (60 F254). NMR spectra were recorded at 400 and 300 MHz for ^{1}H and 100 and 75 MHz for ^{13}C on a *Bruker Avance* 400 and 300 spectrometers. Chemical shifts (δ) are expressed in ppm using the residual solvent signal as an internal reference. Melting points are uncorrected. Mass spectra were recorded in ESI mode. Compounds **9**,[41] **10**,[42] **TOABr@AuNPs**,[19] **C12S@AuNPs**,[38] **PyC12Py** [15] were synthesized according to published procedures.

1-octylpyridinium iodide (**NOPI**).[15] In a sealed glass reactor, pyridine (0.4 mL, 5 mmol), 1-iodoctane (1.1 mL, 6 mmol) in CH_3CN (10 mL) were heated at 90°C for 2 days. Afterwards, the solution was evaporated to dryness under reduced pressure. The oily residue was purified trough recrystallization from cold ethyl acetate to afford the product as a very hygroscopic low-melting yellow solid (1.28 g, 80%). ^{1}H NMR (300 MHz, $CDCl_3$): δ (ppm) = 9.38 (d, 2H J= 5.4 Hz), 8.59 (t, 1H, J= 7.2 Hz), 8.19 (t, 2H, J= 7.2 Hz), 4.92 (t, 2H, J= 7.45 Hz), 2.04 (bs, 2H), 1.40-1.22 (m, 10H), 0.83 (t, 3H, J= 6.75 Hz). ^{13}C NMR (75 MHz, $CDCl_3$): δ (ppm) = 149.0; 147.6; 131.6; 65.1; 34.6; 34.2; 31.8; 31.7; 28.8; 25.5; 17.0. MS-ESI (+): m/z = 192 (100) $[MH]^+$.

Bis-calix[4]arene (**11**).[30] In a 100 mL two-necked round bottom flask, calix[4]arene **10** (1 g, 2.4 mmol) and K_2CO_3 (0.63 g, 5 mmol) in CH_3CN (50 mL) were refluxed for 1 hour. Afterwards, at room temperature **9** (2.2 g, 5 mmol) was added to the mixture. The resulting heterogeneous solution was refluxed for 4 days. The solvent was evaporated to dryness under reduced pressure. The residue was treated with HCl solution (30 mL, 10% v/v in H_2O), followed by extraction with 30 mL of CH_2Cl_2. The separated organic phase was separated and dried over Na_2SO_4. The solvent was removed under reduced pressure and the product **11** was obtained by precipitation from acetone (0.27 g, 11%). ^{1}H NMR (300 MHz, $CDCl_3$): δ (ppm) = 8.47 (s, 4H), 7.01 (d, 8H, J=7.5 Hz), 6.92 (d, 8H, J = 7.5 Hz), 6.76 (t, 4H, J = 7.5 Hz), 6.65 (t, 4H, J = 7.5 Hz), 4.26 (d, 8H, J = 12.7 Hz), 4.06 (t, 8H, J = 6.8 Hz), 3.23 (d, 8H, J = 12.7 Hz), 2.31 (bs, 8H), 2.02 (bs, 8H). ^{13}C NMR (75 MHz,

CDCl$_3$): δ (ppm) = 153.3; 151.7; 133.6; 128.8; 128.4; 128.0; 125.3; 118.8; 75.9; 31.2; 30.1; 24.9. MS-ESI (+): m/z (%) = 1035.4 [M+Na]$^+$; 1051.5 [M+K]$^+$.

undec-10-en-1-yl 4-methylbenzenesulfonate (12). In a 250 mL two-necked round bottom flask, 10-undecen-1-ol (6.8 g, 40 mmol) was solubilized with triethylamine (6.36 mL, 60 mmol) in 50 ml of anhydrous CH$_2$Cl$_2$. A solution *p*-methylbenzenesulfonyl chloride (TsCl) (8.36 g, 43.8mmol) in CH$_2$Cl$_2$ (20 mL) was added dropwise. Subsequently, 4-dimethylaminopyridine (DMAP) was added in catalytic quantity and the reaction mixture was stirred at rt overnight. Afterwards, the reaction mixture was treated with HCl solution (30 mL, 10% v/v in H$_2$O), the organic phase was washed with H$_2$O and it was dried over Na$_2$SO$_4$. The solvent was removed under reduced pressure to yield **12** as a yellow oil (12.5 g, 96%), used in the following step without any further purification. ^{1}H NMR (400 MHz, CDCl$_3$): δ (ppm) = 7.79 (d, 2H, J=8 Hz), 7.35 (d, 2H, J=8 Hz), 5.82-5.78 (m, 1H), 5.02-4.92 (m, 2H), 4.02 (t, 2H, J= 6.8 Hz), 2.45 (s, 3H), 2.05-2.03 (m, 2H), 1.65-1.62 (m, 2H), 1.37-1.23 (m, 12H). ^{13}C NMR (100 MHz, CDCl$_3$): δ (ppm) = 144.6, 139.1, 133.3, 129.8, 127.9, 114.16, 70.7, 33.8, 29.3, 29.0, 28.9, 28.8, 25.3, 21.6.

S-(11-(tosyloxy)undecyl) ethanethioate (13). In a 250 mL three-necked round bottom flask equipped with degassing valve, **12** (12.4 g, 38.2 mmol) and thioacetic acid (13.5 mL, 0.19 mol) were solubilized in anhydrous toluene (100 mL). The solution was degassed for 20 minutes bubbling nitrogen. Subsequently, 2-2'-azobisisobutyrronitrile (AIBN) was added and the reaction mixture was stirred heating at 50°C for 12 hours. The mixture was then treated with a saturated aqueous solution of K$_2$CO$_3$, the separated organic phase was washed with H$_2$O and it was dried over Na$_2$SO$_4$. The solvent was removed under reduced pressure and the product **13** was obtained as a deliquescent white solid after a recrystallization from ethyl acetate/*n*-hexane (7.8 g, 51%). ^{1}H NMR (400 MHz, CDCl$_3$): δ (ppm) = 7.81 (d, 2H, J= 8 Hz), 7.36 (d, 2H, J=8 Hz), 4.04 (t, 2H, J= 6.4 Hz), 2.88 (t, 2H, J=7.2 Hz), 2.47 (s, 3H,), 2.34 (s, 3H), 1.68-1.23 (m, 18H). ^{13}C NMR (75 MHz, CDCl$_3$): δ (ppm) = 195.0, 144.6, 133.2, 129.8, 127.9, 70.7, 30.7, 29.5, 29.4, 29.3, 29.1, 28.9, 28.8, 25.3, 21.6. MS-ESI (+): m/z (%) = 347 (100) [M+Na]$^+$.

Calix[4]arene (14). In a 100 mL round bottom flask, calix[4]arene **10** (1.5 g, 3.53 mmol) and K$_2$CO$_3$ (0.94 g, 7.07 mmol) were solubilized in anhydrous CH$_3$CN (50 mL). Subsequently, a solution of **9** (3.03 g, 7.56 mmol) in CH$_3$CN (10 mL) was added. The mixture was stirred at reflux for 48 hours. The reaction mixture was then treated with HCl solution (20 mL, 10% v/v in H$_2$O), the organic phase was washed with H$_2$O and it was dried over Na$_2$SO$_4$. The solvent was removed under reduced

pressure and the residue was purified by column chromatography (SiO_2, CH_2Cl_2/n-hexane 85:15) to obtain the product **14** as a white solid (1.99 g, 64%). ^{1}H NMR (400 MHz, $CDCl_3$): δ (ppm) = 8.25 (s, 2H), 7.52 (d, 4H, J= 7.6Hz), 6.94 (d, 4H, J= 7.6 Hz), 6.76 (t, 2H, J=7.2 Hz), 6.67 (t, 2H, J=7,2 Hz), 4.35 (d, 4H, J=12.8 Hz), 4.03 (t, 4H, J=6.8 Hz), 3.40 (d, 4H, J=13.2 Hz), 2.89 (t, 4H, J=7.6 Hz), 2.34 (s, 6H), 2.16-2.08 (m, 36H). ^{13}C NMR (75 MHz, $CDCl_3$): δ (ppm) = 153.3, 152.0, 133.3, 128.8, 128.3, 128.1, 125.1, 118.9, 76.5, 31.4, 30.5, 29.9, 29.5, 29.4. MS-ESI (+): m/z (%) = 904 (100) [M+Na]$^+$.

Calix[4]arene (2a). In a 250 mL round bottom flask, **14** (1.5 g, 1.7 mmol) was solubilized in a mixture 1:1 of THF (50 mL) and HCl solution (50mL, 10% v/v in H_2O) and it was stirred at refluxed for 3 days. The reaction mixture was extracted with CH_2Cl_2 (30 mL) and the separated organic phase was washed with H_2O and it was dried over Na_2SO_4. The solvent was removed under reduced pressure and the product **2a** was obtained as a white solid (1.35 g, quant. yield). ^{1}H NMR (300 MHz, $CDCl_3$): δ (ppm) = 8.24 (s, 2H), 7.08 (d, 4H, J= 6 Hz), 6.94 (d, 4H, J=6 Hz), 6.76 (t, 2H, J= 6 Hz), 6.67 (t, 2H, J= 6 Hz), 4.34 (d, 4H, J= 12 Hz), 4.02 (t, 4H, J= 6 Hz), 3.40 (d, 4H, J= 12 Hz), 2.58-2.51 (m, 4H), 2.14-2.07 (m, 4H), 1.76-1.32 (m, 32H). ^{13}C NMR (75 MHz, $CDCl_3$): δ (ppm) = 153.3, 133.4, 128.8, 128.3, 128.1, 125.2, 118.9, 75.6, 31.4, 31.3, 30.1, 29.9, 29.7, 29.5, 29.1, 29.0, 28.5, 26.1, 25.9. MS-ESI (+) m/z (%) = 818 (100) [M+Na]$^+$.

11-(tritylthio)undecan-1-ol (15).[43] In a 100 mL round bottom flask, triphenylmethanethiol (3.3g, 11.9 mmol) was solubilized in a 1:1 mixture toluene/ethanol (30 mL) and a NaOH solution (0.67g, 16.8mmol in 6mL of H_2O) was then added. Subsequently, a solution of 11-bromo-undecenol (3g, 11.9mmol) in 1:1 mixture toluene/ethanol (30 mL) was added dropwise and the reaction mixture was stirred at rt for 6 hours. The mixture was treated with a saturated solution of $NaHCO_3$ (30 mL). The separated organic phase was dried over Na_2SO_4 and evaporated to dryness under reduced pressure. The residue was dissolved in CH_2Cl_2 and purified by filtration over a small plug of silica gel (SiO_2, CH_2Cl_2 100%) to yield the product **15** as a pale-yellow oil (4.7 g, 88%). ^{1}H NMR ($CDCl_3$, 300 MHz): δ (ppm) = 7.42-7.39 (m, 5H), 7.29-7.16 (m, 8H), 3.61 (t, 2H, J = 6.6 Hz), 2.13 (t, 2H, J = 7.2 Hz), 1.57-1.16 (m, 20H).

11-(tritylthio)undecyl 4-methylbenzenesulfonate (16). In a 100 mL two-necked round bottom flask, **15** (4.6 g, 10 mmol) and triethylamine (2.1 ml, 15 mmol) were solubilized in CH_2Cl_2 (30 mL). A solution of TsCl (2.1 g, 11 mmol) in CH_2Cl_2 (20 mL) was added dropwise and DMAP was then added in catalytic quantity. The reaction mixture was stirred at rt overnight. Afterwards, it was washed with H_2O and the

separated organic phase was dried over Na_2SO_4 and it was evaporated to dryness under reduced pressure. The residue was purified by column chromatography (SiO_2, *n*-hexane/CH_2Cl_2 5:5) to yield the product **16** as a yellowish oil (5.88 g, 98%). ^1H NMR ($CDCl_3$, 400 MHz): δ (ppm) = 7.82 (d, 2H, J = 8 Hz), 7.45 (d, 6H, J = 7.6 Hz), 7.38-7.23 (m, 12H), 4.05 (t, 2H, J = 6.4 Hz), 2.47 (s, 3H), 2.17 (t, 2H, J = 7.2 Hz), 1.67-1.64 (m, 2H), 1.44-1.16 (m, 20H).

Calix[6]arene (18). In a Schlenk tube, **17** (1.0 g, 1.02 mmol), **16** (3.68 g, 6.12 mmol), KI (cat. quantity) and K_2CO_3 (0.70 g, 5.1 mmol) were solubilized in anhydrous DMF (50 mL). The heterogeneous reaction mixture was heated at 110°C for 10 days. The solvent was then evaporated under reduced pressure. The solid residue was taken up with CH_2Cl_2 (50 mL) and treated with a HCl solution (30 mL, 10% v/v in H_2O). The separated organic phase was dried over Na_2SO_4 and evaporated to dryness under reduced pressure. The residue was purified by a column chromatography (SiO_2, *n*-hexane/ethyl acetate 9:1) to yield the pure product **18** as a pale yellow solid (0.59 g, 26%). ^1H NMR (400 MHz, $CDCl_3$): δ (ppm) = 7.76 (bs, 6H), 7.48-7.23 (m, 51H), 4.56-4.42 (bs, 6H), 3.89 (bs, 6H), 3.69-3.57 (bs, 6H), 2.92 (s, 9H), 1.91 (t, 6H, J=7.3 Hz), 1.54 (bs, 6H), 1.44-1.00 (m, 53H). ^{13}C NMR (100 MHz, $CDCl_3$): δ (ppm) = 146.8, 145.1, 132.1, 129.9, 129.6, 129.5, 129.3, 128.9, 128.7, 128.3, 128.2, 127.9, 127.7, 127.6, 127.4, 127.3, 127.2, 126.6, 126.4, 126.3, 123.1, 115.3, 73.9, 66.33, 34.2, 32.0, 31.4, 30.2, 31.4, 30.2, 29.7, 29.5, 29.4, 29.2, 29.0, 28.6, 25.0. Mp 100-103°C. MS-ESI (+): m/z (%) = 2288.66 (100) [M+Na]$^+$.

Calix[6]arene (19). In a 250 mL round bottom flask, **18** (0.5 g, 0.22 mmol) and $SnCl_2\cdot2H_2O$ (0.74 g, 3.3 mmol) were dissolved in ethyl acetate (100mL) and the reaction mixture was heated to reflux overnight. The reaction mixture was washed with H_2O (3 x 50 mL). The separated organic phase was dried over Na_2SO_4 and evaporated to dryness under reduced pressure. The resulting white solid was used in the following step without any further purification (0.36 g, 76%).

Calix[6]arene (20).[44] In a 50 mL two-necked round bottom flask, **19** (0.36 g, 0.17 mmol) was dissolved in anhydrous CH_2Cl_2 (30mL) under nitrogen flow. Subsequently, phenyl isocyanate (73 µL, 0.67 mmol) was added and the reaction mixture was stirred at room temperature for 5 hours. The solvent was removed under reduced pressure and the product **20** was isolated by trituration from isopropanol as a white solid (0.16 g, 37%). ^1H NMR (400 MHz, $CDCl_3$): δ (ppm) = 7.41-7.11 (m, 72H), 6.94 (bs, 6H), 4.42 (d, 6H, J = 15.1 Hz), 3.92 (bt, 6H), 3.57 (d, 6H, J = 15.4 Hz), 2.84 (bs, 9H), 2.17 (t, 6H, J = 7.2 Hz), 1.91 (bs, 6H), 1.59 (bs, 6H), 1.42-1.22 (m, 47H). ^{13}C NMR (100 MHz, $CDCl_3$): δ (ppm) = 154.9, 154.4, 152.0, 146.8, 145.0, 138.0, 135.5, 132.9, 132.3, 129.5, 128.8,

128.2, 127.8, 127.7, 127.2, 126.4, 122.5, 120.5, 73.1, 66.3, 60.2, 34.2, 32.0, 31.5, 30.9, 30.5, 29.5, 29.3, 29.1, 28.9, 28.5, 26.2.

Calix[6]arene (21).[44] In a 50 mL two-necked round bottom flask, **20** (80 mg, 0.03 mmol) was solubilized in a 2:1 mixture of anhydrous CH_2Cl_2/trifluoroacetic acid (45 mL) under nitrogen flow. Subsequently, $NaBH_3CN$ (10 mg; 0.16 mmol) was added and the reaction mixture was stirred at rt for 3 hours. The solvent was evaporated to dryness under reduced pressure and the residue was washed with *n*-hexane (2 x 20 mL) to yield a pale yellow solid (58 mg, quant. yield). ^{1}H NMR (400 MHz, $CDCl_3$): δ (ppm) = 7.28-7.12 (m, 27H), 6.30 (bs, 6H), 4.43 (d, 6H, J = 15.4 Hz), 3.93 (t, 6H, J = 6.0 Hz), 3.58 (d, 6H, J = 15.6 Hz), 2.85 (bs, 9H), 2.54 (q, 6H, J = 7.2 Hz), 1.89 (m, 6H), 1.79-1.0 (m, 53H). ^{13}C NMR (100 MHz, $CDCl_3$): δ (ppm) = 154.9, 154.5, 152.3, 146.7, 138.2, 135.7, 133.0, 132.3, 129.4, 129.3, 128.8, 128.7, 128.20, 127.6, 126.2, 123.4, 123.1, 120.5, 73.0, 60.2, 34.1, 34.0, 31.8, 31.5, 31.0, 30.5, 29.6, 29.5, 29.4, 29.3, 29.2, 29.0, 28.8, 28.3, 26.2, 24.6. M.p. = 137-142°C. MS-ESI (+) m/z (%) = 1808.6 (100), 1809.6 (100), 1810.6 (75), 1807.6 (48), 1806.6 (38), 1811.6 (31), 1812.6 (28) [MH]⁺, 1831.6 (100), 1830.6 (88), 1832.6 (65), 1833.6 (35), 1829.6 (32), 1828.6 (27) [M+Na]⁺.

C12NH₂@AgNPs.[22] A solution of dodecylamine (1.5 g) in cyclohexane (50 mL) was stirred for 10 min with an aqueous solution of formaldehyde (37%, 12 mL). The organic phase was separated out and washed twice with water (2 x 50 mL). Then, an aqueous solution of $AgNO_3$ (0.4 g in 20 ml H_2O) was added, left to stir for 40 min. The organic phase was separated and used without further purification in following exchange reactions.

C12S@AgNPs.[22] To the 50 mL of solution of **C12NH₂@AgNPs** in cyclohexane previously prepared,[22] 1-dodecanethiol (0.3 molar eq. of dodecylamine) was added and the reaction was stirred overnight at rt. The organic phase was separated, and the resulting NPs were precipitated by addition of ethanol (50 mL). The suspension was centrifuged at 9000 rpm for 15 minutes. The precipitated **C12S@AgNPs** can be dispersed in CH_2Cl_2.

OAM@CuNPs.[25] In a 100 mL three-necked round bottom flask, previously dried and equipped with condenser, copper acetylactonate, $Cu(acac)_2$, (0.65 g, 0.25 mmol) was dissolved in of phenyl ether (10 mL) and oleylamine, OAM, (12 mL). To this so-called royal blue solution 1,2-tetradecanediol (0.921 g, 4 mmol) was added. The solution was stirred and degassed by three vacuum pump/backfill cycles under Ar. The temperature of the solution was slowly increased (at ∼2 °C/min) over 1 hour to 155 °C and held there for another hour. Afterward, the solution was allowed to cool to rt, and the NPs were precipitated from

phenyl ether by addition of ethanol (50 mL). The suspension was centrifuged at 9000 rpm for 15 minutes. The precipitated **OAM@CuNPs** can be dispersed in toluene (40 mL) for further exchange reactions.

C12S@CuNPs. To the 40 mL of solution of **OAM@CuNPs** in toluene,[25] 1-dodecanethiol (0.21 mL, 1 mmol) was added and the reaction was stirred overnight at rt. The resulting NPs were precipitated by addition of ethanol (80 mL). The suspension was centrifuged at 9000 rpm for 15 minutes. The precipitated **C12S@CuNPs** can be dispersed in CH_2Cl_2.

2a|C12S@AgNPs (general procedure). To an aliquot of **C12NH₂@AgNPs** solution in cyclohexane,[22] a 1:5 mixture solution of 1-dodecanethiol and calix[4]arene **2a** (in total, 0.3 molar eq. of dodecylamine) in CH_2Cl_2 was added. Afterwards, NPs were precipitated by addition of ethanol. The suspension was centrifuged at 9000 rpm for 15 minutes. The precipitated **2a|C12S@AgNPs** can be dispersed in CH_2Cl_2.

References

[1] S. A. Maier, in *Plasmonics: Fundamentals and Applications*, Springer US, New York, NY, **2007**, 109–139.

[2] F. Vetrone, F. Rosei, *Science* **2017**, *357*, 452–453.

[3] E. M. Roller, L. V. Besteiro, C. Pupp, L. K. Khorashad, A. O. Govorov, T. Liedl, *Nat. Phys.* **2017**, *13*, 761–765.

[4] P. Gómez-Romero, C. Sanchez, *Functional Hybrid Materials*, Wiley, **2006**.

[5] R. Banerjee, *Functional Supramolecular Materials : From Surfaces to MOFs*; RSC Publishing, **2017**.

[6] G. Kickelbick, *Hybrid Materials: Synthesis, Characterization, and Applications*, Wiley, **2007**.

[7] S. Connolly, S. N. Rao, R. Rizza, N. Zaccheroni, D. Fitzmaurice, *Coord. Chem. Rev.* **1999**, *185–186*, 277–295.

[8] A. B. Descalzo, R. Martínez-Máñez, F. Sancenón, K. Hoffmann, K. Rurack, *Angew. Chemie Int. Ed.* **2006**, *45*, 5924–5948.

[9] K. Rurack, R. Martínez-Máñez, in *The Supramolecular Chemistry of Organic-Inorganic Hybrid Materials*, Eds. K. Rurack, and R. Martínez-Máñez, John Wiley & Sons, Inc., Hoboken, NJ, USA, **2010**, 689–700.

[10] A. Arduini, D. Demuru, A. Pochini, A. Secchi, *Chem. Commun.* **2005**, 645.

[11] A. Arduini, E. Brindani, G. Giorgi, A. Pochini, A. Secchi, *J. Org. Chem.* **2002**, *67*, 6188–6194.

[12] M. Orda-Zgadzaj, V. Wendel, M. Fehlinger, B. Ziemer, W. Abraham, *European J. Org. Chem.* **2001**, 1549–1561.

[13] T. R. Tshikhudo, D. Demuru, Z. Wang, M. Brust, A. Secchi, A. Arduini, A. Pochini, *Angew. Chemie Int. Ed.* **2005**, *44*, 2913–2916.

[14] L. Guerrini, J. V. Garcia-Ramos, C. Domingo, S. Sanchez-Cortes, *Phys. Chem. Chem. Phys.* **2009**, *11*, 1787–1793.

[15] F. Ciesa, A. Plech, C. Mattioli, L. Pescatori, A. Arduini, A. Pochini, F. Rossi, A. Secchi, *J. Phys. Chem. C* **2010**, *114*, 13601–13607.

[16] A. Boccia, F. D'Orazi, E. Carabelli, R. Bussolati, A. Arduini, A. Secchi, A. G. Marrani, R. Zanoni, *Chem. - A Eur. J.* **2013**, *19*, 7999–8006.

[17] A. Boccia, V. Lanzilotto, R. Zanoni, L. Pescatori, A. Arduini, A.

Secchi, *Phys. Chem. Chem. Phys.* **2011**, *13*, 4444–4451.

[18] A. Arduini, R. Ferdani, A. Pochini, A. Secchi, F. Ugozzoli, *Angew. Chemie - Int. Ed.* **2000**, *39*, 3453–3456.

[19] J. Fink, C. J. Kiely, D. Bethell, D. J. Schiffrin, *Chem. Mater.* **1998**, *10*, 922–926.

[20] B. A. Korgel, D. Fitzmaurice, *Adv. Mater.* **1998**, *10*, 661–665.

[21] M. Brust, M. Walker, D. Bethell, D. J. Schiffrin, R. Whyman, *J. Chem. Soc., Chem. Commun.* **1994**, 801–802.

[22] W. Lewandowski, M. Fruhnert, J. Mieczkowski, C. Rockstuhl, E. Górecka, *Nat. Commun.* **2015**, *6*, 6590.

[23] Y. Chen, X. Wang, *Mater. Lett.* **2008**, *62*, 2215–2218.

[24] Y. Y. Huang, T. Yao, Z. H. Sun, S. Q. Wei, *J. Phys. Conf. Ser.* **2013**, *430*, 012033.

[25] Y. Wei, S. Chen, B. Kowalczyk, S. Huda, T. P. Gray, B. A. Grzybowski, *J. Phys. Chem. C* **2010**, *114*, 15612–15616.

[26] S. Basiruddin, A. Saha, N. Pradhan, N. R. Jana, *J. Phys. Chem. C* **2010**, *114*, 11009–11017.

[27] A. Swami, A. Kumar, M. Sastry, *Langmuir* **2003**, *19*, 1168–1172.

[28] W. Sun, W. Wu, K. M. McMahon, J. S. Rink, C. S. Thaxton, *Part. Part. Syst. Charact.* **2016**, *33*, 300–305.

[29] N. Lala, A. G. Chittiboyina, S. P. Chavan, M. Sastry, *Colloids Surfaces A Physicochem. Eng. Asp.* **2002**, *205*, 15–20.

[30] F. Vita, M. Vorti, G. Orlandini, V. Zanichelli, C. Massera, F. Ugozzoli, A. Arduini, A. Secchi, *CrystEngComm* **2016**, *18*, 5017–5027.

[31] P. R. A. Webber, P. D. Beer, G. Z. Chen, V. Felix, M. G. B. Drew, *J. Am. Chem. Soc.* **2003**, *125*, 5774–5785.

[32] P. R. A. Webber, P. D. Beer, *Dalt. Trans.* **2003**, 2249.

[33] P. K. Jain, W. Huang, M. A. El-Sayed, *Nano Lett.* **2007**, *7*, 2080–2088.

[34] U. Kreibig, M. Vollmer, *Optical Properties of Metal Clusters*, Springer Berlin Heidelberg, **2013**.

[35] S. K. Ghosh, T. Pal, *Chem. Rev.* **2007**, *107*, 4797–4862.

[36] L. Pescatori, A. Boccia, F. Ciesa, F. Rossi, V. Grillo, A. Arduini, A. Pochini, R. Zanoni, A. Secchi, *Chem. - A Eur. J.* **2010**, *16*, 11089–11099.

[37] J. J. González, R. Ferdani, E. Albertini, J. M. Blasco, A. Arduini, A. Pochini, P. Prados, J. De Mendoza, *Chem. - A Eur. J.* **2000**, *6*, 73–80.

[38] F. Vita, A. Boccia, A. G. Marrani, R. Zanoni, F. Rossi, A. Arduini, A. Secchi, *Chem. - A Eur. J.* **2015**, *21*, 15428–15438.

[39] L. Pescatori, A. Arduini, A. Pochini, A. Secchi, C. Massera, F. Ugozzoli, *Org. Biomol. Chem.* **2009**, *7*, 3698.

[40] A. Arduini, A. Pochini, A. Secchi, *Eur. J. Org. Chem.* **2000**, *2000*, 2325–2334.

[41] V. Pejanović, V. Piperski, D. Uglješić-Kilibarda, J. Tasić, M. Dačević, L. Medić-Mijačević, E. Gunić, M. Popsavin, V. Popsavin, *Eur. J. Med. Chem.* **2006**, *41*, 503–512.

[42] A. Arduini, A. Casnati in *Macrocycle Synthesis: A Practical Approach*, Ed.: D. Parker, Oxford University Press, **1996**, 145-173.

[43] F. della Sala, E. R. Kay, *Angew. Chem. Int. Ed.* **2015**, *54* , 4187–4191.

[44] B. Gadenne, I. Yildiz, M. Amelia, F. Ciesa, A. Secchi, A. Arduini, A. Credi, F. M. Raymo, *J. Mater. Chem.* **2008**, *18*, 2022-2027.

CHAPTER 3

Synthesis of Anisotropic Gold Nanoparticles and their Functionalization with Calixarene Derivatives

3.1 Introduction

The increasing use of nanotechnologies has led to a growing interest in nanosciences, disciplines within which the study of the properties of the hybrid organic-inorganic materials is placed. As briefly discussed in the introduction and more extensively in Chapter 2, these materials, in which the constituent parts are combined at the molecular level and thus on a nanometric scale, have interesting novel properties, different from those of the single components, and generally deriving from the phenomenon called as quantum confinement.[1]

The propagation of surface plasmons can be exploited for the construction of plasmonic waveguides, which are devices capable of transporting light below the diffraction limit.[2–5] For example, thin metal plates inserted in a homogeneous dielectric medium can guide surface plasmons over distances of many centimeters with frequencies close to infrared,[6] but the associated fields are weak and confined only in the perpendicular propagation direction. In the opposite case, there are metallic nanowires or waveguides of nanoparticles with transversal confinement modes, lower than the diffraction limit of the surrounding medium, but with significant attenuation losses, obtaining propagation lengths of the order of a few micrometers.[5]

81
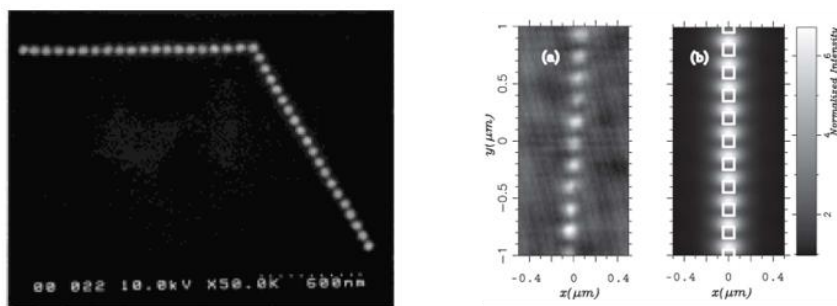
Figure 3.1 *(left) scanning electron microscopy image of a 60° corner in a plasmon waveguide, fabricated using electron beam lithography (adapted from ref. [3], Copyright © 2001 WILEY-VCH Verlag GmbH); (middle) Optical near-field around a one-dimensional arrays of closely spaced Au nanoparticles obtained using collection mode near-field optical microscopy; (right) numerical simulations (adapted from ref. [7], Copyright © 1999 The American Physical Society).*

The direction of propagation of surface plasmons on the interface between a thin metallic layer and a dielectric (even air) can be controlled by scattering two-dimensional waves, creating defects in the metal layer that would otherwise be planar. It is possible to drive electromagnetic waves with transverse confinement lower than the diffraction limit, for

example, with the near field coupling between nanoparticles (Figure 3.1).[7,8]

When more particles are approached, electromagnetic coupling effects are present, and the resonances of the surface plasmons are determined by the collective behavior of the whole system.[9] Generally, there are two different interactions, which differ according to the interparticle distance d: for close particles, $d << \lambda$, where λ is the wavelength of the beam immersed in the surrounding dielectric, the near field interactions are dominant, and the particles can be described as an array of interacting dipole points. However, because of the rapid decrease of the interaction force with distance, this regime is valid for distances between particles lower than about 150 nm. For larger distances, the near field can be neglected, and dipolar coupling occurs mainly through the far-field of diffused light. Thanks to the near field coupling, the nanoparticle array supports two propagation modes, one longitudinal and one transverse, of polarization waves. Due to the resonant excitation at the plasmon resonance frequency, the fields are strongly confined to the waveguide structure.[5] This involves propagation lengths of the order of 1 μm or smaller, depending on the incident wavelength and the dielectric constant of the surrounding material. Longer propagation lengths can be obtained using excitations of non-resonant particles at low frequencies. However, while the absorption losses are minor, the radiative losses begin to overwhelm the routing, and therefore a different approach is needed compared to the one-dimensional chains to be able to maintain the energy confined in the waveguide. A solution to achieve this goal is to consider a waveguide of NPs that is a two-dimensional lattice.[5]

As already mentioned in Chapter 2, to exploit the optical properties of plasmonic nanostructures, it is necessary to exercise control over the aggregation process. The possibility of functionalizing nanostructures such as NPs, or to a lesser extent with NRs, with a large variety of organic monolayers suggests various strategies for their aggregation. For example, it is possible to exploit an aggregation based on the formation of covalent bonds using bidentate thiolate ligands which act as a bridge between two NPs,[10] or by inserting on the surface of the nanoparticles particular functional groups that lead to aggregation through a chemical reaction.[11] This approach has the theoretical advantage of conferring high stability to the aggregates but has the disadvantage of being difficult to control the aggregation degree. Systems of this type show a high propensity to form large aggregates that tend to precipitate, but above all, the aggregation obtained is obviously irreversible. Therefore, it seems more convenient to exploit a spontaneous aggregation process (*self-assembly*) of plasmonic

82

nanostructures based on non-covalent interactions, as described in the previous chapter.

Among the nanostructures to be used for the realization of plasmon waveguides, *gold nanorods* (GNRs) look very enticing because of their shape and optical properties.[12] In fact, these rod-shaped anisotropic nanoparticles possess two characteristic absorption plasmon bands in the UV-Vis-NIR region, corresponding to two different resonance conditions, giving rise therefore to the transversal SPRB (TSPRB) and the longitudinal one (LSPRB) (see Chapter 1, section 1.3). The distance (in terms of the wavelength) between these the maxima of the two bands is closely related to an important parameter, called *Aspect Ratio* (AR). This parameter corresponds to the length to diameter ratio, i.e., the ratio between the transversal axle and the longitudinal one. For this reason, UV-Vis-NIR spectrophotometry is a practical and immediate way to characterize the resulting nanostructures. Most important, the LSPRB can show a significant red-shift with respect to the resonance plasmon of a sphere of the same volume, and the higher is the AR, the greater is the *red-shift* observed (Figure 3.2).[12] Through a controlled chemical synthesis, it is possible to obtain NRs characterized by different AR, to shift the LSPRB up to the NIR region (Figure 3.2).
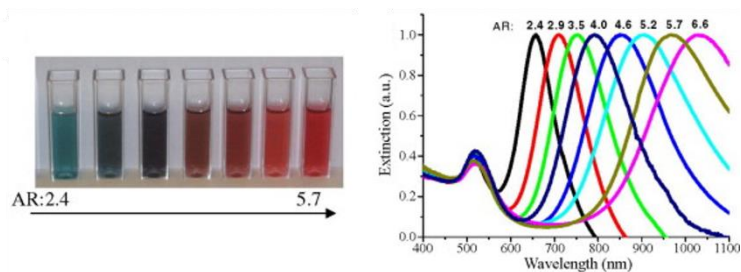
Figure 3.2 *GNRs of different AR exhibit different color of the solution (left) and different SPR wavelength (right).*[13] *Reproduced with permission from ref.* [13] *Copyright © 2009 University of Cairo. All rights reserved.*

These plasmonic optical properties, especially in the NIR region, allow the exploitation of GNRs in several fields of application. As previously discussed in Chapter 1 (see section 1.4.3), recently, several examples were reported concerning the biomedical field, exploiting the GNRs absorption in the region known as the *biological window* (700 – 1300 nm) for applications such as sensing, bioimaging, drug delivery, etc. (Figure 3.3).[14]
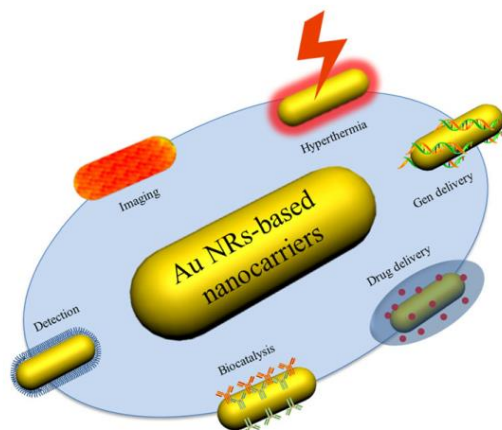
Figure 3.3 *Schematic representation of biomedical applications of GNRs-based nano-carriers. Reproduced from ref. [14] Copyright © Springer Science+Business Media Dordrecht 2013.*

It is also known that NRs show a higher reactivity on the {111} transverse faces, present on their ends with respect to the {100} longitudinal faces.[12,15,16] The covalent or reversible aggregation of GNRs through their minor ends, called *end-to-end*, should also favor the coupling of longitudinal plasmons and, therefore, the formation of a two-dimensional arrangement potentially capable of propagating electromagnetic radiations below the limit of diffraction.

{100}   {111}
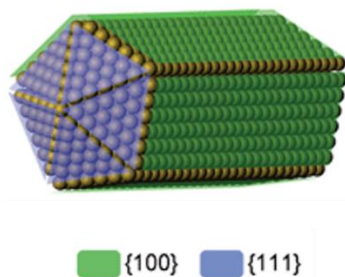
Figure 3.4 *Structural models of gold nanorods, defining the {111} and {100} faces.[17] adapted from ref. [17] Copyright © The Royal Society of Chemistry 2011.*

In this chapter, it will be briefly introduced the synthesis of a series of thiolate calixarene derivatives in the *cone* and 1,3-*alternate* conformations for the covalent functionalization of GNRs. Successively, a series of methods for the preparation of GNRs with AR>5 and characterized by a longitudinal SPRB in the NIR region ($\lambda_{max} > 800$ nm) will be discussed. This part is then followed by the discussion of the attempts made to perform a selective functionalization of the ends of high AR GNRs with the thiolate calixarene derivatives previously synthesized (see also Chapter 2). In the final part of the chapter, the

possibility to make an *end-to-end* controlled aggregation of calixarene-functionalized GNRs is presented.

3.2 Results and discussion

3.2.1 Synthesis of high aspect ratio gold nanorods

The development of reproducible and reliable synthetic methods for the preparation of GNRs with high AR (> 5) and thus characterized by an LSPRB with λ_{max} > 800 nm, was the aim of the first part of this study. Many preparation methods of GNRs are known in the literature. Well-documented are the synthetic methodologies using hard templating agents, where the metal ion precursors are reduced inside pores of a metal oxide (i.e., alumina)[18] or polymeric membranes made of composed of polystyrene and polymethylmethacrylate (diblock copolymers).[19] Equally important and widespread is the so-called *Seed-Mediated Growth* (SMG) method.[20] Such an approach is very enticing since it is a wet-chemical method easily reproducible in the laboratory. It initially involves the preparation of a solution of ~1 nm gold nanoparticles, which act as "seeds" during the growth of the GNRs. These seeds, thanks to the presence of a surfactant such as the cetyltrimethylammonium bromide (CTAB), have more reactive crystalline faces than others and grow in an anisotropic rod-shaped manner.[20,21] Given that the GNRs show two characteristic plasmonic bands (vide supra), the UV-Vis-NIR spectroscopy was used as a practical and immediate characterization method for the prepared nanostructures. TEM measurements were then used to confirm the obtained data.

3.2.1.1 Synthesis of GNRs with AR~3.5 (NR750)

In the literature is reported that the SMG method allows the preparation of GNRs with an AR~3.5 and having the LSPRB centered at ~750 nm, that is at the edge between the visible and NIR region of the electromagnetic spectrum.[22] In few attempts made to reproduce the method, a *seeds* solution was prepared by reduction of the tetrachloroauric acid (HAuCl₄) as the gold precursor with a strong reducing agent such as sodium borohydride (NaBH₄) in the presence of CTAB. This surfactant has a long alkyl chain forming a double layer, with the positively charged "head" (quaternary ammonium salt) towards the metal surface on one side and the other towards the

external water bulk (Figure 3.5). The molar ratios used were indicated in Table 3.1 (see also the experimental part). The *growth* solution that contains the Au(I) precursor was obtained by the reduction *in situ* of HauCl₄ with a mild reducing agent, i.e., ascorbic acid, in the presence of CTAB and AgNO₃ according to the molar ratios shown in Table 3.1. An aliquot of the *seeds* solution was then added to the *growth* solution, and within one hour of stirring at room temperature, the uncolored growth solution turns to an increasingly intense purple color (see the experimental part for further details).
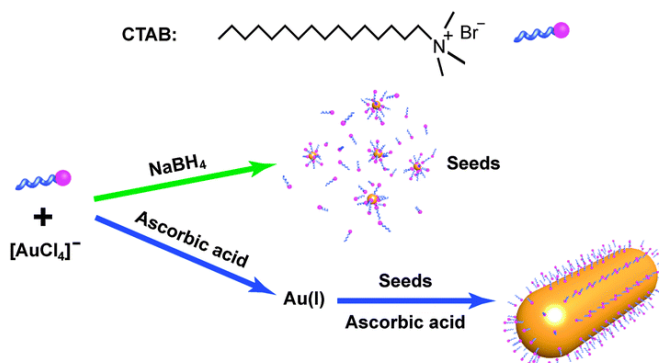

Figure 3.5 *Schematic illustration of the seed-mediated method for the growth of GNRs.*[23] *Reproduced from ref. [23] Copyright © The Royal Society of Chemistry 2013.*

The mechanism by which Ag⁺ ions modify the metal nanoparticle shape is not really understood. It has been hypothesized that Ag⁺ adsorbs at the particle surface in the form of AgBr (Br⁻ coming from CTAB) and allows the growth along the longitudinal direction, i.e., the axis [110].[24] This because preferential adsorption of CTAB to the different crystal faces in a bilayer fashion was suggested. The instability of the {111} faces, less stabilized by the CTAB double layer, also allows the preferential functionalization of these longitudinal endings of the GNRs.

The UV-Vis-NIR spectrum of the resulting GNRs (**NR750**) has been depicted in Figure 3.6. As expected, it presents the two characteristic plasmon band, the transversal one (TSPRB) at ~545 nm, while the longitudinal one (LSPRB) centered at ~780 nm. Nevertheless, the GNRs have impurities, since the two bands have more or less the same intensity, while it would be expected, considering the hypothesized AR, an intensities ratio of about 3 in favor of the LSPRB. The sample impurity was further confirmed by taking several STEM images. As an example, Figure 3.6C evidences that in addition to the expected GNRs, with their typical rod shape, several other nanostructures having different geometries such as spheres, squares, and stars are present in the sample. It was thus necessary to perform a purification procedure of

the resulting sample solution just after the synthesis. The solution containing the mixture of AuNPs and GNRs was initially filtered off through a paper filter to eliminate the excess of CTAB that tends to precipitate from the solution in the form of white crystals. The filtered solution was then centrifuged at 6000 rpm for 30 minutes at room temperature. The supernatant was discarded, and the solid residue dispersed again in distilled water. From the comparison of the UV-Vis-NIR spectra of the sample before and after the purification (Figure 3.6A and B), it is possible to observe a significant reduction of the TSPRB intensity with respect to the LSPRB in the case of the purified sample (Figure 3.6B). The decrease in the intensity of this band, therefore, indicates that through the filtration and ultracentrifugation process, it was possible to eliminate most of the by-product and thus decrease their contribution to the sample absorption spectrum. As a result, the intensities ratio between the two bands changes from ~1 to ~3.8. These results were also confirmed by the comparison between the STEM images of the sample before and after the purification, and depicted in Figure 3.6C and Figure 3.6D. The shot of the purified sample (Figure 3.6D) shows a notable decrease of the nanostructures having a different geometry from that of the nanorods. Thanks to the analysis of these STEM images, it was possible to calculate an average aspect ratio of 3.5 with an average length of ~32 nm.

87
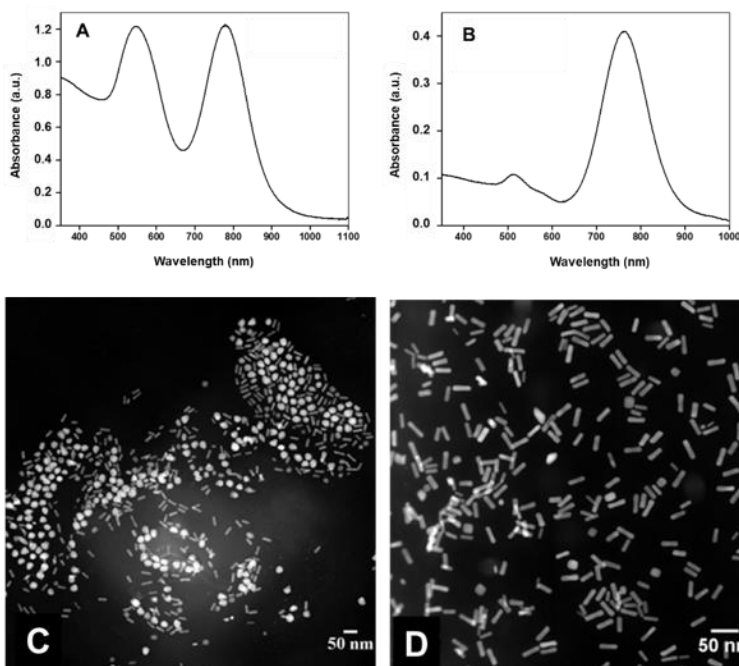
Figure 3.6 *UV-Vis-NIR spectra of water solutions of GNRs with AR ~3.5 before (A) and after (B) the purification procedure; the TEM images were taken on the same samples before (C) and after (D) the samples ultracentrifugation.*

3.2.1.2 Synthesis of GNRs with AR~5.5 (NR900)

To obtain GNRs capable of absorbing at wavelengths higher than 750 nm, it is necessary to increase the AR. Further analysis of the literature revealed that this task could be accomplished by using different molar ratios among the components in the *growth* solution (see Table 3.1) and, most important, by adding another surfactant together with CTAB in the growth solution, that is the benzyldimethylammonium chloride (BDAC).[20]

	NR750	NR900
***Seeds* Solution**	Molar ratio	
HAuCl$_4$ x 3H$_2$O	1	1
CTAB	400	400
NaBH$_4$	2.4	2.4
***Growth* Solution**		
HAuCl$_4$ × 3H$_2$O	1	1
CTAB	199	44
BDAC	–	174
AgNO$_3$	0.2	0.16
Ascorbic Acid	2	1.1

Table 3.1 *Synthesis of gold nanorods with an aspect ratio of 3.5 (**NR750**) and 5.5 (**NR900**).*
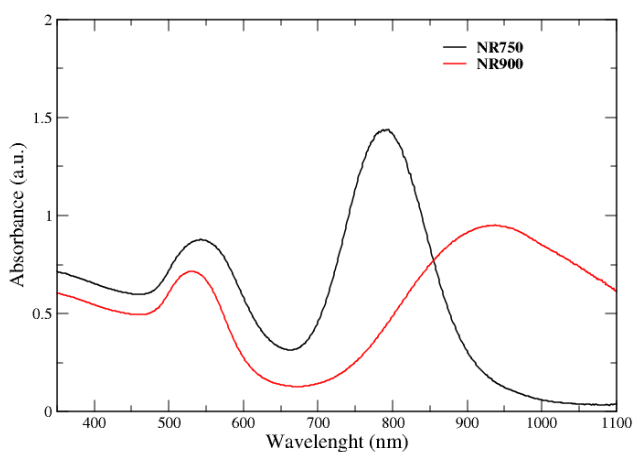

Figure 3.7 *UV-Vis spectrum of water solutions of GNRs **NR900** (red line) and **NR750** (black line).*

The UV-Vis-NIR spectra of the GNRs solutions obtained with the two procedures (after the usual purification step) were depicted in Figure 3.7. It is well-evident the bathochromic shift endured by the LSPRB in the sample in which BDAC was used as co-surfactant (**NR900**). With the instrumentation used for the measurement, it was difficult to correctly estimate the position of the maximum of the LSPRB that, nevertheless, should be around 950 nm, which is well inside the NIR biological window.

As in the case of the **NR750** sample, also this new sample of GNRs was submitted to TEM and STEM measurements (Figure 3.8). The dimensional analysis of the depicted nanostructures evidenced an average *AR* of 10 and an average length of the nanorods of 100 nm.
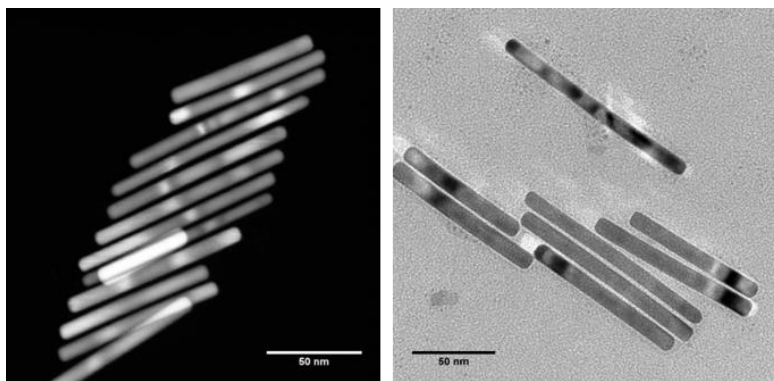

Figure 3.8 *STEM (left) and TEM (right) images of GNRs* **NR900**.

3.2.2   Synthesis of the calix[n]arene hosts

For the functionalization of the GNRs, the calixarene hosts depicted in Figure 3.9 were considered. The synthesis of thiolate calixarene host **Cx4(SH)₂** was already described in Chapter 2 (indicated as compound **2a**), while the synthesis of the dithiolate monophenylureido calix[4]arene **PUCx4(SH)₂** and the tetrathiolate **alt-Cx4(SH)₄** will be dealt in this study. The terminal SH group on the several alkyl chains of all these calixarene hosts would indeed favor their covalent anchoring on the surface of noble metal nanostructures.[25–31]

Host **PUCx4(SH)₂** is blocked in the *cone* conformation and thus possess a preorganized aromatic cavity equipped with an ancillary phenylureido (PU) unit placed on its upper rim. As shown in previous papers on the complexation properties of some 1,3-dipropoxy calix[4]arenes,[32,33]

this potent hydrogen-bond donor group facilitate the complexation of pyridinium-based guest, through a cooperative effect of the "soft" π-rich aromatic cavity of the calixarene that interacts with π-poor pyridinium ring of the guest, and the "hard" H-bond donor group that coordinates the guest halide counteranion. The functionalization of the GNRs with this host would, in principle, favor the end-to-end aggregation of the gold nanorods using a difunctional bis-pyridinium guest.
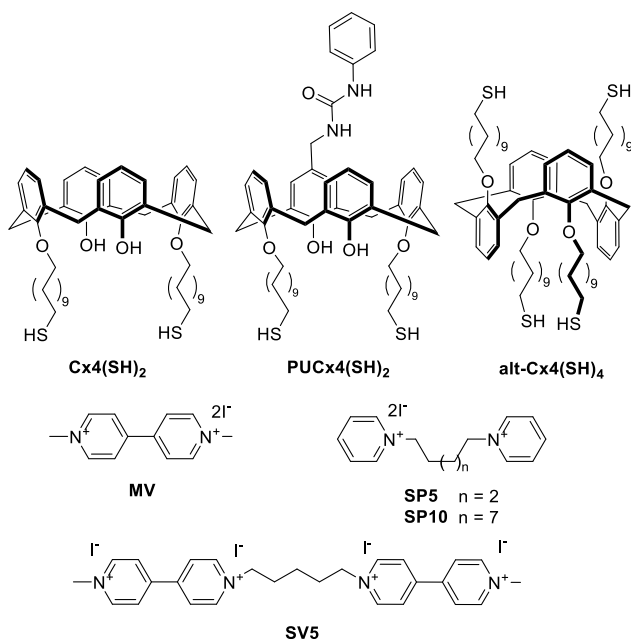

Figure 3.9 *Thiolate calix[4]arene hosts **Cx4(SH)₂**, **PUCx4(SH)₂**, and **alt-Cx4(SH)₄** used for the functionalization of the GNRs {111} faces, and the bifunctional supramolecular linkers **MV**, **SP5-10**, and **SV5** used for the end-to-end aggregation of the GNRs.*

The synthesis of **PUCx4(SH)₂** was accomplished as illustrated in Scheme 3.1. In the first step, the 1,3-(11-acylthio-undecyl)calix[4]arene **1**, whose synthesis was described in Chapter 2, was reacted with *N*-hydroxymethyl phenylurea (**2**) in a Tscherniac-Einhorn amidomethylation reaction promoted by AlCl₃.[34]. The use of a Lewis acid such as AlCl₃ instead of a protic acid (typically CF₃COOH) reduces the hydrolysis of the *S*-acetyl terminal group present on the undecyl chains and favors the regioselective attack of methylene-phenylurea on the more reactive non-alkylated phenolic rings of **1**. A careful choice of the stoichiometric ratio between the reagents (**1** : **2** : AlCl₃ = 1 : 2 : 2) allowed to synthesize the calix[4]arene derivative **3** in 20% yield.
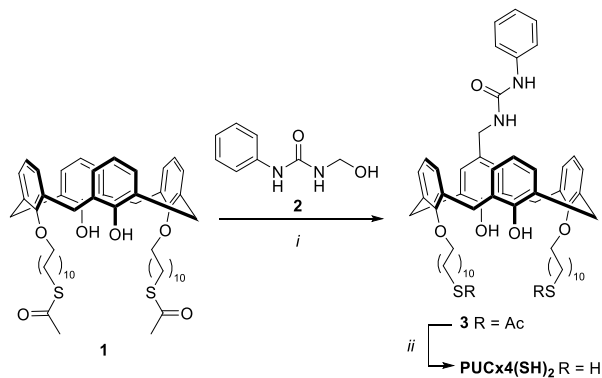
Scheme 3.1 *Synthesis of thiolate calix[4]arene **PUCx4(SH)₂**. Reagents and conditions: i) AlCl₃, CH₂Cl₂, 0 °C, 30 min, then rt, 3h, 20%; ii) NaOEt, THF, rt, 4h, 70%.*

The identity of **3** was confirmed by ¹H and ¹³C NMR spectroscopy in CDCl₃, mass spectrometry ESI-MS, and elemental analysis (see experimental part). The ¹H NMR spectrum in CDCl₃ has been reported in Figure 3.10.

91
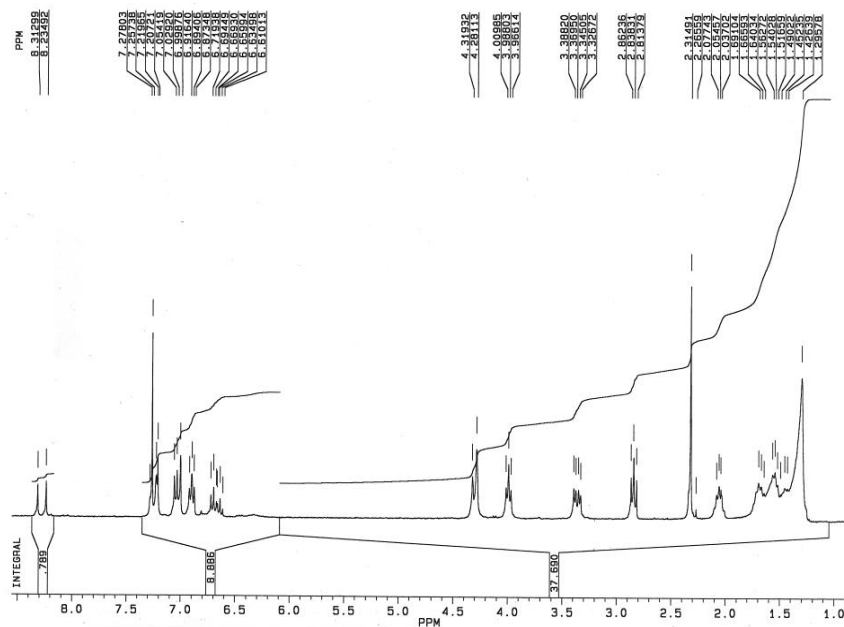
Figure 3.10 *¹H NMR spectrum (CDCl₃, 300 MHz) of calix[4]arene derivative **3**.*

The spectrum shows two singlets at δ = 8.31 and 8.23 ppm in a 1:1 ratio that are diagnostic for the two protons of the phenolic groups: one for the non-substituted phenolic ring and one for the substituted one. The complicated pattern of signals in the aromatic region of the spectrum reflects the presence in the compound of three types of aromatic rings in 1:2:1 ratio. Unlike the symmetric host **Cx4(SH)₂** (see

Chapter 2), which presents a C_{2v} symmetry, the diasterotopic axial and equatorial methylene protons of the asymmetric host **3** give rise to a system of two doublets of doublets at δ = 4.3 ppm (axial) and 3.35 ppm (equatorial). The *dd* system assigned to the axial methylene protons is partially overlapped with a singlet at δ = 4.28 ppm. This singlet is assigned to the protons of the methylene group connecting the phenylurea with an aromatic ring of the calixarene. The presence of a singlet integrating for six protons at δ = 2.31 ppm demonstrates that the two thiol functions of this derivative are still protected with the acyl groups.

In the second step of the synthetic pathway, the thiol functions were deprotected by ethanolysis at room temperature (Scheme 3.1). The deprotection by acid hydrolysis, previously used for **Cx4(SH)₂**, induced in **3** a partial hydrolysis of the phenylurea group. After ethanolysis, the desired host **PUCx4(SH)₂** was recovered in 70% yield after chromatographic purification. Its identity was confirmed by ¹H and ¹³C NMR spectroscopy in CDCl₃, ESI-MS mass spectrometry, and elemental analysis (see experimental part).
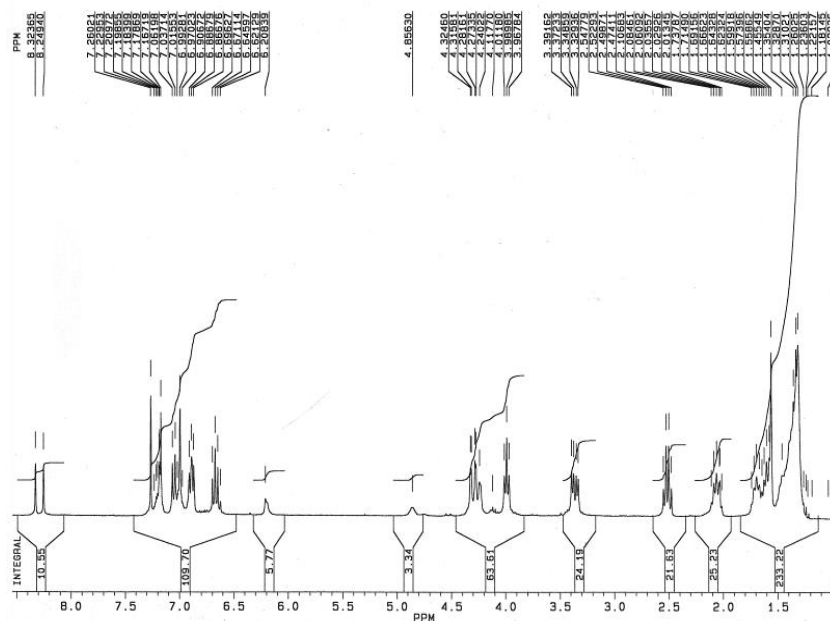
*Figure 3.11 ¹H NMR spectrum (CDCl₃, 300MHz) of **PUCx4(SH)₂**.*

The ¹H NMR spectrum in CDCl₃ (Figure 3.11) of **PUCx4(SH)₂** shows a change of multiplicity of the signal associated with the protons of the two methylene groups in α-position to the sulfur (-C<u>H</u>₂-S-). In **3**, these protons resonate as a triplet at δ = 2.83 ppm (see Figure 3.10), while in **PUCx4(SH)₂** as a quadrupled at δ = 2.51 ppm. The multiplicity change

is due to the coupling of the CH₂ protons with the SH proton. The signal of the latter protons is found at higher fields hidden by more intense aliphatic resonances. The small upfield shift (~0.3 ppm) endured by the above signal is likely due to the loss of the electron-withdrawing effect that was exerted in **3** by the COMe group. In the spectrum of **PUCx4(SH)₂**, the singlet relative to the COMe group, previously found at δ = 2.31 ppm, is correctly disappeared (cf. Figure 3.10 and Figure 3.11).

The calix[4]arene derivative **alt-Cx4(SH)₄** adopts instead a 1,3-*alternate* conformation in which pairs of ω-thioundecanyl chains are placed on opposite sides of the aromatic cavity. This host was designed to promote a covalent linking between the GNRs. To prepare this compound, the synthetic approach described in Scheme 3.2 was used. The calix [4] arene **4** was tetra-alkylated with 11-bromo-1-undecene, used in large stoichiometric excess (10:1), using cesium carbonate (Cs₂CO₃) as the base in DMF. Cesium carbonate, in addition to the deprotonation of the phenolic protons of **4**, favors the blocking of the calix[4]arene macrocycle in the 1,3-alternate conformation.[35] The resulting tetra-alkylated derivative **5** was purified by repeated precipitations in cold *n*-hexane and recovered in 30% yield. Its ¹H NMR in CDCl₃ characterization has been reported in Figure 3.12.

93
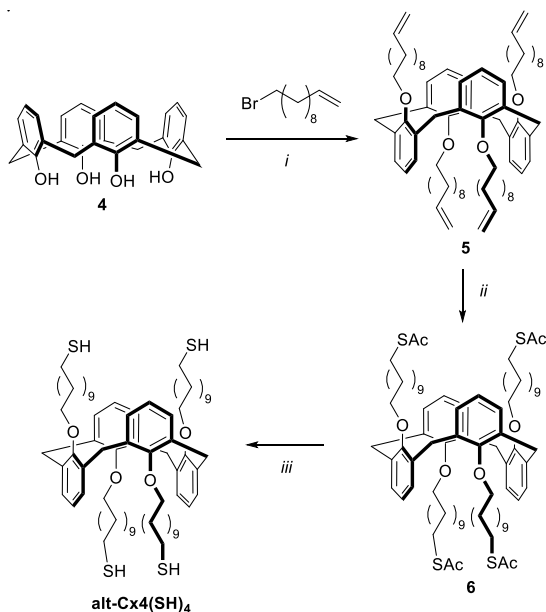
Scheme 3.2 *Synthesis of thiolate calix[4]arene* **alt-Cx4(SH)₄**. *Reagents and conditions: i) Cs₂CO₃, DMF, 80°C, 10 days, 30%; ii) CH₃COSH, AIBN, toluene, reflux, 5h, 78%; iii) HCl 10% v/v, THF, reflux, 72h, quant. yield.*
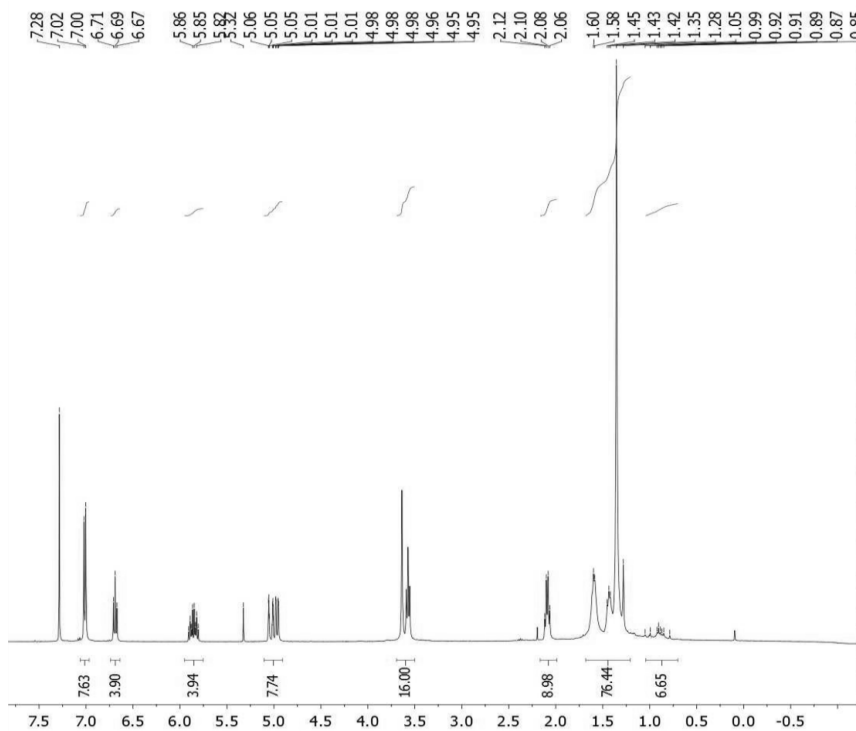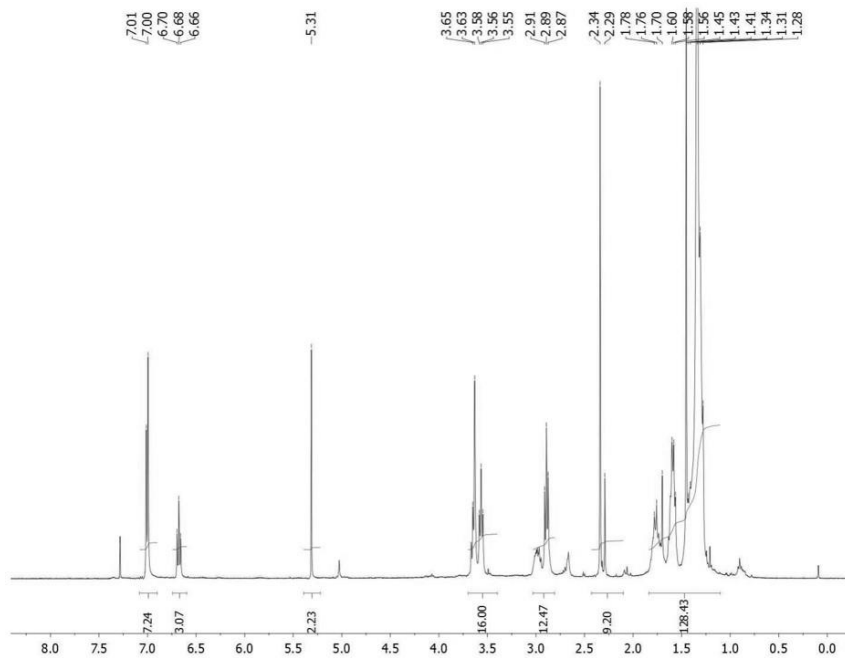
Figure 3.12 *¹H NMR spectrum (400 MHz, CDCl₃) of calix[4]arene derivative 5.*

The diagnostic signals for the successful blocking of macrocycle **5** in the 1,3-alternated conformation are, in addition to the high symmetry of the spectrum, the presence at δ = 3.55 ppm of a singlet integrating for 8 protons. This signal is ascribed to the eight bridging methylene protons between the phenolic rings, which, unlike the case of the calix[4]arene in the *cone* conformation, they are chemically and magnetically equivalent. The effective alkylation of the phenolic hydroxyl groups is evidenced by the intense signals of aliphatic protons at high fields (between 1.20 and 2.0 ppm). At δ = 3.52 ppm it is present a triplet, integrating for eight protons, relative to the methylene groups linked to the phenolic groups. Finally, between 4.8 and 6 ppm, the typical pattern of signals for the four vinyl groups is found: at ca. 5.8–5.9 a multiplet integrating for four protons, and two doublets with *trans* (16 Hz) and *cis* (12 Hz) couplings at δ = 4.97 and 5.0 ppm, each integrating for 4 protons.

In the following synthetic step, the thioacetic function was added to the terminal double bonds of **5** through an anti-Markovnikov radical addition of thioacetic acid, used in large stoichiometric excess, promoted by AIBN as the radical initiator. The thioacetylated derivative **6** was obtained pure in 78% yield by simple evaporation of the solvent under reduced pressure. It was characterized as usual by ¹H and ¹³C NMR

spectroscopy. The ^{1}H NMR spectrum depicted in Figure 3.13 shows the appearance of the diagnostic signals relative to the protecting group: a triplet at δ = 2.88 ppm, for the methylene protons in α to the SCOCH$_3$ unit, and a singlet at δ = 2.36 ppm for the methyl group of the thioacetate. The disappearance of the signals of the alkyl chains terminal unsaturation, confirms the insertion of the thioaceyl functions.


Figure 3.13 ^{1}H NMR spectrum (400 MHz, CDCl$_3$) of calix[4]arene derivative **6**.

Finally, the thiol functions were deprotected by acid hydrolysis. During the chromatographic purification step, however, the target thiolate calix[4]arene **alt-Cx4(SH)$_4$** spontaneously oxidize to give intra- and inter-molecular disulfide bonds and resulting in the formation of insoluble polymers. To overcome this problem, after the hydrolysis step, **alt-Cx4(SH)$_4$** was characterized exclusively by ESI-MS (see experimental part) and used immediately after its deprotection for the functionalization of gold nanostructures.

The possibility to insert calix[6]arene derivatives on the surface of noble metal nanostructures has been already tackled in Chapter 2 where the synthesis of **PUCx6(SH)$_3$** has been discussed. Unfortunately, these previous studies have highlighted the synthetic incompatibility of alkylthiol groups at the lower rim of the calix[6]arene macrocycle and the phenylurea units present on its upper rim, which leads to the obtainment of the above host with very low overall yield. To overcome this problem, the synthesis of the calix[6]arene derivative

PUCx6(NH₂)₃ was designed (Scheme 3.3). This host is functionalized at its lower rim with three alkylamino chains. As will be seen later, these amino-terminal groups can be used for the covalent anchoring of the macrocycle on the surface of gold nanostructures by the formation of amide bonds with lipoic acid molecules previously chemisorbed on the surface of the nanostructures.
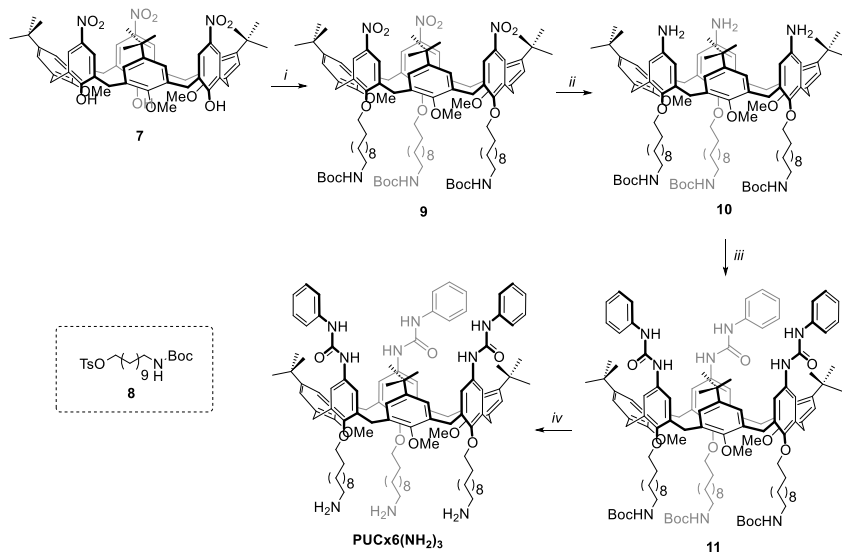
Scheme 3.3 *Synthesis of amino calix[4]arene **PUCx6(NH₂)₃**. Reagents and conditions: i) **8**, K₂CO₃, KI, CH₃CN, 110°C, 10 days, 31%; ii) NH₂-NH₂•H₂O, Pd/C, CH₃OH, reflux, 6h, quant. yield; iii) PhNCO, CH₂Cl₂, rt, 16h, 69%; iv) TFA, CH₂Cl₂, rt, 2h, quant. yield.*

The synthesis of **PUCx6(NH₂)₃** is described in Scheme 3.3. The synthesis of the starting trinitro calix[6]arene **7** was already developed and reported by our research group,[36] while the synthesis of the alkylating agent **8** will be discussed in Chapter 4 (indicated as **L-7**). The alkylation of the phenolic groups of **7** required strong reaction conditions since the reaction must take place, three times, on hydroxyl groups that are made weak nucleophilic by the presence, in the para position, of the electron-withdrawing nitro group. The reaction was carried out in a glass autoclave in refluxing acetonitrile and in the presence of KI and K₂CO₃ as the base. KI was used in catalytic amounts to promote the *in situ* tosylate/iodide exchange. The mixture was reacted for 10 days, and after chromatographic purification, the desired alkylated product **9** was obtained pure in 31% yield. The compound was characterized as usual by ¹H and¹³C NMR spectroscopy and MS-ESI measurements. The nitro groups of **9** were then reduced to amino groups through a catalytic hydrogenation reaction carried out in methanol solution using hydrazine and Pd/C (palladium on carbon) as the catalyst. The reaction took about 6 hours, and it is worth to note

that, even when using hydrazine in place of hydrogen, the Boc protecting group of the lower rim remained unaffected. After the removal of the catalyst by filtration on celite, the desired amino derivative **10** was isolated quite pure by evaporation of the solvent under reduced pressure and used without any further purification in the following step. The insertion of the phenylureido groups on the upper rim of the host was indeed accomplished by reacting compound **10** with phenylisocyanate (PhNCO) in anhydrous CH_2Cl_2 at room temperature for 16 hours. After purification by column chromatography, compound **11** was isolated in 69% yield.

In the ^1H NMR spectrum of **11** in $CDCl_3$ (Figure 3.14), it is possible to recognize several diagnostic signals of the successful condensation reaction. At $\delta = 6.29$ ppm is found a broad signal, integrating for six protons, which is ascribed to the protons of the macrocycle aromatic nuclei bearing the phenylurea groups. The broadness of this signal is indicative of the fluxionality of the macrocycle on the NMR time-scale, while its unusual upfield-shifted resonance is due to the shielding effect exerted by the nearby anisole-type aromatic nuclei. In the pseudo cone conformation adopted by this macrocycle in chloroform solution, the three *N*-phenylureido substituted aromatic nuclei tend to be almost parallel, forming a trigonal prism, while those bearing the tert-butyl groups are bent outward. The AX system of two doublets at $\delta = 4.40$ and 3.58 ppm, coupled with a geminal coupling of 15.5 Hz, also witnesses the pseudo cone conformation adopted by the macrocycle. These signals are assigned to the diasterotopic axial (at lower fields) and equatorial (at higher fields) protons of the methylene groups bridging the six aromatic nuclei of the calixarene skeleton, and by the broad signal relative to the nine methoxy protons at ca. 2.81 ppm. This signal is upfield-shifted of ca. 0.6-0.7 ppm respect with its usual resonance, because, as stated before, the anisole-type aromatic rings are oriented with the methoxy group inward the cavity. Diagnostic is also the presence of another broad signal at $\delta = 4.54$ ppm, which was ascribed to the NH protons of the NHBoc groups present on the macrocycle lower rim. The high and sharp signal relative to the *tert*-butyloxy group of the Boc protecting groups as well of the *tert*-butyl groups on the calix[6]arene upper rim is witnessed by the two high and sharp singlets at $\delta = 1.46$ and 1.31 ppm.

97
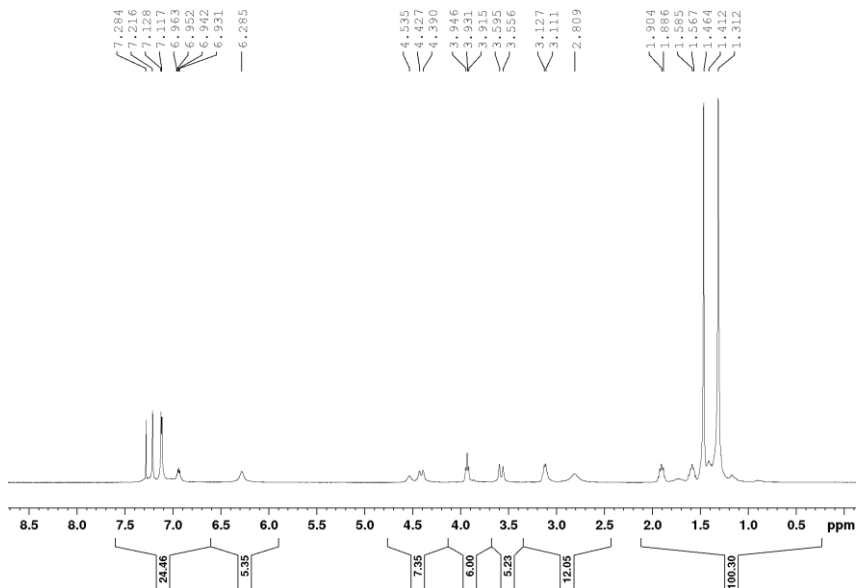
Figure 3.14 *¹H NMR spectrum (CDCl₃, 400 MHz) of the calix[6]arene derivative* **11**.

The last reaction step was the deprotection of the terminal amino groups of the alkyl chains at the lower rim of **11** (Scheme 3.3). The deprotection of the Boc protecting group was accomplished by treating a solution of **11** in CH₂Cl₂ with trifluoroacetic acid (TFA) in the presence of triethyl silane (TES) as the *tert*-butyl scavenger. The desired product **PUCx6(NH₂)₃** was isolated after work-up up to basic condition and characterized by ¹H NMR spectroscopy and ESI-MS.
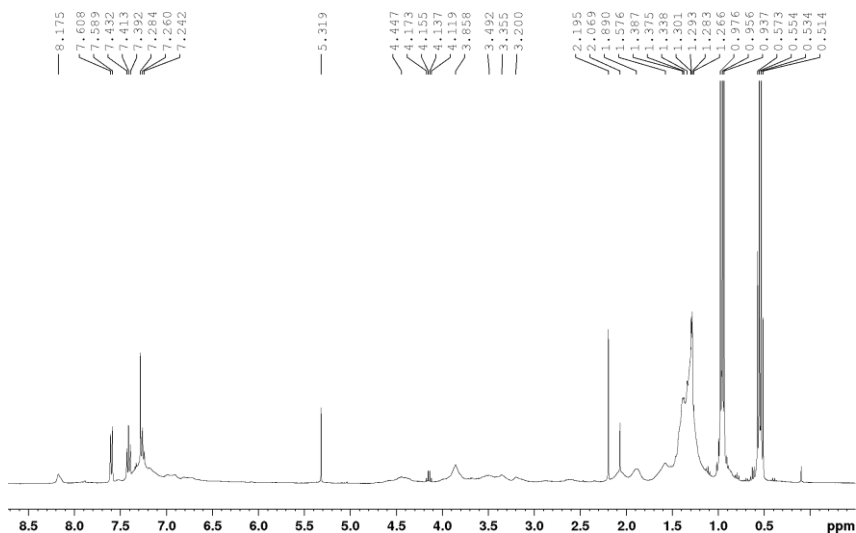
Figure 3.15 *¹H NMR spectrum (CDCl₃, 400 MHz) of the calix[6]arene derivative* **PUCx6(NH₂)₃**.

Despite the overall signals broadness, likely due to extensive aggregation, in the ^{1}H NMR spectrum of **PUCx6(NH$_2$)$_3$** (Figure 3.15), it is possible to observe the disappearance of the singlet at $\delta = 1.31$ ppm, relative to the *t*ert-butyl moiety of the Boc protecting groups (cf. Figure 3.14 and Figure 3.15). The two very intense signals at $\delta = 0.96$ ppm and 0.54 ppm are relative to the impurity of TES, which were not removed during the work-up process. The ESI-MS analysis allowed the identification of the product, showing a signal at m/z = 1757 [M+H]$^+$.

3.2.3 GNRs/calixarenes hybridization

From the literature, it is known that GNRs are preferentially functionalized with thiol-based derivatives on the {111} faces present on their ends (see Figure 3.4).[37] A proper functionalization of the GNRs endings offerings the advantage to obtain a 2D array of aligned nanostructures, and, indeed, this approach has been adopted to promote the *end-to-end* assembly of these nanostructures.[38,39] In these arrays, the coupling of the surface plasmons could allow, in principle, the construction of plasmonic waveguides (see section 3.1).

Considering that GNRs are water-soluble because of their bilayer of CTAB molecules, such functionalization of the nanorods endings is limited to water-soluble thiol derivatives.[38,39] Nevertheless, it is possible to hypothesize the formation of micellar structures exploiting the presence in the water solution of CTAB surfactant molecules, in which the very lipophilic calixarene derivatives can be incorporated. Once dispersed in the solution, the thiol derivative might diffuse inside the nanorods bilayer, thus reaching the reactive {111} faces. To explore the reliability of the latter approach, some preliminary attempts of GNRs endings functionalization were carried out using samples of GNRs indicated as **NR750**, which are characterized by a longitudinal plasmon band at ca. 750nm. The first challenging step was to find the correct amount of calixarene derivative to add to the GNRs solution to promote the exclusive functionalization of the {111} faces. In this context, the first thiolate calix[4]arene used was **alt-Cx4(SH)$_4$**, which is blocked in the 1,3-alternate conformation (see Scheme 3.2). It has a tubular shape exposing two ω-thiolate undecanyl chains on each side. Therefore, this host is suitable to bridge GNRs through the formation of covalent bonds with the {111} faces present on the endings of these nanostructures.
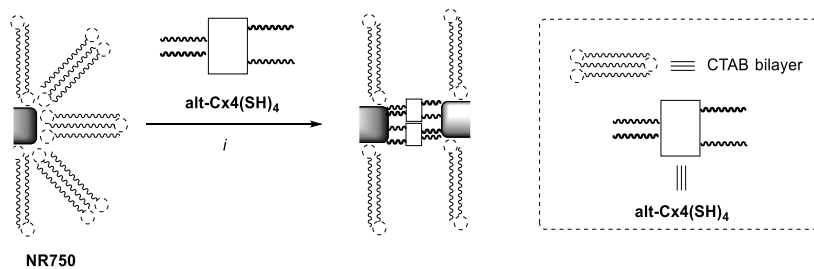
Scheme 3.4 *Schematic synthesis for the hybridization of GNRs* **NR750** *with the calix[4]arene derivative* **alt-Cx4(SH)₄** *as the supramolecular linker. Reagents and conditions: i) water/THF, rt, 4h.*

To this aim, aliquots of 30, 60, 90, and 120 μL of a 0.04 M solution of **alt-Cx4(SH)₄** in THF were added to 2 mL of a water dispersion of GNRs **NR750** to obtain the functionalized GNRs (Scheme 3.4). After each addition, the solution was stirred at room temperature, and a UV-Vis spectrum was recorded to monitor the degree of the GNRs aggregation (Figure 3.16). The collected spectra show that increasing the concentration of **alt-Cx4(SH)₄** solution, a progressive red-shift (~30 nm) of the maximum of the LSPRB (up to 810 nm) is observed. These results seem to suggest that the addition of the thiolate calix[4]arene-based linker led to the formation of increasingly longer GNR chains.

100
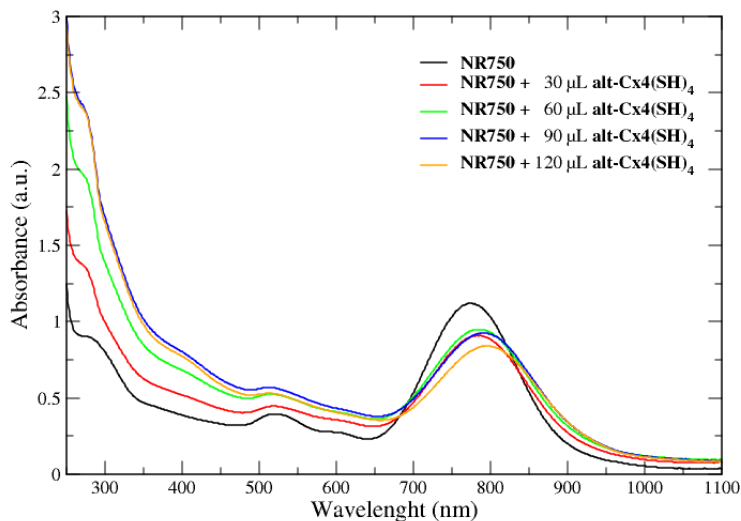
Figure 3.16 *UV-Vis spectra collected during the hybridization experiment of GNRs* **NR750** *with a 0.04 M solution in THF of thiolate calix[4]arene derivative* **alt-Cx4(SH)₄.**

The promising results obtained with GNRs **NR750** prompted us to repeat the hybridization experiment using the GNRs **NR900**, which have a high aspect ratio and a maximum of the LSPRB centered at ~900

nm. As before, two aliquots of 60 and 90 μl of the calix[4]arene derivative solution in THF were added to the GNRs solution, and the aggregation phenomenon was studied through UV-Vis measurements.

The spectra collected in Figure 3.17 clearly show the damping of the longitudinal SPRB and the formation of a weak band at ~670 nm. Unfortunately, the instrumentation at our disposition was not equipped with a detector for the measurements at wavelengths higher than 1100 nm. Therefore, it was not fully disclosed whether the addition of **alt-Cx4(SH)₄** further shifts the LSPRB to lower energy in the NIR region, or it changes the shape of these nanostructures, for example, losing the rod-shaped to give rise to spherical nanostructures.
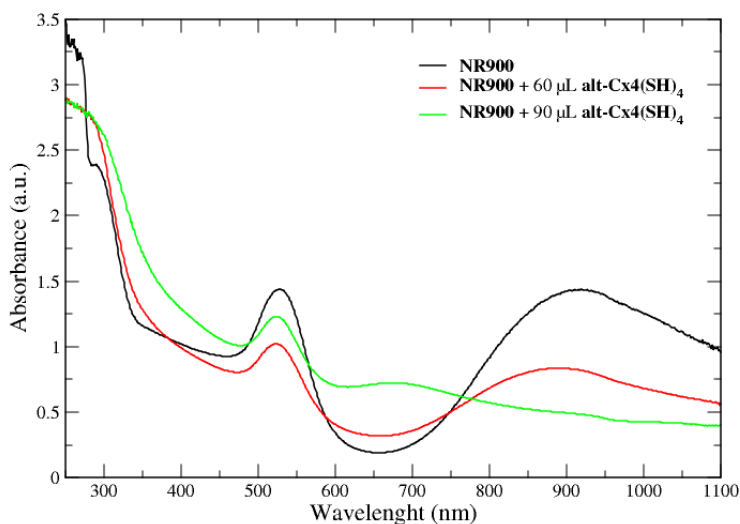

Figure 3.17 *UV-Vis spectra collected during the hybridization experiment of GNRs* **NR900** *with a 0.04 M solution in THF of thiolate calix[4]arene derivative* **alt-Cx4(SH)₄**.

Few drops of the GNRs solution treated with calix[4]arene **alt-Cx4(SH)₄** (and for this reason called **alt-Cx4(SH)₄@NR900**) were transferred on a TEM grid and evaporated to dryness under vacuum. The following STEM measurements in Figure 3.18 revealed the presence in the **alt-Cx4(SH)₄@NR900** sample of short NRs with AR~3.5 along with the expected longer ones (AR > 10). Most important, as depicted in Figure 3.18, several of these GNRs look *end-to-end* enchained. These interesting results deserve to be further investigated.

101
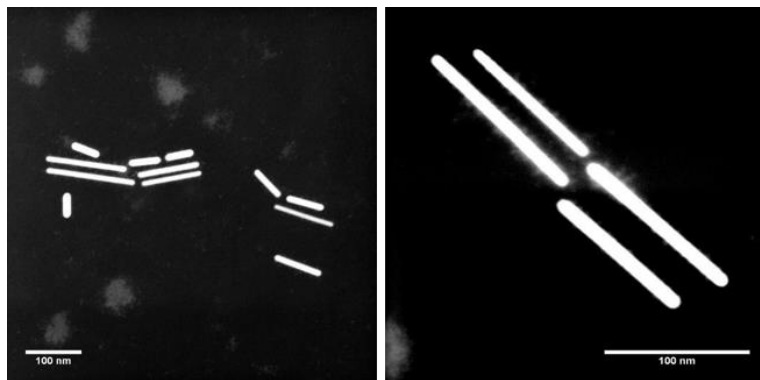
Figure 3.18 *STEM images of* **alt-Cx4(SH)₄@NR900**.

As previously stated (see Chapter 2), a supramolecular approach that exploits non-covalent weak interactions to guide the assembly of GNRs could present some advantages with respect to the covalent networking just discussed. To follow and exploit a supramolecular approach, in particular, a *Strategy II* type in Figure 2.2 in Chapter 2, it is essential to find the proper host/guest partners. The former must be selectively inserted on the {111} faces of GNRs, and the latter has to be a bifunctional guest (supramolecular linker) of proper length and sufficiently rigid to avoid its recognition by host sites present on the same nanostructure. As far as the nature of the interactions guiding the host/guest assembly, we thought that was most important their number more than their intrinsic strength because their co-operativity, a sort of "Velcro effect," should overcome solvation and the loss of entropy of the assembled system. On these premises, we initially chose the thiolate calix[4]arene **Cx4(SH)₂** and **PUCx4(SH)₂** as hosts and a series of bis-pyridinium salts (**MV**, **SP5**, and **SP10**) as the bifunctional guests (Figure 3.9). These host/guest systems have been demonstrated capable of forming 2:1 H⊃G-G⊂H adduct, where H indicates the host and G-G the bifunctional guest.[32]

NR750

Cx4(SH)₄

i
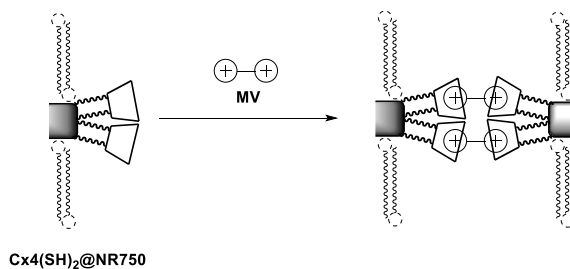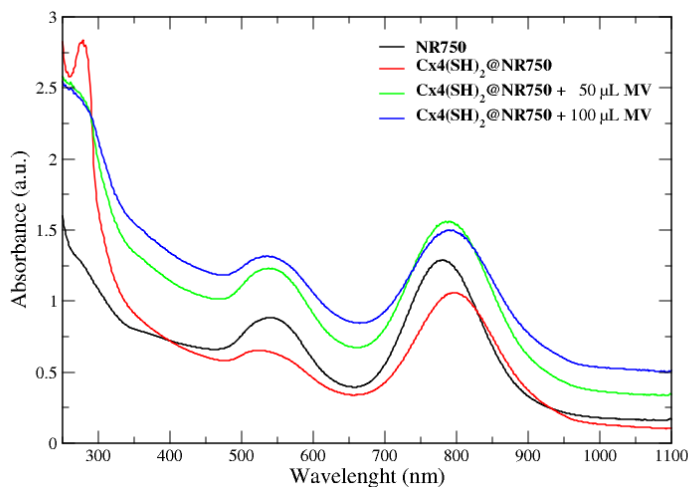
Cx4(SH)₂@NR750

CTAB bilayer
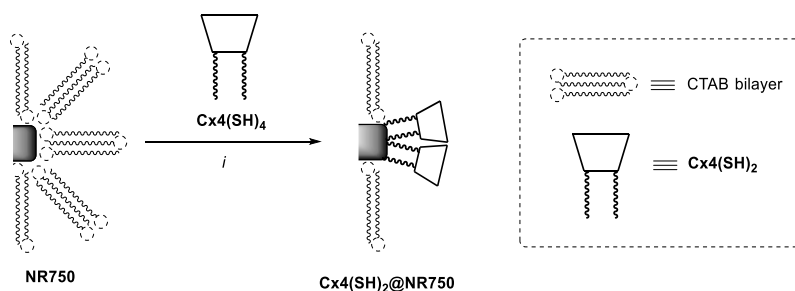
Cx4(SH)₂

Scheme 3.5 *Schematic representation of the synthesis of* **Cx4(SH)₂@NR750**, *obtained through functionalization of GNRs* **NR750** *with the calix[4]arene derivative* **Cx4(SH)₂**. *Reagents and conditions: i) water/THF, rt, 4h.*

After some attempts, satisfying results were obtained by adding several aliquots (30, 50, and 100 μL) of a 7 mM solution of **Cx4(SH)₂** in THF to a 1 mL solution of **NR750** in water (Scheme 3.5). The resulting mixture was kept under magnetic stirring for 4 hours at room temperature, and the course of the GNRs functionalization was monitored by UV-Vis spectroscopy in the 250-1100 nm range (Figure 3.19). For the sake of comprehension, the sample of these hybridized GNRs was indicated as **Cx4(SH)₂@NR750**. As an example, in Figure 3.19, it has been depicted a comparison of the UV-Vis spectra of GNRs **NR750** (black line) and after their hybridization with 30 μL of calix[4]arene **Cx4(SH)₂** solution (red line). It is possible to observe that the hybridization of these nanostructures induces a red-shift of the LSPRB band, whose maximum moves up to ~800 nm. This red-shift is also accompanied by a reduction of the extinction of both SPRBs but is more marked for the transversal one centered at ~525 nm. Such shifts cannot be ascribed to a dilution effect since just 30 μL of calixarene solution were added to 1 mL of nanorods solution. It is more likely due to a change of the nanorods' environment polarity. Much more significative to comment is the appearance of a new band at ~280 nm, which is a characteristic absorption of the aromatic portion of the calix[4]arene derivative. Considering that this compound is not soluble in water in which the GNRs are dispersed, this band indirectly confirms the occurred hybridization with **Cx4(SH)₂** derivative on the surface of the **NR750**.

Another proof of the insertion of **Cx4(SH)₂** on the surface of the GNRs was obtained by the subsequent aggregation studies. To induce GNRs aggregation, a 0.001 M aqueous solution of methyl viologen iodide (**MV**, see Figure 3.9) was used (Scheme 3.6). As witnessed by the spectra depicted with green and blue lines in Figure 3.19, the guest additions determine an enhancement of the extinction of both SPRBs with a broadening of the longitudinal SPRB. The extinctions enhancement is usually ascribed to a coupling of the local fields due to the higher proximity of the plasmonic nanostructures upon aggregation (see the introduction of this chapter). Moreover, the aggregation is witnessed also by the enhancement of the baseline due to the light scattering. It should be noted that the contribution of **MV** to the extinction of the two SPRBs is null since this salt, in water solution, absorbs at a lower wavelength (< 350 nm).[40] The band broadening is instead usually indicative of a loss of size monodispersity with an increment of the light scattering. Therefore, these results were interpreted as deriving from an aggregation of the GNRs that occurs mainly through the endings of these nanostructures on which the thiolate calix[4]arene should likely be grafted.
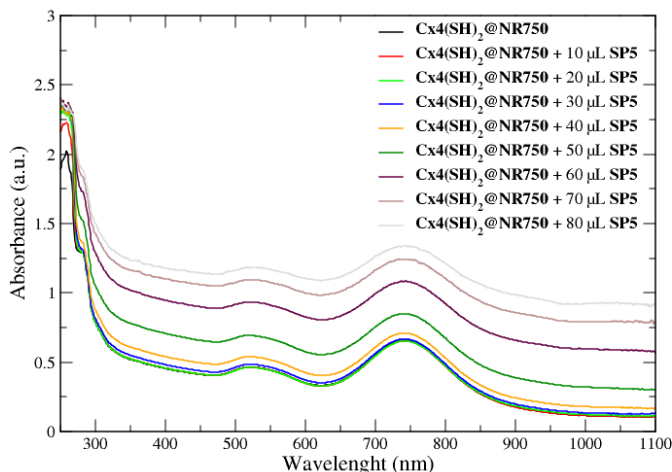
Cx4(SH)₂@NR750

Scheme 3.6 *Aggregation of* **Cx4(SH)₂@NR750** *promoted by the bifunctional guest* **MV** *used as a supramolecular linker.*

Figure 3.19 *UV-Vis spectra of* **NR750**, **Cx4(SH)₂@NR750**, *and of the titration experiment accomplished by adding 50 and 100 µL aliquots of a 0.001 M water solution of methylviologen iodide (* **MV** *).*

The use of a more flexible bifunctional guest than **MV** could allow, in principle, to obtain better control over the GNRs assembly. To this aim, some aggregation on studies were carried out on **Cx4(SH)₂@NR750** using **SP5** and **SP10** as supramolecular linkers In the first experiment, depicted in Figure 3.20, the incremental additions up to 40 µl (blue line) of the **SP5** solution (0.001 M in THF) did not induce an appreciable shift of the two SPRBs. Further additions of the guest solution generate a considerable extinction enhancement of the two bands instead, but still with a no apparent red-shifting. The collection of spectra (not shown) with the normalized extinction at 530 nm, however, shows that the guest addition also induces a considerable broadening of the longitudinal SPRB. Further studies will be required to disclose the observed phenomena.

Figure 3.20 *UV-Vis spectra collected during the titration of a water solution of* **Cx4(SH)₂@NR750** *(black line) with incremental additions of a solution of* **SP5** *(0.001 M in THF).*

In contrast, the additions to the GNRs solution of the longer and more flexible guest **SP10**, which has a C10 alkyl spacer between the pyridinium units, did not induce any apparent effect on the UV-Vis spectrum of these nanostructures (Figure 3.21). These unexpected results were explained considering the higher flexibility and length of guest **SP10** with respect to **SP5**. For this reason, the two guest units of the bifunctional **SP10** could be complexed by two different calixarene hosts on the same GNRs {111} surfaces. Therefore, the result is the saturation of the nearby calixarene recognition sites on the same {111} faces of the GNRs, without any inter-GNRs aggregation.
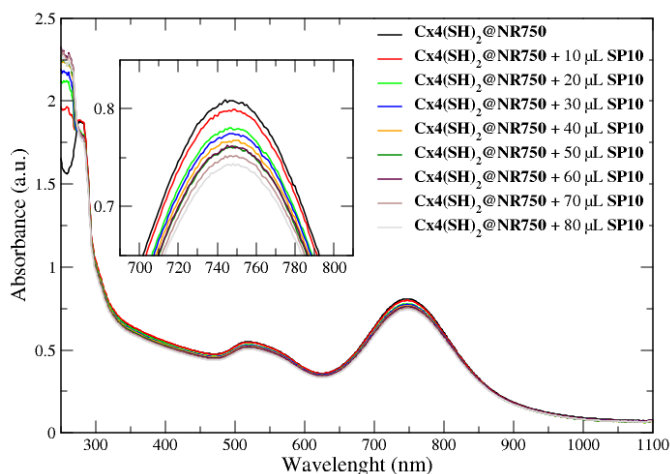
Figure 3.21 *UV-Vis spectra collected during the titration of a water solution of* **Cx4(SH)₂@NR750** *(black line) with incremental additions of a solution of* **SP10** *(0.001 M in THF).*

The second functionalization of the GNRs **NR750** was carried out with the thiolate calix[4]arene derivative **PUCx4(SH)₂** using an experimental procedure identical to the one reported for **Cx4(SH)₂@NR750** (Scheme 3.7). The UV-vis spectra of the GNRs before and after the hybridization were gathered in Figure 3.22. The incremental addition of aliquots of the host solution ($5 \cdot 10^{-3}$ M in THF) induced a blue-shift of the longitudinal plasmonic band to ∼710 nm with an increase of the extinction for both the SPRBs (cf. black and red lines in Figure 3.22). In a preliminary aggregation experiment, the addition of the solution of the difunctional guest **SP10** (0.001 M in THF) induced a further hypsochromic shift of the longitudinal SPRB band.
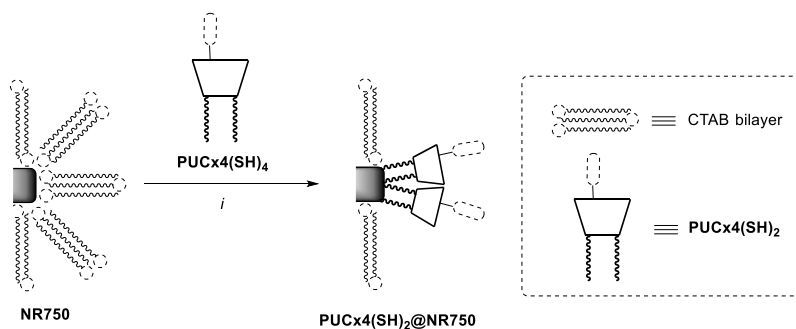
Scheme 3.7 *Schematic synthesis of **PUCx4(SH)₂@NR750**. Reagents and conditions: i) water/THF, rt, 4h.*
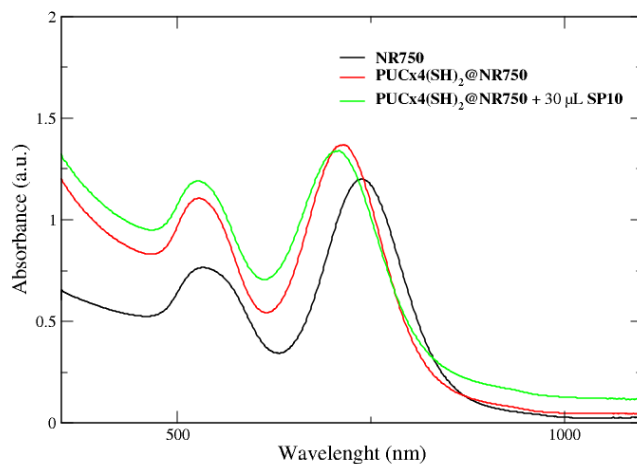
Figure 3.22 *UV-Vis spectra of **NR750**, **PUCx4(SH)₂@NR750**, and titration of the latter with a 10^{-3} M THF solution of **SP10**.*

Because of the difficulty encountered in the synthesis of thiolate tris(*N*-phenylureido) calix[6]arene derivative **PUCx6(SH)₃** (see Chapter 2), to insert this enticing calix[6]arene receptor on the surface of GNRs we used a completely different strategy (Scheme 3.8). The surface of the

GNRs **NR750** endings was initially functionalized with a water solution of lipoic acid (LA),[21] then a solution in a sulfate buffer prepared with a solution of *N*-hydroxysuccinimide and 1-ethyl-3-(3-dimethylaminopropyl)carbodiimmimide (EDC) was added to the solution just prepared. Finally, a solution of **PUCx6(NH₂)₃** was added to the previous resulting mixture. This protocol should promote the formation of amide bonds between the carboxylic acid present in the lipoic acid and the terminal amines of the alkyl chains of the calix[6]arene derivative. The steps of the GNRs functionalization were, as usual, monitored by UV-Vis spectroscopy (Figure 3.23).
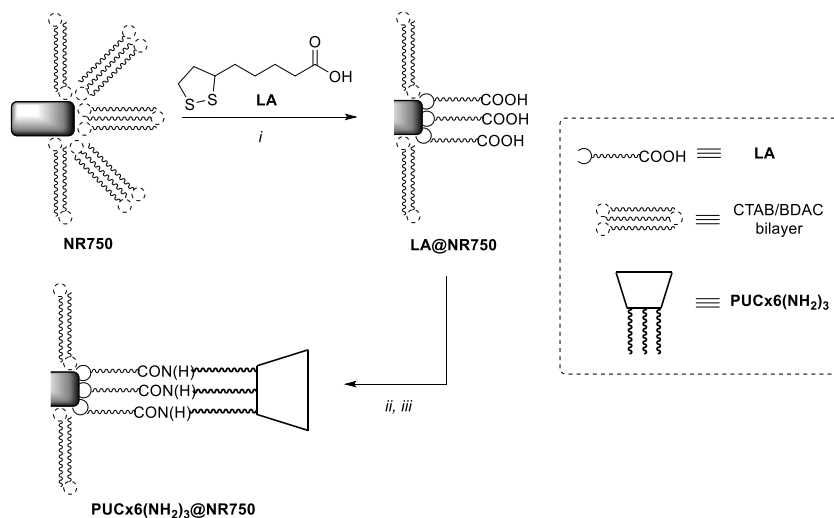
Scheme 3.8 *Functionalization of GNRs with lipoic acid (**LA**) and calix[6]arene derivative* **PUCx6(NH₂)₃**. *Reagents and conditions: i) water/ethanol, rt, 4h; ii) EDC, NHS, water, rt, 30 min; iii)* **PUCx6(NH₂)₃**, *water/THF, rt, 4h.*

Finally, by exploiting the well-established affinity of the cavity of calix[6]arene derivatives towards the *N,N*-dialkylviologen salts,[37] some complexation tests were carried out, monitored by UV-Vis spectroscopy with the bis-viologen salt **SV5** (Figure 3.9). As can be seen from the UV-vis spectra shown in Figure 3.23, a small *redshift* of the longitudinal SPRB band was found (yellow and blue lines): This result suggests a possible complexation between the cavity of **PUCx6(SH)₃** and the two viologen units of **SV5** has occurred. Further studies are underway to improve the methodologies and achieve more accurate characterizations of the aggregated structures.

107
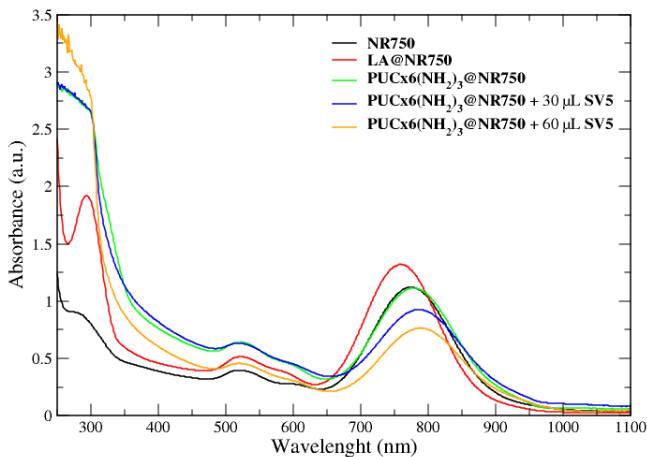
Figure 3.23 *UV-Vis spectra collected during the hybridization experiments between GNRs* ***NR750*** *(black line) with a 0.04 M lipoic acid (LA) solution in THF (red line), followed by the addition of thiolate calix[6]arene derivative* ***PUCx6(SH)₃*** *for the peptide-type coupling (blue line) The spectra indicated with orange and green lines represent the nanorods' aggregation induced by the addition of a 6 mM solution of* ***SV5*** *in water.*

3.3 Experimental Section

All solvents were dried using standard procedures. All other reagents were of reagent-grade quality, obtained from commercial suppliers and were used without further purification. "Brine" refers to a saturated aqueous solution of NaCl. Unless otherwise specified, solutions of common inorganic salts used in workups are aqueous solutions. Reactions were monitored by TLC using 0.25 mm Merck silica gel plates (60 F254). NMR spectra were recorded at 400 and 300 MHz for ^{1}H and 100 and 75 MHz for ^{13}C on a *Bruker Avance* 400 and 300 spectrometers. Chemical shifts (δ) are expressed in ppm using the residual solvent signal as an internal reference. Melting points are uncorrected. Mass spectra were recorded in ESI mode.

17-(N-methylenphenyl-uride)-25,27-bis-[11-(acetylthio)-undecanoxy]-calix[4]arene (**3**). In a 250 mL three-necked round bottom flask, compound **1** (1.78 g, 2.24 mmol) and 1- (hydroxymethyl)-3-phenylurea **2** (0.37 g, 2.24 mmol) were dissolved in anhydrous CH_2Cl_2 (100 mL) under inert atmosphere. The mixture was cooled to 0°C and subsequently $AlCl_3$ (0.75 g, 5.6 mmol) was added. The reaction

mixture was stirred for 30 minutes at 0°C and then for 3 hours at room temperature. The reaction mixture was quenched with the addition of water (100 mL). The organic layer was separated, dried over Na_2SO_4, filtered and evaporated to dryness under reduced pressure. The residue was purified by column chromatography (*n*-hexane/ethyl acetate 7:3) to afford **3** (20%). ^{1}H NMR (300 MHz, CDCl$_3$): δ (ppm) = 8.33 (s, 1H), 8.27 (s, 1H), 7.3-6.6 (4m, 15H), 6.3 (br.s, 1H,), 4.4-4.2 (m, 6H), 3.99 (t, 4H, J = 6.5 Hz), 3.36 (dd, 4H, J = 6.4 Hz, J = 12.9 Hz), 2.84 (t, 4H, J = 7.2 Hz), 2.30 (s, 6H), 2.2-2.0 (m, 4H), 1.8-1.2 (m, 32H). ^{13}C NMR (75 MHz, CDCl$_3$): δ (ppm) = 196.5, 156.1, 153.3, 152.6, 151.9, 138.9, 133.4, 133.3, 129.1, 128.9, 128.7, 128.4, 128.1, 128.0, 125.2, 122.7, 119.7, 119.0 , 76.7, 43.9, 31.4, 31.3, 30.4, 30.0, 29.6, 29.5 (2 resonances), 29.2, 28.8, 25.9. MS-ESI (m/z): 1051 (100) [M+Na]$^+$. M.p. = 45.5-46.5°C. Elemental analysis: calculated = C, 72.37; H, 7.78; N, 2.72; S, 6.22; found = C, 72.10; H, 7.59; N, 2.69; S, 6.06.

PUCx4(SH)$_2$. In a 50 mL two-necked round bottom flask, compound **3** (0.1 g, 0.097 mmol) was dissolved in THF (30 mL) under inert atmosphere. A 0.7 M NaOH solution (10 mL) in ethanol (prepared dissolving 0.4 g of NaOH in 15 mL of absolute ethanol) was added to the mixture and it was stirred at room temperature for 4 hours. The reaction mixture was quenched with water and extracted with ethyl acetate. The separated organic layer was dried over Na_2SO_4, filtrated and evaporated to dryness under reduced pressure to afford **PUCx4(SH)$_2$** as a white solid (70%). ^{1}H NMR (300 MHz, CDCl$_3$): δ (ppm) = 8.32 (s, 1H), 8.25 (s, 1H), 7.3-6.6 (m, 16H), 6.2 (br.s, 1H), 4.9 (br.t, 1H), 4.4-4.2 (m, 6H), 3.99 (t, 4H, J = 6.5 Hz), 3.36 (dd, 4H, J = 6.4 Hz, J = 12.9 Hz), 2.51 (m, 4H), 2.2-2.0 (m, 4H), 1.8-1.2 (m, 16H). ^{13}C NMR (75 MHz, CDCl$_3$): δ (ppm) = 155.6, 153.3, 152.7, 151.9, 138.4, 133.4, 133.2, 129.0, 128.9, 128.7, 128.5, 128.4, 128.1, 128.0, 125.1, 123.5, 120.6, 119.0 , 76.7, 44.1, 34.0, 31.4, 31.3, 29.9, 29.6 (2 resonances), 29.5, 29.4, 29.1, 28.3, 25.9, 24.6. MS-ESI (m/z): 967 (100) [M+Na]$^+$. M.p. = 67.5-68.5 °C. Elemental analysis: calculated = C, 73.72; H, 8.05; N, 2.97; S, 6.78; found = C, 73.53; H, 8.30; N, 2.86; S, 6.71.

25,26,27,28-tetraundecene-calix[4]arene (5). In a 100 mL two-necked round bottom flask, compound **4** (0.5 g, 1.18 mmol) and Cs_2CO_3 (3.84 g, 11.8 mmol) were solubilized in anhydrous DMF (30 mL). The mixture was heated at 80°C for 30 minutes and 11-bromo-1-undecene (1.38 g, 9.44 mmol) was then added and stirred at 80°C for 10 days. The reaction mixture was quenched by the addition of a 10% v/v solution of HCl (50 mL) and extracted with CH_2Cl_2. The organic layer was washed with brine and it was then separated, dried over Na_2SO_4 and evaporated to dryness under reduced pressure. The residue was recrystallize from cold hexane to afford **5** as a white solid (30%). ^{1}H NMR (300 MHz,

CDCl$_3$): δ (ppm) = 7.0 (d, 2H, J = 7.5 Hz), 6.7 (t, 1H, J = 7.5 Hz), 5.9 (ddt, 1H, J = 16.9 - 10.9 - 6.7 Hz), 5 (m, 2H), 3.6 (dd, 2H, J = 20.3 - 13.0 Hz), 2.1 (m, 2H), 1.5 (m, 19H J), 0.9 (m, 3H). ^{13}C NMR (100 MHz, CDCl$_3$): δ (ppm) = 156.5, 139.3, 133.7, 129.7, 121.5, 114.1, 72.1, 33.9, 30.2, 29.7, 29.5, 29.2, 29.0, 26.1

25,26,27,28-tetra-[11-(acetylthio)-undecanossi]-calix[4]arene
(**6**). In a 100 mL two-necked round bottom flask, compound **5** (0.113 g, 0.11 mmol) and thioacetic acid (0.067 g, 87 mmol) were solubilized in anhydrous toluene (50 mL). The solution was degassed for 30 minutes bubbling nitrogen. Subsequently, 2-2'-azobisisobutyrronitrile (AIBN) was added and the reaction mixture was heated to reflux for 5 hours. The mixture was then treated with a saturated aqueous solution of K$_2$CO$_3$, the separated organic phase was washed with H$_2$O, dried over Na$_2$SO$_4$, filtered and evaporated to dryness under reduced pressure to afford **6** as a yellow oil (78% yield). ^{1}H NMR (300 MHz, CDCl$_3$): δ (ppm) = 7.01 (d, 8H, *J* = 7.5 Hz), 6.68 (t, 4H, J = 7.5 Hz), 3.65-3.55 (m, 16H), 2.34 (s, 12H), 1.60-1.28 (m, 72H).

alt-Cx4(SH)$_4$. In a 50 mL two-necked round bottom flask, compound **6** (0.113 g, 0.084 mmol) was dissolved in THF (20 mL). A solution 10% v/v of HCl (20 mL) was the added and the mixture was heated to reflux for 3 days. The reaction was quenched by the addition of water (50 mL) and the organic layer was separated, dried over Na$_2$SO$_4$, filtered and evaporated to dryness under reduced pressure to afford **alt-Cx4(SH)$_4$** as a brown solid (85%). ESI-MS: m/z (%) = 1170.8 (100) [M+H]$^+$.

Calix[6]arene (**9**). In a Schlenk tube, **7** (1.0 g, 1.02 mmol), **8** (2.4 g, 5.3 mmol), KI (30 mg, 0.2 mmol) and K$_2$CO$_3$ (0.70 g, 5.1 mmol) were solubilized in anhydrous CH$_3$CN (70 mL). The heterogeneous reaction mixture was heated at 110°C for 10 days. The solvent was then evaporated under reduced pressure. The solid residue was taken up with CH$_2$Cl$_2$ (50 mL) and treated with a HCl solution (30 mL, 10% v/v in H$_2$O). The separated organic layer was dried over Na$_2$SO$_4$, filtered and evaporated to dryness under reduced pressure. The residue was purified by a column chromatography (SiO$_2$, CH$_2$Cl$_2$/ethyl acetate 97:3) to yield **9** as a pale yellow solid (31%). ^{1}H NMR (400 MHz, CDCl$_3$): δ (ppm) = 7.7 (br.s, 6H), 7.2 (br.s, 6H), 4.3–4.5 (m, 6H), 3.55–3.84 (m, 12H), 3.11 (s, 6H), 2.87 (s, 9H), 1.3–1.9 (m, 11H). ^{13}C NMR (100 MHz, CDCl$_3$): δ (ppm) = 28.44, 29.30, 29.55, 29.70, 30.08, 30.29, 31.49, 34.27, 40.67, 59.62, 60.24, 73.99, 79.03, 123.16, 127.35, 132.17, 135.73, 143.64, 146.82, 156.00. ESI-MS: m/z (%) = 1813 (100) [M+Na]$^+$ 1829 (100) [M+K]$^+$. M.p. = 88-89°C.

Calix[6]arene (**10**). In a 250 mL round bottom flask, **9** (0.57 g, 0.32 mmol), idrazine (1.6 g, 32 mmol) and Pd/C as the catalyst were

solubilized in methanol (100 mL) and the reaction mixture was heated to reflux for 6 hours. The reaction mixture was filtered on celite and the filtrate was concentrated under reduced pressure. The mixture was diluted with CH_2Cl_2 and was washed with water. The separated organic layer was dried over Na_2SO_4, filtered and evaporated to dryness under reduced pressure. The resulting white solid was used in the following step without any further purification (quant. yield).

Calix[6]arene (**11**). In a 50 mL two-necked round bottom flask, **10** (0.22 g, 0.31 mmol) was dissolved in anhydrous CH_2Cl_2 (50mL) under inert atmosphere. Subsequently, phenyl isocyanate (0.52 g, 1.84 mmol) was added and the reaction mixture was stirred at room temperature for 16 hours. The reaction mixture was washed with water and the separated organic layer was dried over Na_2SO_4, filtered and evaporated to dryness under reduced pressure. The residue was purified by a column chromatography (SiO_2, CH_2Cl_2/ethyl acetate 97:3) to yield **11** as a white solid (69%). ^1H NMR (400 MHz, $CDCl_3$): δ (ppm) = 6.93–7.22 (m, 22H), 6.30 (s, 6H), 4.55 (s, 3H), 4.40 (d, 6H, J = 15.6Hz), 3.92 (t, 6H, J =6.5), 3.58 (d, 6H, J = 15.6), 3.1 (m, 6H), 2.86 (s, 9H). ^{13}C NMR (100 MHz, $CDCl_3$): δ (ppm) = 26.28, 26.80, 28.44, 29.28, 29.53, 29.55, 29.57, 29.61, 30.08, 30.29, 31.05, 31.42, 31.52, 34.27, 40.65, 60.22, 73.11, 120.57, 122.87, 123.46, 127.72, 128.70, 128.85, 132.17, 133.05, 135.68, 138.19, 146.81, 152.26, 154.55, 154.98, 156.00. M.p. = 117-118°C.

PUCx6(NH$_2$)$_3$. In a 25 mL round bottom flask, compound **11** (0.04 g, 0.02 mmol) was dissolved in anhydrous CH_2Cl_2 (2 mL). Subsequently, trifluoroacetic acid (0.22 ml, 1.95 mmol) was added and the mixture was stirred at room temperature for 2 hours. The mixture was evaporated to dryness under reduced pressure. The residue was dissolved in CH_2Cl_2, and washed with an aqueous saturated solution of K_2CO_3. The separated organic layer dried over Na_2SO_4, filtered and evaporated to dryness under reduced pressure to afford **PUCx6(NH$_2$)$_3$** as a white impure solid (quant. yield). ^1H NMR (400 MHz, $CDCl_3$): δ (ppm) = 7.3 (br.s., 6H), 7.0 (s, 6H), 6.8 (br.s., 9H), 6.2 (br.s., 6H), 5.3 (br.s., 6H), 4.4 (br.s., 6H), 3.8 (br.s., 17H), 3.5 (br.s., 6H), 2.7 (br.s., 6H), 1.9 (br.s., 12H), 1.6-1.2 (m, 78H). ESI-MS: m/z (%) = 1757 (100) [M+H]$^+$.

NR750. *Preparation of the SEED solution*. In a 50 ml round bottom flask, cetyltrimethylammonium bromide (CTAB) (0.364 g, 1 mmol) was dissolved in water (5 mL) at 28°C, a 4.57 mM HAuCl$_4$ water solution (0.55 mL) was then added. Afterward, a 10 mM NaBH$_4$ solution (0.60 mL, freshly prepared and kept at 0°C by dissolving 38 mg in 100 mL of water), was added and the mixture was vigorously stirred still at 28°C for 2 minutes and left without stirring for 5 minutes at 28°C. The solution turns from colorless to yellow to brown. *Preparation of the GROWTH solution*. In a 50 ml round bottom flask,

cetyltrimethylammonium bromide (CTAB) (0.364 g, 1 mmol) was dissolved in water (5 mL) at 28°C, a 40 mM $AgNO_3$ solution (25 µL, prepared by dissolving 0.0679 g in 10 mL of water) was then added, followed by the addition of a 4.57 mM $HAuCl_4$ water solution (1.1 mL) and a 0.1 M ascorbic acid solution (100 µL, prepared by dissolving 0.176 g in 10 mL of water) in this order. 12 µL of previously prepared *SEED* solution were added to this latter *GROWTH* solution and the mixture was vigorously stirred for 10 seconds and then kept at 28°C for 1 hour without stirring. The color of the solution turned to intense purple. **UV–Vis** = 550 nm (TPB), 790 nm (LPB).

NR850. *Preparation of the SEED solution*. In a 50 ml round bottom flask, cetyltrimethylammonium bromide (CTAB) (0.364 g, 1 mmol) was dissolved in water (5 mL) at 28°C, a 4.57 mM $HAuCl_4$ water solution (0.55 mL) was then added. Afterward, a 10 mM $NaBH_4$ solution (0.60 mL, freshly prepared and kept at 0°C by dissolving 38 mg in 100 mL of water), was added and the mixture was vigorously stirred still at 28°C for 2 minutes and left without stirring for 5 minutes at 28°C. The solution turns from colorless to yellow to brown. *Preparation of the GROWTH solution*. In a 50 ml round bottom flask, cetyltrimethylammonium bromide (CTAB) (0.08 g, 0.22 mmol) and benzyldimethylhexadecylammonium chloride (BDAC) (0.297 g, 0.75 mmol) were dissolved in water (5 mL) at 28°C, a 40 mM $AgNO_3$ solution (20 µL, prepared by dissolving 0.0679 g in 10 mL of water) was then added, followed by the addition of a 4.57 mM $HAuCl_4$ water solution (1.1 mL) and a 0.1 M ascorbic acid solution (55 µL, prepared by dissolving 0.176 g in 10 mL of water) in this order. 12 µL of previously prepared *SEED* solution were added to this latter *GROWTH* solution and the mixture was vigorously stirred for 10 seconds and then kept at 28°C for 1 hour without stirring. The color of the solution turned to intense purple. **UV-Vis** = 550 nm (TPB), 900 nm (LPB).

Cx4(SH)₂@NR750. In three 25 mL round bottom flasks were added 2 mL, respectively, of **NR750** solution. To these latter solutions, 30, 50 and 100 µL of a 6.74 mM **Cx4(SH)₂** solution in THF were respectively added. The three mixtures were stirred for 4 hours at room temperature.

PUCx4(SH)₂@NR750. In three 25 mL round bottom flasks were added 2 mL, respectively, of **NR750** solution. To these latter solutions, 30, 50 and 100 µL of a 5.20 mM **PUCx4(SH)₂** solution in THF were respectively added. The three mixtures were stirred for 4 hours at room temperature.

alt-Cx4(SH)₄@NR750. In three 25 mL round bottom flasks were added 2 mL, respectively, of **NR750** solution. To these latter solutions, 30, 60, 90 and 100 μL of a 41.4 mM **alt-Cx4(SH)₄** solution in THF were respectively added. The four mixtures were stirred for 4 hours at room temperature.

LA@NR750. In a 25 mL round bottom flask, 7 mL of **NR750** solution were added. To this latter solution, 100 μL of a 1 mM lipoic acid (**LA**) solution (prepared by dissolving 21 mg in 100 mL of ethanol) were added and the mixture was stirred at room temperature for 4 hours. Ultracentrifugation was performed at 5000 rpm for 10 minutes to remove the precipitated unbound species. The supernatant solution contains **LA@NR750**.

PUCx6(NH₂)₃@NR750. A 10 mM buffer solution was prepared by dissolving 11.5 mg of NHS and 19.2 mg of EDC in 10 mL of water. 1 mL of this buffer solution was added to the resulting supernatant solution of **LA@NR750** and the mixture was stirred at room temperature for 30 minutes. 2 mL of the resulting solution was taken up and a 4.41 mM THF solution of **PUCx6(NH₂)₃** (100 μL) was added to this portion. The mixture was stirred at room temperature for 4 hours.

References

[1] G. N. Blackman, D. A. Genov, *Phys. Rev. B* **2018**, *97*, 115440-115450.

[2] E. Ozbay, *Science* **2006**, *311*, 189–193.

[3] S. A. Maier, M. L. Brongersma, P. G. Kik, S. Meltzer, A. A. G. Requicha, H. A. Atwater, *Adv. Mater.* **2001**, *13*, 1501–1505.

[4] D. K. Gramotnev, S. I. Bozhevolnyi, *Nat. Photonics* **2010**, *4*, 83–91.

[5] S. A. Maier, P. G. Kik, H. A. Atwater, S. Meltzer, E. Harel, B. E. Koel, A. A. G. Requicha, *Nat. Mater.* **2003**, *2*, 229–232.

[6] M. Kadic, G. Dupont, S. Enoch, S. Guenneau, *Phys. Rev. A* **2014**, *90*, 043812.

[7] J. R. Krenn, A. Dereux, J. C. Weeber, E. Bourillot, Y. Lacroute, J. P. Goudonnet, G. Schider, W. Gotschy, A. Leitner, F. R. Aussenegg, et al., *Phys. Rev. Lett.* **1999**, *82*, 2590–2593.

[8] S. A. Maier, H. A. Atwater, *J. Appl. Phys.* **2005**, *98*, 011101.

[9] W. Rechberger, A. Hohenau, A. Leitner, J. R. Krenn, B. Lamprecht, F. R. Aussenegg, *Opt. Commun.* **2003**, *220*, 137–141.

[10] I. Hussain, Z. Wang, A. I. Cooper, M. Brust, *Langmuir* **2006**, *22*, 2938–2941.

[11] G. A. DeVries, M. Brunnbauer, Y. Hu, A. M. Jackson, B. Long, B. T. Neltner, O. Uzun, B. H. Wunsch, F. Stellacci, *Science* **2007**, *315*, 358–361.

[12] J. Pérez-Juste, I. Pastoriza-Santos, L. M. Liz-Marzán, P. Mulvaney, *Coord. Chem. Rev.* **2005**, *249*, 1870–1901.

[13] X. Huang, M. A. El-Sayed, *J. Adv. Res.* **2010**, *1*, 13–28.

[14] X. Wang, M. Shao, S. Zhang, X. Liu, J. *Nanoparticle Res.* **2013**, *15*, 1892-1908.

[15] N. D. Burrows, W. Lin, J. G. Hinman, J. M. Dennison, A. M. Vartanian, N. S. Abadeer, E. M. Grzincic, L. M. Jacob, J. Li, C. J. Murphy, *Langmuir* **2016**, *32*, 9905-9921.

[16] N. D. Burrows, A. M. Vartanian, N. S. Abadeer, E. M. Grzincic, L. M. Jacob, W. Lin, J. Li, J. M. Dennison, J. G. Hinman, C. J. Murphy, *J. Phys. Chem. Lett.* **2016**, *7*, 632–641.

[17] K. Liu, N. Zhao, E. Kumacheva, *Chem. Soc. Rev.* **2011**, *40*, 656–671.

[18]   C. R. Martin, *Chem. Mater.* **1996**, *8*, 1739–1746.

[19]   J. Shi, S. Gider, K. Babcock, D. D. Awschalom, *Science* **1996**, *271*, 937–941.

[20]   B. Nikoobakht, M. A. El-Sayed, *Chem. Mater.* **2003**, *15*, 1957–1962.

[21]   J.-Y. Chang, H. Wu, H. Chen, Y.-C. Ling, W. Tan, *Chem. Commun.* **2005**, 1092-1094.

[22]   F. Ratto, P. Matteini, F. Rossi, R. Pini, J. *Nanoparticle Res.* **2010**, *12*, 2029–2036.

[23]   H. Chen, L. Shao, Q. Li, J. Wang, *Chem. Soc. Rev.* **2013**, *42*, 2679–2724.

[24]   N. R. Jana, L. Gearheart, C. J. Murphy, *J. Phys. Chem. B* **2001**, *105*, 4065–4067.

[25]   A. Arduini, D. Demuru, A. Pochini, A. Secchi, *Chem. Commun.* **2005**, 645-647.

[26]   T. R. Tshikhudo, D. Demuru, Z. Wang, M. Brust, A. Secchi, A. Arduini, A. Pochini, *Angew. Chemie Int. Ed.* **2005**, *44*, 2913–2916.

[27]   L. Pescatori, A. Boccia, F. Ciesa, F. Rossi, V. Grillo, A. Arduini, A. Pochini, R. Zanoni, A. Secchi, *Chem. - A Eur. J.* **2010**, *16*, 11089–11099.

[28]   F. Ciesa, A. Plech, C. Mattioli, L. Pescatori, A. Arduini, A. Pochini, F. Rossi, A. Secchi, *J. Phys. Chem. C* **2010**, *114*, 13601–13607.

[29]   A. Boccia, F. D'Orazi, E. Carabelli, R. Bussolati, A. Arduini, A. Secchi, A. G. Marrani, R. Zanoni, *Chem. - A Eur. J.* **2013**, *19*, 7999–8006.

[30]   F. Vita, A. Boccia, A. G. Marrani, R. Zanoni, F. Rossi, A. Arduini, A. Secchi, *Chem. - A Eur. J.* **2015**, *21*, 15428–15438.

[31]   F. Vita, A. Arduini, A. Secchi, in *Calixarenes and Beyond*, Eds: P. Neri, J. L. Sessler, M.-X. Wang, Springer, **2016**, 941–963.

[32]   L. Pescatori, A. Arduini, A. Pochini, A. Secchi, C. Massera, F. Ugozzoli, *Org. Biomol. Chem.* **2009**, *7*, 3698-3708.

[33]   F. Vita, M. Vorti, G. Orlandini, V. Zanichelli, C. Massera, F. Ugozzoli, A. Arduini, A. Secchi, *CrystEngComm* **2016**, *18*, 5017–5027.

[34]   A. Arduini, E. Brindani, G. Giorgi, A. Pochini, A. Secchi, *Tetrahedron* **2003**, *59*, 7587–7594.

[35] C. D. Gutsche, *Calixarenes* Revisited, Royal Society Of Chemistry, Cambridge, **1998**.

[36] J. J. González, R. Ferdani, E. Albertini, J. M. Blasco, A. Arduini, A. Pochini, P. Prados, J. De Mendoza, *Chem. - A Eur. J.* **2000**, *6*, 73–80.

[37] L. Vigderman, B. P. Khanal, E. R. Zubarev, *Adv. Mater.* **2012**, *24*, 4811–4841.

[38] K. K. Caswell, J. N. Wilson, U. H. F. Bunz, C. J. Murphy, J. Am. *Chem. Soc.* **2003**, *125*, 13914–13915.

[39] K. G. Thomas, S. Barazzouk, B. I. Ipe, S. T. S. Joseph, P. V. Kamat, *J. Phys. Chem.* B **2004**, *108*, 13066–13068.

[40] J. Ma, Q. Meng, X. Hu, B. Li, S. Ma, B. Hu, J. Li, X. Jia, C. Li, *Org. Lett.* **2016**, *18*, 5740–5743.

[41] V. Pejanović, V. Piperski, D. Uglješić-Kilibarda, J. Tasić, M. Dačević, L. Medić-Mijačević, E. Gunić, M. Popsavin, V. Popsavin, *Eur. J. Med. Chem.* **2006**, *41*, 503–512.

[42] A. Arduini, A. Casnati in *Macrocycle Synthesis: A Practical Approach*, Ed.: D. Parker, Oxford University Press, **1996**, 145-173.

[43] J. Fink, C. J. Kiely, D. Bethell, D. J. Schiffrin, *Chem. Mater.* **1998**, *10*, 922–926.
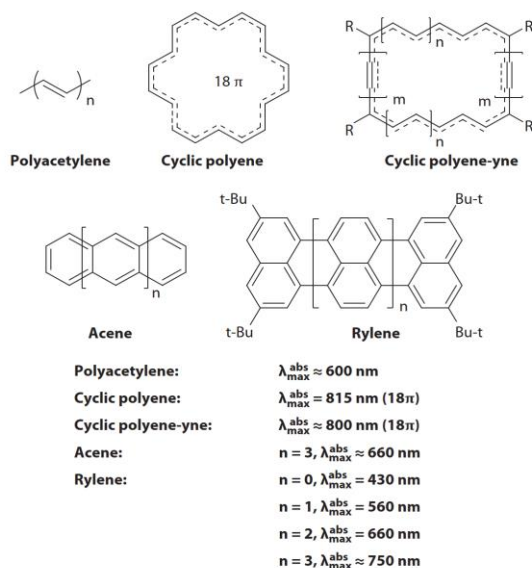
CHAPTER 4
Synthesis of NIR-harvesting functional dyes

4.1 Introduction

4.1.1 NIR Dyes

In recent years there has been a growing interest in the synthesis of organic chromophores capable of absorbing in the near-infrared (NIR) region of the electromagnetic spectrum typically between 780 and 2500 nm.[1] The optical and electronic properties of these organic molecules are determined by their *energy gap*, which is the separation in energy between their highest occupied molecular orbital (HOMO) and their lowest unoccupied one (LUMO), also called as *HOMO-LUMO gap* (HLG). This aspect is fundamental in the construction of organic materials with high optical absorption and often involves structural chemical changes at the molecular level. In particular, to get a red-shift in the absorption spectrum (towards the NIR in fact), it is necessary to decrease the HLG and, to this aim, several factors must be taken into consideration. Typically, the organic materials that absorb in the NIR region, more commonly known as *NIR dyes*, contain chromophores having an extensive π-conjugation (Figure 4.1).[1]

Polyacetylene: $\lambda_{max}^{abs} \approx 600$ nm
Cyclic polyene: $\lambda_{max}^{abs} = 815$ nm (18π)
Cyclic polyene-yne: $\lambda_{max}^{abs} \approx 800$ nm (18π)
Acene: $n = 3$, $\lambda_{max}^{abs} \approx 660$ nm
Rylene: $n = 0$, $\lambda_{max}^{abs} = 430$ nm
$n = 1$, $\lambda_{max}^{abs} = 560$ nm
$n = 2$, $\lambda_{max}^{abs} = 660$ nm
$n = 3$, $\lambda_{max}^{abs} \approx 750$ nm

Figure 4.1 Examples of highly π-conjugated systems. Reproduced from ref. [1] Copyright © 2013 by Taylor & Francis Group, LLC.

The most straightforward π-conjugate system is represented by the class of trans-polyacetylenes (Figure 4.1). If these compounds are cyclized, they are called π-conjugated cyclic polyenes, and benzene can be considered as the simplest and smallest molecule of this class.

Another strategy used to extend the π conjugation can, for example, be the increase in the number of benzene rings that can be fused to form compounds called *acenes* (see Chapter 5). This class of compounds shows a progressive *red-shift* of their main absorption band as the number of fused rings increases. The main disadvantage of these compounds, however, remains their synthesis, especially when a high number of fused rings is required.
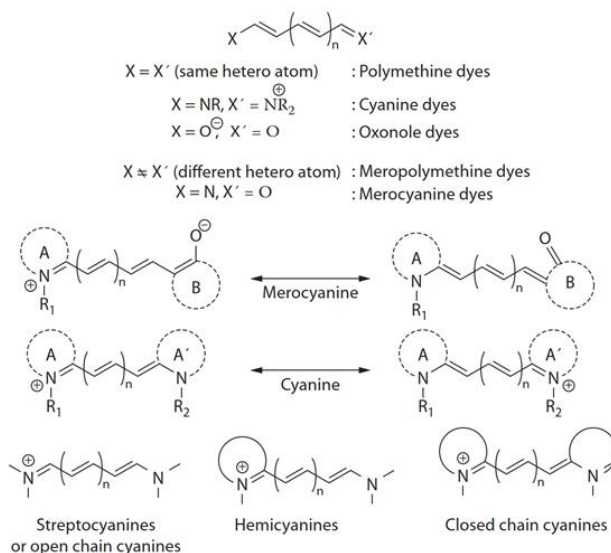
Figure 4.2 *Generic structures of polymethine-based chromophores (PMDs). Reproduced from ref. [1] Copyright © 2013 by Taylor & Francis Group, LLC.*

Among the plethora of NIR chromophores and NIR dyes found in the literature, the class of polymethine-based compounds (*polymethine dyes* or PMDs) (Figure 4.2),[1,2] have found considerable attention given their different fields of application such as bioimaging,[3–5] photovoltaics,[6,7] and nonlinear optics.[8] Systems of this type are treated as three-component systems, being formed by a polymethine chain and two terminal groups containing heteroatoms. A subset of PMDs is historically represented by cyanines and hemicyanines, which have a delocalized positive charge (Figure 4.2) and therefore are cationic species.

Another structural motif widely used for the design of NIR dyes is based on *donor-acceptor* (D-A) dyad or *donor-acceptor-donor* (D-A-D) systems. They consist of several linked π-conjugated units (electron-donors, D, and electron-attractors, A), realized through the formation of covalent bonds (Figure 4.3). Such arrangement induces an extension of the chromophore conjugation with the electrons which are well-delocalized over all the structure. This delocalization promotes a decrease of the

HLG, with a consequent increase in the absorption wavelengths in the near-infrared region.[1] The conjugation of DA and DAD systems consequently guarantees a reduction in the difference in length between single bonds and double conjugated bonds. As an example, DA chromophores exhibit two forms of resonance (D–A, $^+$D = A$^-$) that cause an increase in the double bond character between the D and A units and therefore the decrease of the HLG (in these systems sometimes called *Peierls gap*).

Figure 4.3 *Schematic representation of a symmetric DAD triad.*

The above-described chromophores are usually fluorescent, and their emissive properties depend on the length of the polymethine chain, on the nature of terminal groups, and, most importantly, on their rigidity. Although some characteristics are favorable for the development of NIR materials, their quantum yield of fluorescence, due to the flexibility of the chain is still very low (less than 15%). As an example, very long polymethine chains can, in fact, lose their planarity with a loss of the degree of conjugation. The emissive properties of very long polymethine dyes are consequently reduced.

To maintain the chromophore's absorption properties with a simultaneous increase of the quantum emission yield, it is possible to insert in the polymethine chain cyclic systems with at least one unsaturation. The cycle reduces the distortions of the conjugated system from the planarity without interrupting the conjugation. As we will see later, it is then possible to insert, on these unsaturated cycles, electronegative atoms or electron-withdrawing groups that act directly on the HLG.

4.1.2 Zwitterionic NIR Dyes

It has been recently demonstrated that the use of zwitterionic fluorophores (*zwitterionic dyes*, ZD), having a D-A-D motif, allows absorption at greater wavelengths (~ 1100 nm), given by their electron-attracting mesoionic unit.[9] Zwitterionic units, therefore, act as "*super-acceptor groups*", increasing the normal properties of common carbocationic or neutral electron-attractor groups. By introducing rings such as chlorocyclohexenes or oxo-carbonic acids (Figure 4.4) it is possible to obtain not only zwitterionic dyes but also to generate

more rigid systems in such a way to increase the fluorescence quantum yield.[2,9]
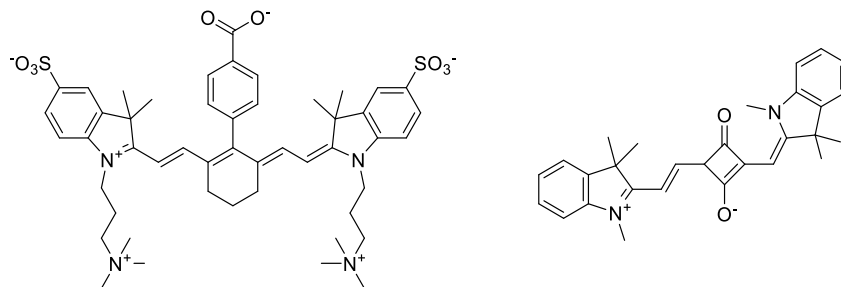
Figure 4.4 *Examples of chlorocyclohexene (left)[9] and squaraine (right)[10] zwitterionic NIR fluorophores.*

In particular, a vast range of derivatives can be synthesized by using as an accepting unit a member of the family of oxo-carbonic acids, such as squaric acid or croconic acid (Figure 4.5).
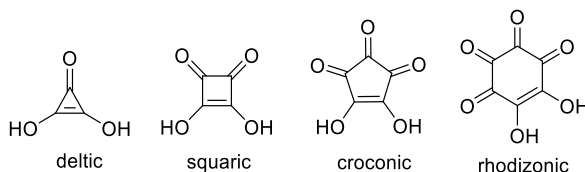
Figure 4.5 *Oxo-carbonic acids family.*

The *squaraines* are NIR dyes deriving from the squaric acid with very low *bandgap* and thus with excellent optical properties. One of the first compounds belonging to this class, was a polymer, more precisely a polysquaraine, synthesized by condensation of the acid with *N*-alkylcarbazoles (Figure 4.6a).[11] However, this polymer had the disadvantage of being an insoluble dusty black solid that made its characterization difficult. For this reason, attention soon shifted to the condensation of squaric acid with a pyrrole derivative. These new polysquaraines (Figure 4.6b),[12] although quite soluble and therefore characterizable, had disappointing optical properties that neglected the expectation of their possible application as a NIR-harvesting material as they showed a maximum absorption of ~580 nm. Finally, it was shown that the absorption of the material could be strongly influenced both by the length of the aliphatic bridging chain between the donor group (D) and the acceptor group (A) and by the nature of units inserted in it. Introducing, therefore, longer polymethine chains, with aromatic groups that increased the conjugation of the system, complex polysquaraines were obtained (Figure 4.6c),[13] characterized by a

122

strong interaction and conjugation between the D and A units, with the result of improving absorption towards NIR region (Figure 4.7).
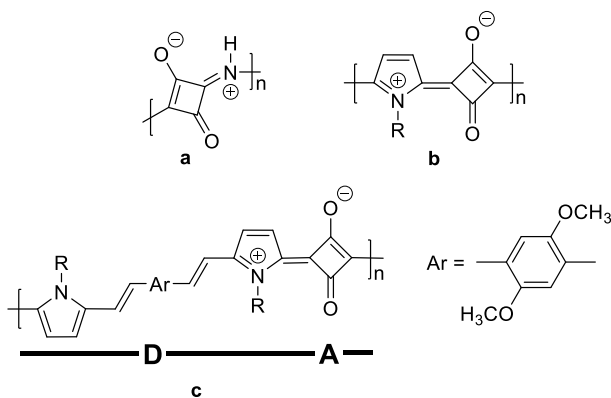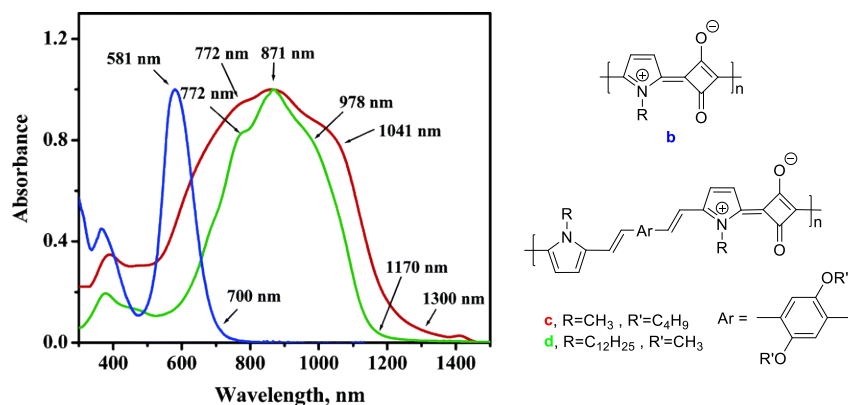

Figure 4.6 *Evolution of polysquaraine synthesis.*

Figure 4.7 *Absorption spectra of polysquaraine **b** (λ$_{max}$ = 581 nm), **c**, and **d** (λ$_{max}$ =871 nm). Reproduced from ref. [12] Copyright © 2005 American Chemical Society.*

In addition to the above findings, it was soon demonstrated how the increase in the absorption wavelength could also be influenced by the degree of conjugation of the donor terminal groups. Figure 4.8 shows three squaraines **(A-C)** presenting donor groups with an increasing degree of conjugation obtained by fusion of the aromatic system. The absorption indeed undergoes a large red-shift going from **A** up to **C**.
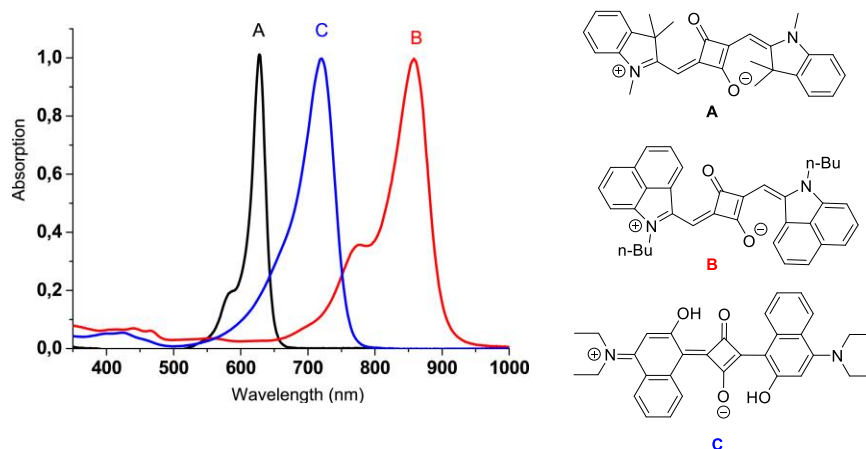
Figure 4.8 *Normalized absorption spectra of squaraine: **A**: λmax = 626 nm; **C**: λmax = 720 nm; **B**: λmax = 855 nm. Reproduced from ref. [2] Copyright © 2015 Elsevier Ltd.*

As regards the chromophores obtained from croconic acid, also called *croconates* or *croconaines*, these dyes differ from the squaraines due to the increase in the size of the central cycle, which in turn leads to an increase in the delocalization of electrons in the whole structure. Indeed, passing from a 4-membered ring to a 5-one, a considerable shift of the maximum absorption towards lower energies (~100 nm) is observed.[2] Croconic acid or 4,5-dihydroxycyclopent-4-ene-1,2,3-trione (Figure 4.5), in fact, is a pentagonal ring of carbons, with oxygen and hydroxyl groups connected to each carbon atom. Its chemistry is similar to that of squaric acid in terms of reactivity towards nucleophiles. As the squaric acid, also the croconic acid, can react with benzobisthiazoles and benzobispyrrolines forming the corresponding polychroconates, which, due to a stronger interaction between the D and A units, show a lower *bandgap* compared to the polysquaraines. These croconaines have a donor-acceptor-donor type structure (Figure 4.11), and their absorption in the NIR region can be tuned by varying the donor unit. Moreover, these systems exhibit a strong solvatochromic effect.

4.1.3 Plasmon-enhanced Fluorescence (PEF)

A different approach to improve the low fluorescence quantum yields of the above NIR chromophores and, consequently, of the corresponding dyes can be tackled by exploiting the intrinsic optical properties of NPs and NRs based on noble metals, described in Chapters 2 and 3. These nanostructures can indeed play a significant role in improving the quantum yield of organic fluorophores with which they interact through a phenomenon referred to *plasmon-enhanced fluorescence* (PEF).[14–17]
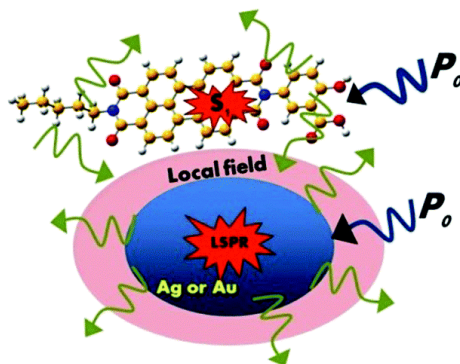
Figure 4.9 *Simplified schematic illustration of the PEF phenomenon. Reproduced from ref.* [18] *Copyright ©The Royal Society of Chemistry 2017*

It is known that the plasmonic interactions between coupled (i.e., closed in space) metallic NPs generate an amplification of the local electric field typical of electromagnetic waves with wavelengths falling in the spectral region associated with the HLG of organic fluorophores (Figure 4.9). This effect could, in principle, amplify the excitation efficiency and the increase in the radiative decay rate of fluorophores placed near the NP surface, thus significantly improving their overall fluorescence intensities. Indeed, it has been shown that coupled metallic NPs exhibit stronger fluorescence enhancement effects than unpaired metallic NPs.[18,19] It has also been observed that the PEF phenomenon depends on other factors such as the morphology and composition of the NPs, the intrinsic quantum yield of the fluorophores, the metal–fluorophore surface separation, as well as the spectral overlap between the SPR of the NPs and the spectrum absorption/emission of fluorophores. Moreover, it is expected that it also depends on the coupling force which is determined by the separation distance between the coupled metallic NPs.

125
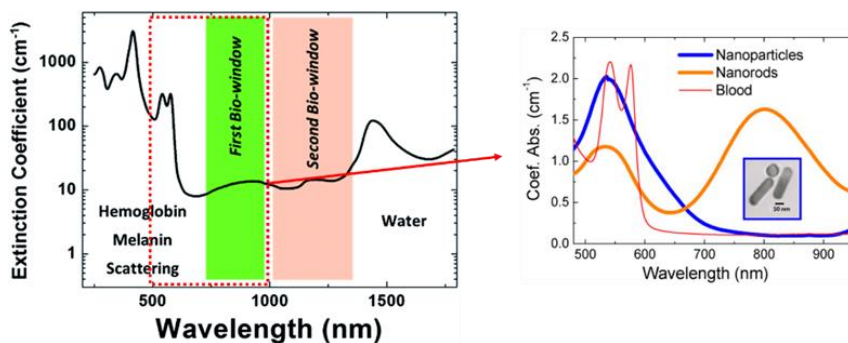
Figure 4.10 *Extinction coefficient of a tissue, in which it is possible to identify the "biological window" (divided into first and second).*[20] *On the right, comparison of absorption of AuNPs, gold NRs and blood. Reproduced from ref.* [20] *Copyright © The Royal Society of Chemistry 2014 (left) and from ref.* [21] *Copyright © 2012 IOP Publishing Ltd (right).*

Starting from the above theoretical considerations, it becomes fundamental to design coupled/aggregated nanostructures with plasmonic properties adequate to obtain an improvement in the fluorescence of fluorophores in the NIR. As previously stated, the fluorescence properties of these organic chromophores can be used in the field of telecommunications, for the development of novel sensors, and other emerging biomedical applications. In the latter context, it is worth to note that the emission of these organic substances falls into the so-called "*biological window*" between 700 and 1300 nm (Figure 4.10), in which blood and tissues are transparent.[21] However, in the absence of coupling with plasmonic nanostructures, this emission may be insufficient for bioimaging purposes. In the PEF phenomenon, the plasmonic nanostructure, therefore, acts as a *nano-amplifier* to improve fluorescence and therefore increase the sensing capabilities of the fluorophore.[22]
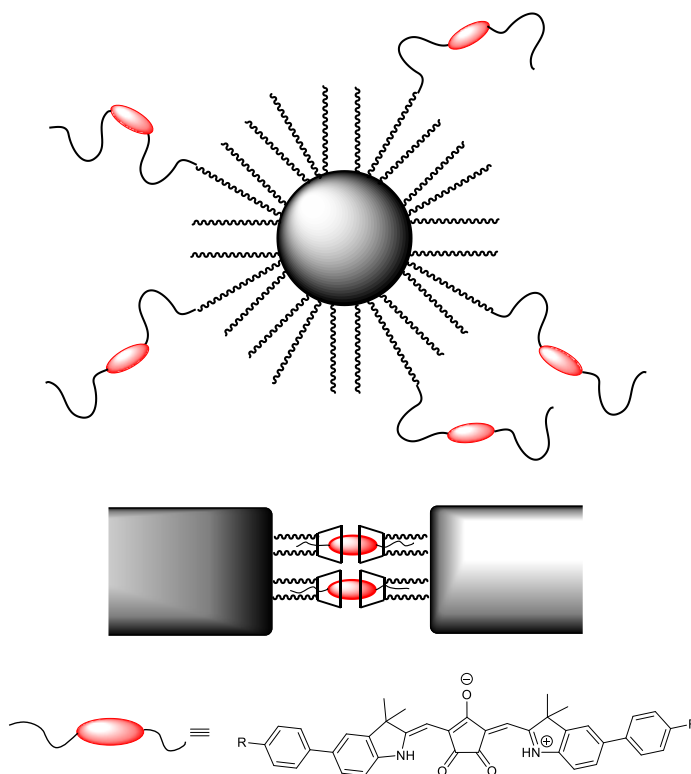
Figure 4.11 *(above) covalent approach in which NIR fluorophores are covalently grafted on the surface of NP or NR; (below) supramolecular approach in which NIR chromophores are functionalized with guest groups that can be complexed by host covalently grafted on the nanomaterial surface.*

In this chapter, the synthesis and the optical characterization of a series croconaines will be discussed. The synthesis of these compounds is

indeed inserted into a broader scientific context aimed at their hybridization with plasmonic nanostructures (NPs and NRs) using a covalent approach. In the first case, that will be discussed in detail because it was almost totally addressed, the croconaines were designed to bear on their donor moieties functional groups (R) allowing the covalent grafting of the dyes on the surface of the nanostructures (Figure 4.11). In the second case, not concluded yet, the NIR chromophore is functionalized with groups behaving as *guests* for synthetic molecular *hosts* covalently linked to the surface of the nanostructures and to exploit the complexation event to promote the aggregation.
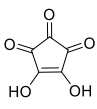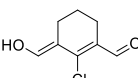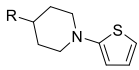
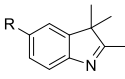## 4.2   Result and Discussion

4.2.1   Design
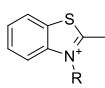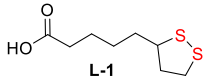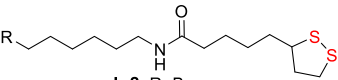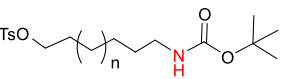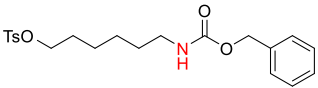
The NIR chromophores were treated as a three-component system, made of Acceptor (**A**), Donor (**D**), and Linker (**L**) units (Figure 4.12). Most of the design has focused mainly on donors and linkers. As indicated briefly in the introduction, the acceptor component must contain electrophilic groups on which the donor systems can be anchored, creating a highly conjugated system. In contrast, donor components should be characterized by the following requisites: *i*) a high degree of conjugation, *ii*) a nucleophilic site to be exploited for the linkage with the acceptor unit, and *iii*) a functional group on which the linker can be bound. The linker, in turn, must be equipped with an appropriate functional group (**G**) on its end to allow the grafting of the NIR chromophore on the surface of the plasmonic nanostructures.
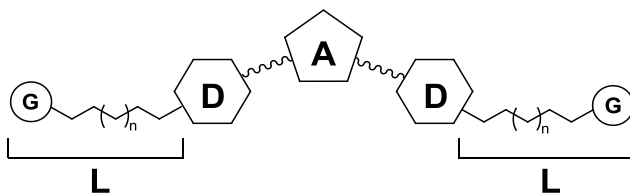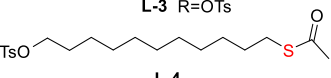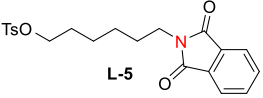
Figure 4.12 *General scheme of a DAD NIR chromophore matter of this study.*

In Table 4.1 were gathered the structures of the components chosen as potential building blocks for the synthesis of the NIR chromophores. As acceptor units, the croconic acid and the (*E*)-2-chloro-3-(hydroxymethylene)cyclohexene-1-carbaldehyde were initially

selected. The use of the former compound as an acceptor precursor for the DAD chromophores synthesis has been very recently documented in a few papers.[23–26] The latter of the two acceptors looks indeed very promising since the commercial dyes based on its use as a precursor are characterized by absorptions maxima beyond 1000 nm. As regards the donor components, differently substituted thiophene, indole, and benzothiazole derivatives were selected as potential candidates. On the indole scaffolds, a linker can be attached by exploiting the reactivity of an X substituent presents on the aromatic system (X = O, N, S, …). For the benzothiazole derivatives, the linker can be introduced by alkylating the nitrogen of the five-member ring with R groups. A series of disulfide and amino-protected derivatives were instead identified as potential linkers. Once deprotected, these functional groups present a well-documented high affinity for the surface of plasmonic noble metal nanomaterials. It is worth to note that linkers of different lengths were designed to explore the effect of the spacing between the surface and the NIR chromophore on the emission properties of the NIR dyes.

Acceptors	Donors	Linkers
A-1	TD	L-1
A-2	ID	L-2 R=Br
		L-3 R=OTs
	BTD	L-4
		L-5
		L-6 n=1
		L-7 n=6
		L-8

Table 4.1 *Acceptor, donor, and linker building blocks for the synthesis of the DAD triads as NIR-harvesting chromophores.*

In the first part of the chapter, the synthesis of the building blocks of the DAD triads is tackled, focusing on the use of croconic acid as an acceptor. Therefore, different types of donors with varying degrees of

conjugation and different functional groups that could anchor on the croconic acid and manifest different properties were explored.

## 4.2.2 Synthesis of Acceptor Building Blocks

Croconic acid (**A-1**) is a 5-member cyclic compound belonging to the family of oxo-carbonic acids together with its most known lower homolog, the squaric acid. To each of its carbon atoms, oxygen and hydroxyl groups are attached, which give the molecule its acceptor character. It is an expensive commercial product; for this reason, it was prepared with a two-step procedure reported in the literature[23] from the cheaper tetrahydroxy-1,4–benzoquinone (Scheme 4.1).
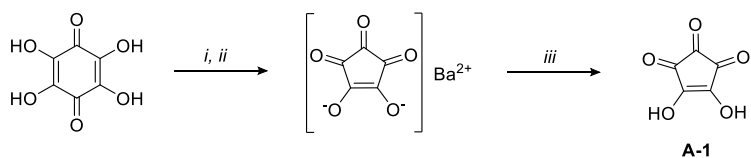
Scheme 4.1 *Synthesis of croconic acid* **A-1** *from tetrahydroxy-1,4–benzoquinone. Reagents and conditions: i) NaOH, MnO₂, H₂O, reflux, 45 min, ii) HCl$_{(aq)}$ (37%), BaCl₂, H₂O, 80%; iii) H₂SO₄, 60°C, 2h, quant. yield.*

In the first step, an aqueous solution of tetrahydroxy-1,4–benzoquinone is refluxed in the presence of manganese oxide and sodium hydroxide. The quinone undergoes a rearrangement whose mechanism is not reported in the literature. The reaction is quenched after one hour of refluxing by treatment with a 37% w/v solution of hydrochloric acid. To the obtained yellow solution, a hot aqueous solution of barium chloride dihydrate is added. The resulting solution is first heated to 90°C and then cooled to favor the precipitation of the barium croconate as shiny yellow crystals. In the second step, the solid barium croconate is added to a solution of sulfuric acid kept at 60 °C. This treatment promotes the precipitation of the insoluble barium sulfate which is removed by filtration. The desired croconic acid (**A-1**) is finally obtained by precipitation from the filtrate as a yellow solid in 80% yield.

Compound **A-1** was characterized by ^{13}C NMR spectroscopy, and its spectrum, taken in D₂O (Figure 4.13), presents three signals (δ = 181.79, 149.14, and 86.74 ppm) which correspond to the five carbons of the cycle since the molecule has a plane of symmetry. Instead, the low-field signal at δ = 191.87 ppm, is hypothesized to be relative to the dianionic form generated by the deprotonation of both hydroxyl groups.[27]
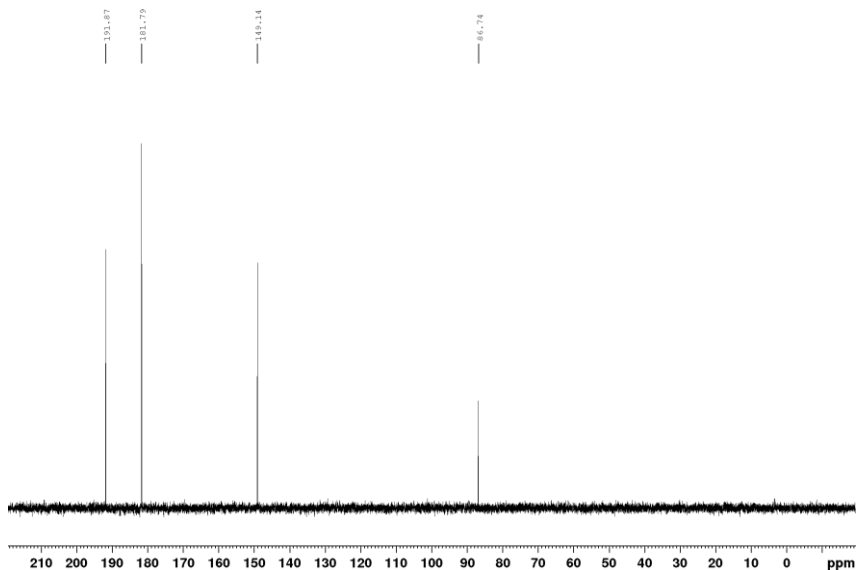
Figure 4.13 *^{13}C NMR spectrum (100 MHz, D$_2$O) of croconic acid **A-1**.*

The 2-chlorocyclohex-1-enyl moiety represents another acceptor component that has been used as an alternative to croconic acid unit.[24,26] This structural motif can be inserted in DAD chromophores using the (*E*)-2-chloro-3-(hydroxymethylene)cyclohex-1-ene-1-carbaldehyde (**A-2**) as the precursor. The synthesis of **A-2** is not trivial since, once formed, the compound tends to degrade very quickly if not stored in proper conditions. Nevertheless, compound **A-2** was prepared through a Vilsmeier-Haack formylation reaction by reacting cyclohexanone with *N,N*-dimethylformamide and phosphorous oxychloride (Scheme 4.2).[28] The product is isolated in 70% of yields as a yellow solid precipitate after the quenching of the reaction with crushed ice. It was characterized by ^{1}H and ^{13}C NMR spectroscopy in DMSO-d6 and with ESI-MS measurements.
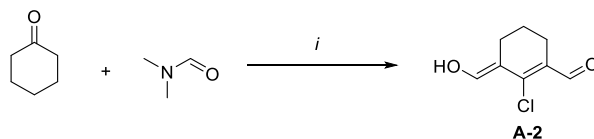
Scheme 4.2 *Synthesis of acceptor **A-2**, starting from cyclohexanone and dimethylformamide. Reagents and conditions: i) POCl$_3$, CH$_2$Cl$_2$, 80°C 3h, 70%.*

The ^{1}H NMR spectrum of **A-2** (Figure 4.14) is characterized by a broad signal at δ ~10.9 ppm, integrating for one proton, and assigned to the enol hydroxyl proton. Slightly more upfield-shifted, at δ ~10.1 and ~7.6 ppm, are found two very broad resonances, each integrating for one proton. These resonances have been assigned to the aldehyde and vinyl

protons, respectively, which are exchanging on the NMR time-scale. The upfield region of the spectrum shows at δ = 2.36 ppm a triplet, integrating for four protons, which was assigned to the methylene protons of the cyclohexene ring at the 5- and 3-position, while at δ = 1.58 ppm there is a pentuplet, integrating for two, relative to methylene protons in 4-position.
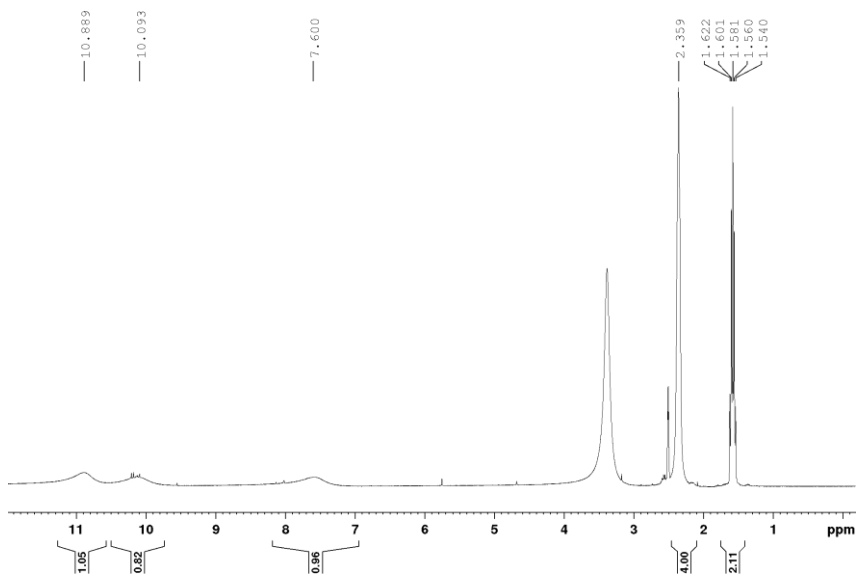
Figure 4.14 *¹H NMR spectrum of A-2 (300 MHz, DMSO-d6).*

The ¹³C NMR spectrum taken in the same solvent confirms the identity of **A-2**. The UPLC-MS analysis detects a product with a retention time of 0.79 min and mass peaks at m/z = 173 (100) [MH]⁺, 175 (40) [MH+2]⁺ in agreement with the structure of **A-2**.

4.2.3   Synthesis of Donor Building Blocks

4.2.3.1   Benzothiazole-based Donors (BTD)

In Table 4.1 have been reported the typology of donors chosen as building blocks for the synthesis of the DAD triads. Structurally-simple benzothiazole donor building blocks were synthesized, since the versatility and the commercial availability of this starting material. Moreover, they were studied to improve the alkylation methodology on this donor moiety, to introduce alkyl linkers (see Table 4.1) for further functionalization. The two synthesized compounds belonging to this class (**BTD-1, BTD-2**) are gathered in Scheme 4.3.
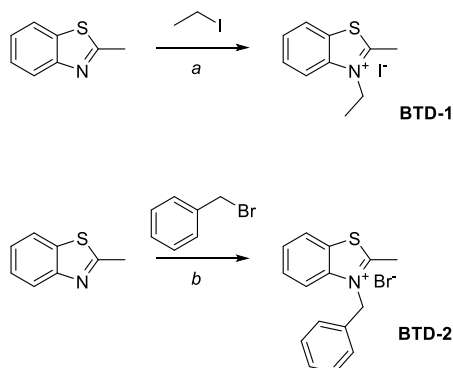
Scheme 4.3 *Synthesis of* **BTD-1** *and* **BTD-2**. *Reagents and conditions: a) toluene, reflux, 24h, 46%; b) toluene, reflux, 24h, 65%.*

The commercial benzothiazole was reacted with the proper alkylating agents in toluene at reflux. For the synthesis of **BTD-1**, 1-iodoethane was employed, while benzyl bromide was used to obtain **BTD-2**. In both cases, the products were isolated as crystalline solids by concentrating the reaction mixture under reduced pressure and by inducing the crystals precipitation through the addition of diethyl ether to the concentrated solution.
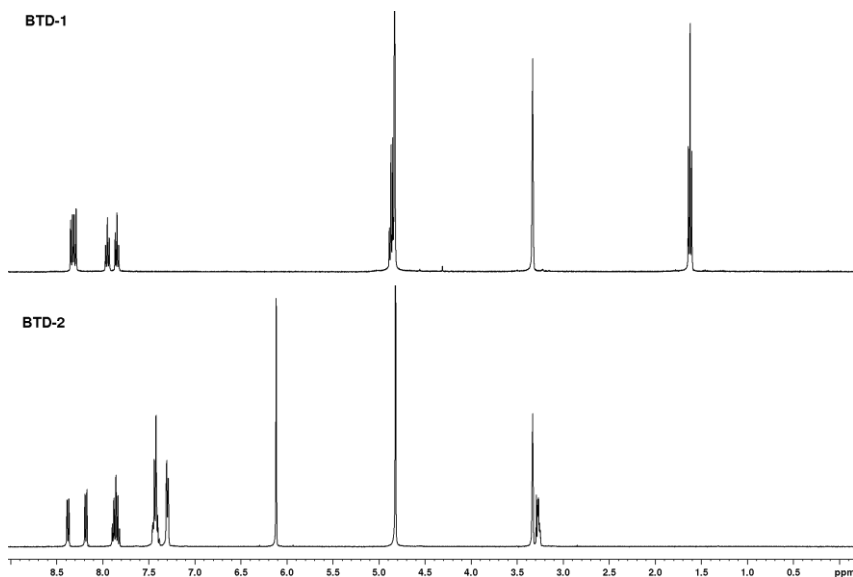
Figure 4.15 *¹H NMR stack plot (400 MHz, CD₃OD) of benzothiazole donor* **BTD-1** *(top),* **BTD-2** *(bottom).*

The ¹H NMR spectra of the two compounds, taken in CD₃OD, were gathered in Figure 4.15. The benzothiazole moiety gives rise, in both cases, to the singlet at $\delta = 3.33$ ppm, related to the methyl group of the thiazole ring, while a slightly different pattern of signals is visible in the

aromatic region between 8.5 and 7.7 ppm. As regards **BTD-1**, the diagnostic signals are the triplet at δ = 1.62 ppm, integrating for three protons, and related to the -CH$_3$ ending group of the alkyl chain, while the methylene group resonates as a quartet at δ = 4.87 ppm, partially overlapped to the water residual signal. The ^{1}H NMR spectrum of **BTD-2** (Figure 4.15, bottom) shows the diagnostic singlet at δ = 6.12 ppm, belongings to the methylene group of the benzyl moiety, together with the aromatic doublet at δ = 7.30 ppm and the multiplet at δ = 7.4-7-5 ppm.

4.2.3.2   Thiophene-based Donors (TD)

The thiophene-based donors were only recently introduced as components of DAD triads. As the benzothiazole-based donors, the thiophene ones are particularly enticing for the functionalization of the noble metal nanostructures because they can be, in principle, easily functionalized with the linkers indicated in Table 4.1.
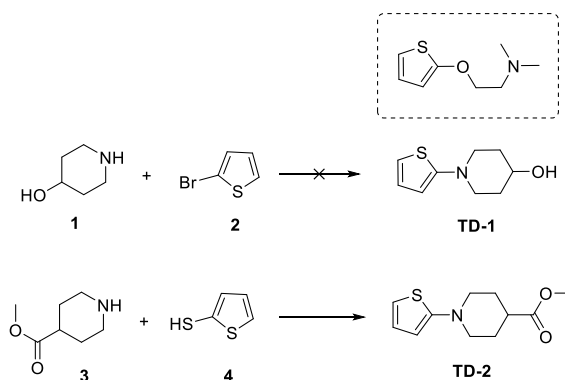
Scheme 4.4 *Synthesis of donor building blocks* **TD**. *Reagents and conditions: a) Cu/CuI, deanol, 80°C, 72h; b) toluene, reflux, 3h, 84%.*

The first donor building block of which the synthesis has been tackled is **TD-1** (Scheme 4.4). Its thiophene ring is substituted in the 2-position with a piperidine-4-ol unit. The hydroxyl group present in the piperidine cycle represents an ideal functionalization site for the introduction of linkers through S$_N$2 alkylation reactions. A perusal of the literature shows that this compound can be prepared through an Ullmann-type coupling between 2-bromo thiophene (**2**) and 4-hydroxy piperidine (**1**) and a Cu/CuI catalytic system.[29] The reaction makes use of dimethylethanolamine (deanol) that would play the key role in solvating the copper salts favoring the coupling of the reactants. After several attempts accomplished changing the catalyst loading, temperature, and co-solvent, the desired donor **TD-1** was never isolated. The only by-product separated in a considerable amount in all

these attempts was due to the nucleophilic attack of the solvent on **2**. To overcome the encountered problems, the synthesis of an alternative thiophene based donor building block (**TD-2**) was tackled. This donor, the methyl-1- (2-thiophenyl) piperidine-4-carboxylate, was synthesized by reacting the methyl piperidine-4-carboxylate (**3**) and 2-mercaptothiophene (**4**), which are commercial compounds, in refluxing toluene for 3 hours according to a procedure reported in the literature (Scheme 4.4).[30] In this reaction, the piperidine nitrogen makes a nucleophilic attack on the carbon substituted with the thiol group of the mercaptothiophene, releasing hydrogen sulfide (condensation reaction). The progress of the reaction was monitored by UPLC-MS, an analytical technique in which liquid chromatography is combined with mass spectroscopy. After chromatographic purification, donor **TD-2** was isolated in 84% yield as a pale yellow solid. The characterization was in agreement with those reported in the literature.[30]
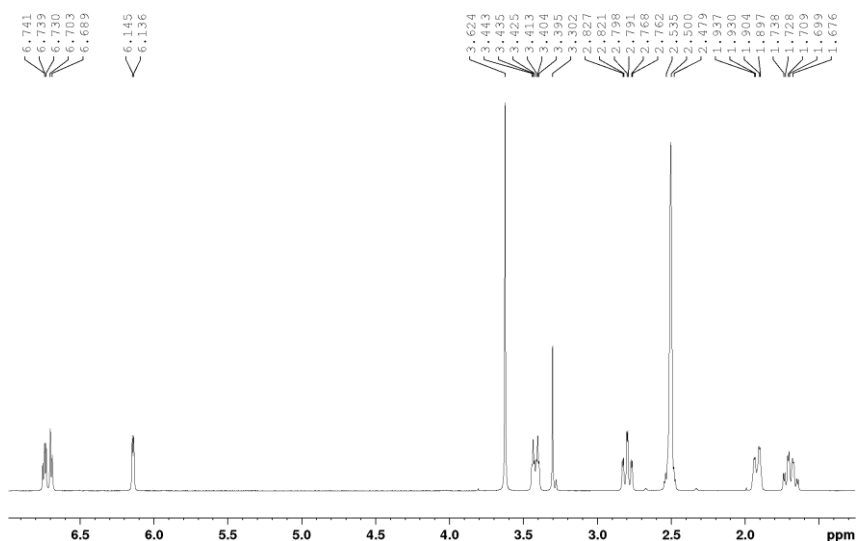
*Figure 4.16 ¹H NMR (400 MHz, DMSO-d6) of donor **TD-2**.*

The ¹H NMR spectrum of **TD-2** taken in DMSO-d6 (Figure 4.16), presents, in the low-fields region, a multiplet and a doublet of doublets at δ = 6.7-6.6 and 6.14 ppm, respectively, assigned to the three magnetically different aromatic protons of the thiophene ring, while at δ = 3.62 ppm there is a singlet, integrating for 3 protons, relative to the ester methyl group. As regards the piperidine ring, the equatorial protons in α to nitrogen give rise to a doublet of triplets integrating for two protons at δ = 3.42 ppm, while the axial ones give rise to a triplet of doublets at δ = 2.79 ppm integrating for the same value. At δ = 2.52 ppm, partially superimposed to the solvent residual signal, resonates a multiplet relative to the proton in the 4-position of the piperidine ring.

Finally, the equatorial and axial protons at the 3- and 5-position of the piperidine ring give rise to two multiplets, each integrating for two protons, at $\delta = 2.0$-1.9 and 1.7-1.6 ppm, respectively.

4.2.3.3 Indole-based Donors (ID)

The synthesis of the donor building blocks belonging to this class (**ID-1-3**) was gathered in Scheme 4.5. Most of them were prepared from a common intermediate, the 5-bromo-2,3,3-trimethyl-3H-indole (**5**). This compound was prepared in 84% of yield according to the known Fischer synthesis of indoles by reacting isopropyl methyl ketone and (4-bromophenyl) hydrazine hydrochloride in acetic acid (Scheme 4.5).[31] Through a Suzuki cross-coupling reaction, **5** was converted into the desired indoles **ID-1** and **ID-2** in high yields using commercial phenylboronic acids. In particular, **5** and (4-hydroxyphenyl)boronic acid were reacted in a 1:1 mixture of THF/H$_2$O using a microwave reactor. The reaction was carried out using K$_2$CO$_3$ as the base and tetrakis(triphenylphosphine)palladium(0) as the catalyst. To overcome the problem of the low conversion of **5**, three successive additions of boronic acid were carried out after every hour until **5** disappears from the reaction mixture. After chromatographic purification, **ID-1** was obtained as an orange solid with a 94% yield. The same reaction carried out using the (4-nitrophenyl)boronic acid yielded **ID-2** in almost quantitative yields. Donor **ID-3** was instead obtained in 91% yield through the reduction of **ID-2** with ammonium chloride and iron powder in a solution of water and isopropanol (1:3) (Scheme 4.5).
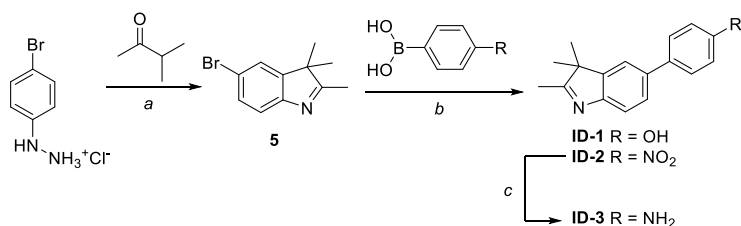
Scheme 4.5 *Synthesis of the indole-based donor building blocks (**ID**). Reagents and conditions: a) CH$_3$COOH, 120°C, 3h, 84%; b) Pd(PPh$_3$)$_4$, K$_2$CO$_3$, THF/H$_2$O, MW 110°C, 1h, 60% (**ID-1**), 98% (**ID-2**); c) Fe, NH$_4$Cl, H$_2$O/IprOH, 80°C, 2h, 94%.*

All indoles **ID-1-3** were characterized by ¹H NMR, ¹³C NMR, and MS-ESI measurements. The ¹H NMR spectra of the three indoles, taken in DMSO-d6, were gathered in Figure 4.17. The common features of the spectra are the two singlets in the spectrum upfield region at δ~2.5 and 1.3 ppm, which are assigned, as for **5**, to the protons of the methyl group in α position with respect to nitrogen and the two chemically equivalent methyl groups of the 5-member ring, respectively. The effect of substituent -R on the compounds resonances is well visible in the

spectra downfield region. The electron-withdrawing effect of the nitro group downfield shifts the two doublets (♥) and (♣) relative to the four protons of the aromatic ring of **ID-2** with respect to the same signals in **ID-1** and **ID-3**. The protons in ortho to the substituent (♣) in **ID-2** resonate at δ = 8.30 ppm, while in **ID-1** and **ID-3**, they are found at δ = 6.64 and 6.84 ppm, respectively. In **ID-1**, the OH substituent resonates at δ ~9.5 ppm as a broad signal, while the amino group of **ID-3** gives rise to another broad signal at δ ~ 5.2 ppm. The ESI-MS spectra of the three isolated compounds (see experimental part) confirm their identity.
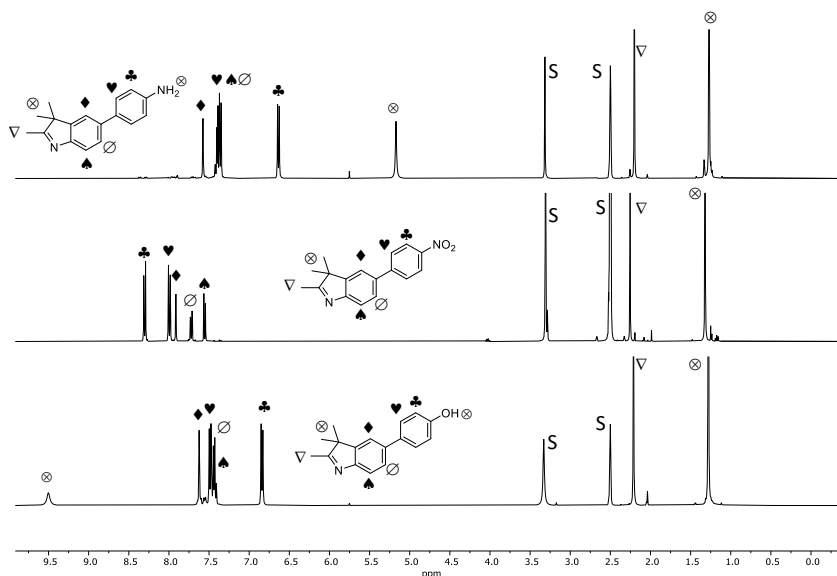
Figure 4.17 *¹H NMR stack plot (400 MHz, DMSO-d6) of indole donor **ID-3** (top), **ID-2** (middle) and **ID-1** (bottom).*

4.2.4 Synthesis and Studies of the DAD Dyes

4.2.4.1 Synthesis of Croconaines DAD-type

First examples of croconaine dyes were reported between 1970-1987 in several industrial patents.[32–37] However, the first scientific paper about croconaine dyes was published in 1988, referring to the first patent as regards the synthetic procedure and details.[38] In general, the procedure consists of a one-pot reaction between the croconic acid (i.e., the acceptor) and the donor unit in a 2:1 stoichiometric ratio. The two components are refluxed in a 1:1 mixture of toluene and *n*-butanol, in some cases, in the presence of a base (e.g. pyridine).

In this thesis, the first NIR chromophores synthesized were the croconaine **C-1** and **C-2**. These compounds are zwitterion species consisting of an acceptor component based on croconic acid (**A-1**) and the two benzothiazole-based donors, **BTD-1** and **BTD-2**, previously synthesized. Their synthesis was accomplished in order to test and improve the methodology typically reported for the synthesis of croconaines.

BTD-1 R=CH₃, X=I⁻
BTD-2 R=Ph, X=Br⁻

C-1 R = CH₃, 19%
C-2 R = Ph, 18%
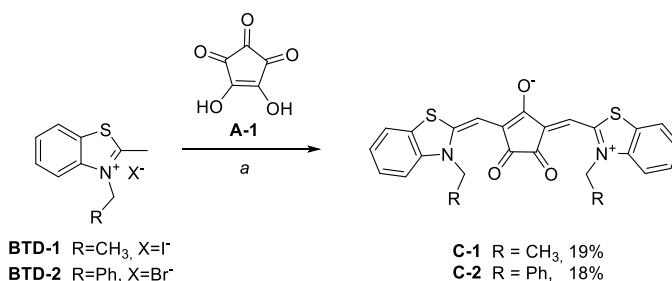
Scheme 4.6 *Synthesis of croconaine* **C-1**. *Reagents and conditions: a) pyridine, toluene/n-butanol (1:1), reflux, 6h.*

While the synthesis and characterization of croconaine **C-2** were reported by Ye et al. in 2017,[39] croconaine **C-1** was only present in some industrial patents.[34,40] Croconic acid (**A-1**) and two molar equivalents of **BTD-1** were refluxed in the 1:1 mixture of toluene and *n*-butanol in the presence of pyridine (Scheme 4.6). This latter base allows the deprotonation of the methyl group on the benzothiazole for the coupling with the core. The croconaine was isolated, as a pure compound in 19% yield through chromatographic separation (SiO₂, CH₂Cl₂/CH₃OH 95:5). The resulting croconaines **C-1** and **C-1** were characterized as usual by ¹H NMR spectroscopy in DMSO-d6 and ESI-MS mass spectroscopy.

In the ¹H NMR spectra, taken in DMSO-d6, the diagnostic signal related to the vinyl proton is centered at $\delta = 6.34$ ppm. In the aromatic region of the spectrum relative to the croconaine **C-2** (Figure 4.18, bottom), overlapped to the signals related to the benzothiazole unit, it is possible to distinguish the presence of the signals deriving from the benzyl aromatic ring. The whole integration of the aromatic region stands indeed for eighteen protons. The singlet at $\delta = 5.69$ ppm is related to the methylene group of the benzyl moieties. On the contrary, the presence of the ethyl alkyl chain of the croconaine **C-1** is evidenced by the triplet resonating at $\delta = 1.39$ ppm, related to the methyl groups coupled with the methylene ones, which indeed give rise to a broad quadruplet at $\delta \sim 4.5$ ppm (Figure 4.18, top).

Figure 4.18 *¹H NMR stack plot (400 MHz, DMSO-d6) of croconaines **C-1** (top), **C-2** (bottom).*

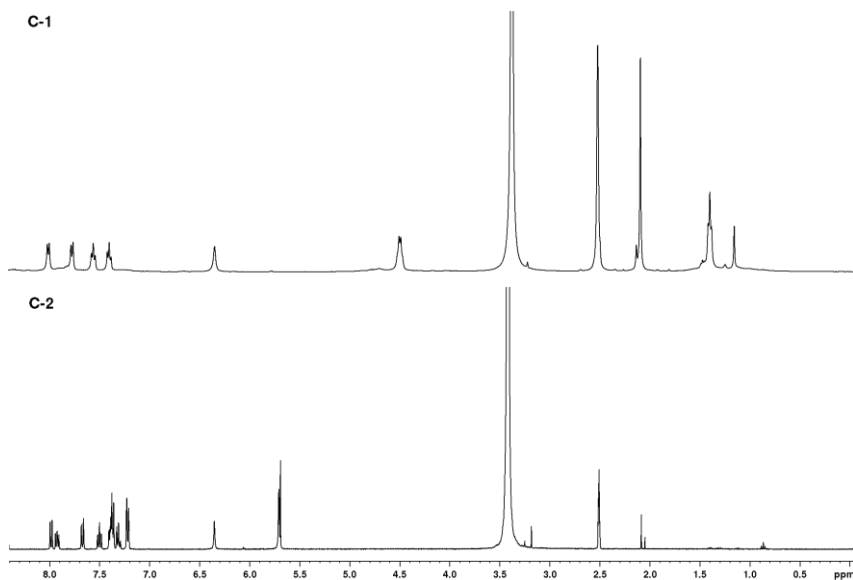Regarding the croconaines having a thiophene-based donor, the synthesis of **C-3** was not trivial, and it has been described in Scheme 4.7. The two reactants, in a 2:1 stoichiometric ratio, were refluxed in a 1:1 mixture of toluene and n-butanol according to a procedure reported in the literature.[41] The dye was obtained by precipitation induced by the addition of methanol to the reaction mixture followed by Buchner filtration. In this way, **C-3** was isolated in 66% yield without any further purification. It was characterized by ¹H NMR spectroscopy and ESI-MS mass measurements.
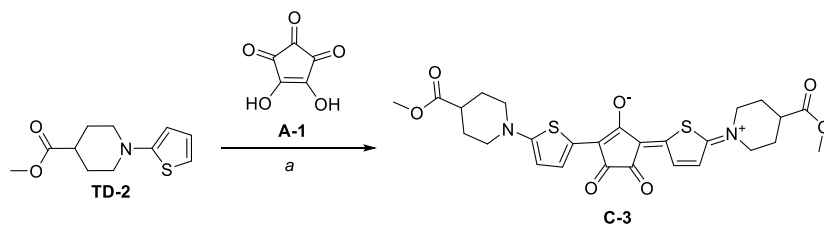
Scheme 4.7 *Synthesis of croconaine **C-3**. Reagents and conditions: a) toluene/n-butanol (1:1), reflux, 3h, 66%.*

The ¹H NMR spectrum of **C-3**, taken in DMSO-d6 (Figure 4.19), shows, in the aromatic zone, a broad signal and a doublet at δ = 8.6 and 7.04 ppm, respectively. These signals, both integrating for two protons, are related to the protons of the two thiophene rings. In the region of the aliphatic protons, a pattern of signals similar to that of **TD-2** (Figure

4.16) was found together with some signals deriving by solvents impurities. All other characterizations are in agreement with the reported ones.[41]
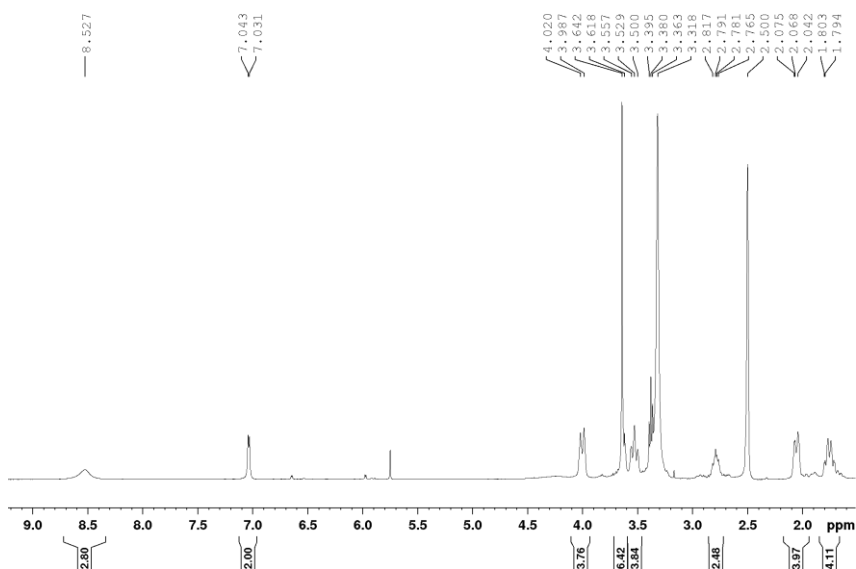
Figure 4.19 ^{1}H NMR *(400 MHz, DMSO-d6) of croconaine* **C-3**.

139

Croconaine **C-4** (Scheme 4.8) was obtained in a similar way to the previously discussed ones by reacting the croconic acid **A-1** with the indole donor **ID-1** in a 1:2 stoichiometric ratio. The croconaine was isolated, as a pure compound in 60% of yield, by precipitation induced by the addition of methanol to the reaction mixture. The compound was characterized as usual by ^{1}H NMR spectroscopy in DMSO-d6 and ESI-MS mass spectroscopy.

ID-1 R = OH
ID-2 R = NO$_2$
ID-3 R = NH$_2$

C-4 R = OH, 60%
C-5 R = NO$_2$, 0%
C-6 R = NH$_2$, 0%
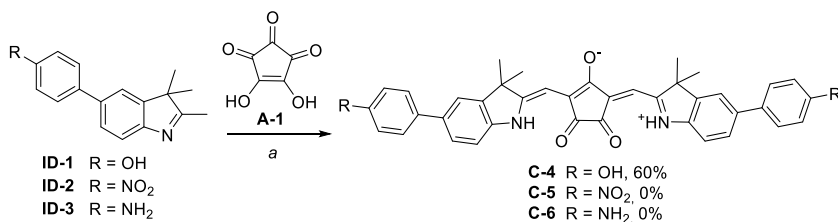
Scheme 4.8 Synthesis of croconaine **C-4**. *Reagent and conditions: a) pyridine, toluene/n-butanol (1:1), 110°C, 3h, 60% (**C-2**).*

The ^{1}H NMR spectrum of **C-4**, taken in DMSO-d6 (Figure 4.20), shows a singlet at δ = 9.5 ppm, integrating for two, relative to the protons of the hydroxyl groups. In the aromatic zone are present a singlet at δ= 7.8 ppm, integrating for two, relative to the protons in α to the indole

iminium groups, a multiplet at δ = 7.7-7.6 ppm, integrating for eight, relative to the remnants protons of the indole aromatic rings and to the protons of the phenolic rings in meta to the OH group. Finally, at δ = 6.8 ppm resonates a doublet, integrating for four, assigned to the protons of the phenolic rings in ortho to the OH. At δ ~ 6 ppm, on the other hand, is found a broad signal relative to the vinyl protons. This resonance is diagnostic of the successful condensation reaction between **A-1** and **ID-1**. At high fields (δ = 1.54 ppm), it is recognizable a singlet integrating for twelve protons, of the four identical methyl groups.
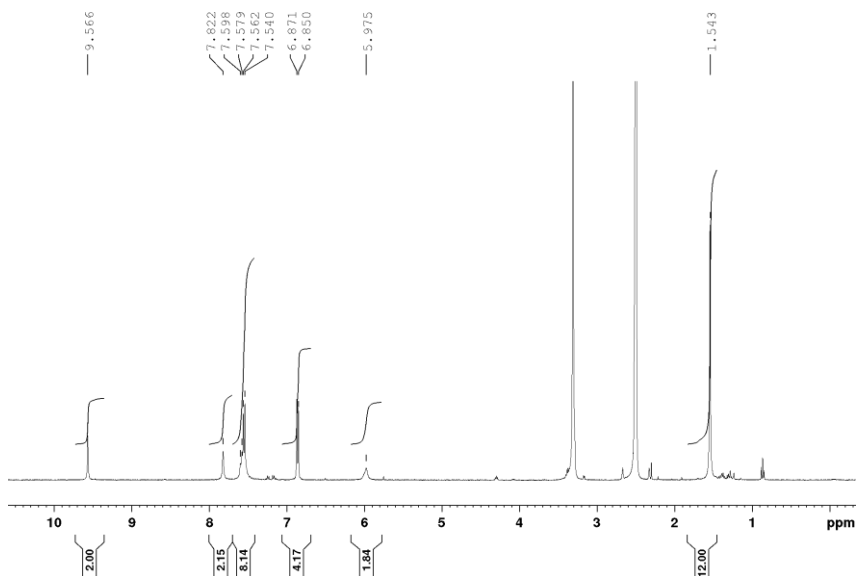
Figure 4.20 *¹H NMR spectrum (400 MHz, DMSO-d6) of croconaine **C-4**.*

The UPLC-MS(ESI) analysis finally detects a peak with a retention time (inverse phase, C18, eluent: gradient water/ACN) of 1.27 min with an isotopic pattern, m/z = 608.2 (100) $[MH]^+$, 608.7 (93) $[MH+1]^+$, 609.9 (58) $[MH+2]^+$, in good agreement with the theoretical one.

On the other hand, when the condensation reaction was carried out in the same experimental conditions employed for **ID-1**, but using **ID-2** (R = NO$_2$) or **ID-3** (R = NH$_2$) as the reagent, the desired croconaines **C-3** and **C-4** were never isolated from the reaction mixture (Scheme 4.8).

To overcome these unexpected results, a new synthetic approach to croconaines **C-5** and **C-6** was devised and summarized in the retrosynthetic analysis depicted in Scheme 4.9.
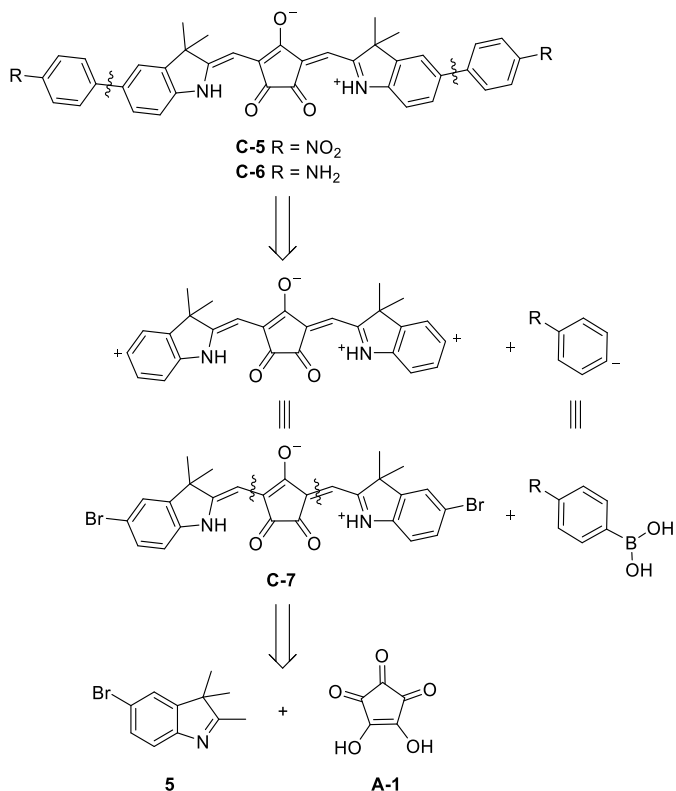
Scheme 4.9 *Retrosynthetic analysis for the synthesis of croconaines **C-5** and **C-5**.*

This approach is different from that used for the synthesis of **C-4** (Scheme 4.8). The first disconnection generates two synthons that could have, as synthetic equivalents, a *p*-substituted phenylboronic acid and a bromo-substituted DAD dye (**C-7**) already known in the literature.[31] This latter can be, in turn, prepared by the reaction between **A-1** and **5**, whose syntheses have already been previously discussed in Scheme 4.1 and Scheme 4.5, respectively.
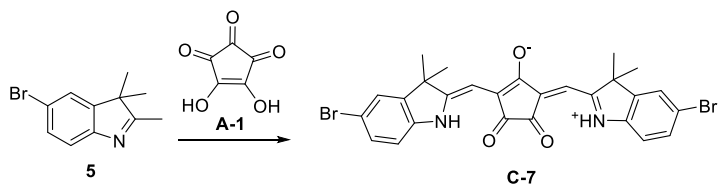
Scheme 4.10 *Synthesis of croconaine **C-7** from croconic acid (**A-1**) and indole **5**. Reagents and conditions: a) pyridine, toluene/n-butanol (1:1), 110°C, 3h, 79%.*

Compound **C-7** was obtained with the usual procedure by reacting **5** with **A-1** in a 2:1 stoichiometric ratio (Scheme 4.10). After its precipitation from the reaction mixture through methanol addition, it

was isolated in 79% yield and characterized by ¹H NMR spectroscopy and ESI-MS mass measurements.

Its ¹H NMR spectrum, taken in DMSO-d6 (Figure 4.21), shows, in the aromatic zone, a broad singlet at δ = 7.85 ppm, integrating for two, and two broad doublets at δ = 7.54 and 7.46 ppm, each integrating for two. These signals were assigned to the aromatic protons of the indole moieties. The two vinyl protons, on the other hand, resonate as one broad signal at δ = 5.95 ppm. This signal witnesses the effective formation of **C-7** and suggests the high mobility in solution on NMR time-scale of the molecule. Finally, a singlet at δ = 1.5 ppm integrating for twelve protons, was assigned to the protons of the four methyl groups.
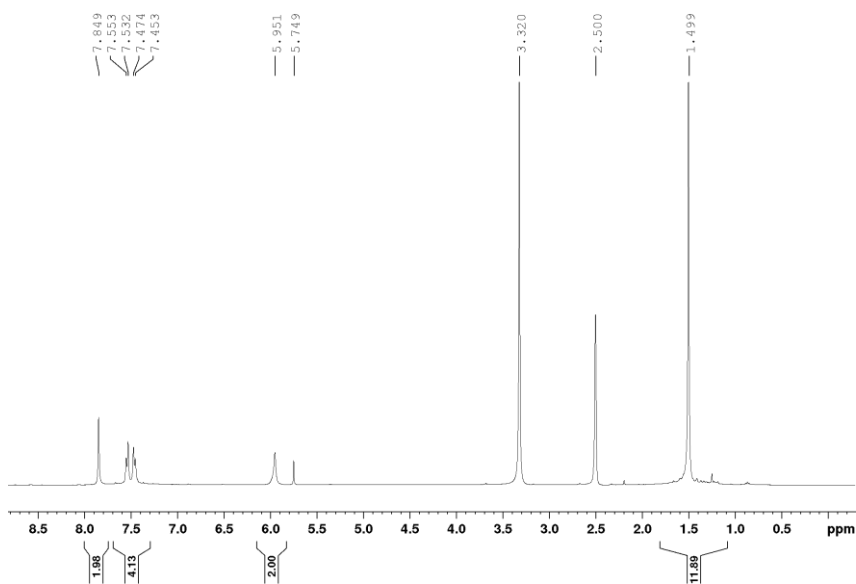
Figure 4.21 *¹H NMR (400 MHz, DMSO-d6) spectrum of croconaine **C-7**.*

The mass spectrum (ESI) reveals a species with isotopic pattern of m/z = 583.3 (100) [MH+2]⁺, 581.1 (30) [MH]⁺, 585.2 (32) [MH+4]⁺ in agreement with the structure of **C-7**.

The resulting croconaine **C-7** proved to be a useful substrate for Pd-catalyzed cross-coupling reactions, in particular in the Suzuki-Miyaura reaction with differently substituted commercial boronic acids, leading to the preparation of several DAD dyes in higher yields (Scheme 4.11).
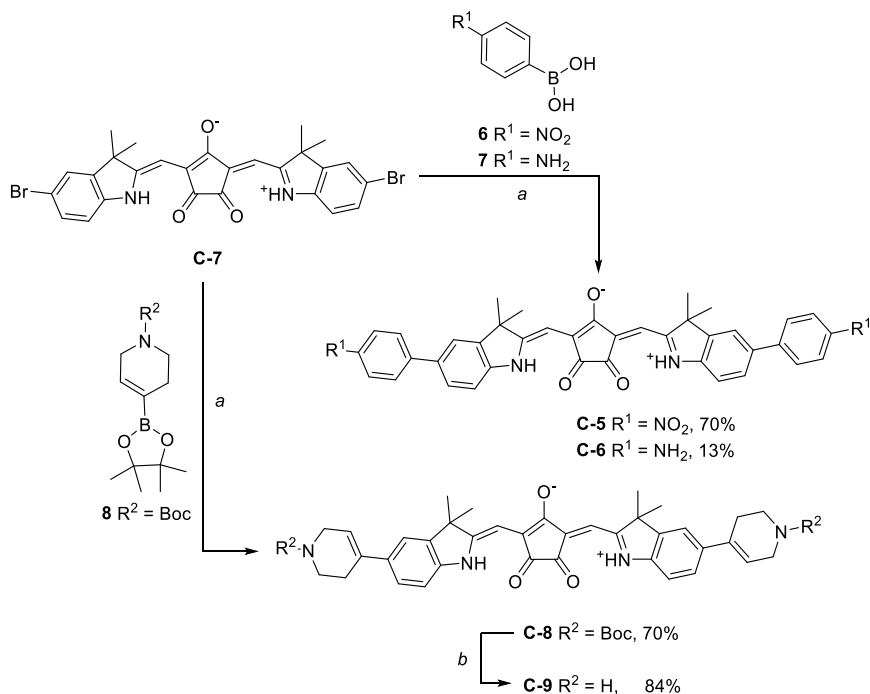
Scheme 4.11 *Synthesis of croconaines* **C-5**, **C-6**, **C-8**, *and* **C-9** *through Suzuki-Miyaura cross-coupling reaction between* **C-7** *and boronic acid derivatives. Reagents and conditions: a) Pd(PPh₃)₄, K₂CO₃, THF/H₂O, MW, 110°C, 1h; b) TFA, CH₂Cl₂, rt, 1h.*

Croconaines **C-5** and **C-6** were synthesized by reacting *p*-substituted phenylboronic acid (**6** or **7**, respectively) with **C-7** in 2:1 stoichiometric ratio in the presence of K_2CO_3 and tetrakis(triphenylphosphine) palladium(0) (Pd(PPh₃)₄) as the catalyst. The reaction was carried out for 1 hour in a refluxing 1:1 THF/H₂O mixture in a microwave reactor (Scheme 4.11). The reaction was monitored by UPLC-MS, turned off, and after chromatographic purification, croconaines **C-5** and **C-6** were isolated in 70 and 13% yields, respectively. The low yield obtained with **C-6** was due to purification problems since the UPLC-MS analysis instead revealed a high percentage of the croconaine in the reaction mixture. It is also worth to note that Pd(PPh₃)₄ was the best catalyst among those used. Unexpectedly, using Pd(dba)₂, Pd₂(dba)₃, or Pd(CH₃COO)₂, which are known to be suitable catalysts for the Suzuki reaction, the conversion of **C-7** was instead low if not existent at all. The newly synthesized were fully characterized by ¹H NMR spectroscopy and ESI-MS mass spectroscopy. The ¹³C NMR spectrum was not recorded due to the poor solubility of these zwitterions.

As an example, in Figure 4.22 it has been reported the ¹H NMR spectrum of **C-6**, taken in DMSO-d6. At $\delta = 7.78$ ppm is visible a broad singlet because of the meta *J*-coupling and integrating for two that was

assigned to the protons in 4-position of the indole ring. Always at low fields, a multiplet overlapped with a doublet with ortho *J*-coupling is found in the 7.6-7.3 ppm range. Overall, these signals integrate for eight protons, and they are indeed relative to the two protons in 6- and 7-position of the indole rings, and to the two chemically equivalent protons of the aniline rings in meta with respect to the substituent. The other two protons of the latter aromatic system (four overall) in ortho with respect to the amino group resonate as a doublet at δ= 6.7 ppm. Very diagnostic for the identity of **C-6** are the two broad signals at δ ~ 6.0 and 5.3 ppm. The former of these resonances integrates for two protons, and it has been assigned to the vinyl protons, while the latter, integrating for four protons, was ascribed to the protons of the amino groups present on the two donor systems. Finally, at δ = 1.53 ppm, is easily recognizable a singlet relative to the twelve protons of the four identical methyl groups of the dye. The corresponding ESI-MS spectrum presents a base peak in agreement with the structure of the compound (see experimental part). The identity of the related croconaine **C-5** was confirmed through the same measurements (see experimental part).
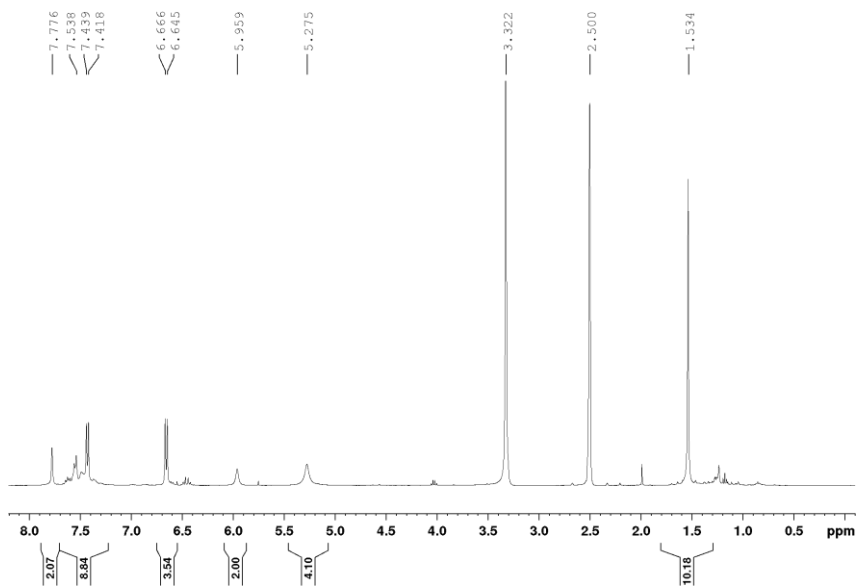
Figure 4.22 *¹H NMR spectrum (400 MHz, DMSO-d6) of croconaine* **C-6**.

Encouraged by these promising results, compound **C-7** was reacted with another commercial boronic derivative: the Boc-protected dihydropyridine boronic (as pinacolate) derivative **8** (Scheme 4.11). Using the same Pd catalyst, croconaine **C-8** was isolated in 70% yield after the usual workup. The Boc protecting group was then removed

with trifluoroacetic acid at room temperature for one hour (Scheme 4.11) to yield the croconaine **C-9** in 84% yield after inverse-phase chromatographic separation (see experimental part).
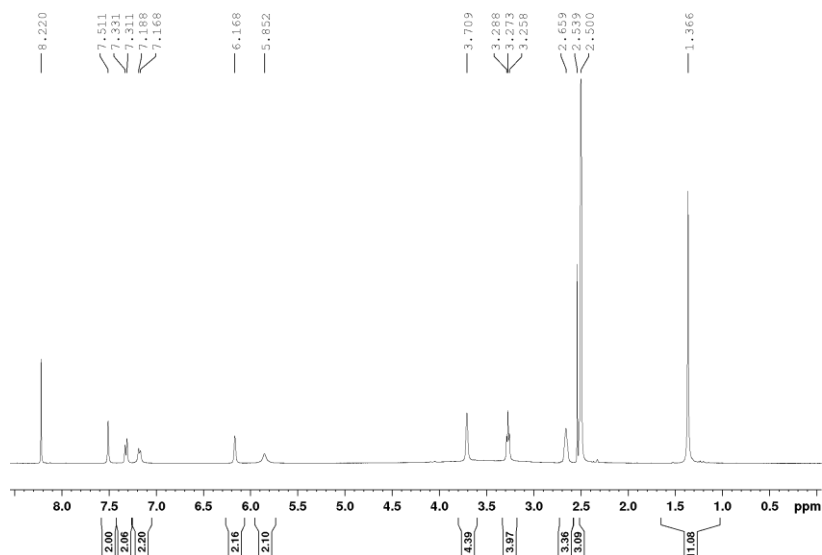
Figure 4.23 *¹H NMR spectrum (400 MHz, DMSO-d6) of croconaine* **C-9.**

The ¹H NMR spectrum of **C-9** (Figure 4.23) presents, at very low fields (δ = 8.2 ppm) a singlet relative to the formate ions deriving from the formic acid contained in the eluent used for the dye purification ($H_2O/CH_3CN/HCOOH$ (0.1%)) and due to which the product is in the form of formate salt. The aromatic zone presents a doublet with meta *J*-coupling at δ = 7.5 ppm, integrating for two, and a doublet of doublets with ortho and meta *J*-couplings at δ = 7.32, and a doublet at δ = 7.18 ppm, each integrating for two protons. These signals were assigned to the protons of the indole rings in 4-, 6- and 7-position, respectively. At δ = 6.17 and 5.85 ppm there are two broad signals, both integrating for two, relative to the vinyl protons. In the aliphatic zone, are observed a broad singlet at δ = 3.71 ppm, a triplet at δ = 3.27 ppm, and a broad signal at δ = 2.66 ppm a singlet, each integrating for four protons. These resonances were assigned to the three different methylene groups of the two piperidine cycles. Finally, at δ = 2.6-2.5 ppm, overlapped with the residual solvent signal, is found a multiplet, probably relative to the amino protons belonging to the indole and piperidine derivatives. Finally, at δ = 1.37 ppm there is a singlet, integrating for twelve, relative to the protons of the four methyl groups on the indole moieties. The corresponding ESI-MS spectrum presents peaks at m/z = 587.1 (100) [MH]⁺ and 585.7 (78) [MH]⁺, confirming the identity of **C-9**.

4.2.4.2   Study of Optical Properties

The optical properties (absorption and emission) of the synthesized croconaines were studied in different organic solvents to study the solvatochromic effects (i.e. the change of the absorption and emission maximum as a function of the polarity of the solvent). All the absorption and emission spectra have been normalized to favour a direct comparison of the bands. The optical properties of **C-1** and **C-2** were not studied.
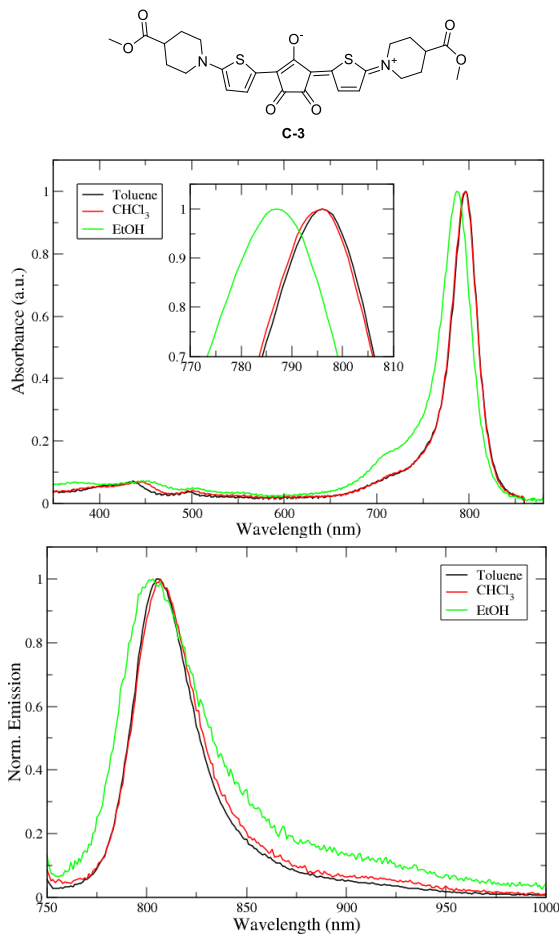
Figure 4.24 Normalized absorption (top) and emission (bottom) spectra of croconaine **C-3** in three different organic solvents.

The absorption spectra of croconaine **C-3** collected in various solvents were gathered in Figure 4.24. In all solvents used, the spectra always present a sharp absorption at the edge between the visible and the NIR regions at ca. 790 nm. In ethanol (green line in Figure 4.24, top) the maximum is centred at 787 nm (1.57 eV) in ethanol, while in less polar and aprotic solvents such as chloroform (red line) and toluene (black

line), a small bathochromic shift (redshift) of ca. 10 nm is observed. Since the maximum of the absorption band endures a hypsochromic shift increasing the solvent polarity, it is possible to say that a negative solvatochromism is observed. This could be due to a higher stabilization of the HOMO (with a more polar character) than the LUMO (less polar) by the solvent. As regards the emission spectrum, a similar behavior was recorded since the maximum of the emission band is at 825 nm in toluene and chloroform solution, while is found at 815 nm in ethanol (see Table 4.3).
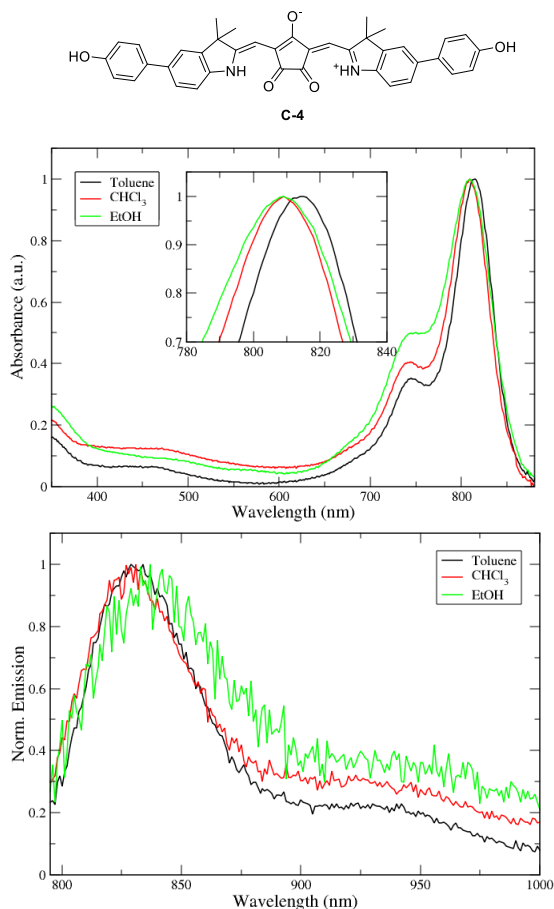
Figure 4.25 *Normalized absorption (top) and emission (bottom) spectra of croconaine* **C-4** *in three different organic solvents.*

Concerning the croconaine **C-4**, the maximum of the absorption band is centered at ~805 nm both in ethanol and in chloroform. In a less polar solvent, the maximum is red-shifted of ~10 nm, showing a bathochromic effect. Indeed, in ethanol, the band is centered at ~815 nm. On the other hand, in the emission spectra is not observed a relevant solvatochromic effect, and the maximum of the band is around

840 nm. As previously specified, the fluorescence intensity is normalized for both cases, in order to have a direct comparison. However, the emission intensity of **C-3** is approximately one order of magnitude greater than the intensity of **C-4**. This fact was confirmed by the determination of the fluorescence quantum yields of the two compounds (see Table 4.2). The results obtained for the croconaine **C-4** are in agreement with those found for analogous compounds by Punzi et al.[31] It is worth to note that the quantum yield calculated for **C-3** in toluene ($\Phi = 0.272$) is very high for this type of compound.

	C-3	**C-4**
Toluene	0.272	0.04
CHCl₃	0.101	0.07
EtOH	0.027	0.02

Table 4.2 *Fluorescence quantum yields (Φ) of croconaines* **C-3** *and* **C-4**.

For the indole-based croconaine **C-5**, **C-6**, and **C-9**, only the UV-Vis-NIR measurements were performed. Compound **C-5** shows a very sharp absorption at ~805 nm both in toluene (Figure 4.26, black line) and chloroform (Figure 4.26, red line). On the contrary, a strange behavior was observed in the more polar ethanol. In this solvent, the band is blue-shifted by ~20 nm and an increase in the intensity of a sideband centered at ~710 nm is observed (Figure 4.26, green line).

This fact was ascribed to a lower solubility in this polar solvent or also to a different stabilization of the possible conformations that this molecule can assume in solution.[1] To disclose the latter effect, the UV-Vis spectra of the three conformers indicated as **Down**, **Up**, and **Up&Down** in Figure 4.26 were simulated using the ORCA quantum chemistry package[42] with the ZINDO/S semi-empirical quantum chemistry method[43] on PM3[44] minimized structure of the conformers. Indeed, the ZINDO/S method allows the calculation of excited states. As indicated in Figure 4.26, because of its high electrons delocalization, in the simulated spectra (not shown), the conformer **Down** gives rise to a band centered at $\lambda = 822$ nm with an oscillator strength f = 1.43. As expected, the simulation relative to the conformer **Up** yields a less intense (f = 0.75) and blue-shifted band ($\lambda = 773$ nm).

---

[1] Because of the mesomerism, it is difficult to discriminate whether the rotation occurs around a single or a double bond; therefore the denotation conformer was chosen instead of geometrical isomer.

It thus seems that in ethanol, the contribution of the conformer **Up** (or **Up&Down**) is higher than in the other two solvents used.
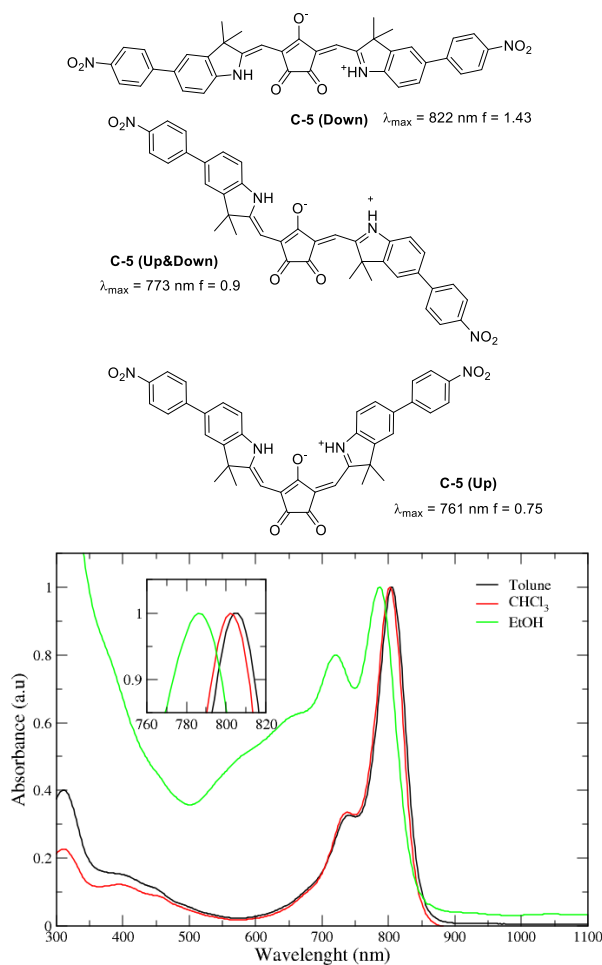
*Figure 4.26 Normalized absorption spectra of croconaine **C-5** in three different organic solvents. The λ_{max} are indicated close to the structure of the several conformers.*

The UV-Vis-NIR absorption spectra of croconaine **C-6** show a similar position of the band maximum (823 nm) in chloroform (Figure 4.27, red line) and ethanol solution (Figure 4.27, green line). In toluene solution, the band is centered at 828 nm (Figure 4.27, black line), thus no significant solvatochromic effect was observed. However, even in this case, in ethanol, the intensity of the shoulder band at higher energy is increased than in the other two low polarity solvents.
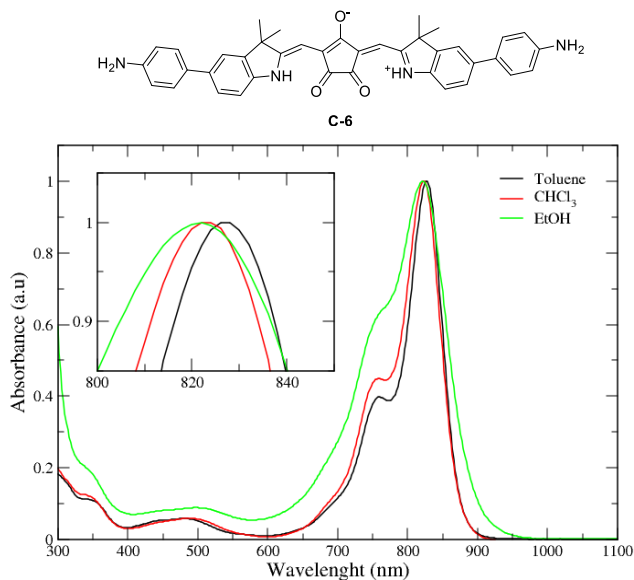
Figure 4.27 *Normalized absorption spectra of croconaine **C-6** in different organic solvents.*

Croconaine **C-9** is characterized by high insolubility in Toluene. For this reason, it was possible to record the spectra only in chloroform and ethanol. In both cases, the shape of the band is very similar, showing a slight solvatochromism (~15 nm). In ethanol the maximum is centered at 792 nm (Figure 4.28, green line), and in chloroform at 806 nm (Figure 4.28, red line).

150
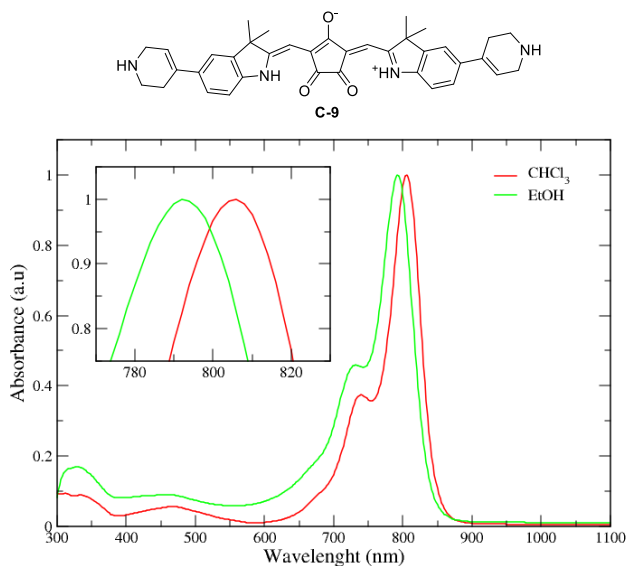
Figure 4.28 *Normalized absorption spectra of croconaine **C-9** in two different organic solvents.*

For each of the synthesized dyes, the molar extinction coefficient (ε), the wavelength corresponding to the maximum of the absorption (λ_{max}) and the energy gap (E_g), calculated from the λ_{onset}, were summarized in Table 4.3 for the different solvents used.

Croconaine	Solvent	λ_{max} (nm)	ε (M^{-1} cm^{-1})	λ_{onset} (nm)	E_g (eV)
C-3	Toluene	796	4.6 x 10^3	825	1.50
	CHCl$_3$	796	4.4 x 10^3	825	1.50
	EtOH	787	5.3 x 10^3	815	1.52
C-4	Toluene	814	5.1 x 10^3	855	1.45
	CHCl$_3$	809	4.9 x 10^3	850	1.46
	EtOH	808	5.5 x 10^3	860	1.44
C-5	Toluene	806	3.2 x 10^4	850	1.46
	CHCl$_3$	802	5.8 x 10^4	845	1.47
	EtOH	786	2.7 x 10^4	843	1.47
C-6	Toluene	828	4.1 x 10^4	870	1.43
	CHCl$_3$	824	2.4 x 10^4	875	1.42
	EtOH	822	2.1 x 10^4	895	1.39
C-9	CHCl$_3$	806	8.3 x 10^4	850	1.46
	EtOH	792	5.7 x 10^4	840	1.48

Table 4.3 *Molar extinction coefficient (ε) and energy gap (E_g) of the synthesized croconaines in toluene, CHCl$_3$ and ethanol.*

4.2.5 Synthesis of Linkers

In Table 4.1 were listed a series of possible linkers (L) to be used for the functionalization of the donor moieties and thus for the realization of a functional triad (indicated as LDADL). As briefly discussed in the introduction, the linkers are characterized by the presence of terminal functional groups (G) of different nature (Table 4.1) that can act as anchor points for a further grafting on an inorganic surface (e.g. noble metals NPs or NRs). Several combinations of donors coupled with linkers of various lengths have been evaluated and synthesized.

The mainly used functional alkyl chain was the lipoic acid (**L-1**) (see Scheme 4.12), which is characterized by an aliphatic chain made of six carbon atoms with a terminal five-membered ring with an S-S bond. It can be considered as a self-protecting group; in fact, it is very often used

in place of a thiol free function (-SH) because it has no oxidability problems and cannot act as a nucleophile. On the other hand, its propensity to form stable anchor points with surfaces of noble metals is well documented since it is a bidentate ligand. The linker **L-2** was obtained by reacting lipoic acid with 6-bromohexane-1-amine in a dichloromethane solution in the presence of diisopropyl ethylamine (DIPEA) and N, N, N ′, N′-tetramethyl-O- (1H-benzotriazole-1-ile) uronium hexafluorophosphate (HBTU), as the coupling agent (see Scheme 4.12). In this way **L-2** was isolated in 46% yield. NMR and ESI-MS measurements confirms the identity of the product.
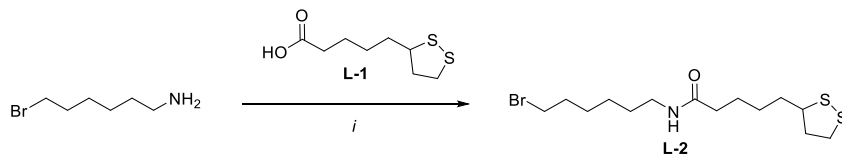
Scheme 4.12 *Synthesis of the linker **L-2**. Reagents and conditions: i) HBTU, DIPEA, CH₂Cl₂, rt, 16h, 46%.*
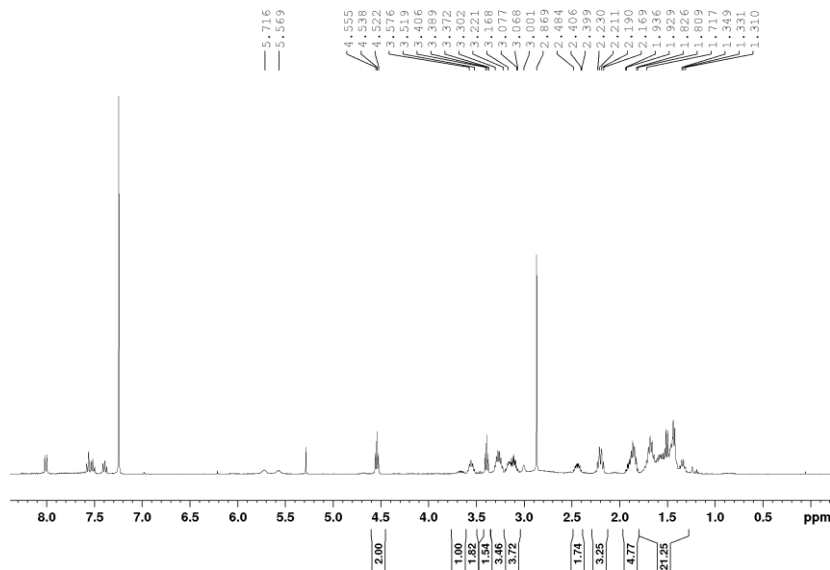
Figure 4.29 *¹H NMR spectrum (400 MHz, CDCl₃) of the linker **L-2**.*

The ¹H NMR spectrum of **L-2**, taken in CDCl₃, shows in the aromatic region, at low fields, signals related to a byproduct deriving from the HBTU (Figure 4.29). This impurity was not isolated to avoid the degradation of the disulfide bond in the chromatographic step. **L-2** was thus used in the following reactions without any further purification step. At ~5.7 and 5.6 ppm two broad signals, overall integrating for one

proton, were assigned to the proton amide group, thus indicating that the coupling between **L-1** and 6-bromohexane-1-amine occurred correctly. Finally, in the aliphatic region, it is possible to identify the signals related to the remaining protons of the two alkyl chains.

The ESI-MS analysis, combined with reverse-phase liquid chromatography (UPLC) detected a peak with a retention time of 1.18 min and a isotopic mass distribution of $m/z = 335.9$ (100) $[MH]^+$, 337.8 (94) $[MH+1]^+$ that is in agreement with the formation of **L-2**.

A similar linker, **L-3**, was prepared by changing the leaving group from bromo to tosylate as depicted in Scheme 4.13. As in the previous case, the first reaction was a coupling between 6-aminohexanol and lipoic acid (**L-1**) in the presence of DIPEA and HBTU. The product detected with the UPLC-MS analysis presented two peaks characterized by an equal ratio of m/z and retention time of 0.84 min and 0.85 min, respectively. The subsequent characterization by ^{1}H NMR showed the presence of a side product, presumably generated by the nucleophilic attack of the hydroxyl group on the lipoic acid. Therefore, further purification was accomplished through a cation exchange chromatography (SCX), so that the isomer having the amino group (after its protonation) could be retained by the sulfonic groups (-SO$_3^-$) of the resin. The pure product **L-3** was obtained in 60% yield and characterized by NMR and ESI-MS spectroscopy.
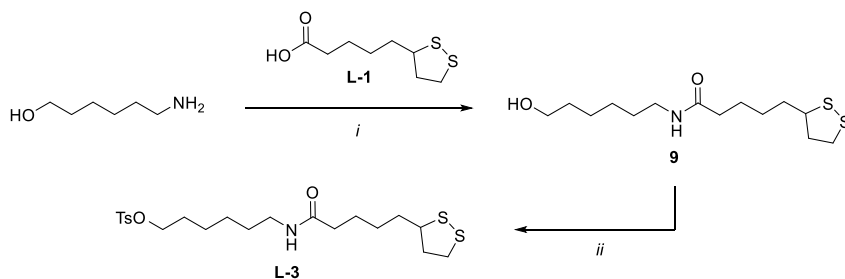
Scheme 4.13 *Synthesis of the linker L-3. Reagents and conditions: i) HBTU, DIPEA, CH₂Cl₂, rt, 16h, 60%; ii) TsCl, Et₃N, DMAP, CH₂Cl₂, rt, 16h, 63%.*

The linker **L-3** was then obtained by reaction of **9** with tosyl chloride (TsCl) in the presence of triethylamine (Et$_3$N) and DMAP (Scheme 4.13). After a chromatographic purification step, **L-3** was obtained in 63% yield and it was characterized by NMR and ESI-MS spectroscopy.

The ^{1}H NMR spectrum of the isolated compound, taken in DMSO-d$_6$ (**Figure 4.30**), shows two doublets at $\delta = 7.59$ ppm and 7.29 ppm, integrating for two protons, respectively, and a singlet at $\delta = 2.23$ ppm, integrating for three protons, related to the OTs group. The triplet at $\delta = 3.81$ ppm, integrating for two protons, is related to the methylene

protons in α to the -OTs group, whereas the methylene protons in α to amide nitrogen give rise to a quadruplet at $\delta = 2.78$ ppm. The 5-membered ring, containing the S-S bond, originate a series of diagnostic multiplets at ~3.5-3.4 ppm, integrating for one proton, 3.0-2.8 ppm, two overlapped signals, integrating for two protons, 2.3-2.2 ppm and 1.7-1.6 ppm, integrating for one proton, respectively. These four multiplets are originated because of the four diasterotopic protons of the dithiolane ring. The ESI-MS analysis combined with reverse-phase liquid chromatography detects a peak with retention time of 1.23 min, having in the related mass spectrum an isotopic distribution of m/z = 459.9 (100) [MH]$^+$, 460.8 (35) [MH+1]$^+$, 462 (21) [MH+2]$^+$ that is in agreement with the structure of **L-3**.
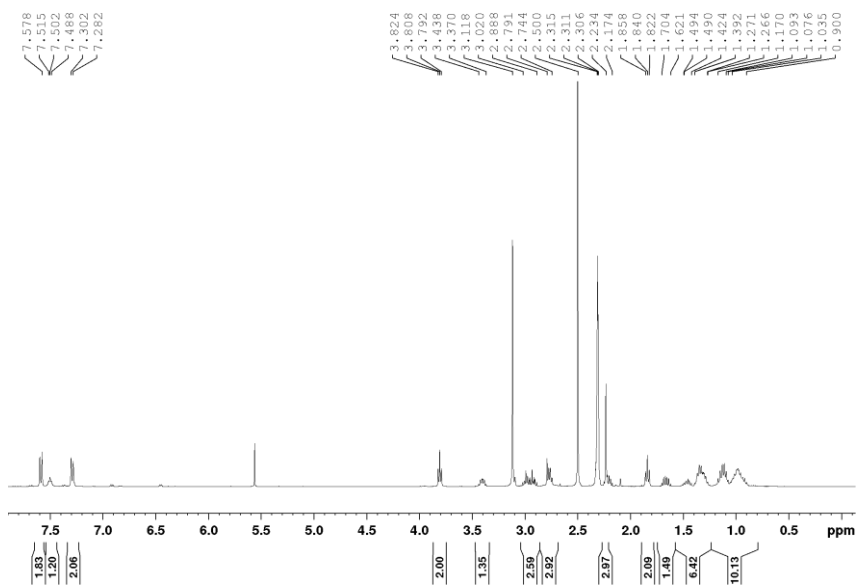
Figure 4.30 ^{1}H NMR spectrum (400 MHz, DMSO-d6) of the linker **L-3**.

The synthesis of linkers **L-4** was already discussed in Chapter 2 (Scheme 2.5). The functional thiol-anchoring group was protected as a thioester group (-SCOCH$_3$) to avoid oxidation, with the formation of disulfide bridges, and to prevent unwanted side-reactions.
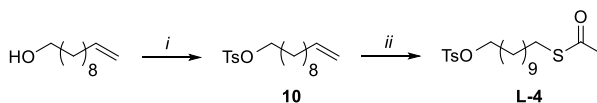
Scheme 4.14 Synthesis of linker **L-4**. Reagents and conditions: i)TsCl, Et$_3$N, DMAP, CH$_2$Cl$_2$, rt, overnight, 96%; ii)CH$_3$COSH, AIBN, toluene, reflux, 5h, 70%.

In the ^{1}H NMR spectrum, recorded in CDCl$_3$, the presence of three diagnostic signals can be observed: the triplet at $\delta = 4.03$ ppm relative

to the methylene protons in α-position with respect to the tosylate protecting group (-OTs), the triplet to δ = 2.87 ppm relative to methylene protons in α-position with respect to the thioester functional group and the singlet at δ = 2.33 ppm relative to the methyl protons of the thioester (Figure 4.31). Moreover, the methyl protons of the thioester resonate at δ = 2.46 ppm.
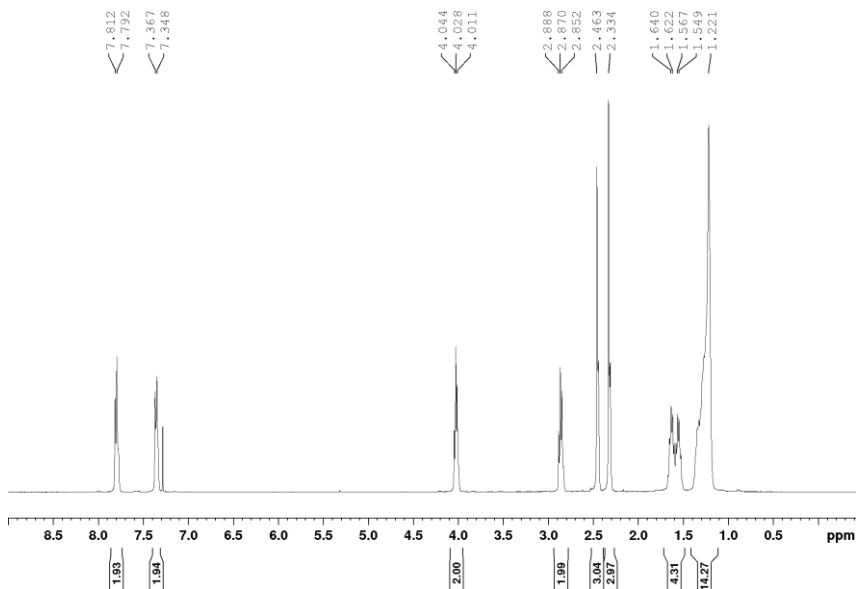
Figure 4.31 ^1H NMR spectrum (400 MHz, CDCl$_3$) of the linker **L-4**.

Besides a thiol group, another possible anchoring group **G** for the surfaces is the amino function. For its protection, several protecting groups were used: phthalimide (Phthal), tert-butoxycarbonyl (Boc), and benzyl chloroformate (Cbz).

The linker **L-5** was synthesized in two steps. The first one is the reaction of 6-aminohexan-1-ol with phthalic anhydride in a microwave reactor to yield the derivative **11** in quantitative yield (Scheme 4.15). Without any further purification, **11** was used in the subsequent reaction with TsCl in the same conditions already discussed for the synthesis of **L-3** and **L-4**. The product was then characterized through NMR and ESI-MS measurements and the result obtained were in agreement with the theoretical ones (see the experimental part).
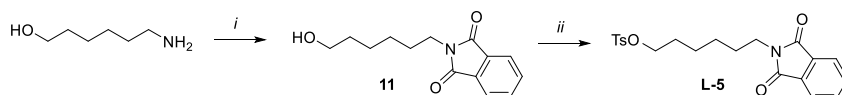
Scheme 4.15 Synthesis of linker **L-5**. Reagents and conditions: i) phthalic anhydride, MW, 160°C, 5 min, quant. yield; ii) TsCl, Et$_3$N, DMAP, CH$_2$Cl$_2$, rt, 16h, 98%.

In the ^{1}H NMR spectrum, taken in CDCl$_3$ (Figure 4.32), a multiplet at ~7.8-7.6 ppm is related to the four aromatic protons of the phthalimido group and two protons of the -OTs. The other two aromatic protons of this latter group resonate at δ = 7.29 ppm. The triplets at δ = 3.97 ppm and δ = 3.58 ppm are related to the methylene protons in α position with respect to the amino-protected group and the O atom of the tosylate, respectively. The methyl protons of the -OTs resonate at δ = 2.40 and the other two broad multiplets at 1.6-1.2 ppm are related to the aliphatic protons of the alkyl chain.

Figure 4.32 ^{1}H NMR spectrum (300 MHz, CDCl$_3$) of the linker **L-5**.

Using the *Boc* as protecting group, two linkers were synthesized: one with six carbon atoms (**L-6**) and one with eleven carbon atoms (**L-7**). The first step is the reaction with the di-*tert*-butyl dicarbonate (Boc$_2$O) to give **12** (n=1) and **13** (n=6). The two target linkers were obtained after the reaction with TsCl in the usual conditions, previously reported (Scheme 4.16).

Scheme 4.16 Synthesis of the linker **L-6** and **L-7**. Reagents and conditions: i) Boc$_2$O, Et$_3$N, THF, rt, 16h; ii) TsCl, Et$_3$N, DMAP, CH$_2$Cl$_2$, rt, 16h.

In the ^{1}H NMR spectra, both taken in CDCl$_3$, besides the diagnostic signals arising from the -OTs group, already previously discussed, it is

clearly visible the intense singlet relative to the *tert*-butyl group in both the linkers (Figure 4.33). The triplets at $\delta = 3.9$ and the broad signal at ~3.1 ppm, both integrating for two protons, are related to the methylene protons in α position with respect to the functional ending groups.

L-6

L-7
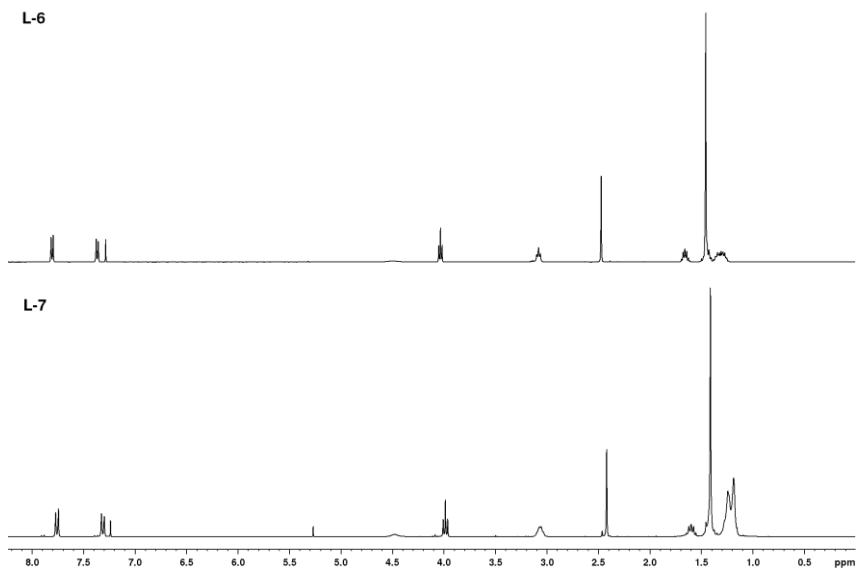
Figure 4.33 *^{1}H NMR stack plot of linkers **L-6** (400 MHz, CDCl₃, top), **L-7** (300 MHz, CDCl₃, bottom).*

With a similar procedure, it was also synthesized the linker **L-8**, which is a known compound. After the protection of the amino function with benzyl chloroformate (Cbz-Cl), the reaction with TsCl was carried out to afford the linker in 70% overall yield (Scheme 4.17). The isolated product was characterized by NMR and ESI-MS spectroscopy and the results obtained were in agreement with the published ones.[45]
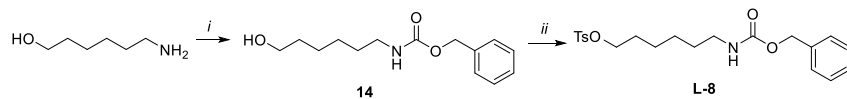
Scheme 4.17 *Synthesis of the linker **L-8**. Reagents and conditions: i) Cbz-Cl, Na₂CO₃, THF/H₂O (1:1), rt, 16h, 81%; ii) TsCl, Et₃N, DMAP, CH₂Cl₂, rt, 16h, 87%.*

In the ^{1}H NMR, taken in CDCl₃, of **L-8** it is possible to recognize some diagnostic signals for the *Cbz* group (Figure 4.34). The singlet at $\delta = 4.89$ ppm is generated by the benzylic methylene protons, while the aromatic protons resonate as a multiplet in the aromatic region around 7.2-7.3 ppm, overlapped to the doublet of the two aromatic protons of the -OTs group. The presence of the tosylate is also confirmed by the

singlet at δ = 2.40 ppm, integrating for three protons. The methylene protons in α-position with respect to the OTs and to the protected nitrogen atom generate the triplet at δ = 3.96 ppm and the quadruplet at δ = 3.09 ppm, respectively. The multiplets in the aliphatic region are generated by the remaining methylene protons of the alkyl chain.
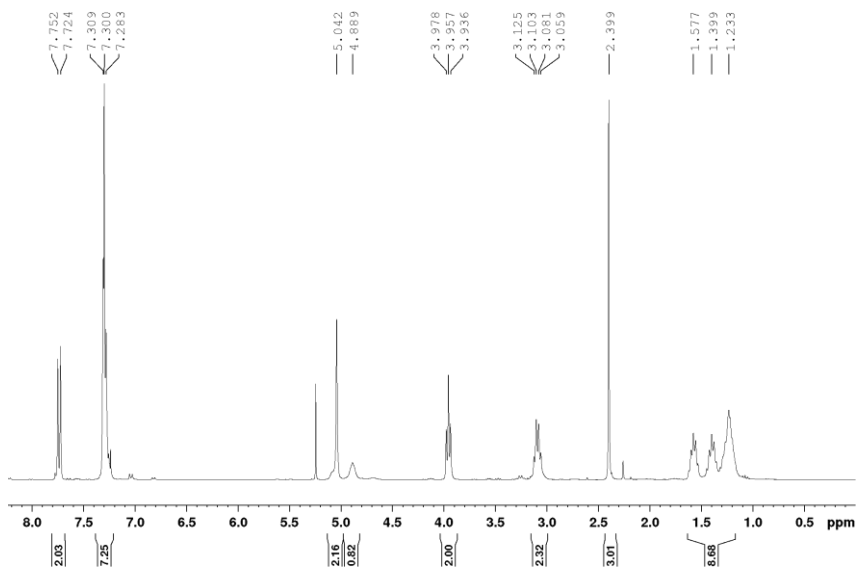
Figure 4.34 ¹*H NMR spectrum (300 MHz, CDCl₃) of the linker* **L-8**.

4.2.6 Synthesis of the functionalized Donors with Linkers (DL)

Some synthetic strategies have been adopted to form amide, ester and ether bonds between the indole derivatives (**ID-1** and **ID-3**) and some of the synthesized linkers (**L-1** and **L-3**).
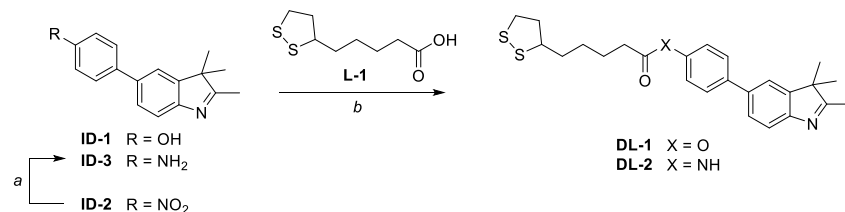
Scheme 4.18 Synthesis of functionalized donors **DL-1** *and* **DL-2**, *starting from* **ID-1** *and* **ID-2**, *respectively. Reagents and conditions: a) Fe, NH₄Cl, H₂O/iPrOH (1:3), 80°C, 2h, 94%; b)* **ID-1**, *EDC, DMAP, ET₃N, CH₂Cl₂, rt, 16h, 46% or* **ID-3**, *HBTU, DIPEA, CH₂Cl₂, rt, 16h, 90%.*

The lipoic acid **L-1**, exploiting its "self-protecting" nature of the thiol function, can be used directly for the coupling reactions with the donor

moieties. Its reaction with **ID-1** in the presence of 1-ethyl-3-(3-dimethylaminopropyl)carbodiimide (EDC-Cl) as the coupling agent, gave the functionalized donor **DL-1** in 46% yield after purification by column chromatography (Scheme 4.18).

Functionalized donor **DL-2** was obtained by reaction between **ID-3** and **L-1**, employing HBTU as the coupling agent, in the presence of DIPEA as the base (Scheme 4.18). After purification step through silica gel column chromatography, **DL-2** was obtained in 90% yield. Both **DL-1** and **DL-2** were characterized by NMR and ESI-MS analysis (see also experimental section).
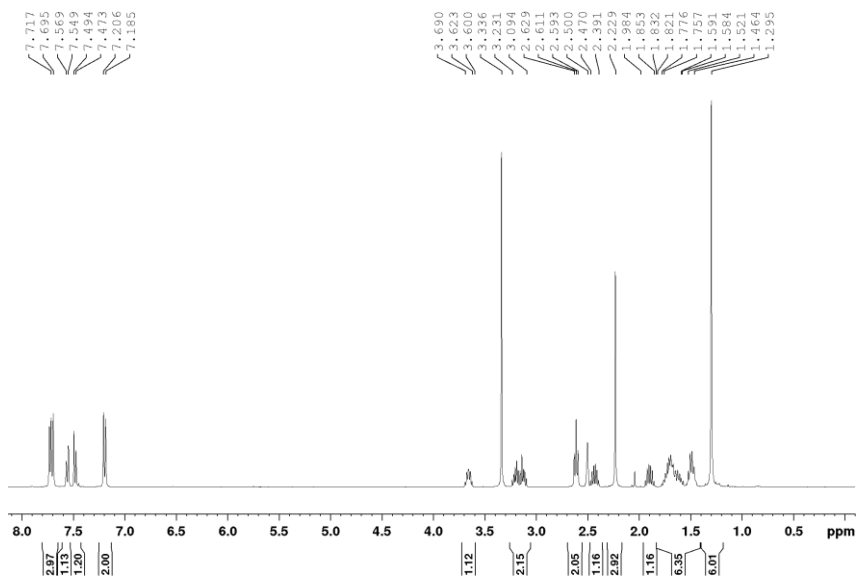
Figure 4.35 *¹H NMR spectrum (400 MHz, DMSO-d6) of the functionalized donor **DL-1**.*

As an example, the ¹H NMR spectrum of **DL-1**, taken in DMSO-d$_6$, is reported in **Figure 4.35**. It presents, in the aromatic region, a series of signals relative to the typical pattern of aromatic protons of the substituted indole moieties (Figure 4.35), as previously described i.e. for compound **ID-2**. Besides the typical multiplets deriving from the diasterotopic protons of the dithiolane ring, previously discussed in the synthesis of the linkers, the occurred functionalization of the donor moieties is confirmed by the presence of the triplet at δ = 2.61 ppm, relative to the methylene group in α-position to the carbonyl group, and from the series of multiplets between δ = 1.8-1.4 ppm, integrating in total for six protons, generated by the remaining three methylene groups of the aliphatic chain of **L-1** unit. Finally, at δ = 2.23 and 1.30 ppm, there are two intense singlets, integrating respectively for three and six protons, relative to the methyl groups of the indole unit. Moreover, mass spectroscopy (ESI) combined with reverse-phase liquid

chromatography detects a peak with retention time of 1.38 min having an isotopic pattern of m/z = 440 (100) [MH]$^+$, 441 (18) [MH + 1]$^+$, 441.9 (19) [MH + 2]$^+$ that is in agreement with the identity of **DL-1**.

The linker **L-3** presents a good leaving group (-OTs), which was exploited for the alkylation of the -OH function of **ID-1**. The reaction was conducted in a 1:1 mixture of THF and acetone in the presence of cesium carbonate (Cs$_2$CO$_3$) as the base (Scheme 4.19). After the purification chromatographic step, the isolated **DL-3** was characterized by NMR and ESI-MS measurements.
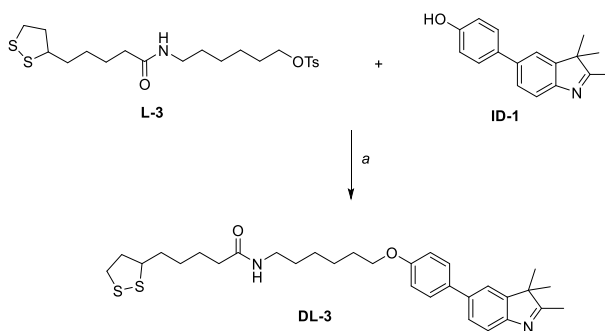
Scheme 4.19 *Synthesis of functionalized donor **DL-3**. Reagents and conditions: a) Cs$_2$CO$_3$, THF/Acetone (1:1), 60°C, 24h, 49%.*
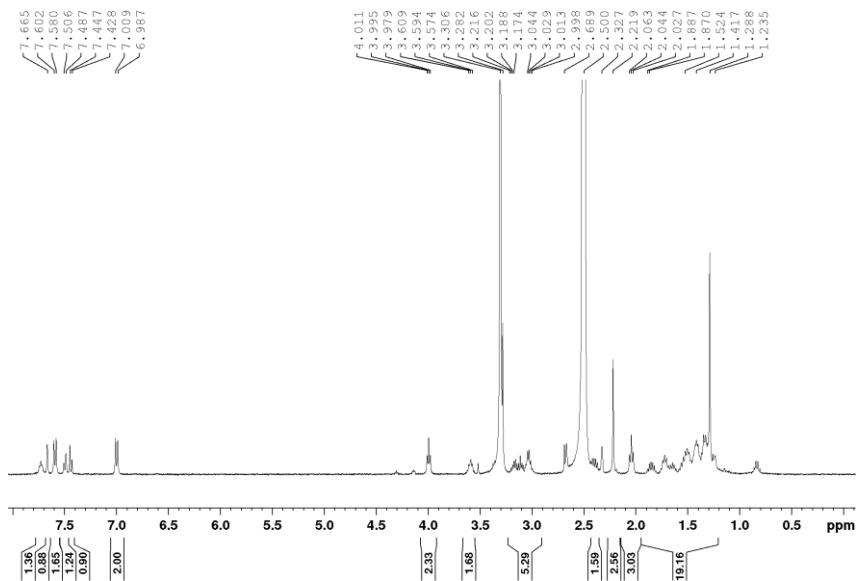
Figure 4.36 *^{1}H NMR spectrum (400 MHz, DMSO-d6) of the functionalized donor **DL-3**.*

The ^{1}H NMR spectrum (**Figure 4.36**) of the **DL-3**, taken in DMSO-d6, shows the diagnostic signals belonging to the chain of the linker **L-3** (see Figure 4.30) and to the donor **ID-1** (see Figure 4.17, bottom). The

disappearance of the singlet relative to the -OH function of the indole-based donor and the signals relative to the protons of the tosylate group confirms the occurred reaction. The mass spectroscopy (ESI) analysis combined with reverse-phase liquid chromatography detects a peak with retention time of 1.31 min and isotopic pattern of m/z = 539.2 (100) [MH]$^+$, 540.2 (37) [MH+1]$^+$, 541.2 (13) [MH+2]$^+$ that is in agreement with the identity of **DL-3**.

The alkylation conditions of the 2-methyl benzothiazole (**BT**) were investigated in section 4.2.3.1. A possible strategy for the functionalization of this donor moiety could be the insertion on the N atom of the thiazole ring with an alkyl chain bearing a "grafting" ending group **G**. To this aim, the synthesis of two functionalized benzothiazole-based donors **DL-4** and **DL-5** was tackled (Scheme 4.20). In separated experiments, **BT** was refluxed in toluene with the proper linker, **L-4** or **L-5**, for 24 hours. The desired products **DL-4** and **DL-5** were obtained through precipitation from ethyl acetate in 33 and 36% yields and characterized by NMR and ESI-MS measurements.
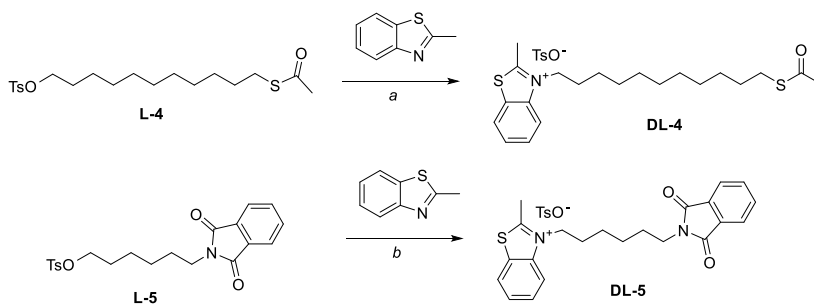
Scheme 4.20 *Synthesis of functionalized donors* **DL-4** *and* **DL-5**. *Reagents and conditions: a) toluene, reflux, 24h, 36%; b) toluene, reflux, 24h, 33%.*

In the ^{1}H NMR spectrum, taken in CDCl$_3$, the presence of the **BT** unit is confirmed by the presence of the typical patterns of signals in the aromatic region (Figure 4.37): two doublets at δ = 8.17 and 7.88 ppm, and two triplets at δ = 7.72 and 7.6 ppm, partially overlapped with a doublet relative to two tosylate protons. The signals arising from the protons of the alkyl chain of the linkers are visible in the upfield region of the spectrum. The positive outcome of the reaction is indeed confirmed by the downfield shift endured by the signal of the methylene protons in α-position with respect to the benzothiazole ring. In **L-4**, the corresponding triplet is found at δ = 4.03 ppm (cf. Figure 4.31), while in **DL-4** it resonates at δ = 4.74 ppm because of the electron-withdrawing effect generated by the positively charged N atom. The mass spectroscopy (ESI) analysis detects peaks at m/z = 378.3 (100)

[M-OTs]⁺, 379.3 (69) [M-OTs+1]⁺, 380.3 (45) [M-OTs+2]⁺, 381.2
(11) [M-OTs+3]⁺, in agreement with the theoretical prediction.
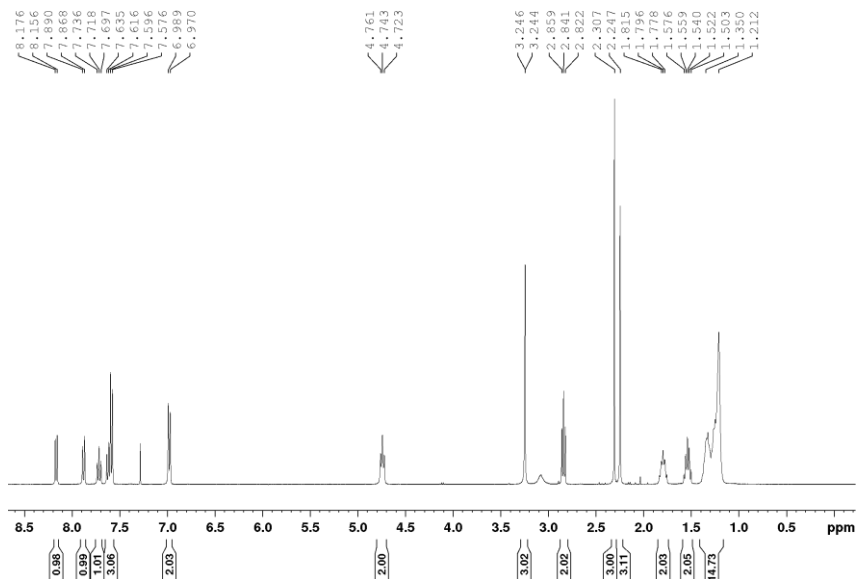
Figure 4.37 ¹H NMR spectrum (400 MHz, CDCl₃) of functionalized donor **DL-4**.
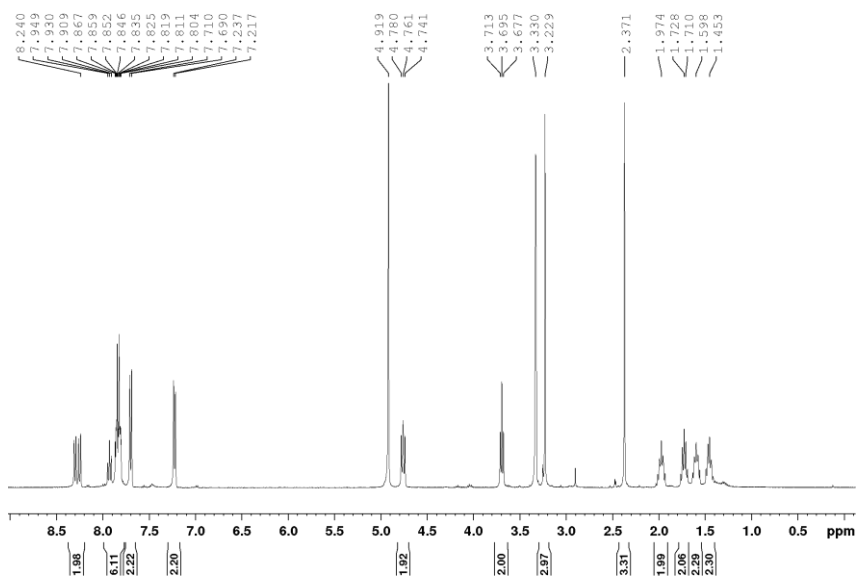
Figure 4.38 ¹H NMR spectrum (400 MHz, CD₃OD) of the functionalized donor **DL-5**.

In Figure 4.38 is shown the ¹H NMR spectrum of **DL-5**, taken in
CD₃OD. Also in this case, the positive outcome of the alkylation
reaction is confirmed by the disappearance of the triplet, at δ = 3.97
ppm (cf. Figure 4.32), relative to the methylene protons in α-position

with respect to the -OTs group, together with the appearance of the triplet at δ = 4.76 ppm generated by the methylene protons in α-position with respect to the positively charged N atom. In the aromatic region, besides the signals relative to the **BT** unit and the tosylate as counterion, the presence of a multiplet at 7.8-7.9 ppm is due to the aromatic protons of the -Phthal protecting group.
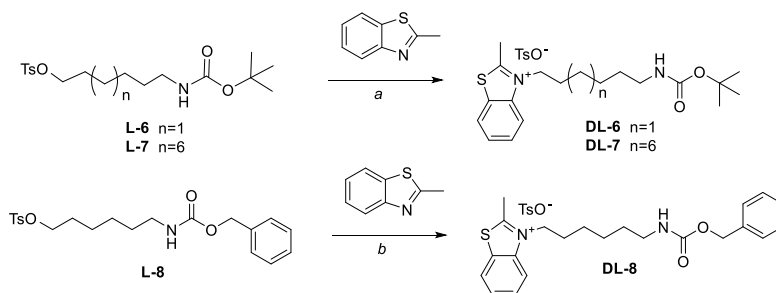
Scheme 4.21 *Synthesis of functionalized donors* **DL-6**, **DL-7**, *and* **DL-8**. *Reagents and conditions: a) toluene/CH₃CN (1:1), reflux, 24h; b) toluene, reflux, 24h, 0%.*

The same synthetic approach was used for the reaction of **BT** with linkers **L-6** and **L-7**, which are characterized by the presence of a good leaving group (-OTs) at one end and an amino-protecting group (-NH*Boc*) on the other end (Scheme 4.21). The former linker is characterized by a C6 alkyl chain, instead the latter one by a longer C11 chain. The **BT** was refluxed in a 1:1 mixture of toluene and CH₃CN for 24 hours with the proper linker, but neither **DL-6** nor **DL-7** were isolated from the reaction mixture in appreciable amount. Therefore, another attempt was made to alkylate **BT** with another C6 linker (**L-8**, Scheme 4.21), which presents the tosylate as the leaving group, and an amine function protected with -*Cbz* group. However, also in this case, the alkylation reaction was not successful.

4.2.7   Synthesis and optical properties of LDADL dyes

4.2.7.1   Synthesis of croconaine LDADL-type dyes

In the last part of this study, several attempts were carried out to conjugate the previously prepared **DL-1-5** units with the acceptor units **A-1** and **A-2** to obtain a series of LDADL dyes. Unfortunately, the harsh reaction conditions used to promote the condensation between the DL units and the acceptor core (high temperatures and basic conditions) were not compatible with the dithiolane ring present in **DL1-3**, and all the condensation reactions carried out using these DL were unsuccessful. Contrarywise, the robustness of the two functionalized donor units containing the benzothiazole ring, **DL-4** and

DL-5, allowed us to isolate the new LDADL croconaine dyes **C-10** and **C-11** (Scheme 4.22). The reactions were carried out in the typical conditions reported for the synthesis of the unfunctionalized croconaines (**C-1** to **C-9**) discussed in section 4.2.4.1. In brief, croconaine **C-10** was obtained by reaction between **A-1** and **DL-4** in a refluxing 1:1 mixture of toluene and *n*-butanol in the presence of pyridine as the base. The purification of this product was accomplished through precipitation induced by the addition of methanol to the concentrated reaction mixture, followed by a centrifugation step to isolate **C-10** in15% yield as a solid compound.
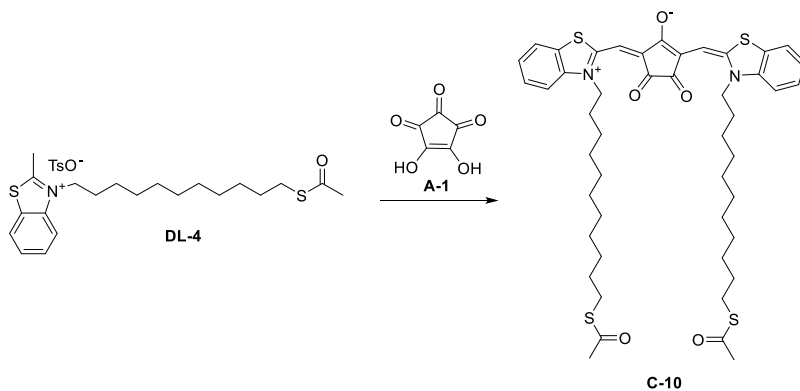
Scheme 4.22 *Synthesis of croconaine* **C-10**. *Reagents and conditions: pyridine, toluene/n-butanol (1:1), 110 °C, 6h, 15%.*
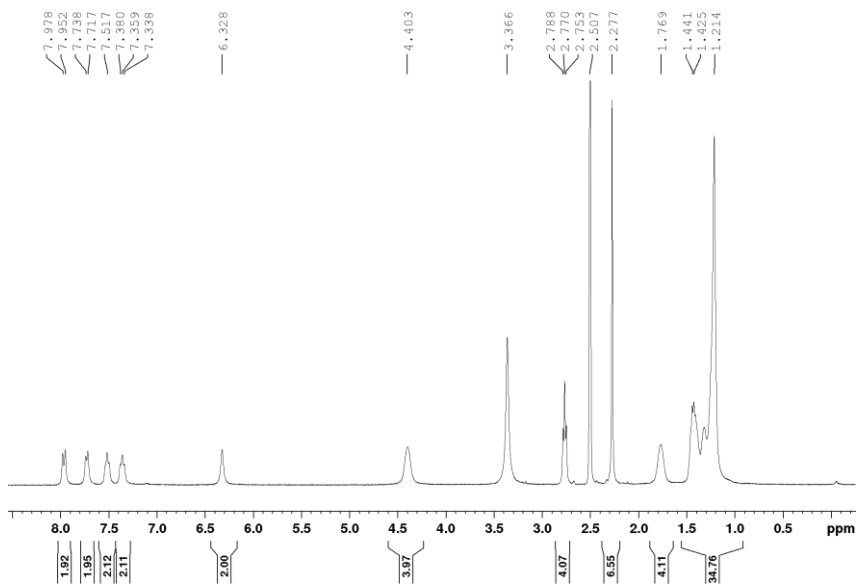
Figure 4.39 *¹H NMR spectrum (400 MHz, DMSO-d6) of* **C-10**.

The ^{1}H NMR spectrum, taken in DMSO-d6, reflects the tendency of **C-10** to aggregate in solution (Figure 4.39). The positive outcome of the reaction is confirmed by the presence of several diagnostic signals. The broad singlet at δ = 6.33 ppm is related to the vinyl protons of the bridging unit between **A-1** and **DL-4**. With respect to the spectrum of the starting reagent **DL-4** (cf. Figure 4.37), it is possible to observe the disappearance of the singlet at δ = 3.24 ppm relative to the methyl protons of the benzothiazole donor unit. The integration of all the signals evidences the correct ratio of 2:1 between the acceptor (A) and donor (D) units. The croconaine **C-10** was further analyzed by ESI-MS spectrometry, revealing diagnostic peaks at m/z = 860.5 (100) [M]$^+$, 861.5 (80) [M+H]$^+$.

The reaction between **A-1** and **DL-5** was carried out in the same experimental condition, to give croconaine **C-11** in 12% yield (Scheme 4.23). In this case, however, in addition to the croconaine precipitation, it was necessary to perform a further purification step through column chromatography (SiO$_2$, CH$_2$Cl$_2$/CH$_3$OH 92:8). The isolated pure croconaine **C-11** was characterized as usual through NMR and ESI-MS spectroscopy.
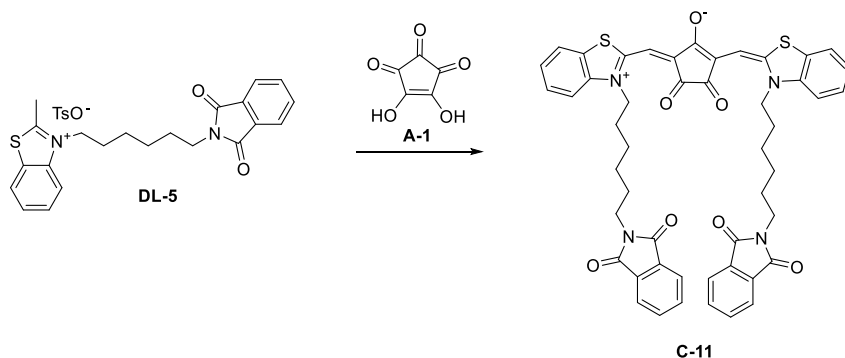
Scheme 4.23 *Synthesis of croconaine **C-11**. Reagents and conditions: pyridine, toluene/n-butanol (1:1), 110°C, 6h, 12%.*

In the ^{1}H NMR spectrum of **C-11**, taken in DMSO-d$_6$ (Figure 4.40), the broad signal relative to the vinyl protons at δ = 6.32 ppm witnesses the positive outcome of the condensation reaction. The other signals are almost superimposable with the ^{1}H NMR spectra of the two separated components (**A-1** and **DL-4**); nevertheless, the correct ratio of the integrals confirms the structure of **C-11**. The ESI-MS analysis shows as expected, the diagnostic peaks at m/z = 863.4 (100) [MH]$^+$, 864.4 (62) [MH+1]$^+$, 865.4 (32) [MH+2]$^+$.
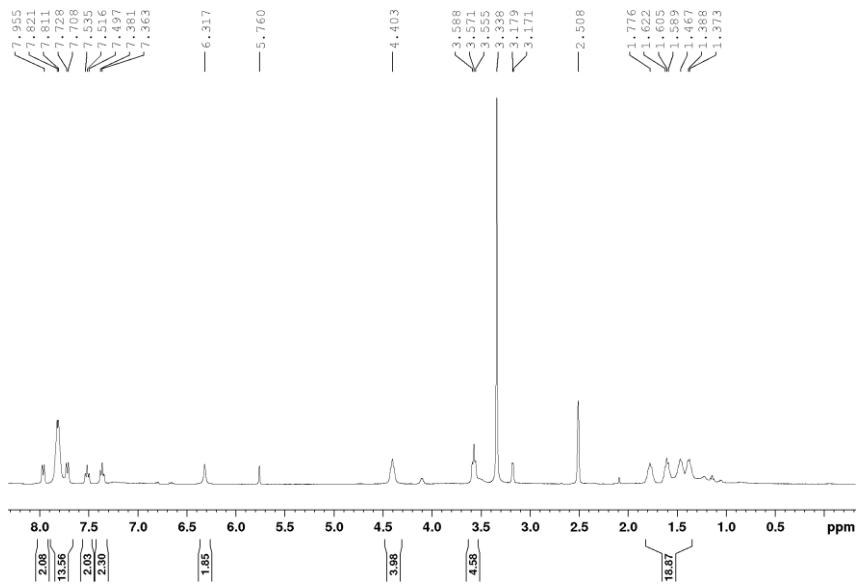
Figure 4.40 *¹H NMR spectrum (400 MHz, DMSO-d6) of **C-11**.*

4.2.7.2   Optical Properties

The optical properties of the synthesized LDADL-type croconaines **C-10** and **C-11** were studied as usual in different organic solvents. All the absorption and emission spectra have been normalized to favor a direct comparison of the bands.

The absorption spectra of croconaine **C-10** in various solvents were collected in Figure 4.41. In all solvents is present a sharp absorption in the NIR region, significantly affected by a solvatochromic effect (~40 nm). In methanol (green line in Figure 4.41) the maximum is centered at 759 nm (1.63 eV), while in a less polar and aprotic solvents such as CCl_4 the maximum is red-shifted and centered at 798 nm(1.55 eV). As in the previous optical studies reported in section 4.2.4.2, since the maximum of the absorption band shows a hypsochromic shifting with the increase of the solvent polarity, it is possible to assert that a negative solvatochromism is observed. As regards the emission spectrum, a similar behavior was recorded since the maximum of the emission band is centered at 816 nm (1.52 eV) in CCl_4, while is found at 803 nm (1.54 eV) in methanol (Figure 4.41).

Therefore, the calculate Stokes shift (i.e. the difference between the positions of the band maxima of the absorption and emission spectra of the same electronic transition[46]) was calculated and reported in Table 4.4.
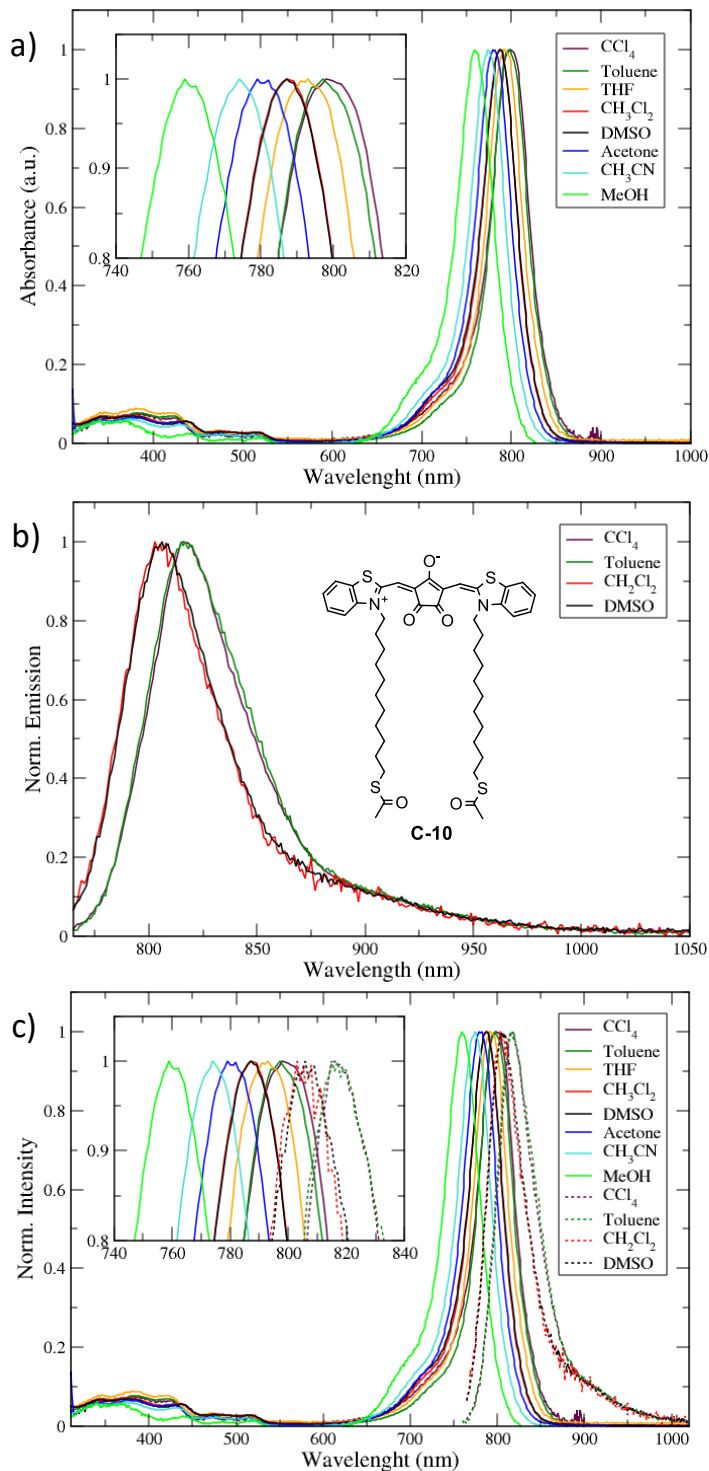
Figure 4.41 *Normalized absorption (a) and emission (b) spectra of croconaine **C-10** in different organic solvents. In c) absorption spectra are indicated as solid lines, while emission spectra as dotted lines.*
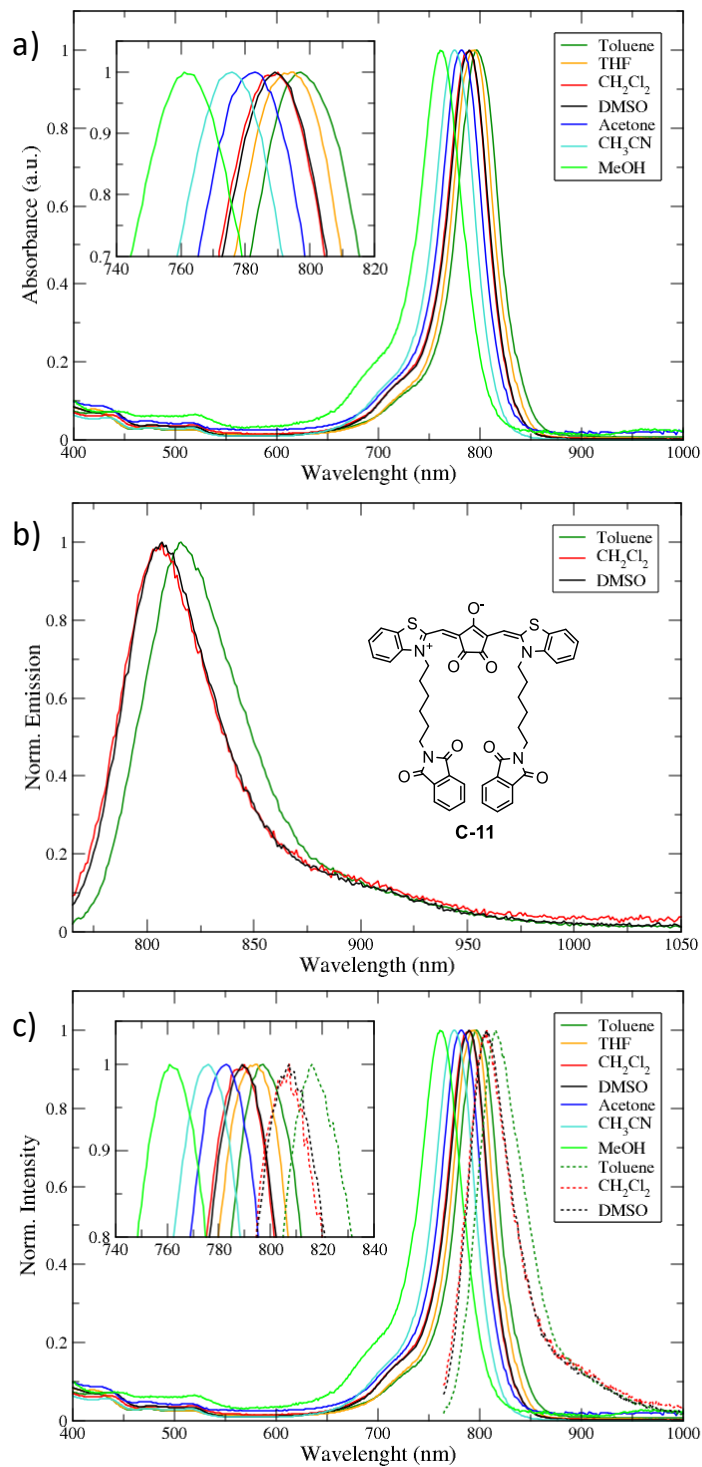
Figure 4.42 *Normalized absorption (a) and emission (b) spectra of croconaine C-11 in different organic solvents. In c) absorption spectra are indicated as solid lines, while emission spectra as dotted lines.*

As regards the croconaine **C-11**, a similar trend was observed both in the absorption and in the emission spectra, even in the shape of the band. The solvatochromic effect is estimated at ~35 nm (Figure 4.42). In the emission spectra, the maximum of the band is found at 807 nm for both CH_2Cl_2 and DMSO, while in toluene the band is centered at 816 nm, showing Stokes shifts of 299 cm^{-1}, 283 cm^{-1} and 292 cm^{-1}, respectively (Table 4.4).

Stokes shift	**C-10**	**C-11**
CCl$_4$	276	-
Toluene	356	292
CH$_2$Cl$_2$	269	299
DMSO	283	283

Table 4.4 *Calculated Stokes shifts (cm-1) of croconaine **C-10** and **C-11** in the reported solvents.*

The fluorescence quantum yields were then calculated, according to the not normalized emission intensities (for details, see Experimental Section). The values are reported in Table 4.5, showing a similar behavior of the croconaine **C-10** and **C-11** in the same solvents. In CH_2Cl_2, both the compounds show a lower Φ with respect to the values obtained from the other two solvents. As expected, these types of compounds, in general, show a low intensity in emission, strictly correlated to the increased red-shift towards higher wavelengths in the NIR region. Even if normalized, the emission spectra show indeed a higher signal to noise ratio with respect to the absorption spectra.

Φ	**C-10**	**C-11**
CCl$_4$	0.044	-
Toluene	0.044	0.036
CH$_2$Cl$_2$	0.005	0.009
DMSO	0.014	0.013

Table 4.5 *Fluorescence quantum yields (Φ) of croconaines **C-10** and **C-11** in the reported solvents.*

Croconaine	Solvent	λ_{max} (nm)	λ_{onset} (nm)	E_g (eV)
	CCl_4	798	849	1.46
	Toluene	792	849	1.46
	THF	793	840	1.48
	CH_2Cl_2	786	825	1.50
C-10	DMSO	788	825	1.50
	Acetone	779	820	1.51
	CH_3CN	774	815	1.52
	MeOH	759	805	1.54
	Toluene	797	849	1.46
	THF	795	845	1.47
	CH_2Cl_2	790	835	1.48
C-11	DMSO	789	835	1.48
	Acetone	783	825	1.50
	CH_3CN	776	820	1.51
	MeOH	761	810	1.53

Table 4.6 *Molar extinction coefficient (ε) and energy gap (E_g) of the synthesized croconaines in different solvents*

4.3 Experimental Section

Anhydrous solvents were purchased from Aldrich and used as received and all other reagents were of reagent grade quality, obtained from commercial suppliers and were used without further purification. "Brine" refers to a saturated aqueous solution of NaCl. Unless otherwise specified, solutions of common inorganic salts used in workups are aqueous solutions. Reactions were monitored by TLC using 0.25 mm Merck silica gel plates (60 F254) or LC–MS analysis. Automated column chromatographic purifications were done using a *Biotage Isolera* apparatus with prepacked silica gel or C18 columns of different sizes (from 10 to 120 g). UV purity and m/z of compounds were assessed by ESI(+) LC–MS analysis, performed on an *Acquity Waters* UPLC BEH C18 1.7 µm 50×2.1 mm column with *Waters ZQ* interfaced with 2996 PDA detector. NMR spectra were recorded at 400 and 300 MHz for ¹H

and 100 and 75 MHz for ¹³C on a *Varian* AS400 or on a *Bruker Avance* 400 and 300 spectrometers. Chemical shifts (δ) are expressed in ppm using the residual solvent signal as the internal reference. Melting points are uncorrected. Coupling constants (*J* values) are given in hertz (Hz) and multiplicities are reported using the following abbreviation: s = singlet, d = doublet, t = triplet, q = quartet, m = multiplet, br. s = broad signal. Compounds **BTD-1**,[47] **BTD-2**,[39] **C-2**,[39] **L-5**,[48] **12**,[49] **L-6**, [49] **14**,[50] **L-8** [45] were synthesized according to published procedures.

4,5-dihydroxycyclopent-4-ene-1,2,3-trione (or **croconic acid**) (**A-1**).[23] To a stirred solution of sodium hydroxide (8 g, 0.2 mol) in water (240 ml), disodium tetrahydroxy-p-benzoquinone (4.2 g, 0.02 mol) and activated manganese dioxide (11.2 g, 0.13 mol) (previously activated at 160°C for 16 hours) were added. The reaction mixture was stirred at room temperature for 5 minutes and then was refluxed for 45 minutes. When it is still hot, the mixture was filtered through a frit funnel to remove the manganese dioxide. The solid residue left on the filter was washed with hot water (80 ml), and the combined filtrates were treated with concentrated hydrochloric acid (42 ml) in few portions, to yield a bright-yellow solution. A solution of barium chloride dihydrate (10 g, 0.05 mol) in water (30 ml) was then added and the mixture was heated at 90°C for 1 hour. After cooling to room temperature, the mixture was filtrated on a Buchner filter and the solid was washed with water and then ethanol and air-dried to yield barium croconate as yellow crystals (4.88 g, 80%), used in the following step without any further purification. The obtained barium croconate (4.88 g, 17.6 mol) was added in small portions to a stirred aqueous solution of sulfuric acid (prepared by dissolving 1.71 ml of 98% H_2SO_4 in 5.5 ml of water) kept at 55 to 60°C. The reaction mixture was stirred at this temperature for 30 to 45 min, then the precipitated barium sulfate was separated by filtration, washed with a small volume of hot water, and discarded. The combined filtrates were concentrated under reduced pressure, and the residue was dissolved with a hot solution of absolute ethanol (5 ml) and dioxane (27 ml). The resulting yellow solution was decolourised with a small amount of activated charcoal and filtered. The filtrate was concentrated under reduced pressure until crystallisation begins, then the mixture was diluted with toluene to incipient turbidity. The resulting crystals were separated by Buchner filtration, washed with a small volume of toluene, and dried in a vacuum desiccator. By concentration of the mother liquor, additional crystals were obtained in 80% overall yield. M.p.: 150-151 °C; ¹³C NMR (D_2O, 100 MHz): δ (ppm) = 191.87, 181.79, 149.14, 86.74.

171

2-chloro-3-(hydroxymethylene)cyclohex-1-ene-1-carbaldehyde
(**A-2**). [28] To a solution of *N,N*-dimethylformamide (2.69 ml, 0.04 mol) in dry CH_2Cl_2 (8 ml), cooled at 0°C by an external ice salt bath, a solution of phosphoryl trichloride (1.59 ml, 0.02 mol) in DCM (8 ml) was dropwise added. After stirring for 30 minutes, cyclohexanone (1 ml, 0.007 mol) was added. The resulting reaction mixture was stirred at 80°C for 3 hours, poured into a flask containing crushed ice, and then extracted twice with CH_2Cl_2. The combined organic layers were dried over anhydrous Na_2SO_4, filtered and concentrated under reduced pressure. The product **A-2** was obtained as a yellow solid in 70% yield. The product must be stored in the refrigerator to avoid its decomposition. M.p.: 120-121°C; ^1H NMR (DMSO-d_6, 400 MHz): δ (ppm) = 10.6-11.1 (bs, s, 1H), 8.4-9.2 (bs, s, 2H), 2.36 (t, 4H, *J* = 6.1 Hz), 1.58 (m, 2H, *J* = 6.1 Hz). LC-MS (ESI): Rt= 0.79 min, m/z (%) =173 [MH]+, 175 (40) [MH+2]+.

Methyl 1-(thiophen-2-yl)piperidine-4-carboxylate (**TD-2**).[30] A solution of methyl piperidine-4-carboxylate (1.74 ml, 12.9 mmol) and thiophene-2-thiol (0.8 ml, 8.6 mmol) in toluene (20 ml) was refluxed, under argon, for 3 hours. The reaction mixture was then cooled down to room temperature, and the solvent was evaporated to dryness under reduced pressure. The residue was purified by column chromatography (SiO$_2$, gradient of *n*-heptane/ethyl acetate) to afford **TD-2** as a pale yellow solid in 84% yield. M.p.: 78-80 °C. ^1H NMR (DMSO-d_6, 400 MHz): δ (ppm) = 6.8-6.7 (m, 2H), 6.14 (dd, 1H, *J* = 3.7 and 1.2 Hz), 3.62 (s, 3H), 3.42 (dt, 2H, *J* = 12.2 and 3.6 Hz), 2.79 (td, 2H, *J* = 11.8 and 2.9 Hz), 2.51-2.52 (m, 1H, overlapped with solvent signal), 2.0-1.9 (m, 2H), 1.7-1.6 (m, 2H). LC-MS (ESI): Rt = 0.98 min, m/z (%) = 226 (100) [MH]+, 227 (12) [MH+1]+.

5-bromo-2,3,3-trimethyl-3H-indole (**5**).[31] (4-Bromophenyl) hydrazine hydrochloride (0.5 g, 2.24 mmol) and 3-methylbutan-2-one (0.48 ml, 4.47 mmol) were dissolved in acetic acid (5 ml). The resulting solution was refluxed for 3 hours and then cooled to room temperature. The solution was diluted with diethyl ether and washed with a saturated solution of Na_2CO_3. The organic phases were combined and dried over anhydrous Na_2SO_4, filtered, and evaporated under reduced pressure to afford **5** as a red oil in 96% yield. ^1H NMR (DMSO-d_6, 400 MHz): δ (ppm)= 7.67 (d, 1H, *J* =1.8 Hz) 7.44 (dd, 1H, *J* = 8.2 and 1.9 Hz), 7.37 (d, 1H, *J* = 8.2 Hz), 2.19 (s, 3H), 1.25 (s, 6H). LC-MS (ESI): Rt= 0.99 min, m/z (%) = 240.1 (100) [MH+2]+, 238.2 (83) [MH]+.

4-(2,3,3-trimethyl-3H-indol-5-yl)phenol (**ID-1**). To a solution of compound **5** (0.5 ml, 2.1 mmol) in THF (5 ml) and water (5 ml), K_2CO_3 (1.45 g, 10.5 mmol), tetrakis(triphenylphosphine)palladium(0) (0.1 g, 0.08 mmol), and (4-hydroxyphenyl) boronic acid (0.58 g, 4.2 mmol)

were added. The boronic acid was added in three portions (1x0.29 g, 2x0.15 g) and after each addition, the reaction mixture was refluxed and stirred in a microwave reactor (250 W) for 1 hour at 110°C. The reaction mixture was then cooled to room temperature, quenched with water and extracted with ethyl acetate (3x10 mL). The combined organic layers were dried over anhydrous Na_2SO_4, filtered and evaporated to dryness under reduced pressure. Purification of the residue by column chromatography (SiO_2, gradient of CH_2Cl_2/ CH_2Cl_2-CH_3OH (10%)), afforded **ID-1** as a sticky red solid in 60% yield. M.p.: 210-212 °C. ^{1}H NMR (DMSO-d_6, 400 MHz): δ (ppm)= 9.4 (br. s, 1H), 7.62 (s, 1H), 7.5-7.4 (d and m, 4H), 6.84 (d, 2H, J = 8.6 Hz), 2.1 (s, 3H), 1.28 (s, 6H). ^{13}C NMR (DMSO-d_6, 100 MHz): δ (ppm)= 187.9, 157.3, 152.7, 147.1, 137.6, 131.7, 128.2, 125.6, 119.9, 119.7, 116.1, 53.7, 23.1, 15.5. LC-MS (ESI): Rt = 0.75 min, m/z (%) = 252.3 (100) [MH][+], 253.3 (15) [MH+1][+].

2,3,3-trimethyl-5-(4-nitrophenyl)-3*H*-indole (**ID-2**).[31] To a solution of compound **5** (0.3 ml, 1.26 mmol) in THF (4 ml) and water (4 ml), K_2CO_3 (0.87 g, 6.30 mmol), tetrakis(triphenylphosphine) palladium(0) (0.06 g, 0.05 mmol), and (4-nitrophenyl)boronic acid (0.42 g, 5.52 mmol) were added. The boronic acid was added in three portions (1x0.21 g and 2x0.11 g). After each portion, the reaction mixture was refluxed and stirred in a microwave reactor (250 W) for 1 hour at 110°C. The reaction mixture was then cooled to room temperature, quenched with water and extracted with ethyl acetate (3x10 mL). The combined organic layers were dried over anhydrous Na_2SO_4, filtered and concentrated under reduced pressure. After purification of the residue by column chromatography (SiO_2, gradient of *n*-heptane/ethyl acetate), product **ID-2** was obtained as brown solid in 98% yield. M.p.: 142-143°C. ^{1}H NMR (DMSO-d_6, 400 MHz): δ(ppm) = 8.31 (d, 2H, J = 8.9 Hz), 7.99 (d, 2H, J = 8.9 Hz), 7.91 (d, 1H, J = 1.8 Hz), 7.72 (dd, 1H, J =8.0 and 1.9 Hz), 7.56 (d, 1H, J = 7.9 Hz), 2.25 (s, 3H), 1.32 (s, 6H). ^{13}C NMR (CDCl_3, 100 MHz): δ(ppm) = 189.7, 154.7,148.0, 147.0, 146.9, 136.0, 127.9, 127.4, 124.2, 120.5, 120.5, 54.1, 23.2, 15.7. LC-MS (ESI): Rt = 1.09 min, m/z (%) = 281.2 (100) [MH][+], 282.3 (19) [MH+1][+].

4-(2,3,3-trimethyl-3*H*-indol-5-yl)aniline (**ID-3**). In a 50 mL round bottom flask, **ID-2** (0.42 g, 1.5 mmol), iron powder (0.25 g, 4.5 mmol) and ammonium chloride (1.6 g, 30 mmol) were dissolved in a mixture of 2-propanol (10 ml) and water (6 ml). The resulting reaction mixture was stirred at 80°C for 2 hours, then filtered through a pad of celite to remove the undissolved solids. The pad was copiously rinsed with ethyl acetate, and the separated organic phase was washed with brine, dried over anhydrous Na_2SO_4, filtered and evaporated to dryness to afford **ID-3** in 94% yield as a yellow solid. M.p.: 145-146°C. ^{1}H NMR (DMSO-

d$_6$, 400 MHz): δ(ppm) = 7.57 (d, 1H, J = 1.7 Hz), 7.5–7.3 (m, 4H), 6.7–6.6 (m, 2H), 5.16 (s, 2H), 2.20 (s, 3H), 1.27 (s, 6H). ^{13}C NMR (DMSO-d$_6$, 100 MHz): δ(ppm) = 187.4, 152.2, 148.5, 147.0, 138.2, 138.1, 128.2, 127.7, 124.9, 119.7, 119.3, 114.6, 53.6, 23.1, 15.5. LC-MS (ESI): Rt = 0.59 min, m/z (%) = 251.3 (100) [MH]$^+$, 252.3 (19) [MH+1]$^+$.

Croconaine C-1. In a 100 mL two-necked round-bottom flask equipped with a Dean-Stark apparatus, **A-1** (0.43 g, 3.04 mmol), **BTD-1** (1.85 g, 6.08 mmol) and pyridine (2.1 mL) were added to a 1:1 mixture of toluene and *n*-butanol (60 ml). The reaction mixture was heated at 110 °C for 6 hours. After cooling to room temperature, the solvents were evaporated under reduced pressure, and methanol was added. The mixture was centrifuged at 9000 rpm for 15 minutes. The residue was then purified by column chromatography (SiO$_2$, CH$_2$Cl$_2$/CH$_3$OH 95:5) to give **C-1** as a dark-green solid (0.260 g, 19%). ^{1}H NMR (DMSO-d$_6$, 400 MHz): δ (ppm) = 7.90 (d, 2H, J = 7.8 Hz), 7.67 (d, 2H, J = 8.4 Hz), 7.46 (t, 2H, J = 7.2 Hz), 7.30 (t, 2H, J = 7.5 Hz), 6.25 (s, 2H), 4.39 (q, 4H, J = 7.2 Hz), 1.30 (t, 6H, J = 7.2 Hz). ^{13}C NMR (DMSO-d$_6$, 100 MHz): δ (ppm) = 159.2, 141.0, 129.9, 128.4, 125.5, 123.2, 113.7, 92.3, 42.1, 13.0. ESI-MS (+): m/z (%) = 461 (100) [MH]$^+$, 462 (30) [MH+1]$^+$, 463 (15) [MH+2]$^+$.

Croconaine C-3.[41] In a 25 mL two-necked round-bottom flask equipped with a Dean-Stark apparatus, **A-1** (30 mg, 0.2 mmol) and **TD-2** (95 mg, 0.42 mmol) were added to a 1:1 mixture of toluene and *n*-butanol (6 ml). The reaction mixture was heated at 110 °C for 3 hours. After cooling to room temperature, the solvents were evaporated under reduced pressure, and methanol was added. The mixture was centrifuged at 9000 rpm for 15 minutes to afford the product **C-3**, which was used without any further purification (66%). M.p.: 236-237°C. ^{1}H NMR (DMSO-d$_6$, 400 MHz): δ(ppm) = 8.6 (br. s, s, 2H), 7.04 (br. s, d, 2H, *J* = 4.8 Hz), 4.01 (br. s, d, 4H, *J* = 13.4 Hz), 3.6-3.7 (m, 6H), 3.55 (br. s, d, 4H, *J* = 11.6 Hz), 2.8-2.9 (m, 2H), 2.0-2.1 (m, 4H), 1.7-1.8 (m, 4H). LC-MS (ESI): Rt= 0.95 min, m/z (%) = 555.5 (100) [M-H]$^+$, 556.9 (53) [MH]$^+$, 557.9 (12) [MH+1]$^+$.

Croconaine C-4. In a 25 mL two-necked round-bottom flask equipped with a Dean-Stark apparatus, **A-1** (30 mg, 0.21 mmol), **ID-1** (0.106 g, 0.42 mmol) and pyridine (34 µl) were added to a 1:1 mixture of toluene and *n*-butanol (6 ml). The reaction mixture was heated at 110 °C for 3 hours. After cooling to room temperature, the solvents were evaporated under reduced pressure, and methanol was added. The mixture was filtrated to afford the product **C-4**, which was used without any further purification (60%). ^{1}H NMR (DMSO-d$_6$, 400 MHz) δ (ppm) = 9.5 (s, 2H), 7.8 (s, 2H), 7.7-7.6 (m, 10H), 6.86 (d, 4H, *J* = 8.6 Hz), 6.0 (bs, s,

2H), 1.4 (s, 12H). ^{13}C-NMR spectrum was not collected because of the poor solubility of the product. LC-MS (ESI): Rt= 1.27 min, m/z (%) = 608.2 (100) [MH]$^+$, 608.7 (93) [MH+1]$^+$, 609.9 (58) [MH+2]$^+$.

Croconaine C-7.[31] In a 25 mL two-necked round-bottom flask equipped with a Dean-Stark apparatus, **A-1** (20 mg, 0.14 mmol), **5** (0.07 ml, 0.28 mmol) and pyridine (20 µl) were added to a 1:1 mixture of toluene and *n*-butanol (6 ml). The reaction mixture was heated at 110 °C for 3 hours. After cooling to room temperature, the solvents were evaporated under reduced pressure, and methanol was added. The mixture was centrifugated at 9000 rpm for 15 minutes to afford the product **C-4**, which was used without any further purification (79%). M.p.: 298-299°C. ^{1}H NMR (400 MHz, DMSO-d$_6$): δ(ppm) = 7.85 (s, 2H), 7.54 (d, J = 8.4 Hz, 2H), 7.46 (d, J = 8.5 Hz, 2H), 5.95 (s, 2H), 1.50 (s, 12H). LC-MS (ESI): Rt= 1.55 min, m/z (%) = 583.3 (100) [MH+2]$^+$, 581.1 (30) [MH]$^+$, 585.2 (32) [MH+4]$^+$.

Croconaine C-5.[31] In a microwave tube, **C-7** (50 mg, 0.09 mmol), potassium carbonate (59 mg, 0.43 mmol) and tetrakis(triphenylphosphine)palladium(0) (14.8 mg, 0.02 mmol) were solubilized in THF (2 ml) and water (2 ml). To the resulting mixture (4-nitrophenyl)boronic acid **6** (29 mg, 0.17 mmol) was then added. The reaction mixture was heated at 110°C for 1 hour in a microwave reactor. After cooling to room temperature, the reaction was extracted with ethyl acetate (3×10 mL). The combined organic layers were dried over anhydrous Na$_2$SO$_4$, filtered and concentrated under reduced pressure. The product **C-5** was obtained after its precipitation from the reaction mixture upon the addition of methanol and centrifugation at 4000 rpm for 20 min (70%). ^{1}H NMR (DMSO-d$_6$, 400 MHz) :δ (ppm) = 8.3-8.4 (d, 2H), 8.32 (br.s., d, 4H, J =8 Hz), 8.1 (bs, d, 4H), 8.04 (bs, d, 4H, J = 8 Hz),7.92 (br.s., s, 2H), 6.0 (s, 2H), 1.56 (br.s., s, 12H). ^{13}C-NMR spectrum was not collected because of the poor solubility of the product. LC-MS (ESI): Rt= 1.59 min, m/z (%) = 667.9 (100) [MH]$^+$, 666.4 (91) [M-H]$^+$, 667.1 (82) [MH]$^+$.

Croconaine C-6. In a microwave tube, **C-7** (30 mg, 0.05 mmol), potassium carbonate (36 mg, 0.26 mmol) and tetrakis(triphenylphosphine) palladium(0) (9 mg, 0.01 mmol) were solubilized in THF (2 ml) and water (2 ml). to the resulting mixture (4-aminophenyl)boronic acid • HCl **7** (18 mg, 0.1 mmol) was then added. The reaction mixture was heated at 110°C for 1 hour in a microwave reactor. After cooling to room temperature, the reaction was extracted with ethyl acetate (3×10 mL). The combined organic layers were dried over anhydrous Na$_2$SO$_4$, filtered and concentrated under reduced pressure. The residue was purified by column chromatography (SiO$_2$, gradient of CH$_2$Cl$_2$/CH$_2$Cl$_2$- CH$_3$OH (10%)) to afford **C-6** as a brown

solid (13%). ^{1}H NMR (DMSO-d$_6$, 400 MHz): δ (ppm) = 7.7-7.8 (br. s, s, 2H), 7.6-7.4 (br.s, m, 6H), 7.43 (d, 4H, J = 8.6 Hz), 6.66 (d, 4H, J = 8.3 Hz), 5.9-6.0 (br. s, s, 2H), 5.2-5.3 (br.s, s, 4H), 1.53 (s, 12H). ^{13}C-NMR spectrum was not collected because of the poor solubility of the product. LC-MS (ESI): Rt = 1.14 min, m/z (%) = 607.11 (100) [MH]$^+$, 605.7 (63) [M-2H]$^+$.

Croconaine C-8. In a microwave tube, tert-butyl 4-(4,4,5,5-tetramethyl-1,3,2-dioxaborolan-2-yl)-3,6-dihydropyridine-1(2H)-carboxylate **8** (11 mg, 0.03 mmol), potassium carbonate (12 mg, 0.09 mmol) and tetrakis(triphenylphosphine)palladium(0) (2 mg, 1.7 μmol) were solubilized in THF (2 ml) and water (2 ml) and **C-5** (10 mg, 0.02 mmol) was then added. The resulting reaction mixture was heated at 110°C for 1 hour in a microwave reactor. After cooling to room temperature, the reaction was extracted with ethyl acetate (3×10 ml). The combined organic layers were dried over anhydrous Na$_2$SO$_4$, filtered and concentrated under reduced pressure. After trituration of the residue with methanol, product **C-8** was isolated by centrifugation at 4000 rpm for 20 min (70%). ^{1}H NMR (DMSO-d$_6$, 400 MHz): δ(ppm) = 7.7 (s, 2H), 7.6-7.7 (m, 2H), 7.5-7.6 (m, 2H), 7.4-7.5 (m, 2H), 6.2 (s, 2H), 5.9 (s, 1H), 5.7 (s, 1H), 4.0-4.1 (m, 4H), 3.5-3.6 (m, 4H), 2.3-2.4 (br.s, t, 2H), 2.2 (bs, s, 2H), 1.5 (s, 6H), 1.4 (s, 18H), 1.3 (s, 6H). ^{13}C-NMR spectrum was not collected because of the poor solubility of the product. LC-MS (ESI): Rt= 1.71 min, m/z (%) = 786.2 (37) [MH]$^+$.

Croconaine C-9. In a 25 mL round bottom flask, croconaine **C-8** (35 mg, 0.04 mmol) was dissolved in CH$_2$Cl$_2$ (5 ml) and treated with trifluoroacetic acid (1 ml, 12.98 mmol). The resulting reaction mixture was stirred at room temperature for 1 hour and it was then evaporated under reduced pressure. The residue was purified by column chromatography (C$_{18}$, H$_2$O/CH$_3$CN) to afford **C-9** as a formate salt (84%). ^{1}H NMR (DMSO-d$_6$, 400 MHz): δ(ppm) = 8.22 (s, 2H), 7.5-7.6 (br.s, s, 2H), 7.3-7.4 (br.s, d, 2H), 7.1-7.2 (br.s, d, 2H), 6.17 (br.s, s, 2H), 5.8 (br.s, s, 2H), 3.71 (br.s, s, 4H), 3.2-3.3 (t, 4H, J = 6 Hz), 2.6-2.7 (m, 4H), 2.5 (s, 4H), 1.37 (s, 12H). ^{13}C-NMR spectrum was not collected because of the poor solubility of the product. LC-MS (ESI): Rt= 0.64 min, m/z(%) = 587.1 (100) [MH]$^+$, 585.7 (78) [M-H]$^+$.

***N*-(6-bromohexyl)-5-(1,2-dithiolan-3-yl)pentanamide** (**L-2**). In a 25 mL round bottom flask, a solution of lipoic acid **L-1** (100 mg, 0.49 mmol), HBTU (184 mg, 0.49 mmol) and DIPEA (0.25 ml, 1.45 mmol) in CH$_2$Cl$_2$ (3 ml) was stirred for 15 minutes at room temperature, then 6-bromohexan-1-amine (87 mg, 0.49 mmol) was added. The resulting reaction mixture was stirred at room temperature for 16 hours, then quenched with a saturated solution of NH$_4$Cl (10 ml). The organic layer was separated, and aqueous phase was extracted with diethyl ether

(3x10 ml). The combined organic layers were dried over anhydrous Na_2SO_4, filtered and evaporated to dryness under reduced pressure. The yellow oily residue was purified by column chromatography (SiO_2, gradient of *n*-heptane/ethyl acetate) to afford **L-2** as a yellow oily compound (46%), which was used without any further purification. ^{1}H NMR (CDCl$_3$, 400 MHz): δ(ppm) = 5.7 and 5.6 (2 br.s, 1H), 4.54 (t, 1H, J = 6.6 Hz), 3.7-3.5 (2m, 3H), 3.39 (t, 1H, J = 6.6 Hz), 3.3-3.2 and 3.2-3.0 (2m, 8H). LC-MS (ESI): Rt = 0.35min, m/z (%) = 369.7 (100) [MH+2]$^+$, 367.8 (95) [MH]$^+$.

5-(1,2-dithiolan-3-yl)-*N*-(6-hydroxyhexyl) pentanamide (9). In a 25 mL round bottom flask, a solution of lipoic acid **L-1** (0.88 g, 4.27 mmol), HBTU (1.62 g, 4.27 mmol) and DIPEA (2.24 ml, 12.8 mmol) in CH_2Cl_2 (10ml) was stirred for 15 minutes at room temperature, then 6-aminohexan-1-ol (0.5 g, 4.27 mmol) was added. The reaction mixture was stirred at room temperature for 16h, then was quenched with a saturated solution of $NaHCO_3$. The separated organic layer was washed with a brine solution, dried over anhydrous Na_2SO_4, filtered and evaporated under reduced pressure. The residue was purified by column chromatography (SiO_2, gradient of CH_2Cl_2/CH_2Cl_2- CH_3OH (10%)), followed by a further purification by a strong cation exchange (SCX) ion chromatography to afford **9** as a yellow oil (60%). ^{1}H NMR (DMSO-d$_6$, 400 MHz): δ(ppm) = 7.71 (br.s. t, 1H, J = 5.0 Hz), 4.00 (br.s, s, 3H), 3.5-3.7 (m, 1H), 3.37 (t, 2H, J = 6.5 Hz), 3.1-3.2 (m, 2H), 3.01 (br.s, q, 2H, J = 6.1 Hz), 2.3-2.5 (m, 1H), 2.04 (t, 2H, J = 7.2 Hz), 1.8-1.9 (m, 1H), 1.6-1.7 (m, 1H), 1.4-1.6 (m, 3H), 1.2-1.4 (m, 8H). ^{13}C NMR (DMSO-d$_6$, 100 MHz): δ(ppm) = 172.1, 61.1, 56.6, 38.8, 38.5, 35.7, 34.5, 32.9, 29.7, 28.7, 26.8, 25.7, 25.5. LC-MS (ESI): Rt= 0.84 min, m/z (%) = 306.1 (100) [MH]$^+$, 307 (21) [MH+1]$^+$, 308 (15) [MH+2]$^+$.

6-(5-(1,2-dithiolan-3-yl)pentanamido)hexyl tosylate (L-3). In a 25 mL round bottom flask, **9** (0.2 g, 0.66 mmol), triethylamine (0.14 ml, 0.98 mmol) and DMAP (8 mg, 0.07 mmol) were solubilized in CH_2Cl_2 (2 ml). A solution of 4-methylbenzenesulfonyl chloride (TsCl) (140 mg, 0.72 mmol) in CH_2Cl_2 (2 ml) was then added dropwise. The resulting reaction mixture was stirred at room temperature for 24 hours, then quenched by addition of a saturated solution of NH_4Cl. The separated organic phase was washed with water, dried over anhydrous Na_2SO_4, filtered and evaporated under reduced pressure to give **L-3** as a brown oil (63%). ^{1}H NMR (DMSO-d$_6$, 400 MHz): δ(ppm) = 7.59 (d, 2H, J = 8.3 Hz), 7.50 (br.s, t, 1H, J = 5.4 Hz), 7.29 (d, 2H, J = 7.9 Hz), 3.81 (t, 2H, J = 6.4 Hz), 3.5-3.4 (m, 1H), 3.0-2.9 (m, 2H), 2.8-2.7-(m, 2H), 2.23 (s, 3H), 2.1-2.2 (m, 1H), 1.83 (t, 2H, J = 7.5 Hz), 1.7-1.6 (m, 1H), 1.5-1.4 (m, 2H), 1.4-1.2 (m, 6H), 1.19 (m, 6H). LC-MS (ESI): Rt = 1.23 min,

m/z (%) = 459.9 (100) [MH]$^+$, 460.8 (35) [MH+1]$^+$, 462 (21) [MH+2]$^+$.

undec-10-en-1-yl 4-methylbenzenesulfonate (10). In a 250 mL two-necked round bottom flask, 10-undecen-1-ol (6.8 g, 40 mmol) was solubilized with triethylamine (6.36 mL, 60 mmol) in 50 ml of anhydrous CH$_2$Cl$_2$. A solution of TsCl (8.36 g, 43.8mmol) in CH$_2$Cl$_2$ (20 mL) was added dropwise. Subsequently, 4-dimethylaminopyridine (DMAP) was added in catalytic quantity and the reaction mixture was stirred at rt overnight. Afterwards, the reaction mixture was treated with HCl solution (30 mL, 10% v/v in H$_2$O), the organic phase was washed with H$_2$O and it was dried over Na$_2$SO$_4$. The solvent was removed under reduced pressure to yield **10** as a yellow oil (12.5 g, 96%), used in the following step without any further purification. ^{1}H NMR (400 MHz, CDCl$_3$): δ (ppm) = 7.79 (d, 2H, J=8 Hz), 7.35 (d, 2H, J=8 Hz), 5.82-5.78 (m, 1H), 5.02-4.92 (m, 2H), 4.02 (t, 2H, J= 6.8 Hz), 2.45 (s, 3H), 2.05-2.03 (m, 2H), 1.65-1.62 (m, 2H), 1.37-1.23 (m, 12H). ^{13}C NMR (100 MHz, CDCl$_3$): δ (ppm) = 144.6, 139.1, 133.3, 129.8, 127.9, 114.16, 70.7, 33.8, 29.3, 29.0, 28.9, 28.8, 25.3, 21.6.

S-(11-(tosyloxy)undecyl) ethanethioate (L-4). In a 250 mL three-necked round bottom flask equipped with degassing valve, **10** (12.4 g, 38.2 mmol) and thioacetic acid (13.5 mL, 0.19 mol) were solubilized in anhydrous toluene (100 mL). The solution was degassed for 20 minutes bubbling nitrogen. Subsequently, 2-2'-azobisisobutyrronitrile (AIBN) was added and the reaction mixture was stirred heating at 50°C for 12 hours. The mixture was then treated with a saturated aqueous solution of K$_2$CO$_3$, the separated organic phase was washed with H$_2$O and it was dried over Na$_2$SO$_4$. The solvent was removed under reduced pressure and the product **L-4** was obtained as a deliquescent white solid after a recrystallization from ethyl acetate/*n*-hexane (7.8 g, 51%). ^{1}H NMR (400 MHz, CDCl$_3$): δ (ppm) = 7.81 (d, 2H, J= 8 Hz), 7.36 (d, 2H, J=8 Hz), 4.04 (t, 2H, J= 6.4 Hz), 2.88 (t, 2H, J=7.2 Hz), 2.47 (s, 3H,), 2.34 (s, 3H), 1.68-1.23 (m, 18H). ^{13}C NMR (75 MHz, CDCl$_3$): δ (ppm) = 195.0, 144.6, 133.2, 129.8, 127.9, 70.7, 30.7, 29.5, 29.4, 29.3, 29.1, 28.9, 28.8, 25.3, 21.6. MS-ESI (+): m/z (%) = 347 (100) [M+Na]$^+$.

2-(6-hydroxyhexyl)isoindoline-1,3-dione (11).[51] In a microwave tube, phthalic anhydride (1.5 g, 10 mmol) and 6-amino-1-hexanol (1.18 g, 10 mmol) were added. The reaction was carried out stirring in a microwave apparatus at 80 W, heating to 160°C for 5 minutes to yield the product **11** as a brown oil (2.52 g, quant. yield), which was used without any further purification. ^{1}H NMR (400 MHz, CDCl$_3$): δ (ppm) = 7.83 (dd, 2H, J$_1$ = 5.6 Hz, J$_2$ = 3.2 Hz), 7.71 (dd, 2H, J$_1$ = 5.6 Hz, J$_2$ = 3.2 Hz), 3.67 (t, 2H, J = 7.2 Hz), 3.62 (t, 2H, J = 6.4 Hz), 2.03 (s, 1H), 1.7 (m, 2H), 1.57 (m, 2H), 1.43 (m, 4H).

tert-butyl (11-hydroxyundecyl)carbamate (13). In a 100 ml round bottom flask, under inert atmosphere, di-tert-butyl dicarbonate (1.0 g, 4.8 mmol) and triethylamine (0.8 g, 4.8 mmol) were added to a solution of 11-aminoundecan-1-ol (0.9 g, 4.8 mmol) in THF (50 mL). The reaction mixture was stirred overnight at room temperature. Afterwards, the solvent was removed under reduced pressure and the residue was portioned between ethyl acetate and water. The separated organic phase was dried over Na_2SO_4 and evaporated under reduced pressure to afford **13** as a white solid (1.3 g, 94%). M.p. = 33-35°C; ^{1}H NMR (CDCl$_3$, 300 MHz) δ (ppm) = 3.68 (t, 2H, J = 6.6 Hz), 3.14 (t, 2H, J =7.0 Hz), 1.54 (m, 2H), 1.46 (s, 11H), 1.29 (m, 14H); ^{13}C NMR (CDCl$_3$, 75 MHz) δ (ppm)= 158.0, 63.0, 40.8, 32.8, 30.0, 29.5, 29.4, 29.2, 28.4, 26.8, 25.7. ESI-MS (+): m/z (%) = 288.3 [M+ H]$^+$.

11-((tert-butoxycarbonyl)amino)undecyl 4-methylbenzenesulfonate (L-7). A solution of 4-toluenesulfonyl chloride (3.0 g, 15.8 mmol) in anhydrous CH_2Cl_2 (100 mL) was slowly added to a solution of **13** (3.5 g, 12.2 mmol) and triethylamine (2.3 g, 24.4 mmol) in 50 mL of anhydrous CH_2Cl_2. A catalytic amount of DMAP were added. After stirring at room temperature for 5 hours, the reaction was quenched with water (100 mL) and the organic phase was separated, dried over anhydrous Na_2SO_4 and filtered. The solvent was removed under reduced pressure and the residue was purified by column chromatography (*n*-hexane/ethyl acetate 85:15) to afford **L-7** as a white solid in (3.9 g, 72%). M.p. = 52-53°C. ^{1}H NMR (CDCl$_3$, 400 MHz) δ (ppm) = 7.82 (d, 2H, J = 8.0 Hz), 7.37 (d, 2H, J = 8.0 Hz), 4.51 (bs, 1H), 4.05 (t, 2H, J = 6.6 Hz), 3.11 (bs, 2H), 2.47 (s, 3H), 1.67 (m, 2H), 1.46 (s, 11H), 1.29 (m, 14H). ^{13}C NMR (CDCl$_3$, 100 MHz): δ = 158.0, 144.6, 133.3, 129.8, 127.9, 70.7, 40.6, 30.1, 29.5, 29.4, 29.2, 29.3, 28.9, 28.8, 28.4, 26.8, 25.3, 21.6; ESI-MS (+): m/z (%) = 464.4 [M+ Na]$^+$.

4-(2,3,3-trimethyl-3*H*-indol-5-yl)phenyl 5-(1,2-dithiolan-3-yl)pentanoate (DL-1). In a 25 mL round bottom flask, to a solution of lipoic acid **L-1** (49 mg, 0.24 mmol) in CH_2Cl_2 (5 ml), DMAP (0.29 mg, 0.002 mmol), EDC (23 mg, 0.12 mmol) and triethylamine (0.04 ml, 0.3 mmol) were added. After 10 minutes of stirring, **ID-1** (30 mg, 0,12 mmol) was added and the reaction mixture was stirred at room temperature for 16 hours. The solvent was then removed under reduced pressure. The yellow oily residue was purified by column chromatography (SiO$_2$, gradient of *n*-heptane/ethyl acetate) to afford the product **DL-1** as a yellow oil (46%). ^{1}H NMR (DMSO-d$_6$, 400 MHz): δ (ppm) = 7.76 (d, 1H, *J* = 1.5 Hz), 7.71 (d, 2H, *J* = 8.4 Hz), 7.55 (dd, 1H, *J* = 8.1 and 1.5 Hz), 7.49 (d, 1H, *J* = 8.1 Hz), 7.20 (d, 2H, *J* = 8.4 Hz), 3.6-3.7 (m, 1H), 3.2-3.1 (2m, 2H), 2.62 (t, 2H, *J* = 7.2 Hz), 2.5-2.4 (m, 1H), 2.2 (s, 3H), 1.9-1.8 (m, 1H), 1.8-1.6 (m, 4H), 1.5-1.4 (m, 2H),

1.30 (s, 6H). ^{13}C NMR (DMSO-d_6, 100 MHz): δ(ppm) = 188.8, 172.2, 153.6, 150.2, 147.2, 138.5, 136.7, 131.9, 128.2, 126.4, 122.6, 121.3, 120.7, 119.9, 56.5, 53.8, 40.6, 40.4 (2 res.), 40.2 (2 res.), 40.0 (2 res.), 39.8, 39.6, 39.4, 38.6, 34.5, 33.8, 28.5, 24.6, 24.4, 23.0, 15.6. LC-MS (ESI): Rt= 1.38 min, m/z (%) = 440 (100) [MH]$^+$, 441 (18) [MH+1]$^+$, 441.9 (19) [MH+2]$^+$.

5-(1,2-dithiolan-3-yl)-*N*-(4-(2,3,3-trimethyl-3*H*-indol-5-yl)phenyl)pentanamide (**DL-2**). In a 25 mL round bottom flask, to a solution of lipoic acid **L-1** (82 mg, 0.4 mmol) in CH_2Cl_2 (10 ml), HBTU (151 mg, 0.4 mmol) and DIPEA (0.21 ml, 1.2 mmol) were added. After stirring for 10 minutes, **ID-3** (100 mg, 0.4 mmol) was added. The reaction mixture was stirred at 40°C for 6 hours and then quenched with a saturated solution of NH_4Cl (10 mL). The organic layer was separated, and the aqueous phase was extracted with diethyl ether (3x10 ml). The combined organic layerswre collected, dried over anhydrous Na_2SO_4, filtered and evaporated under reduced pressure. The yellow oily residue was purified by column chromatography (SiO$_2$, gradient of CH_2Cl_2/CH_2Cl_2-CH_3OH (10%)) to afford **DL-2** as a brown oil (90%), which was used without any further purification. ^1H NMR (DMSO-d_6, 400 MHz): δ (ppm) = 9.94 (s, 1H), 7.70 (d, 1H, J = 1.5 Hz), 7.67 (d, 1H, J = 8.6 Hz), 7.61 (d, 1H, J = 8.6 Hz), 7.52 (dd, 1H, J$_1$ = 8 Hz, J$_2$ = 1.5 Hz), 7.44 (d, 1H J = 8 Hz), 3.7-3.6 (m, 2H), 3.3-3.1 (m, 3H), 2.5-2.4 (m, 1H), 2.32 (t, 2H, J = 7.2 Hz), 2.22 (s, 3H), 1.9-1.8 (m, 1H), 1.8-1.5 (m, 4H), 1.5-1.4 (m, 2H), 1.29 (s, 6H). LC-MS (ESI): Rt = 1.17 min, m/z (%) = 439.3 (100) [MH]$^+$, 440.4 (24) [MH+1]$^+$.

5-(1,2-dithiolan-3-yl)-*N*-(6-(4-(2,3,3-trimethyl-3*H*-indol-5-yl)phenoxy) hexyl)pentanamide (**DL-3**). In a 25 mL round bottom flask, a mixture of **L-3** (0.05 g, 0.2 mmol), **ID-1** (0.18 g, 0.4 mmol), and Cs_2CO_3 (0.16 g, 0.5 mmol) in THF (3 ml) and acetone (3 ml) was refluxed at 60°C for 24 hours. Afterwards, the mixture was cooled down to room temperature and extracted with CH_2Cl_2 (3 x 10 ml). The combined organic layers were dried over anhydrous Na_2SO_4, filtered and evaporated under reduced pressure. The residue was purified by column chromatography (SiO$_2$, gradient of *n*-heptane/ethyl acetate) to afford **DL-3** as a yellow oil (49%), which was used without any further purification. ^1H NMR (DMSO-d_6, 400 MHz): δ (ppm) = 7.73 (br.s, t, 1H), 7.67 (br.s, s, 1H), 7.59 (d, 2H, J = 8.8 Hz), 7.49 (br.s, d, 1H, J = 8.3 Hz), 7.43 (d, 1H, J = 8 Hz), 7.00 (br.s, d, 2H, J = 8.8 Hz), 4.00 (t, 2H, J = 6.2 Hz), 3.59 (br.s, t, 1H), 3.2-2.9-3.0 (2m, 2H), 2.4-2.5 (m, 1H, partially hidden by the solvent signal), 2.22 (s, 3H), 2.04 (t, 2H, J = 7.0 Hz), 1.9-1.8 (m, 1H), 1.78-1.7 (m, 2H), 1.7-1.6 (m, 2H), 1.6-1.5 (m, 4H), 1.5-1.4 (m, 4H), 1.4-1.2 and 1.29 (m and s, 8H). LC-MS (ESI): Rt= 1.31

min, m/z (%) = 539.2 (100) [MH]$^+$, 540.2 (37) [MH+1]$^+$, 541.2 (13) [MH+2]$^+$.

3-(11-(acetylthio)undecyl)-2-methylbenzo[d]thiazol-3-ium 4-methylbenzenesulfonate (DL-4). In a 25 mL round-bottom flask, **L-4** (1.22 g, 3.1 mmol) and 2-methyl benzothiazole (0.43 mL, 3.3 mmol) were solubilized in toluene (2 mL). the mixture was stirred at reflux for 24 hours and then it was allowed to cool to room temperature. The product was obtained through precipitation induced by adding ethyl acetate, to give **DL-4** as a pink solid (0.6 g, 36%). ^{1}H NMR (CDCl$_3$, 400 MHz): δ (ppm) = 8.17 (d, 1H, J = 8 Hz), 7.88 (d, 1H, J = 8 Hz), 7.72 (t, 1H, J = 7.2 Hz), 7.64-7.58 (m, 3H), 6.98 (d, 2H, J = 7.6 Hz), 4.74 (t, 2H, J = 7.2 Hz), 3.24 (s, 3H), 2.84 (t, 2H, J = 7.2 Hz), 2.31 (s, 3H), 2.25 (s, 3H), 1.84-1.76 (m, 2H), 1.58-1.50 (m, 2H), 1.38-1.21 (m, 14H). ^{13}C NMR (CDCl$_3$, 100 MHz): δ (ppm) = 196.1, 176.0, 144.0, 140.9, 138.8, 129.6, 129.3, 128.4, 125.8, 124.4, 116.4, 50.4, 30.7, 29.5, 29.4, 29.3 (2 resonances), 29.1, 29.0, 28.8, 28.6, 26.7, 21.3, 17.7. ESI-MS (+): m/z (%) = 378.3 (100) [M-OTs]$^+$, 379.3 (69) [M-OTs+1]$^+$, 380.3 (45) [M-OTs+2]$^+$, 381.2 (11) [M-OTs+3]$^+$.

3-(6-(1,3-dioxoisoindolin-2-yl)hexyl)-2-methylbenzo[d]thiazol-3-ium 4-methylbenzenesulfonate (DL-5). In a 25 mL round-bottom flask, **L-5** (1.78 g, 4.43 mmol) and 2-methyl benzothiazole (0.56 mL, 4.3 mmol) were solubilized in toluene (2 mL). the mixture was stirred at reflux for 24 hours and then it was allowed to cool to room temperature. The product was obtained through precipitation induced by adding ethyl acetate, to give **DL-5** (0.8 g, 33%). ^{1}H NMR (CDCl$_3$, 400 MHz): δ (ppm) = 8.30 (d, 1H, J = 8.2 Hz), 8.25 (d, 1H, J = 8.5 Hz), 7.93 (t, 1H, J = 7.5 Hz), 7.87-7.80 (m, 4H), 7.70 (d, 2H, J = 8.0 Hz), 7.22 (d, 2H, J = 8.0 Hz), 4.76 (t, 2H, J = 7.9 Hz), 3.70 (t, 2H, J = 7.0 Hz), 3.23 (s, 3H), 2.37 (s, 3H), 2.02-1.93 (m, 2H), 1.77-1.69 (m, 2H), 1.64-1.56 (m, 2H), 1.49-1.41 (m, 2H). ESI-MS (+): m/z (%) = 379.3 (100) [M-OTs]$^+$, 380.3 (69) [M-OTs+1]$^+$, 381.2 (45) [M-OTs+2]$^+$, 382.2 (11) [M-OTs+3]$^+$.

Croconaine C-10. In a 25 mL two-necked round-bottom flask equipped with a Dean-Stark apparatus, **A-1** (64 mg, 0.45 mmol), **DL-4** (0.34 g, 0.9 mmol) and pyridine (0.2 mL) were added to a 1:1 mixture of toluene and *n*-butanol (12 ml). The reaction mixture was heated at 110 °C for 6 hours. After cooling to room temperature, the solvents were evaporated, and methanol was added. The mixture was centrifuged at 9000 rpm for 15 minutes to afford **C-8** as a green sticky solid (58 mg, 15%). ^{1}H NMR (400 MHz, DMSO-d6): δ (ppm) = 7.96 (d, 2H, J = 10 Hz), 7.73 (d, 2H, J = 8.4 Hz), 7.52 (d, 2H, J = 8.5 Hz), 7.36 (d, 2H, J = 8.5 Hz), 6.33 (bs, 2H), 4.40 (bs, 4H), 2.77 (t, 4H, J = 7.2 Hz), 2.28 (s, 6H), 1.77 (bs, 4H), 1.44-1.21 (m, 32H). ESI-MS (+): m/z (%) = 860.5 (100) [M-H]$^+$, 861.5 (80) [MH]$^+$.

Croconaine C-11. In a 25 mL two-necked round-bottom flask equipped with a Dean-Stark apparatus, **A-1** (50 mg, 0.36 mmol), **DL-5** (0.40 g, 0.73 mmol) and pyridine (0.25 mL) were added to a 1:1 mixture of toluene and *n*-butanol (10 ml). The reaction mixture was heated at 110 °C for 6 hours. After cooling to room temperature, the solvents were evaporated, and methanol was added. The mixture was centrifugated at 9000 rpm for 15 minutes. The residue was then purified through column chromatography (SiO$_2$, CH$_2$Cl$_2$/CH$_3$OH 92:8) to give **C-9** as a sticky solid (37 mg, 12%). ^{1}H NMR (400 MHz, DMSO-d6): δ (ppm) = 7.96 (d, 2H, J = 7.2 Hz), 7.82-7.71 (m, 10H), 7.52 (t, 2H, J = 7.6 Hz), 7.36 (t, 2H, J = 7.6 Hz), 6.32 (bs, 2H), 4.40 (bs, 4H), 3.57 (t, 4H, J = 6.8 Hz), 1.79-1.76 (m, 4H), 1.64-1.37 (m, 12H). ESI-MS (+): m/z (%) = 863.4 (100) [MH]$^+$, 864.4 (62) [MH+1]$^+$, 865.4 (32) [MH+2]$^+$.

Optical Measurements. Absorption measurements were carried out on a *Perkin Elmer* Lambda 750 UV/vis/NIR spectrometer. The emission measurements were performed on an *Edinburgh Instruments* FLS1000 Photoluminescence Spectrometer, using a photomultipliers tube (PMT-NIR) detector. Al the solutions were prepared in a quartz cuvette with an optical path of 1 cm in order to have an absorbance of ca. 0.1 at the λ$_{max}$. Low solubility samples were treated with ultrasonic vibrations using a sonicator and then filtered with PTFE syringe filters (0.45 μm). Fluorescence quantum yields (Φ) were calculated using the following formula:

$$\Phi = \frac{I_{sample}}{A_{sample}(\lambda_{sample}^{exc})} \frac{A_{ref}(\lambda_{ref}^{exc})}{I_{ref}} \frac{\eta_{sample}^2}{\eta_{ref}^2} \Phi_{ref}$$

using 1,1',3,3,3',3'-Hexamethylindotricarbocyanine Iodide (HTCI) as the reference compound (Φ$_{ref}$ = 0,28).

References

[1] Z. Y. Wang, *Near-Infrared Organic Materials and Emerging Applications*, CRC Press, **2013**.

[2] J. L. Bricks, A. D. Kachkovskii, Y. L. Slominskii, A. O. Gerasov, S. V. Popov, *Dye. Pigment.* **2015**, *121*, 238–255.

[3] S. Zhu, B. C. Yung, S. Chandra, G. Niu, A. L. Antaris, X. Chen, *Theranostics* **2018**, *8*, 4141–4151.

[4] S. Luo, E. Zhang, Y. Su, T. Cheng, C. Shi, *Biomaterials* **2011**, *32*, 7127–7138.

[5] L. Prodi, S. Biffi, L. Petrizza, C. Garrovo, E. Rampazzo, L. Andolfi, P. Giustetto, I. Nikolov, G. Kurdi, M. Danailov, et al., *Int. J. Nanomedicine* **2016**, *11*, 4865–4874.

[6] D. Saccone, S. Galliano, N. Barbero, P. Quagliotto, G. Viscardi, C. Barolo, *Eur. J. Org. Chem.* **2016**, 2244–2259.

[7] E. Seliverstova, N. Ibrayev, *IOP Conf. Ser. Mater. Sci. Eng.* **2018**, *289*, 012011.

[8] R. A. Ganeev, R. I. Tugushev, A. A. Ishchenko, N. A. Derevyanko, A. I. Ryasnyanskii, T. Usmanov, *Opt. Spectrosc.* **2003**, *95*, 435–441.

[9] D. Su, C. L. Teoh, A. Samanta, N.-Y. Kang, S.-J. Park, Y.-T. Chang, *Chem. Commun.* **2015**, *51*, 3989–3992.

[10] O. S. Kolosova, S. V. Shishkina, V. Marks, G. Gellerman, I. V. Hovor, A. L. Tatarets, E. A. Terpetschnig, L. D. Patsenker, *Dye. Pigment.* **2019**, *163*, 318–329.

[11] A. Treibs, K. Jacob, *Angew. Chemie Int. Ed. English* **1965**, *4*, 694–694.

[12] A. Ajayaghosh, *Acc. Chem. Res.* **2005**, *38*, 449–459.

[13] J. Eldo, A. Ajayaghosh, *Chem. Mater.* **2002**, *14*, 410–418.

[14] A. M. Glass, P. F. Liao, J. G. Bergman, D. H. Olson, *Opt. Lett.* **1980**, *5*, 368-370.

[15] J. Gersten, A. Nitzan, *J. Chem. Phys.* **1981**, *75*, 1139–1152.

[16] A. Wokaun, H. -P. Lutz, A. P. King, U. P. Wild, R. R. Ernst, *J. Chem. Phys.* **1983**, *79*, 509–514.

[17] M. Moskovits, *Rev. Mod. Phys.* **1985**, *57*, 783–826.

[18] J.-F. Li, C.-Y. Li, R. F. Aroca, *Chem. Soc. Rev.* **2017**, *46*, 3962–3979.

[19] J. Zhang, Y. Fu, M. H. Chowdhury, J. R. Lakowicz, *Nano Lett.* **2007**, *7*, 2101–2107.

[20] D. Jaque, L. Martínez Maestro, B. del Rosal, P. Haro-Gonzalez, A. Benayas, J. L. Plaza, E. Martín Rodríguez, J. García Solé, *Nanoscale* **2014**, *6*, 9494–9530.

[21] M. A. Garcia, *Phys. D Appl. Phys.* **2011**, *44*, 283001.

[22] M. Bauch, K. Toma, M. Toma, Q. Zhang, J. Dostalek, *Plasmonics* **2014**, *9*, 781–799.

[23] A. J. Fatiadi, H. S. Isbell, W. F. Sager, *J. Res. Natl. Bur. Stand. Sect. A Phys. Chem.* **1963**, *67A*, 153.

[24] W. Sun, S. Guo, C. Hu, J. Fan, X. Peng, *Chem. Rev.* **2016**, *116*, 7768–7817.

[25] W. Ghann, H. Kang, E. Emerson, J. Oh, T. Chavez-Gil, F. Nesbitt, R. Williams, J. Uddin, *Inorganica Chim. Acta* **2017**, *467*, 123–131.

[26] C. Shi, J. B. Wu, D. Pan, *J. Biomed. Opt.* **2016**, *21*, 050901.

[27] W. Städeli, R. Hollenstein, W. Von Philipsborn, *Helv. Chim. Acta* **1977**, *60*, 948–958.

[28] C. Han, H. Yang, M. Chen, Q. Su, W. Feng, F. Li, *ACS Appl. Mater. Interfaces* **2015**, *7*, 27968–27975.

[29] V. Maltese, S. Cospito, A. Beneduci, B. C. De Simone, N. Russo, G. Chidichimo, R. A. J. Janssen, *Chem. - A Eur. J.* **2016**, *22*, 10179–10186.

[30] X. Song, J. W. Foley, *Dye. Pigment.* **2008**, *78*, 60–64.

[31] A. Punzi, M. A. M. Capozzi, V. Fino, C. Carlucci, M. Suriano, E. Mesto, E. Schingaro, E. Orgiu, S. Bonacchi, T. Leydecker, et al., *J. Mater. Chem. C* **2016**, *4*, 3138–3142.

[32] G. A. Rillaers, H. Depoorter, *German Patent DE1930224A1*, **1970**.

[33] A. G. N. V, H. Depoorter, P. E. F. Lesmes, A. W. Breiner, *United States Patent US3615417*, **1971**.

[34] G. A. Rillaers, H. Depoorter, N. V Agfa-gevaert, *United States Patent US3793313*, **1974**.

[35] K. Katagiri, Y. Oguchi, Y. Takasu, *United States Patent US4548886*, **1985**.

[36] K. Katagiri, Y. Oguchi, T. Ohtake, K. Arao, Y. Takasu, *United States Patent US4629670*, **1986**.

[37] K. Katagiri, Y. Oguchi, T. Ohtake, K. Arao, M. Kitahara, Y. Takasu, *United States Patent US4673630*, **1987**.

[38] S. Yasui, M. Matsuoka, T. Kitao, *Dye. Pigment.* **1989**, *10*, 13–22.

[39] S. Ye, Q. Liang, Z. Li, S. Xu, C. Yao, *Tetrahedron* **2017**, *73*, 1350–1357.

[40] A. L. Hamilton, M. S. J. Briggs, I. E. Bruce, W. J. Cummins, R. M. West, *European Patent EP0898596A1*, **1997**.

[41] L. X. Guo, M. H. Liu, S. M. Sayed, B. P. Lin, P. Keller, X. Q. Zhang, Y. Sun, H. Yang, *Chem. Sci.* **2016**, *7*, 4400–4406.

[42] F. Neese, *Wiley Interdiscip. Rev. Comput. Mol. Sci.* **2012**, *2*, 73–78.

[43] J. E. Ridley, M. C. Zerner, *Theor. Chim. Acta* **1976**, *42*, 223–236.

[44] J. J. P. Stewart, *J. Mol. Model.* **2004**, *10*, 155–164.

[45] S. J. Krivickas, E. Tamanini, M. H. Todd, M. Watkinson, *J. Org. Chem.* **2007**, *72*, 8280–8289.

[46] J. R. Lakowicz, *Principles of Fluorescence Spectroscopy*, 3rd ed., Springer US, **2006**.

[47] O. A. Okoh, R. H. Bisby, C. L. Lawrence, C. E. Rolph, R. B. Smith, *J. Sulfur Chem.* **2014**, *35*, 42–56.

[48] J. R. Harjani, C. Liang, P. G. Jessop, *J. Org. Chem.* **2011**, *76*, 1683–1691.

[49] A. Arduini, R. Bussolati, A. Credi, G. Faimani, S. Garaudée, A. Pochini, A. Secchi, M. Semeraro, S. Silvi, M. Venturi, *Chem. - A Eur. J.* **2009**, *15*, 3230–3242.

[50] E. Boseggia, M. Gatos, L. Lucatello, F. Mancin, S. Moro, M. Palumbo, C. Sissi, P. Tecilla, U. Tonellato, G. Zagotto, *J. Am. Chem. Soc.* **2004**, *126*, 4543–4549.

[51] V. La Paglia Fragola, F. Lupo, A. Pappalardo, G. Trusso Sfrazzetto, R. M. Toscano, F. P. Ballistreri, G. A. Tomaselli, A. Gulino, *J. Mater. Chem.* **2012**, *22*, 20561-20565.

CHAPTER 5

Synthesis of key precursors for the formation
of starphenes and (a)symmetric acenes

5.1 Introduction

Organic compounds that show an absorption or an emission in the near-infrared (NIR) region of the light spectrum are usually characterised by an extended conjugated π-system, in which the π-electrons are delocalised over the whole structure. An example of π-conjugated systems is represented by the trans-polyacetylene class. If these compounds assume a cyclic structure, they are called cyclic π-conjugated polyenes and benzene can be considered as the smallest molecule of this class.
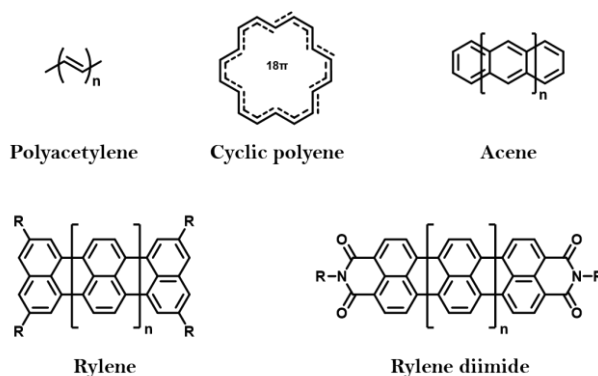
Figure 5.1 *Examples of conjugated π-systems.*

A way to extend the π-conjugation is to increase the number of annulated benzene rings. *Acenes* are a class of aromatic compounds composed of laterally fused benzene rings. These compounds show a red-shift of their low-energy absorption band (i.e. decrease of the HOMO-LUMO gap) with the extension of the π-system. Acenes are considered attractive compounds due to their intriguing electronic and magnetic properties.[1] In recent years, some theoretical works reported the studies of the electronic structures of long acenes, in particular concerning the open-shell singlet state.[2,3]

For these reasons, they are predicted to be good candidates for applications in several scientific fields. For example, they could be employed in organic electronics as semiconducting materials,[4,5] organic-field effect transistors[6] and as organic elements in light-emitting diodes.[7] They could be used also for solar-cell applications,[8] for spintronics,[9] and plasmonic.[10]
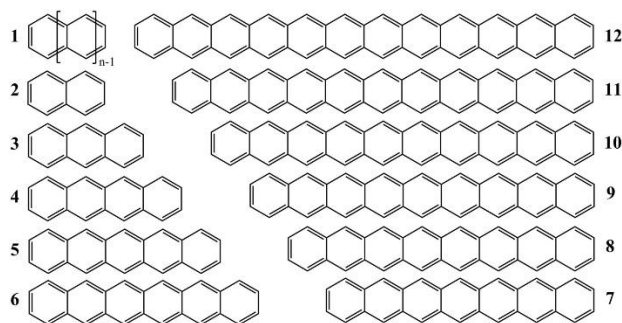
Figure 5.2 *Structure of acenes in one Kekule resonance form.*[11] *Reproduced from ref.* [11] *Copyright © 2016 National Academy of Sciences.*

The increase in the number of annulated benzene rings causes higher chemical reactivity. In fact, long acenes are difficult to obtain, first of all, because of their inherent fragility. They are easily (photo)oxidable, and they tend to dimerize in solution. Moreover, this type of compounds is poorly soluble in common organic solvents.

To improve both the stability and the solubility of acenes, several modifications can be done on their framework.[12] In literature, several examples reported the introduction of electron-deficient or bulky substituents or even heteroatoms (e.g. sulfur or nitrogen) directly into the acene structure.[13–15]

190
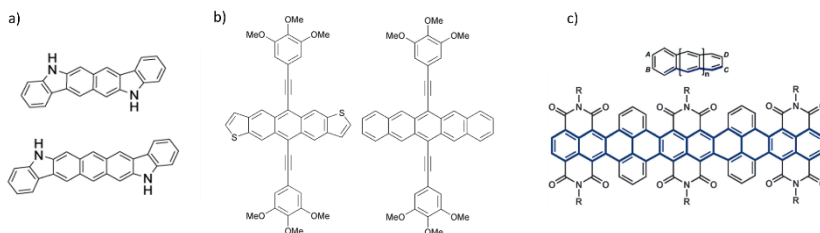
Figure 5.3 *Modification on the acenes framework. a) Adapted from ref.* [13] *Copyright © The Royal Society of Chemistry 2016; b) Adapted from ref.* [14] *Copyright © The Royal Society of Chemistry 2006; c) Adapted from ref.* [15] *Copyright © 2017 Wiley-VCH Verlag GmbH & Co. KGaA, Weinheim.*

It is easily foreseen that these structural modifications lead to a notable change in the electronic properties of these molecules, not more comparable with the unsubstituted ones. As a direct consequence, the synthesis of acenes still remains a challenge, especially their preparation in bulk. In fact, the synthesis of acenes up to undecacene in amount of few molecules in matrices were reported.[16,17] Recently, they have been prepared by on-surface synthesis at low-temperature (5 K) under ultra-high vacuum. Basically, the strategy is based on the synthesis of stable and soluble precursors which, in turn, can be converted in the solid state

into the target acenes. This latter step usually consists of a unimolecular process, such as photochemical bis-decarbonylation,[16–18] deoxygenation of epoxides,[19–21] dehydrogenation[22,23] and bis-decarbonylation of α-diketones.[24,25] The bulk preparation of acenes beyond the pentacene has been described only recently. In 2012, Chow and co-workers reported the preparation of hexacene by using a carbonyl-bridged precursor (**1**, Figure 5.4), which was synthesized in 5 steps in 24% overall yield.[26] The last crucial step consisted of the decarbonylation of a monoketone precursor and can be achieved either by irradiation of the precursor solution at 365±30 nm or by heating the solid sample at 180 °C (Figure 5.4). The formed hexacene was stable in the solid state form for several months.
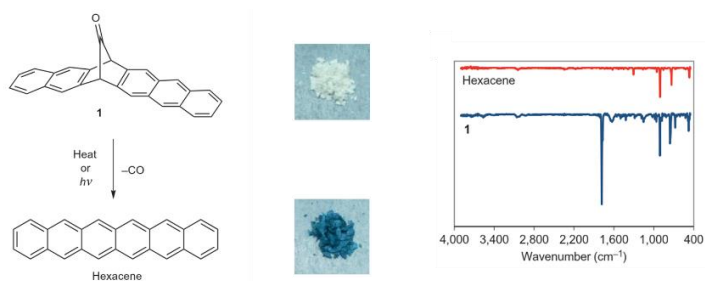
Figure 5.4 *Characterization of the transformation of the monoketone precursor in hexacene: physical appearance and infrared spectra of both the compounds. Reproduced from ref. [26] Copyright © 2012, Springer Nature.*

Heptacene, instead, has been prepared in 2017 by Bettinger et al., more than 70 years after the first attempted synthesis.[27] The reported strategy is based on the thermal cleavage (more precisely, thermal retro Diels-Alder reaction) of the diheptacene dimer precursor. By heating the sample in the solid state form to 300°C for 12 min under inert gas, it is possible to observe the formation of heptacene in the ^{13}C CP-MAS NMR experiment.
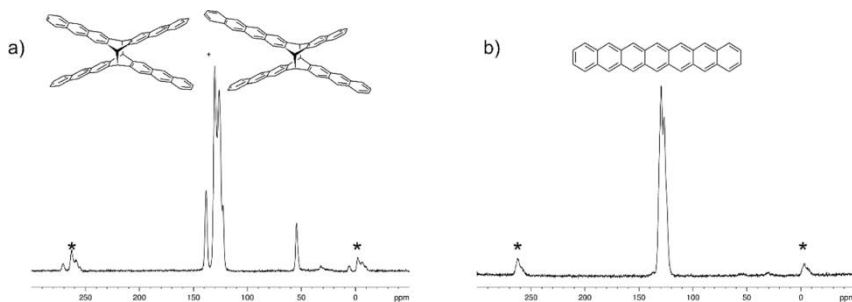
Figure 5.5 *Solid-state ^{13}C CP-MAS NMR spectra (rotational sidebands are marked by asterisks). Reproduced from ref. [27] Copyright © 2017 American Chemical Society.*

In the spectrum is visible a sharpening of the signals in the aromatic region and the disappearance of the bridgehead carbon signals, exclusively suggesting the presence of sp² hybridized carbon atoms (Figure 5.5). In contrast to hexacene, thus formed heptacene was not stable and slowly converted back to its dimer.

In 2019, Jancarik et al. reported a practical general method for the preparation of long acenes beyond pentacene.[28] Even in this case, the precursor is a monoketone (**MK**) derivative, which brings to the quantitative formation of the target acene after decarbonylation by heating in the solid state at moderate temperatures between 155 and 205°C.[29] The strategy employed consists of three steps, excluding the decarbonylation one (Scheme 5.1). The starting compound is the (1S,4S)-7,7-dimethoxy-2,3,5,6-tetramethylenebicyclo[2.2.1]heptane **1**[30] that, in the first step, undergoes a Diels–Alder condensation with arynes to give, after oxidation, the protected mono-ketal (**PMK**) precursors. These soluble compounds represent the non–planar and not fully conjugated and therefore stable protected acene derivatives. The third step is the cleavage of the ketals to yield the CO bridged precursors (**MK**).
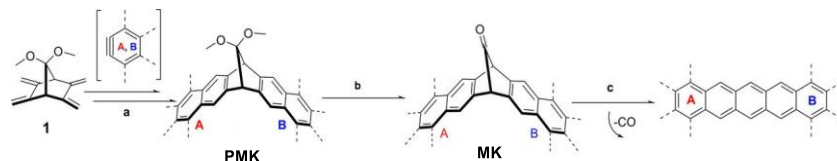
Scheme 5.1 *General method reported by Jancarik et al. a) Diels-Alder reactions of **1** with benzynes in one or two steps; b) cleavage of the ketal (**PMK**) to yield the corresponded ketone (**MK**); c) heating in solid state to yield the corresponding acene. Adapted from ref. [28] Copyright © 2019 Wiley-VCH Verlag GmbH.*

As representative examples, heptacene and other three seven-membered rings acenes have been synthesized, employing different aryne precursors. Heptacene **3** was obtained by Diels-Alder cycloaddition of **1** with 2,3-naphtyne compounds. These latter molecules were prepared in situ employing n-butyllithium (n-BuLi) or caesium fluoride (CsF) with precursors **2a** or **2b**, respectively (Scheme 5.2). The formed heptacene was stable in the solid state form for several months stored under inert gas. The two isomers of dibenzopentacene **4** and **5** were obtained from 1,2-naphtyne (generated in situ from **2c**) in stead of 2,3-naphtyne. After the oxidation and the cleavage of the ketal, the mono-ketone compounds were heated under inert atmosphere, accompanied by a colour change. The effective cheletropic CO extrusion was followed by TGA and the resulting acenes **3**, **4**, and **5**, obtained in quantitative yields, were characterized also by FTIR, solid-state UV-Vis spectroscopy, ¹³C CP-MAS NMR and HR ESI-MS.
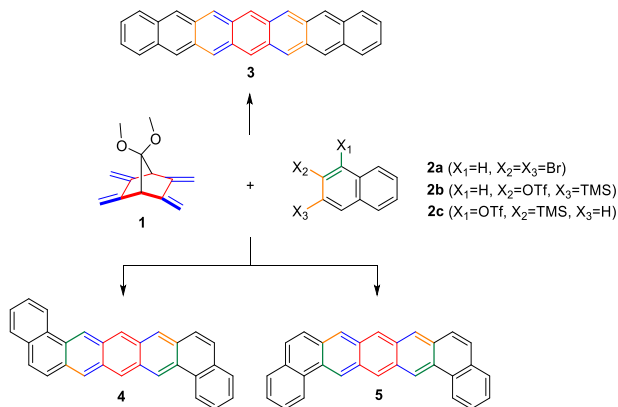
Scheme 5.2 *General scheme for the synthesis of heptacene 3 and dibenzopentacene 4 and 5.*

To extend the potential of the latter approach, the preparation of *asymmetric* acene precursors was attempted. This purpose was achieved by reacting only one side, i.e. the diene, of tetraene **1**, changing the molar ratio of the aryne. Benzo[a]hexacene **9** was prepared by the Diels-Alder reaction of **1** with 1.3 eq. of in situ-generated 2,3-naphtyne (from **2b**). The resulting *cis*-diene **6** was used in another Diels-Alder addition with 1,2-naphtyne (from **2c**) to give the corresponding acene precursor **7** (Scheme 5.3).
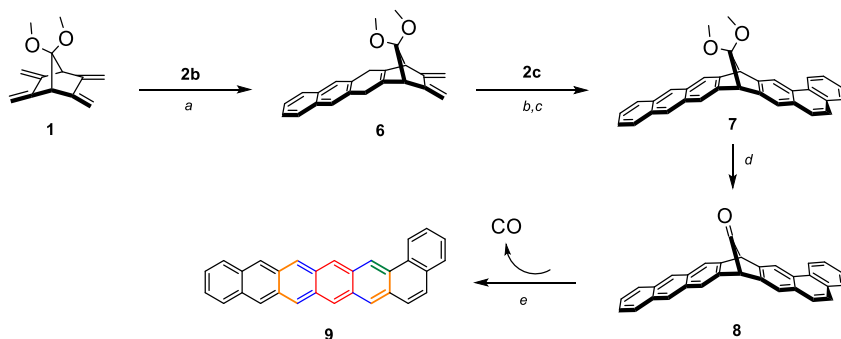
Scheme 5.3 *Synthesis of benzo[a]hexacene 9: a) 2b, CsF, CH₃CN, 46%; b) 2c, CsF, CH₃CN, then c) DDQ, toluene, 80%; d) TMSI, CH₂Cl₂, 96%; e) neat, 200°C, quant. yield.*

The great breakthrough was demonstrated by the synthesis of acenes up to heptacene in bulk. These acenes were stable in the solid state form for several months which breaks the established dogma.

This methodology is general enough to be potentially applied in the preparation of acenes longer then heptacene and their derivatives. My task was to develop a methodology for the construction of branched acenes (starphenes) based on this concept. Starphenes and their multiply branched analogues (cloverphenes, dendrophenes) represent a class of

polyaromatic hydrocarbon compounds. The starphene nomenclature was coined by Clar an Mullen in 1968, referred to benzologues of triphenylene, in which from a central benzene core ring split off three branches in a linear manner.[31] Recently, it was reported the synthesis of asymmetric starphene molecule **A** (Figure 5.6, bottom left) by a combination of solution and on-surface chemistry.[32] It was demonstrated that compound **A** represents the working principle of a single molecule NAND logic gate [33] by selectively contacting single gold atoms by atomic manipulation to the longer branches of the molecules. By scanning tunnelling spectroscopy the output of this system was measured. With this methodology it was possible to obtain only the desired asymmetric starphene **A**, without the formation of any possible by-products generated from the thermally-activated on-surface reaction (**B** and **C**).
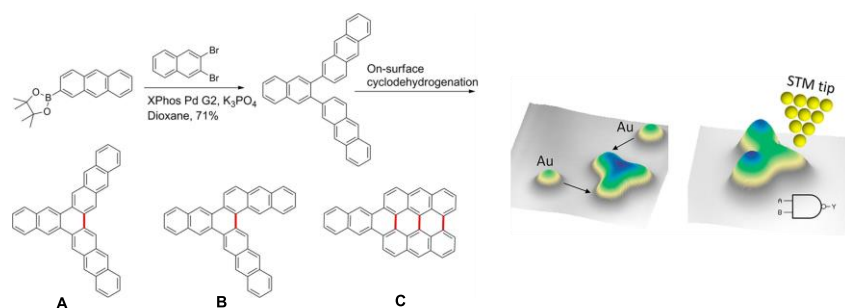
Figure 5.6 *Chemical synthesis of an asymmetric starphene **A** and possible products (**B** and **C**) of thermally activated on-surface reaction. Reproduced from ref. [32] Copyright © 2017 American Chemical Society.*

The bottom-up approach through organic synthesis would avoid the structural inhomogeneity characteristic of current on-surface approaches. Moreover, it could open the way to the synthesis of even more conjugated systems. Generally, the strategy for the formation of starphene-type molecules is based on the cyclotrimerization of polycyclic arynes, efficiently catalyzed by palladium(0) complexes.[34–38] For instance, Alonso et al. reported the synthetic procedure leading to a clover-shaped *cata*-condensed nanographene with sixteen fused benzene rings (compound **15** in Scheme 5.4).[39] The building block employed in the Pd-cyclotrimerization was ortho-(trimethylsilyl)aryl triflate aryne precursor **14**. This compound was synthesized through Diels-Alder reaction from the cyclopentadienone **10** which reacted with *in*-situ generated aryne **12**, deriving from the asymmetric bis(benzyne) precursor **11**, followed by the chelotropic extrusion of CO to yield compound **13**. This latter was reacted with hexamethyldisilazane (HMDS), and then the addition of *n*-BuLi and Tf$_2$O afforded the aryne precursor **14**.
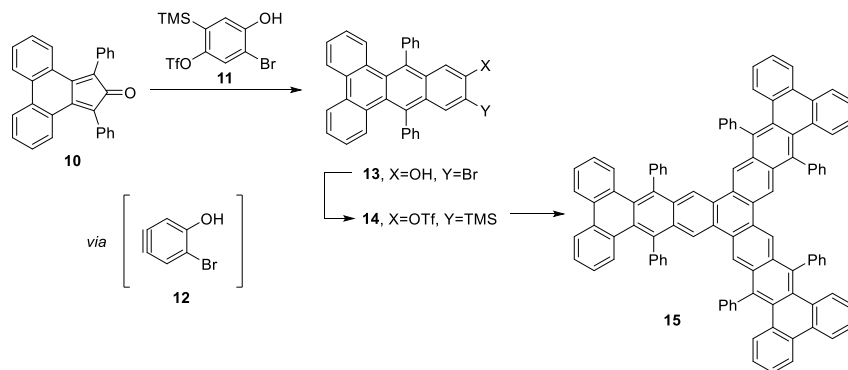
Scheme 5.4 *Synthesis of aryne precursor 14, which in turns undergoes to a Pd-cyclotrimerization to give the cloverphene 15.*

In this Chapter, two alternative methodologies will be discussed. In particular, it will be presented the synthesis of a precursor, which can be employed both in the synthesis of starphenes and asymmetric long acenes.

5.2 Results and Discussion

195

Taking advantage of the methodology reported by Jancarik et al. for the synthesis of heptacene derivative and from those reported by Alonso et al. regarding the synthesis of the [16]Cloverphene, two main strategies are proposed in Scheme 5.5. *Strategy A* is the most straightforward route leading directly to the starphene protected precursor **20** by triple Diels-Alder reaction, where the asymmetric diene precursor **16** and the hexabromotriphenylene **19** are coupled (Scheme 5.5). Besides this "direct" synthetic pathway, another strategy was pointed out for the synthesis of **20**. *Strategy B* is based on palladium-assisted cyclotrimerisation (as depicted in Scheme 5.4) of suitable aryne precursors like compound **18**. This suitable precursor **18**, could be prepared by selective Diels-Alder reaction of asymmetric bis(benzyne) **17** and diene **16**. This key compound employed in the cyclotrimerization will form the triple-bridged [16]starphene(5.5.5) **20**, which, in turn, could undergo a deprotection step of the ketal, to yield the starphene precursor **SP-1**. A decarbonylation step could be accomplished in the solid state, as previously discussed for the synthesis of heptacene derivative, to give the target starphene **S-1**.
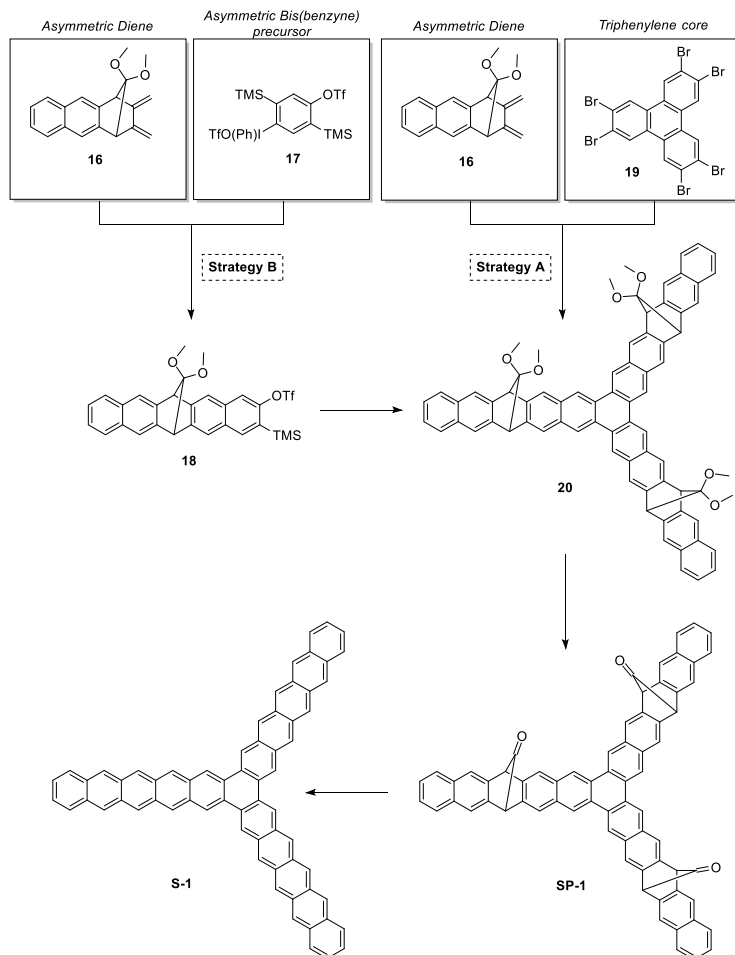
Scheme 5.5 *Synthetic pathways proposed for the synthesis of [16]starphene(5.5.5)* **S–1**.

5.2.1 Strategy A

As reported for the synthesis of benzo[a]hexacene in the general method[28], it is possible to employ a proper stoichiometric ratio between tetraene **1** and the aryne, to obtain the asymmetric precursor as the major product in the Diels–Alder reaction (see section 5.1, Scheme 5.3).

Tetraene **1** is the building block on which the following synthetic methodologies are based. It can be obtained from dimethyl fulvene, following the synthesis reported by Roth et al.[30] in 1991 and recently reinvestigated by Jancarik et al.[40] The revised method allows the synthesis of **1** in a reduced number of simplified steps, without any

column chromatography separation and therefore in gram scale (∼ 10 grams).

*Cis*-diene **16** was indeed synthesized through the Diels-Alder cycloaddition of **1** with 1.3 eq. of 2,3-benzyne precursor **21**, generated in situ by the use of CsF at room temperature in CH₃CN (Scheme 5.6). The resulting not-fully aromatized compound **22** was purified through column chromatography on silica gel and was obtained in 64% yield. This latter molecule, since it is not stable over a long period, was immediately oxidized with 2,3-dichloro-5,6-dicyano- 1,4-benzoquinone (DDQ) in toluene at room temperature to yield the *cis*-diene synthon **16** in 95% yield.
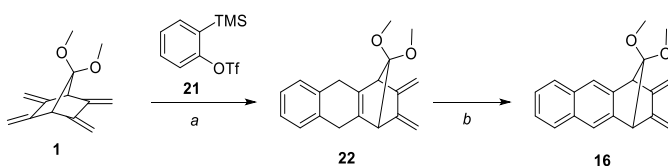
Scheme 5.6 *Synthesis of asymmetric diene synthon **11**: a) CsF, CH₃CN, rt, 16h, 64%; b) DDQ, toluene, rt, 3h, 95%.*
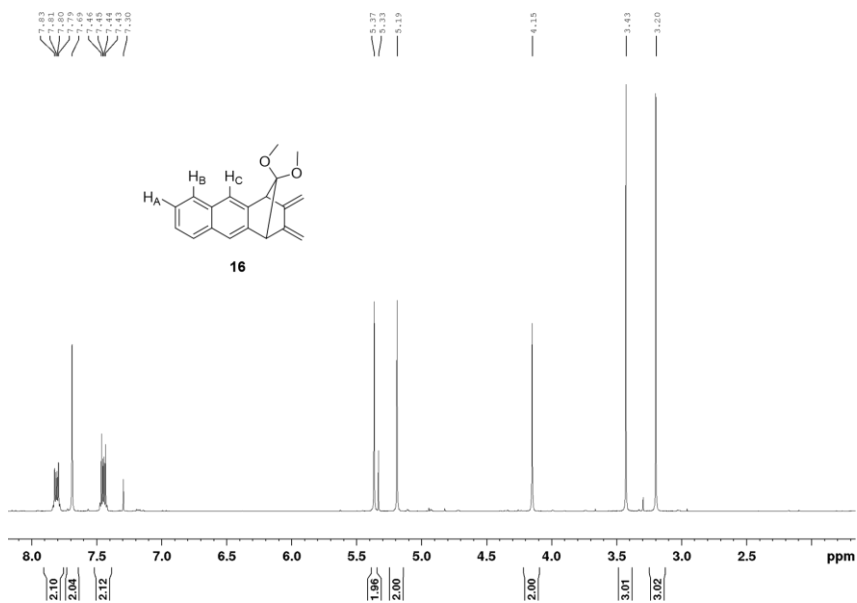
**Figure 5.7** *¹H NMR (300 MHz, CDCl₃) spectrum of **16**.*

In the ¹H NMR spectrum of **16** some diagnostic signals are clearly recognisable (Figure 5.7). The two geminal protons of each terminal double bond give rise to two singlets at δ = 5.37 and δ = 5.19 ppm. The singlet at δ = 4.15 ppm corresponds to the two bridgehead protons. The two intense signals at δ = 3.43 and δ = 3.20 ppm, integrating for three

protons respectively, are relative to the two methyl groups of the ketal protecting group. In the aromatic region, besides the two patterns of signals relative to H_A and H_B, the effective aromatization is confirmed by the presence of the singlet at $\delta = 7.69$ ppm relative to H_C.

The other building block employed in this first strategy consists of a suitable triphenylene core. According to the literature procedure, hexabromotriphenylene **19** was prepared by bromination of the commercially available triphenylene, which was allowed to react with bromine in nitrobenzene in the presence of iron powder as catalyst (Scheme 5.7). [39] Compound **19** was then treated with *n*-BuLi in the presence of synthon **16**. However, this reaction was not successful, and all the analysis seemed to show a complete degradation of the reaction mixture, probably due to a high instability of the lithiated species or due to the elevated probability of side reactions, since the number of active sites on the involved molecules.

198
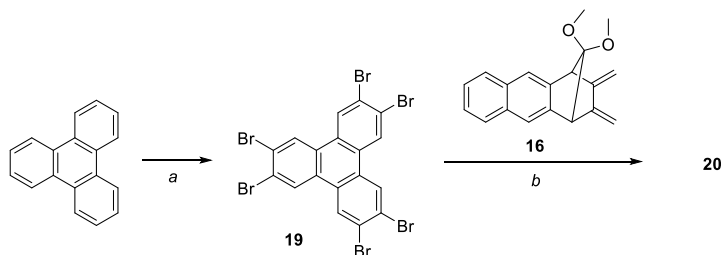
Scheme 5.7 *Synthesis of core* **19** *as building block to obtain the triple-bridged [16]starphene(5.5.5)* **20** *after the reaction with asymmetric diene* **16**. *Reagents and conditions: a) Br₂, iron, nitrobenzene, 16h at rt, then 2h at 205°C, 95%; b)* **16**, *n-BuLi, toluene, 24h.*

5.2.2   Strategy B

In this second strategy, besides synthon **16**, it is necessary to synthesize the asymmetric bis(benzyne) **17**. The design of this latter molecule was related to a different reactivity of the substituents on the benzene rings. In fact, it was demonstrated that the hypervalent iodo–group has a much higher leaving ability than the triflate group (more than 10^6).[41] Thank to this difference in leaving ability, it is possible by temperature to chemoselectively control the generation of mono(aryne) **17a**[42] and therefore to avoid the possible polymerization. The followed synthetic pathway is illustrated in Scheme 5.8.
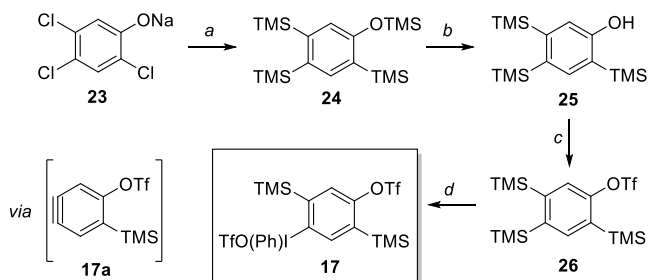
Scheme 5.8 *Synthesis of asymmetric bis(benzyne) precursor **17**. Reagents and conditions: a) Mg, CuCl, LiCl, TMSCl, DMI, 60°C, 48h, 46%; b) KOH, EtOH, rt, 30 min, quant. yield; c) Tf₂O, pyridine, CH₂Cl₂, 0°C, 30 min, 79%; d) PhI(OAc)₂, TfOF, CH₂Cl₂, 0°C, 1h.*

The first step is the trimethylsilylation of sodium 2,4,5-trichlorophenoxide **23** in the presence of Mg, CuCl and LiCl in DMI. All these reagents were managed under inert conditions since the reaction is very sensitive to water. The resulting product **24**, obtained in 46% yield, was treated with a solution of KOH in ethanol to give the desilylated compound **25** quantitatively. Because of its tendency to decompose, even at room temperature, **25** was immediately reacted with triflic anhydride (Tf₂O) in the presence of pyridine at 0 °C to afford 2,4,5- tris(trimethylsilyl)phenyl triflate **26** in 79% yield. Finally, the treatment with phenyliodine(III) diacetate (PhI(OAc)₂)and triflic acid (TfOH) allowed the synthesis of the asymmetric bis(benzyne) precursor **17**, which is reported to be non-hygroscopic and stable over a long period of time.[42]

However, despite an intensive synthetic effort, it was not possible to isolate compound **17**, by reproducing the published synthetic protocol. The reaction led always to a mixture of several compounds. Since this compound cannot be simply purified by column chromatography and precipitation/recrystallization also failed, it was decided to explore the preparation of key compound **18** using an alternative way (see paragraph 5.2.3).

All the intermediate species were characterized and the ¹H NMR stack plot is reported in Figure 5.8.
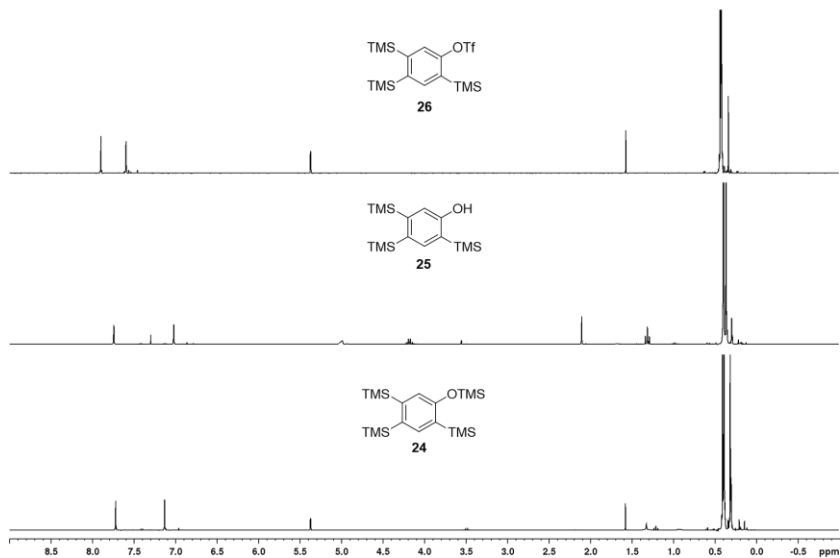
***Figure 5.8*** *¹H NMR stack plot of **24** (300 MHz, CD₂Cl₂), **25** (300 MHz, CDCl₃) and **26** (300 MHz, CD₂Cl₂).*

In all the ¹H NMR spectra, two singlets are present in the aromatic region and these signals (each integrating for one proton) are generated by the two aromatic protons of the compounds. The position of the singlet initially at $\delta = 7.15$ ppm in compound **24** (Figure 5.8, bottom), is down-field shifted up to $\delta \sim 7.5$ ppm in compound **26** (Figure 5.8, top), depending on the different substituents on the aromatic ring. Moreover, the protons of the three TMS groups resonate at $\delta \sim 0.4$ ppm as a singlet, integrating for 27 protons. In the ¹H NMR spectrum of **24** (Figure 5.8, bottom), the identity of the compound is confirmed by the presence of a further singlet at $\delta = 0.3$ ppm, assigned to the nine protons of the OTMS group. In the ¹H NMR spectrum of **25** (Figure 5.8, middle), the disappearance of this latter signal confirms the occurred hydrolysis of the OTMS group and the hydroxyl proton resonates as a broad signal at $\delta \sim 5.1$ ppm.

5.2.3 Alternative route for the synthesis of precursor (18)

The idea was to synthesize the precursor **18** from diene **16** by statistic Diels-Alder reaction. For this purpose, bis(aryne) synthon **27** was prepared. By using the excess of this latter synthon, it could be possible to suppress the formation of unwanted products and to directly afford the key compound **18** in two synthetic steps. Moreover, with the same strategy, it could be possible to obtain a longer precursor (**29**)

employing bis(naphtyne) **28** instead of **27**. To verify this concept, precursor **27** and **28** had to be prepared.
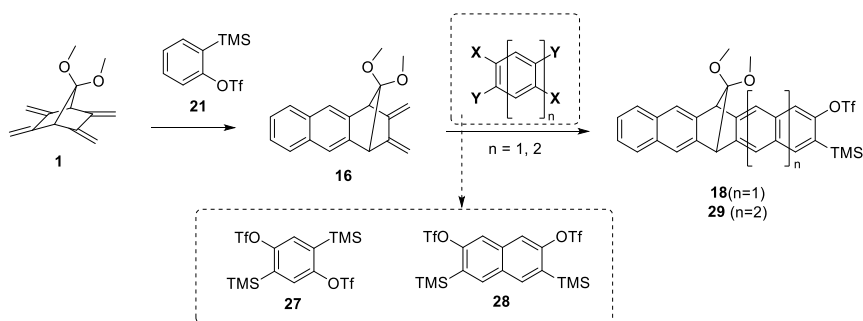
Scheme 5.9 *Schematic synthetic pathway for the synthesis of precursors **19** and **29**.*

5.2.3.1 Synthesis of target bis(arynes) precursors

Bis(naphtyne) precursor **28** was synthesized in two steps (Scheme 5.10). Commercial 3,6-dibromo-2,7-dihydroxynaphtalene was treated with trimethylsilyl chloride (TMSCl) in pyridine and toluene at reflux, to obtain the desired compound **30**. Without any further purification, this latter compound was used directly in the following step. The reaction of **30** with *n*-BuLi and subsequently with trifluoromethanesulfonic anhydride (Tf$_2$O) at -80 °C in THF yielded the target compound **28** (53% yield).
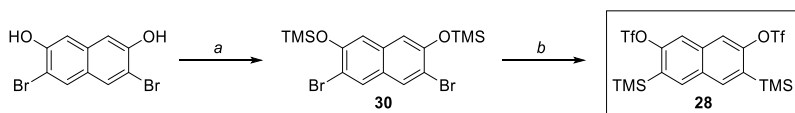
Scheme 5.10 *Synthesis of bis(naphtyne) precursor **28**. Reagents and conditions: a) TMSCl, pyridine, toluene, reflux, 18h, quant. yield; b) n-BuLi, Tf$_2$O, THF, -80°C, 1h, 53%.*

The ¹H NMR spectrum of **28**, measured in CD$_2$Cl$_2$, shows three expected diagnostic signals: the two singlets in the aromatic region (δ = 8.16 and δ = 7.89 ppm) and one single intense signal at δ = 0.49 ppm corresponding to the two trimethylsilyl groups (Figure 5.9).
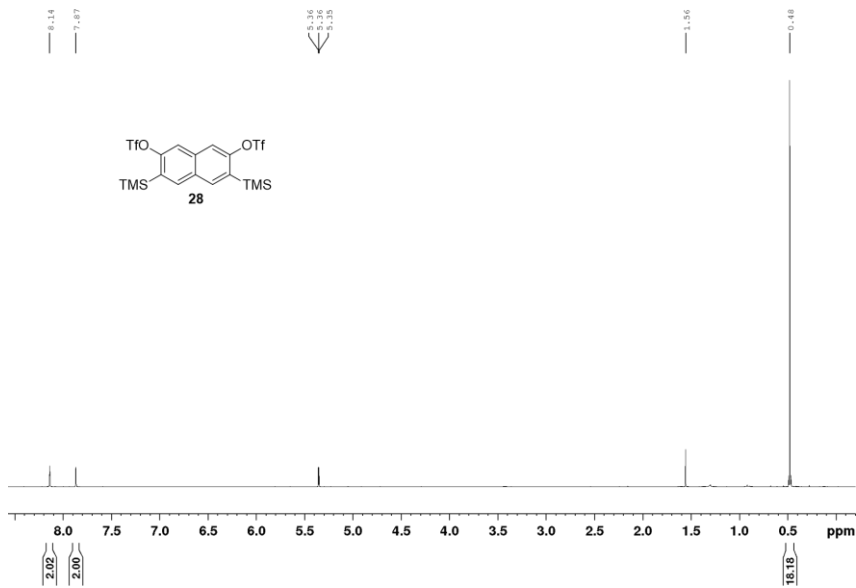
Figure 5.9 *^{1}H NMR (300 MHz, CD$_2$Cl$_2$) spectrum of **28**.*

In a first attempt, the same procedure was followed for the synthesis of bis(benzyne) precursor **27**. Unfortunately, in the lithiation step, complete degradation of the reaction mixture was obtained. It was assumed, it is due to the instability of the lithiated intermediate species. Therefore, an alternative three-step procedure was followed leading to compound **27** (Scheme 5.11). The hydroxylic groups of 2,5-dibromohydroquinone were protected with TMSCl to give compound **31**, which was reacted with *n*-BuLi in THF at -78°C. Then, TMSCl was added dropwise to yield the stable compound **32**. After the isolation of this latter molecule, another lithiation reaction was performed, followed by the addition of Tf$_2$O at 0 °C. After purification by a silica gel column chromatography, target bis(benzyne) precursor **27** was isolated in 44% overall yield and it was completely characterized.
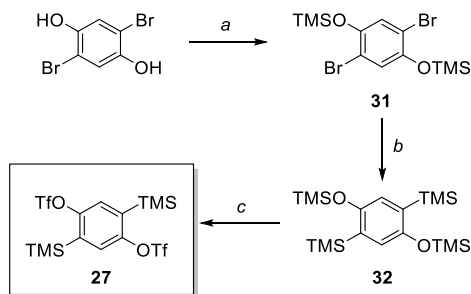
Scheme 5.11 *Synthesis of bis(benzyne) precursor **27**. Reagents and conditions: a) TMSCl, Et$_3$N, THF, rt, 1h, quant. yield; b) n-BuLi, TMSCl, THF, -78°C to rt, 2h, 79%; c) n-BuLi, Et$_2$O, -78°C to rt 2h, then Tf$_2$O, Et$_2$O, 0°C to rt, 1h, 56%.*

As for **28**, the ^{1}H NMR spectrum of **27** is simply due to its symmetry, showing just two signals: one singlet at δ = 7.50 ppm, assigned to the two aromatic protons and one singlet of two trimethylsilyl groups at δ = 0.43 ppm (Figure 5.10).
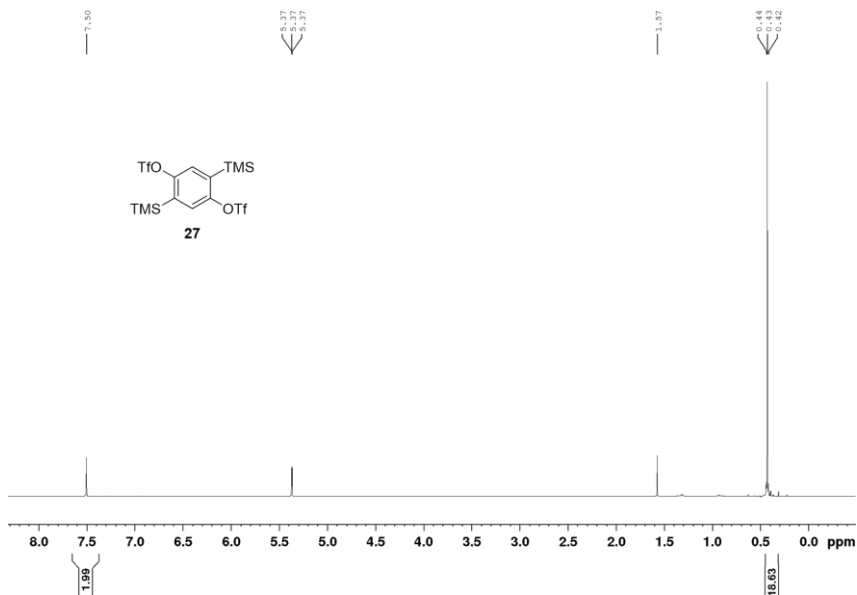
Figure 5.10 ^{1}H NMR (300 MHz, CD$_2$Cl$_2$) spectrum of **27**.

203

5.2.3.2 Synthesis of precursor 18

In a first attempt, the reaction between diene **16** and synthon **27** was carried out following the same reaction conditions employed in the Diels–Alder condensation for the synthesis of **22**, showed in Scheme 5.6. Since **27** is a bifunctional benzyne precursor, to favour the formation of **18** as the major product, the reaction was accomplished with an excess of **27** in CH$_3$CN, using 2 equivalents of CsF at room temperature (Scheme 5.12). However, the reaction was not successful, even upon heating the mixture to 40°C and the formation of the desired product **18** was not observed. In 2015, Rodriguez-Lojo et al. reported the selective generation of the functionalized mono(arynes) **27a** and **28a** and their further Diels–Alder reaction with a dienone.[43] Therefore, the reaction between diene **16** and synthon **27** was carried out in a 4:1 mixture of CH$_3$CN and CH$_2$Cl$_2$ at room temperature in the presence of CsF (2 eq.), as fluoride source. Surprisingly, optimizing the reaction conditions, it was discovered that it is possible to obtain **18** as the major product of the reaction, even using a 1:1 ratio between compounds **27** and **16** (Scheme 5.12). The choice of the solvent mixture seems thus to be crucial for the effective success of the chemoselectivity. The use of

only one of the two solvents resulted in lower conversions due to the poor solubility of either the diene or CsF.[43]
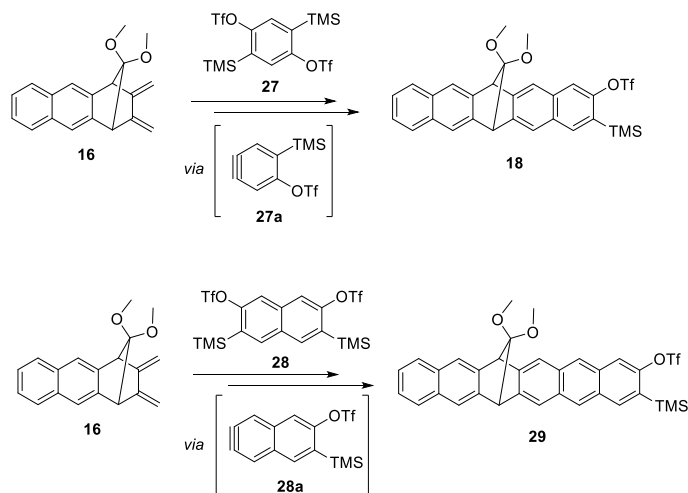
Scheme 5.12 *Synthetic scheme for the synthesis of* **18** *and* **29**.

The identity of the synthesized compound **18** has been confirmed through a series of NMR and ESI–MS measurements. Nevertheless, this data cannot be reported in the dissertation for scientific secrecy reasons.

5.3 Conclusion

The resulting compound **18** will be used for the preparation of the starphene **S-1** (Scheme 5.5). Moreover, the effective development of the synthetic methodology for the synthesis of precursors, as compound **18**, opens the way, in principle, to the preparation of (a)symmetric long acenes. For example, precursor **18** or **29** could be employed, as the aryne precursors, in the reaction with the tetraene building block **1**, to give a triple-bridged acene precursor (as showed in the general method showed in Scheme 5.1).

5.4 Experimental Section

Anhydrous solvents were purchased from Aldrich and used as received and all other reagents were of reagent-grade quality obtained from commercial suppliers and were used without further purification. NMR spectra were recorded at 300 MHz for ^{1}H on a *Bruker Avance* 300 spectrometer. Chemical shifts (δ) are expressed in ppm using the residual solvent signal as the internal reference. Melting points are uncorrected. Coupling constants (J values) are given in hertz (Hz) and multiplicities are reported using the following abbreviation: s = singlet, d = doublet, t = triplet, q = quartet, m = multiplet, br. s = broad signal. Mass spectra were recorded in ESI mode. Compound **19**[39] was synthesized according to published procedures.

(1S)-11,11-dimethoxy-2,3-dimethylene-1,2,3,4,9,10-hexahydro-1,4-methanoanthracene (22). A well-dried flask was charged with **1** (3 g, 14.7 mmol, 1 equiv.) and CsF (4.46 g, 29.4 mmol, 2 equiv.) under argon and then anhydrous CH_3CN was added (300 mL). The reaction mixture was cooled to 0 °C, and then 2-(trimethylsilyl)phenyl trifluoromethanesulfonate **21** (4.64 mL, 19.1 mmol, 1.3 equiv.) was added dropwise. The mixture was stirred at room temperature overnight. After the evaporation of the solvent, the residue was purified by column chromatography (SiO_2, hexane/THF 20:1) to obtain **22** as a pale yellow solid (2.2 g, 64%). ^{1}H NMR (300 MHz, CDCl$_3$) δ: 3.26 (3H, s), 3.30 (3H, s), 3.38 (2H, s), 3.42-3.66 (4H, m), 5.00 (2H, s), 5.23 (2H, s), 7.17 (4H, s).

Asymmetric diene precursor (16). In a well-dried flask, compound **22** (2.17 g, 7.74 mmol, 1 equiv.) was dissolved in anhydrous toluene (250 mL). The mixture was cooled to 0 °C, then DDQ (1.74 g, 7.74 mmol, 1 equiv.) was added in three portions and it was stirred at room temperature for 3 hours. The mixture was filtered over a glass frit filter S4 and the solvents were removed under reduced pressure. The residue was purified by column chromatography (SiO_2, hexane/ethyl acetate 15:1) to yield **16** as a pale yellow solid (2.05 g, 95%). ^{1}H NMR (300 MHz, CDCl$_3$) δ: 3.20 (3H, s), 3.43 (3H, s), 4.15 (2H, s), 5.19 (2H, s), 5.37 (2H, s), 7.43-7.46 (2H, m), 7.69 (2H, s), 7.79-7.83 (2H, m).

[2,4,5- tris(trimethylsilyl)phenyl](trimethylsilyl)ether (24).[42] A well-dried flask was charged with Mg turnings (0.93 g, 35.37 mmol, 8 equiv.), CuCl (0.44 g, 4.42 mmol, 1 equiv.) and LiCl (1.50 g, 35.37 mmol, 8 equiv.) under argon and then DMI (30 mL) was added. Subsequently, trimethylsilyl chloride (9.07 mL, 70.73 mmol, 16 equiv.) was slowly

added and the mixture was stirred at room temperature for 5 min. 2,4,5-trichlorophenol sodium salt (1 g, 4.42 mmol, 1 equiv.) was then added in one portion and the mixture was heated at 60 °C for 2 days. A saturated solution of NaHCO$_3$ was slowly added and the magnesium solid residue was filtered off and the product in the filtrate was extracted with *n*-hexane. The organic layer was washed with brine, dried over MgSO$_4$ and solvent was evaporated under reduced pressure. The residue is treated with methanol to give **24** as a withe solid (0.78 g, 46%). ^{1}H NMR (300 MHz, CD$_2$Cl$_2$) δ: 0.31 (9H, s), 0.38 (18H, s), 0.40 (9H, s), 7.12 (1H, s), 7.71 (1H, s).

2,4,5-tris(trimethylsilyl)phenol (25).[42] Compound **24** (0.76 g, 1.98 mmol, 1 equiv.) was added in one portion to a solution of potassium hydroxide (0.11 g, 1.98 mmol, 1 equiv.) in ethanol (20 mL) and the mixture was stirred at room temperature for 30 minutes. The solvent was evaporated under reduced pressure and the residue was extracted with ethyl acetate and washed with water. The organic layer was dried over MgSO$_4$ and the solvent was evaporated under reduced pressure. Without any further purification, the resulting **25** was directly used in the following step. ^{1}H NMR (300 MHz, CDCl$_3$) δ: 0.36 (9H, s), 0.39 (18H, s), 4.99 (1H, bs), 7.02 (1H, s), 7.74 (1H, s).

2,4,5- tris(trimethylsilyl)phenyl triflate (26).[42] The well-dried white solid **25** was dissolved in anhydrous CH$_2$Cl$_2$ (9.5 mL) and then pyridine (0.80 mL, 9.90 mmol, 5 equiv.) was added. The mixture was cooled to 0 °C and triflic anhydride (0.51 mL, 2.97 mmol, 1.5 equiv.) was added dropwise. After stirring at 0 °C for 30 minutes, a cold solution of NaHCO$_3$ was slowly added. The organic layer was washed with brine, dried over MgSO$_4$ and solvent was evaporated under reduced pressure. The residue was purified by filtration over a small plug of silica gel (SiO$_2$, *n*-hexane with 1% of diethyl ether), to yield **26** as a white solid (0.72 g, 82%). ^{1}H NMR (300 MHz, CD$_2$Cl$_2$) δ: 0.417 (9H, s), 0.423 (9H, s), 0.43 (9H, s), 7.60 (1H, s), 7.90 (1H, s).

Asymmetric bis(benzyne) precursor (17).[42] A suspension of PhI(OAc)$_2$ (772.7 mg, 2.4 mmol) in CH$_2$Cl$_2$ (15 mL) was cooled to 0 °C with an ice bath and triflic acid (425 µL, 4.8 mmol) was added. After stirring for 30 minutes, **26** (884.2 mg, 2.0 mmol) was added and stirred at 0 °C for 30 minutes. The reaction mixture was slowly poured into a cold saturated solution of NaHCO$_3$ and extracted with CH$_2$Cl$_2$. The solvent was evaporated under reduced pressure and the residue was treated with diethyl ether. The resulting solid compound was filtered to give **17** as a mixture of unidentifiable compounds. All the attempts to purify this compound failed.

3,6-dibromo-2,7-bis(trimethylsilyloxy)naphtalene (**35**).[44] A well-dried Schlenk flask was charged with 3,6-dibromonaphthalene-2,7-diol (4 g, 12.6 mmol, 1 equiv.) and toluene (40 mL). The heterogeneous mixture was heated to 85 °C and then pyridine (11.4 mL, 141 mmol, 11 equiv.) was added, obtaining a clear solution. Trimethylsilyl chloride (11.4 mL, 89.3 mmol, 7.1 equiv.) was slowly added and the mixture was stirred at reflux overnight. The mixture was allowed to cool at room temperature and water was cautiously added, the organic layer was separated, washed with brine and dried over $MgSO_4$. After evaporation of the solvent, the product **35** was obtained as a creamy pale yellow solid (5.8 g, quant. yield) and it was used in the next step without any further purification. ^1H NMR (300 MHz, CD_2Cl_2) δ: 0.41 (18H, s), 7.15 (2H, s), 7.96 (2H, s).

Bis(naphtyne) precursor (**28**).[45] In a well-dried Schlenk flask, compound **35** (1g, 2.16 mmol, 1 equiv.) was dissolved in anhydrous THF (25 mL). The solution was cooled to -80 °C, a 1.6 M solution of n-butyllithium in hexane (3.24 mL, 5.19 mmol, 2.4 equiv.) was added dropwise, and the resulting mixture was stirred for 30 minutes at -80 °C. Then, triflic anhydride (1.19 mL, 7.14 mmol, 3.3 equiv.) was added dropwise. After 30 minutes still at -80 °C, the mixture was allowed to warm to room temperature. A saturated solution of $NaHCO_3$ was cautiously added and the mixture was extracted with diethyl ether. The organic layer was washed with brine, dried over $MgSO_4$ and solvents were evaporated under reduced pressure. The residue was purified by column chromatography (SiO_2, hexane 100%) to give a pale yellow solid (0.655 g, 53%). ^1H NMR (300 MHz, CD_2Cl_2) δ: 0.48 (18H, s), 7.87 (2H, s), 8.14 (2H, s).

3,6-dibromo-1,5- bis(trimethylsilyloxy)benzene (**36**).[46] In a well-dried flask 2,5-dibromobenzene-1,4-diol (1 g, 3.73 mmol, 1 equiv.) was dissolved in anhydrous THF (20 mL). Then, triethylamine (1.51 mL, 10.8 mmol, 2.9 equiv.) and trimethylsilyl chloride (1.39 mL, 10.8 mmol, 2.9 equiv.) were added, and the mixture was stirred at room temperature for 1 hour. The solvent was removed under reduced pressure. The residue was taken up in n-hexane, and the resulting solution was filtrated on celite, to obtain the product **36** as a white solid (1.53 g, 99%). Without any further purification, it was used in the next step. ^1H NMR (300 MHz, CD_2Cl_2) δ: 0.34 (18H, s), 7.12 (2H, s).

3,6- bis(trimethylsilane)-1,5- bis(trimethylsilyloxy)benzene (**37**).[46] In a well-dried Schlenk flask, compound **36** (1.37 g, 3.32 mmol, 1 equiv.) was dissolved in anhydrous THF (27 mL), the mixture was cooled to -78 °C, then a 2.5 M solution of n-butyllithium in hexane (3.99 mL, 9.97 mmol, 3 equiv.) was added dropwise. The resulting reaction mixture was stirred for 1 hour. Then, trimethylsilyl chloride (1.70 mL,

13.29 mmol, 4 equiv.) was added dropwise, and the resulting mixture was allowed to warm to room temperature with stirring for 1 hour. The reaction was quenched by water addition and extracted with hexane. The organic layer was washed with brine, dried over $MgSO_4$ and the solvent was evaporated to dryness under reduced pressure. The isolated product **37** (1.24 g, 94%) was used in the next step without any further purification. ^{1}H NMR (300 MHz, CD_2Cl_2) δ: 0.29 (18H, s), 0.34 (18H, s), 6.80 (2H, s).

Bis(benzyne) precursor (27).[46] In a well-dried Schlenk flask, compound **37** (1.24 g, 3.11 mmol, 1 equiv.) was dissolved in anhydrous diethyl ether (20 mL). The mixture was cooled to -78 °C, then a 2.5 M solution of n-butyllithium in hexane (3.11 mL, 7.77 mmol, 2.5 equiv.) was added dropwise. The resulting mixture was stirred for 2 hours at room temperature, then, triflic anhydride (1.55 mL, 9.33 mmol, 3 equiv.) was added dropwise at 0 °C, and the mixture was stirred for 1 hour at room temperature. The reaction was quenched by water addition and the mixture was extracted with hexane. The organic layer was washed with brine, dried over $MgSO_4$ and the solvent was evaporated to dryness under reduced pressure. The residue was purified by column chromatography (SiO_2, hexane 100%), obtaining **27** as a white solid (0,711 g, 44%). ^{1}H NMR (300 MHz, CD_2Cl_2) δ: 0.43 (18H, s), 7.51 (2H, s).

References

[1]   J.-P. Malrieu, G. Trinquier, *J. Phys. Chem. A* **2016**, *120*, 9564–9578.

[2]   H. Chakraborty, A. Shukla, *J. Phys. Chem. A* **2013**, *117*, 14220–14229.

[3]   H. F. Bettinger, C. Tönshoff, M. Doerr, E. Sanchez-Garcia, *J. Chem. Theory Comput.* **2016**, *12*, 305–312.

[4]   C. Wang, H. Dong, W. Hu, Y. Liu, D. Zhu, *Chem. Rev.* **2012**, *112*, 2208–2267.

[5]   J. E. Anthony, *Angew. Chemie Int. Ed.* **2008**, *47*, 452–483.

[6]   A. Naibi Lakshminarayana, A. Ong, C. Chi, *J. Mater. Chem. C* **2018**, *6*, 3551–3563.

[7]   J. Li, Y. Zhao, J. Lu, G. Li, J. Zhang, Y. Zhao, X. Sun, Q. Zhang, *J. Org. Chem.* **2015**, *80*, 109–113.

[8]   T. J. Carey, E. G. Miller, A. T. Gilligan, T. Sammakia, N. H. Damrauer, *Org. Lett.* **2018**, *20*, 457–460.

[9]   Z. Sun, Q. Ye, C. Chi, J. Wu, *Chem. Soc. Rev.* **2012**, *41*, 7857.

[10]   E. B. Guidez, C. M. Aikens, *J. Phys. Chem. C* **2013**, *117*, 21466–21475.

[11]   Y. Yang, E. R. Davidson, W. Yang, *Proc. Natl. Acad. Sci. U. S. A.* **2016**, *113*, E5098–E5107.

[12]   J. E. Anthony, *Chem. Rev.* **2006**, *106*, 5028–5048.

[13]   H. Srour, T.-H. Doan, E. Da Silva, R. J. Whitby, B. Witulski, *J. Mater. Chem. C* **2016**, *4*, 6270–6279.

[14]   R. Schmidt, S. Göttling, D. Leusser, D. Stalke, A.-M. Krause, F. Würthner, *J. Mater. Chem.* **2006**, *16*, 3708–3714.

[15]   W. Fan, T. Winands, N. L. Doltsinis, Y. Li, Z. Wang, *Angew. Chemie Int. Ed.* **2017**, *56*, 15373–15377.

[16]   B. Shen, J. Tatchen, E. Sanchez-Garcia, H. F. Bettinger, *Angew. Chemie Int. Ed.* **2018**, *57*, 10506–10509.

[17]   H. Yamada, Y. Yamashita, M. Kikuchi, H. Watanabe, T. Okujima, H. Uno, T. Ogawa, K. Ohara, N. Ono, *Chem. - A Eur. J.* **2005**, *11*, 6212–6220.

[18]   R. Mondal, B. K. Shah, D. C. Neckers, *J. Am. Chem. Soc.* **2006**, *128*, 9612–9613.

[19] N. Pavliček, P. Gawel, D. R. Kohn, Z. Majzik, Y. Xiong, G. Meyer, H. L. Anderson, L. Gross, *Nat. Chem.* **2018**, *10*, 853–858.

[20] J. Krüger, F. Eisenhut, J. M. Alonso, T. Lehmann, E. Guitián, D. Pérez, D. Skidin, F. Gamaleja, D. A. Ryndyk, C. Joachim, et al., *Chem. Commun.* **2017**, *53*, 1583–1586.

[21] J. Krüger, F. García, F. Eisenhut, D. Skidin, J. M. Alonso, E. Guitián, D. Pérez, G. Cuniberti, F. Moresco, D. Peña, *Angew. Chemie Int. Ed.* **2017**, *56*, 11945–11948.

[22] R. Zuzak, R. Dorel, M. Krawiec, B. Such, M. Kolmer, M. Szymonski, A. M. Echavarren, S. Godlewski, *ACS Nano* **2017**, *11*, 9321–9329.

[23] R. Zuzak, R. Dorel, M. Kolmer, M. Szymonski, S. Godlewski, A. M. Echavarren, *Angew. Chemie Int. Ed.* **2018**, *57*, 10500–10505.

[24] M. Zugermeier, M. Gruber, M. Schmid, B. P. Klein, L. Ruppenthal, P. Müller, R. Einholz, W. Hieringer, R. Berndt, H. F. Bettinger, et al., *Nanoscale* **2017**, *9*, 12461–12469.

[25] J. I. Urgel, H. Hayashi, M. Di Giovannantonio, C. A. Pignedoli, S. Mishra, O. Deniz, M. Yamashita, T. Dienel, P. Ruffieux, H. Yamada, et al., *J. Am. Chem. Soc.* **2017**, *139*, 11658–11661.

[26] M. Watanabe, Y. J. Chang, S.-W. W. Liu, T.-H. H. Chao, K. Goto, M. M. Islam, C.-H. H. Yuan, Y.-T. T. Tao, T. Shinmyozu, T. J. Chow, *Nat. Chem.* **2012**, *4*, 574–578.

[27] R. Einholz, T. Fang, R. Berger, P. Grüninger, A. Früh, T. Chassé, R. F. Fink, H. F. Bettinger, *J. Am. Chem. Soc.* **2017**, *139*, 4435–4442.

[28] A. Jancarik, G. Levet, A. Gourdon, *Chem. - A Eur. J.* **2019**, *25*, 2366–2374.

[29] M. Watanabe, K.-Y. Chen, Y. J. Chang, T. J. Chow, *Acc. Chem. Res.* **2013**, *46*, 1606–1615.

[30] W. R. Roth, R. Langer, T. Ebbrecht, A. Beitat, H.-W. Lennartz, *Chem. Ber.* **1991**, *124*, 2751–2760.

[31] E. Clar, A. Mullen, *Tetrahedron* **1968**, *24*, 6719–6724.

[32] D. Skidin, O. Faizy, J. Krüger, F. Eisenhut, A. Jancarik, K. H. Nguyen, G. Cuniberti, A. Gourdon, F. Moresco, C. Joachim, *ACS Nano* **2018**, *12*, 1139–1145.

[33] W. H. Soe, C. Manzano, N. Renaud, P. De Mendoza, A. De Sarkar, F. Ample, M. Hliwa, A. M. Echavarren, N. Chandrasekhar, C. Joachim, *ACS Nano* **2011**, *5*, 1436–1440.

[34] D. Peña, S. Escudero, D. Pérez, E. Guitián, L. Castedo, *Angew. Chemie - Int. Ed.* **1998**, *37*, 2659–2661.

[35] D. Peña, A. Cobas, D. Pérez, E. Guitián, L. Castedo, *Org. Lett.* **2000**, *2*, 1629–1632.

[36] C. Romero, D. Peña, D. Pérez, E. Guitián, *Chem. - A Eur. J.* **2006**, *12*, 5677–5684.

[37] C. Romero, D. Peña, D. Pérez, E. Guitián, *J. Org. Chem.* **2008**, *73*, 7996–8000.

[38] P. T. Lynett, K. E. Maly, *Org. Lett.* **2009**, *11*, 3726–3729.

[39] J. M. Alonso, A. E. Díaz-Álvarez, A. Criado, D. Pérez, D. Peña, E. Guitián, *Angew. Chemie Int. Ed.* **2012**, *51*, 173–177.

[40] A. Jancarik, G. Levet, H. Nguyen-Kahn, A. Gourdon, **2019**, DOI Manuscript in preparation.

[41] T. Okuyama, T. Takino, T. Sueda, M. Ochiai, *J. Am. Chem. Soc.* **1995**, *117*, 3360–3367.

[42] T. Kitamura, K. Gondo, J. Oyamada, *J. Am. Chem. Soc.* **2017**, *139*, 8416–8419.

[43] D. Rodríguez-Lojo, D. Peña, D. Pérez, E. Guitián, *Synlett* **2015**, *26*, 1633–1637.

[44] C. Kitamura, Y. Abe, T. Ohara, A. Yoneda, T. Kawase, T. Kobayashi, H. Naito, T. Komatsu, *Chem. - A Eur. J.* **2010**, *16*, 890–898.

[45] C. Kitamura, A. Takenaka, T. Kawase, T. Kobayashi, H. Naito, *Chem. Commun.* **2011**, *47*, 6653–6655.

[46] T. Ikawa, S. Masuda, A. Takagi, S. Akai, *Chem. Sci.* **2016**, *7*, 5206–5211.

Ringraziamenti

Prima di tutti vorrei ringraziare il Prof. Andrea Secchi per tutti gli insegnamenti (chimici e non) e per la libertà che mi ha sempre lasciato, permettendomi di sbagliare e imparare dai miei errori.

Grazie al Prof. Arturo Arduini per la disponibilità, per i consigli e per tutti i "*Good lock*" pre-NMR.

Grazie a tutti coloro con cui ho collaborato, soprattutto la Dott.ssa Francesca Rossi dell'istituto IMEM per le misure TEM e la Prof.ssa Francesca Terenziani per le misure ottiche.

A special thanks to Dr André Gourdon for the possibility to join his group at the CEMES-CNRs of Toulouse. And thank you, Andrej, for the patience, the support and the all the scientific suggestions!

Grazie alla Marghe, con cui ho condiviso questi tre anni nel fantastico laboratorio 49. E grazie a tutti i ragazzi che mi hanno accompagnato e aiutato nello sviluppo di questa tesi: Silvia, Federica, Gabriele e Giorgia (a cui dico due volte grazie per la "doppietta"!).

Grazie agli amici del lab 50, Marti (meglio conosciuta come "Zaga") e Ste, con cui, soprattutto negli ultimi due mesi, ho condiviso le gioie e i dolori del dottorato (possiamo scrivere un libro con questo titolo) e per aver sopportato la mia costante presenza in ufficio.

GRAZIE ai fantastici 4: MCGullo (la senatrice), Fede (#poidividiamo), Carlo (il lombardo e non aggiungo altro) e Rix (fedele compagno di mensa). Gaione nel cuore. Grazie anche a tutto il lab 192, il mio "secondo" lab, per tutte le pause caffè!

Grazie a Gio e a Tiz per avermi sempre aiutato anche nelle situazioni più diffcili. Se sono arrivata qui, è proprio grazie a voi e ai 5 anni passati insieme. E grazie alla nostra creazione, Easyidea.

Grazie ai miei amicissimi Dario, Eli, Tecla e Andrea per tutte le nostre innumerevoli avventure. Grazie anche a Marty per le risate, gli inseguimenti e i viaggi in macchina!

Grazie ai miei genitori e a Laura. Grazie alla zia Piera, allo zio To' e a Giulia. Grazie Filo.